

**Assessing the Behaviour of Some Monocationic,  
Dicationic and Binary Mixtures of Monocationic  
Ionic Liquids through Spectroscopic Investigations**

*By*

**MANJARI CHAKRABORTY  
CHEM 11201704008**

**National Institute of Science Education and Research  
Bhubaneswar, Odisha**

*A thesis submitted to the  
Board of Studies in Chemical Sciences  
In partial fulfillment of requirements  
For the degree of*

**DOCTOR OF PHILOSOPHY  
of  
HOMI BHABHA NATIONAL INSTITUTE**



**April, 2022**

# Homi Bhaba National Institute

## Recommendations of the Viva Voce Committee

As members of the Viva Voce Committee, we certify that we have read the dissertation prepared by Ms. Manjari Chakraborty entitled "Assessing the Behaviour of Some Monocationic, Dicationic and Binary Mixtures of Monocationic Ionic Liquids through Spectroscopic Investigations" and recommend that it may be accepted as fulfilling the thesis requirement for the award of Degree of Doctor of Philosophy.

Chairman -

<Name>

Dr. Sanjib Kar

Date:

25/08/2022

Guide / Convener -

<Name>

Dr. Moloy Sarkar

Date:

25.08.2022

Co-guide -

Examiner -

<Name>

Dr. Nilmoni Sarkar

Date:

25/08/2022

Member 1 -

<Name>

Dr. Himansu Sekhar Biswal

Date:

25/08/2022

Member 2 -

<Name>

Dr. Arindam Ghosh

Date:

25/08/2022

Member 3 -

<Name>

Dr. Shantanu Pal

Date:

25/8/22

Final approval and acceptance of this thesis is contingent upon the candidate's submission of the final copies of the thesis to HBNI.

I/We hereby certify that I/we have read this thesis prepared under my/our direction and recommend that it may be accepted as fulfilling the thesis requirement.

Date: 25/08/2022

Place: NISER

Signature

Co-guide (if any)

Signature

Guide

Moloy Sarkar

## **STATEMENT BY AUTHOR**

This dissertation has been submitted in partial fulfilment of requirements for an advanced degree at Homi Bhabha National Institute (HBNI) and is deposited in the library to be made available to borrowers under rules of the HBNI. Brief quotations from this dissertation are allowable without special permission, provided that accurate acknowledgement of source is made. Requests for permission for extended quotation from or reproduction of this manuscript in whole or in part may be granted by the Competent Authority of HBNI when in his or her judgment the proposed use of the material is in the interests of scholarship. In all other instances, however, permission must be obtained from the author.

*Manjari Chakraborty*

**Manjari Chakraborty**

## DECLARATION

I, hereby declare that the investigation presented in the thesis has been carried out by me. The work is original and has not been submitted earlier as a whole or in part for a degree / diploma at this or any other Institution / University.

*Manjari Chakraborty*

**Manjari Chakraborty**

## List of Publications

- #1. Understanding the microscopic behavior of binary mixtures of ionic liquids through various spectroscopic techniques. **Chakraborty, M.**; Ahmed, T.; Dhale, R. S.; Majhi, D.; Sarkar, M. *J. Phys. Chem. B* **2018**, *122*, 12114–12130.
- #2. Understanding the behavior of monocationic and dicationic room-temperature ionic liquids through resonance energy-transfer studies. **Chakraborty, M.**; Ahmed, T.; Sarkar, M. *Langmuir* **2019**, *35*, 16172–16184.
- #3. Binary mixtures of ionic liquids: Ideal, non-ideal, or quasi-ideal? **Chakraborty, M.**; Barik, S.; Mahapatra, A.; Sarkar, M. *J. Chem. Phys.* **2021**, *154*, 224507.
- #4. Effect of Lithium-Ion on the Structural Organization of Monocationic and Dicationic Ionic Liquids. **Chakraborty, M.**; Barik, S.; Mahapatra, A and Sarkar, M. *J. Phys. Chem. B* **2021**, *125*, 13015-13026. (Invited article, “Kankan Bhattacharyya Festschrift”)
5. How does addition of lithium salt influence the structure and dynamics of choline chloride-based deep eutectic solvents? Barik, S.; **Chakraborty, M.**; Sarkar, M. *J. Phys. Chem. B* **2020**, *124*, 2864–2878.
6. An imine linked fluorescent covalent organic cage: the sensing of chloroform vapour and metal ions, and the detection of nitroaromatics. Gajula, R. K.; Mohanty, S.; **Chakraborty, M.**; Sarkar, M.; Prakash, M. *J. New J. Chem.* **2021**, *45*, 4810-4822.
7. Understanding the microscopic structural organization of neat ammonium based ionic liquids through resonance energy transfer (RET) studies. Majhi, D<sup>†</sup>; **Chakraborty, M.**<sup>†</sup>; Barik, S.; Mahapatra, A.; Sarkar, M. *Chemical Physics Impact* **2021**, *3*, 100034.
8. Comparison between pyrrolidinium-based and imidazolium-based dicationic ionic liquids: intermolecular interaction, structural organization, and solute dynamics. Mahapatra, A.;

**Chakraborty, M.;** Barik, S.; Sarkar, M. *Phys. Chem. Chem. Phys.* **2021**, *23*, 21029-21041.

9. Choline Chloride and Ethylene Glycol Based Deep Eutectic Solvent (DES) versus Hydroxyl Functionalized Room Temperature Ionic Liquids (RTILs): Assessing the Differences in the Microscopic Behaviour Between DES and RTILs. Barik, S.; **Chakraborty, M.;** Mahapatra, A.; Sarkar, M. *Phys. Chem. Chem. Phys.* **2022**, *24*, 7093-7106.

# List of publications pertaining to the thesis.

## Conferences

1. Presented poster in National Symposium on Radiation and Photochemistry 2021 (NSRP-2021) organized by Indian Society for Radiation and Photochemistry (June 25-26, 2021).
2. Delivered oral presentation in “National Workshop on Fluorescence and Raman Spectroscopy” (FCS- 2019) December 16 - 21, 2019 organized by TIFR and Fluorescence Society of India.
3. Presented poster in National Symposium on Radiation and Photochemistry 2019 (NSRP-2019) organized by Indian Society for Radiation and Photochemistry (February 7<sup>th</sup> - 9<sup>th</sup> 2019).
4. Presented poster in Trombay International Symposium on Radiation and Photochemistry 2018 (TSRP-2018) organized by Indian Society for Radiation and Photochemistry (3<sup>rd</sup> to 7<sup>th</sup> January 2018).

*Manjari Chakraborty*

**Manjari Chakraborty**

*Dedicated to.....*

*My Beloved Parents and Family*

## ACKNOWLEDGEMENTS

*The summary of my research in these five years has been written in this thesis but the foundation was laid years back when I was first introduced to the subject Chemistry and I started liking the subject. Since then, many people have influenced and contributed to this journey and indeed is the most interesting one till date.*

*The guidance and support of my supervisor Dr. Moloy Sarkar has been the most instrumental in these five years. I humbly express my deep sense of gratitude to him. Time management, knack for perfection and discipline are some of his traits that inspire me and I have been trying to emulate them in my life. I have learned a lot from him not only about research but also many things which eventually helped me to be a better human being.*

*I would like to thank Prof. Sudhakar Panda (Director, NISER) and Prof. T. K. Chandrashekar (Founder Director, NISER) for providing the research opportunities in NISER. It gives me immense pleasure to thank my thesis committee members Dr. Sanjib Kar, Dr. Himansu Sekhar Biswal, Dr. Arindam Ghosh and Dr. Santanu Pal for their cooperation and encouragement during my research work. I would like to thank to Dr. Bidraha Bagh Convenor, PGCS NISER. I wish to extend my warmest thanks to Dr. Himansu Sekhar Biswal, Chairperson, School of Chemical Sciences, NISER. I am thankful to all faculty members and scientific officers of my department for providing me a healthy atmosphere. I acknowledge all non-teaching staffs of my department for their constant support. I gratefully acknowledge NISER, Bhubaneswar for providing financial support and research infrastructure. My sincere regards are due for all the teachers who steered me in the right direction at personal and professional fronts during different stages of my life.*

*I have been fortunate enough to work in a lab where the atmosphere has always been friendly and fun-filled and much of it has to do with the lab members (MS Group). I have not just learned about instruments, designing of experiments and writing manuscripts, but also*

*about leadership and team work from all my former and present labmates. I would like to thank Dr. S. K. Das, P.K. Sahu and Dr. D. Majhi for introducing to the world of ionic liquid. I shall always be grateful to S. Banerjee, Dr. S. Roy, Dr. M. M. Islam and Dr. L. Satish for their suggestions. I would like to acknowledge my past and present lab members Ranu, Samya, Abhilash, Aman, Aditya, Biswa, Nilesh, Aradhana, Ramya and Dinesh for keeping the lab atmosphere lively. I have enjoyed my associations with Preeyanka, Sahadev, Amita, Amit and Debabrata in the lab for their myriad discussions ranging from scientific to non-scientific rantings. Without these wonderful colleagues of mine, life at NISER lab wouldn't have been a memorable one. I cherish my bonding with the SCS and SBS Ph.D students Krishna, Juhi, Namrata, Priyanka, Anwasha, Subrakant, Komal, Sandeep, Prakash, Shalini, Kasturi, Sruti, Shubhranshu, Sohini, Raktim, Uday, Debopam, Unmesh, Subhadip and the list continues. I express my heartfelt gratitude to Prof. Palok Aich and his family for making my research life more enjoyable.*

*Finally, I express my deep sense of gratitude to my late grandparents (maternal and paternal) who were always encouraging towards my education and co-curricular activities. I would like to take this occasion to express my respect to my parents for their teachings help me to face the world with confidence. The blessings, love, patience, care, support and sacrifices of Baba and Maa are unparalleled and I will forever remain indebted to them. I also acknowledge the love and support of my relatives. My sincere apologies if I have missed out your name, but I wish to extend my heartfelt gratitude to everyone who has been involved in my life in some way or the other.*

*Above all, I thank the Almighty for showing me the right path always.*

*Manjari*

# CONTENT

	Page No.
<b>SYNOPSIS</b>	<b>xii</b>
<b>List of Schemes</b>	<b>xxiv</b>
<b>List of Figures</b>	<b>xxv</b>
<b>List of Tables</b>	<b>xxix</b>
<b>Glossary of Acronyms</b>	<b>xxx</b>
<b>Chapter 1</b>	
<b>Introduction</b>	
1.1. Ionic liquids	2
1.1.1. Characteristic feature of ILs	4
1.1.2. Binary mixture of ILs	8
1.1.3. Information on structural and dynamic heterogeneity in ILs and their binary mixtures	10
1.1.4. Applications of ILs and their binary mixtures	12
1.1.5. Photophysical processes in ILs	14
1.1.6. NMR investigations on ILs	18
1.1.7. Fluorescence Correlation Spectroscopic (FCS) studies in ILs	19
1.2. Objective of the thesis	20
<b>Chapter 2</b>	
<b>Materials, Instrumentation and Methods</b>	
2.1. Materials	25
2.2. Synthesis procedure of dicationic ionic liquids (DILs)	26
2.2.1. 1,6-Bis(3-methylimidazolium-1-yl)hexane bromide, [C <sub>6</sub> (Mim) <sub>2</sub> ][Br] <sub>2</sub> (precursor for target six membered DIL)	26
2.2.2. 1,6-Bis(3-methylimidazolium-1-yl)hexane bis(trifluoromethylsulfonyl)amide, [C <sub>6</sub> (Mim) <sub>2</sub> ][NTf <sub>2</sub> ] <sub>2</sub>	26
2.2.3. 1,8-Bis(3-methylimidazolium-1-yl)octane bromide, [C <sub>8</sub> (Mim) <sub>2</sub> ][Br] <sub>2</sub> (precursor for target eight membered DIL)	27
2.2.4. 1,8-Bis(3-methylimidazolium-1-yl)octane	27
2.3. Sample preparation for spectroscopic measurements	28
2.4. Instrumentations	28
2.4.1. Instrumentations used for characterization of samples	28
2.4.2. Instrumental techniques for absorption and steady state emission measurements	28
2.4.2.1. Absorption measurements	28
2.4.2.2. Steady state fluorescence measurements	29
2.4.3. Instrumental techniques for time-resolved studies	30
2.4.3.1. Fluorescence lifetime measurements	30
2.4.3.2. Basic principle of TCSPC setup	31
2.4.4. Experimental technique for single-molecule studies	33
2.4.4.1. Time-resolved confocal fluorescence microscope	33

2.4.4.2.	Fluorescence correlation spectroscopy	34
2.5.	Methods	36
2.5.1.	Analysis of the fluorescence decay curves	36
2.5.1.1.	Data analysis	36
2.5.1.2.	Reduced chi-square ( $\chi^2$ ) values	37
2.5.1.3.	Distribution of weighted residuals	38
2.5.2.	Time-resolved fluorescence anisotropy measurements	38
2.5.3.	Hydrodynamic and Quasihydrodynamic theories	40
2.5.3.1.	The Stokes-Einstein-Debye (SED) theory	40
2.5.3.2.	Quasi-hydrodynamic theories	42
2.6.	NMR measurements	44
2.7.	Quantum yield calculations	45
2.8.	Standard error limits	45

### **Chapter 3**

#### **Thermophysical and Spectroscopic Investigations on Imidazolium-based Monocationic ILs and their Binary Mixtures with Common Cation**

3.1.	Introduction	47
3.2.	Experimental techniques and methods	50
3.3.	Results and discussions	50
3.3.1.	Thermophysical properties of ILs and IL-IL mixtures	50
3.3.2.	Photochromic behavior of spiropyran in ILs and IL-IL mixtures	55
3.3.3.	Time-resolved fluorescence study	58
3.3.3.1.	Perylene	59
3.3.3.2.	MPTS	64
3.3.4.	NMR and FCS studies	65
3.3.4.1.	NMR studies	65
3.3.4.2.	FCS studies	66
3.4.	Conclusion	68

### **Chapter 4**

#### **Thermophysical and Spectroscopic Investigations on Imidazolium and Pyrrolidinium-based Monocationic ILs and their Binary Mixtures with Common Anion**

4.1.	Introduction	70
4.2.	Experimental techniques and methods	73
4.3.	Results and discussions	74
4.3.1.	Thermophysical properties of ILs and their binary mixtures	74
4.3.2.	Time-resolved fluorescence anisotropy	79
4.3.3.	NMR studies	87
4.4.	Conclusion	88

### **Chapter 5**

#### **Understanding the Structural Organisation of Monocationic and Dicationic Room Temperature Ionic Liquids through Resonance Energy Transfer (RET) Studies**

5.1.	Introduction	91
------	--------------	----

5.2.	Experimental techniques and methods	95
5.3.	Results and discussions	95
5.3.1.	Thermophysical properties of neat ILs	95
5.3.2.	Fluorescent property of neat ILs	97
5.3.3.	Resonance energy transfer (RET) study	100
5.3.3.1.	Probing the RET process through steady-state measurements	101
5.3.3.2.	RET process through time-resolved measurements	102
5.4.	Conclusion	110
<b>Chapter 6</b>		
<b>The Effect of Lithium Ions on the Structural Organisation of Monocationic and Dicationic Ionic Liquids</b>		
6.1.	Introduction	113
6.2.	Experimental techniques and methods	117
6.3.	Results and discussions	118
6.3.1.	Steady-state fluorescence studies	118
6.3.2.	Time-resolved fluorescence anisotropy studies	120
6.3.3.	NMR studies	129
6.4.	Conclusion	132
<b>Summary and Future Prospects</b>		<b>134</b>
<b>REFERENCES</b>		<b>136</b>

## **SYNOPSIS**

Ionic Liquids (ILs) are special category of molten salts typically composed of bulky and asymmetrical organic cations and organic or inorganic anions with their melting points below 100 °C. These materials have great promise in terms of their applications in the fields of chemistry, biology and also in industry due to its attractive thermophysical properties.<sup>1, 2</sup> As the properties of ILs are tunable in nature, different ILs can be synthesized to meet the requirements for various applications. While mono cation-based ILs are more widely known, the other exciting classes of ILs are the geminal dicationic ILs (DILs).<sup>3-5</sup> Due to the presence of two cations in DILs, DILs have shown high thermal and chemical stability as compared to monocationic ILs (MILs).<sup>3-7</sup> To effectively use these DILs in various applications, understanding the structure-property correlation for these media are very much necessary. Another important approach to fine tune the properties of ILs can be achieved through the mixing of ILs. This is also interesting as it may allow a prior prediction of the desired properties of the specific target mixtures, to be used for a particular application.<sup>8-10</sup> However, the potential application of binary mixture of ILs can only be realized when the microscopic behavior of these mixtures is well understood. The main objective of the present thesis is to understand the inter-relationship among the intermolecular interaction, structural organization and solute dynamics in various imidazolium and pyrrolidinium based MILs, DILs and binary mixtures of MILs mainly through time-resolved fluorescence anisotropy, NMR and fluorescence correlation spectroscopy (FCS) spectroscopic studies.

### **Organization of thesis**

The present thesis has been divided into six chapters. The contents of the different chapters of thesis are briefly mentioned below.

## **Chapter 1: Introduction**

Chapter 1 starts with a brief introduction about ionic liquids (ILs) and their physicochemical properties. In particular, discussions are made on various imidazolium and pyrrolidinium-based ILs. Various applications of ILs and their binary mixtures in the fields of chemical, biological and material sciences have also been highlighted. Next, the study of kinetics using photochromic probes has been illustrated in this chapter. After this, a detailed discussions on the excitation wavelength dependent emission behavior, solute rotation, translational diffusion phenomena in various ILs have been made by illustrating several literature reports. Lastly, the current challenges in ionic liquids research and objective of the present thesis work have been outlined at the end of this chapter.

## **Chapter 2: Instrumentation and Method**

Basic principles of different experimental techniques used in the present study, such as absorption spectroscopy, steady-state and time-resolved emission spectroscopy have been demonstrated briefly in this chapter. The working principle of time-correlated single photon counting (TCSPC) technique and single molecule fluorescence spectroscopic technique have also been discussed. Further, principles of time-resolved fluorescence anisotropy and pulsed-field-gradient NMR (PFG-NMR) measurements are also described. Methodologies used to obtain the rotational relaxation time and analysis of time resolved fluorescence anisotropy data by using several hydrodynamic models have also been demonstrated. The error limits corresponding to different experimental parameters are provided in the end of this chapter.

## **Chapter 3. Thermophysical and Spectroscopic Investigations on Imidazolium-based Monocationic ILs and their Binary Mixtures with Common Cation**

This chapter discusses the outcomes of combined thermophysical and photophysical investigations of several binary mixtures of ILs along with the constituent pure ILs that they

are composed of. Specifically in this study, the mixtures of ILs are chosen with a common cation and variation in anion namely 1-Butyl-3-methylimidazolium [BMIM] bistrifluoromethylsulfonylimide [NTf<sub>2</sub>], hexafluorophosphate [PF<sub>6</sub>] and tetrafluoroborate [BF<sub>4</sub>] as shown in Figure 1. This has been done by monitoring the role of anion, if any, in governing the behavior of ILs exclusively. Initially, the systems have been investigated by studying the thermophysical properties of the concerned mixtures. The synergistic effect between the pure ILs and their binary mixtures have also been studied through a photochromic probe Spiropyran (SP). Further, investigations on these mixtures have been carried out through steady-state and time-resolved fluorescence spectroscopy, nuclear magnetic resonance (NMR), and fluorescence correlation spectroscopy (FCS). The data obtained from time-resolved fluorescence experiment have been analyzed with the help of Stokes-Einstein-Debye (SED) hydrodynamic theory<sup>11, 12</sup> which shows that the rotation of probes (perylene and sodium 8-methoxypyrene 1,3,6-trisulfonate) are different in neat ILs as well as their mixtures (Figure 2 and Figure 3). Interestingly, the extent of interactions observed through the rotation of probes in ILs as well as their mixtures are found to be different for different mixtures indicating that the binary mixtures of ILs are not only spatially heterogeneous but also dynamically heterogeneous. Further, measurements of translational diffusion coefficients of the diffusing species in ILs as well as their binary mixtures through NMR and FCS studies have independently provided an idea about the nanostructural organization within these IL mixtures. The analysis of data essentially reveals that the mixtures of ILs that are used in the current study do not behave like a non-ideal solution. The behavior of the IL mixtures is observed to be more like quasi-ideal type.

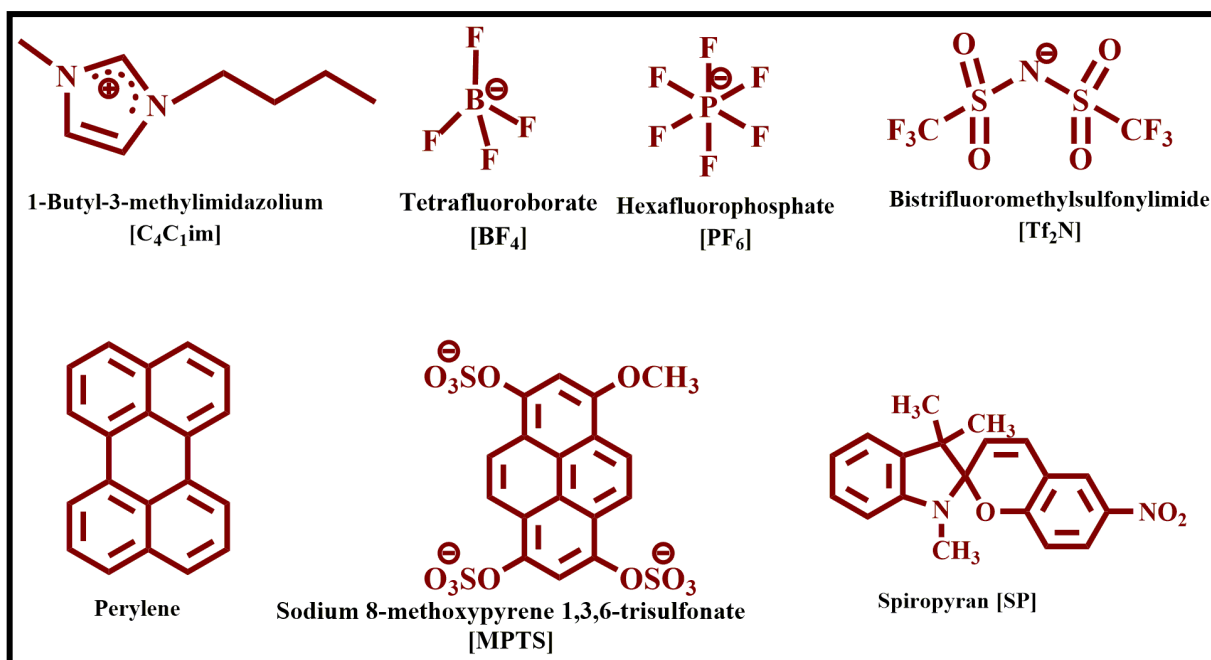


**Figure 1.** Molecular structures of ILs and probes used in the study.

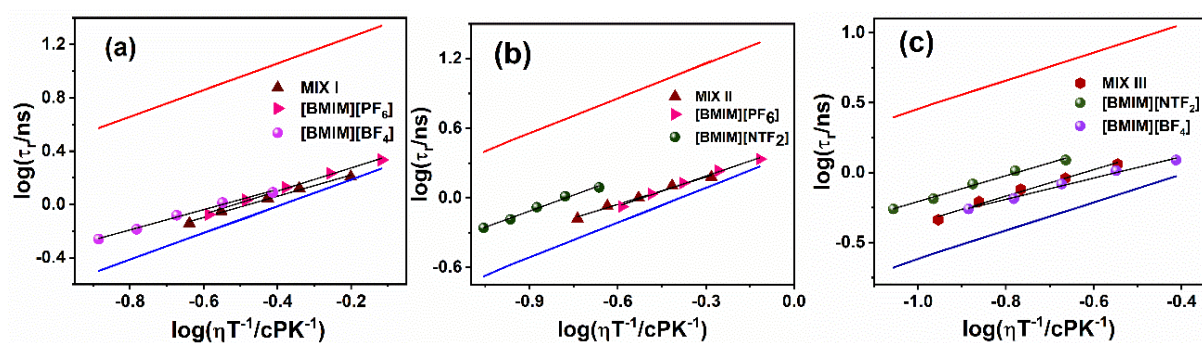


**Figure 2.** Log ( $\tau_r$ ) vs log ( $\eta/T$ ) plot of perylene in (a) mix I, (b) mix II, and (c) mix III with stick and slip boundary condition limits. The solid black lines indicate the fit to the data points.

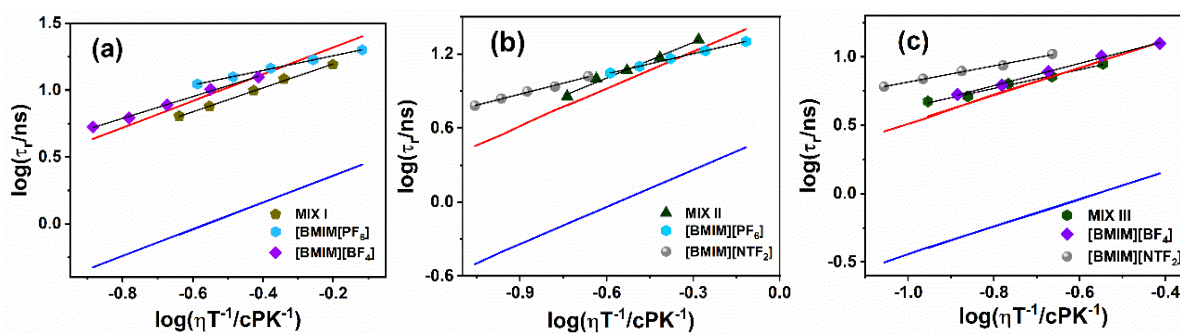


**Figure 3.** Log ( $\tau_r$ ) vs log ( $\eta/T$ ) plot of MPTS in (a) mix I, (b) mix II, and (c) mix III with stick and slip boundary condition limits. The solid black lines indicate the fit to the data points.

#### **Chapter 4. Thermophysical and Spectroscopic Investigations on Imidazolium and Pyrrolidinium-based Monocationic ILs and their Binary Mixtures with Common Anion**

In this chapter the thermophysical properties as well as the structural organization of different binary mixtures of ILs have been investigated by understanding the thermodynamics of mixing ILs. In this work, a systematic study of the IL mixtures has been conducted by taking imidazolium and pyrrolidinium ILs with bis(trifluoromethylsulfonyl)imide [NTf<sub>2</sub>] as the common anion and various cations such as 1-alkyl-3-methylimidazolium with  $n = 2, 3, 4$ , [C<sub>2</sub>C<sub>1</sub>im], [C<sub>3</sub>C<sub>1</sub>im], [C<sub>4</sub>C<sub>1</sub>im], and 1-alkyl-3-methylpyrrolidinium with  $n = 3, 4$ , [C<sub>3</sub>C<sub>1</sub>pyr] and [C<sub>4</sub>C<sub>1</sub>pyr] (Figure 4). Moreover, imidazolium and pyrrolidinium based ILs are chosen so that the role of cations, in governing the behavior of the said mixture, if any, is properly understood. Investigations have been carried out at the macroscopic level by observing the thermophysical properties, such as molar volume and thermal expansion coefficient, and at the microscopic level with time-resolved fluorescence measurements and the pulse field gradient nuclear magnetic resonance (NMR) technique. The results obtained from the thermophysical study have indicated that excess molar volume for imidazolium-based IL–IL mixtures may be linked to the free volume created by the alkyl chain of the imidazolium cation whereas for the mixture of pyrrolidinium ILs, lowering of density can give rise to free volume. Analysis of time-resolved fluorescence anisotropy data through quasi-hydrodynamic theory (DKS model)<sup>13, 14</sup> has provided clear evidence in favor of the presence of free volume in the binary mixture of ILs (Figure 5, Table 1). Further, NMR studies have also supported the fact that free volume has been observed in the binary mixtures of ILs. The outcome of the present investigation reveals that the mixtures show appreciable deviation from ideal behavior and the

deviation from the ideal behavior is caused due to the generation of free volume in the resultant mixture, describing these IL mixtures as quasi-ideal.

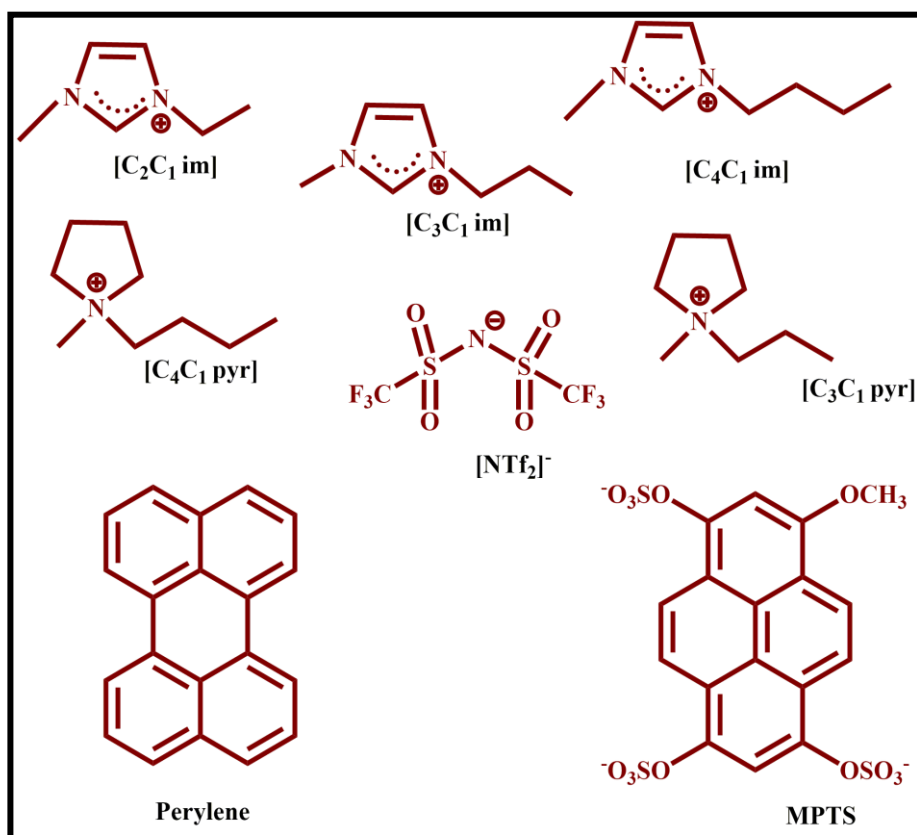


**Figure 4.** Molecular structures of ILs and probes used in the study.

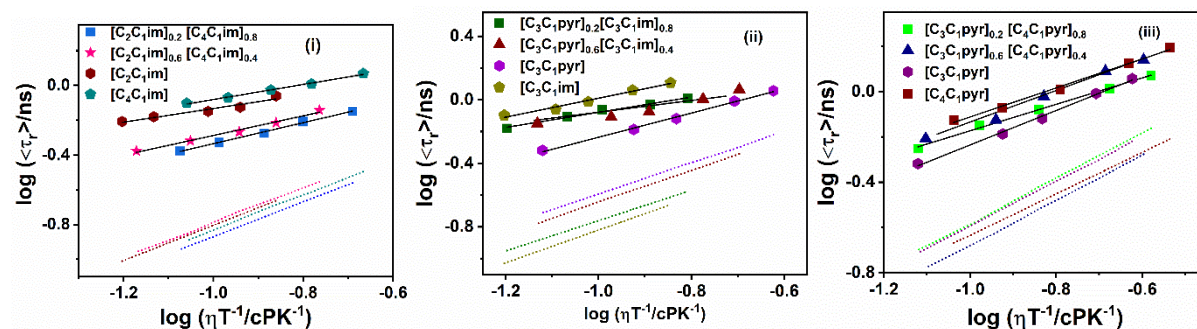


**Figure 5.** Log–log plots of the average rotational relaxation time of perylene in (i) the [C<sub>2</sub>C<sub>1</sub>im] and [C<sub>4</sub>C<sub>1</sub>im] mixture, (ii) the [C<sub>3</sub>C<sub>1</sub>pyr] and [C<sub>3</sub>C<sub>1</sub>im] mixture, and (iii) the [C<sub>3</sub>C<sub>1</sub>pyr] and [C<sub>4</sub>C<sub>1</sub>pyr] mixture, with the dashed line representing the boundary parameters obtained from the DKS model.

**Table 1.** Free volume estimated through DKS theory

System	$C_{DKS}$	$C_{slip}$	Free volume
$[C_2C_1im]_{0.6}[C_4C_1im]_{0.4}$	0.053	0.085	~ 38%
$[C_2C_1pyr]_{0.6}[C_4C_1im]_{0.4}$	0.078		~ 8%
$[C_2C_1pyr]_{0.6}[C_4C_1pyr]_{0.4}$	0.073		~ 14%

## Chapter 5. Understanding the Structural Organization of Monocationic and Dicationic Ionic Liquids through Resonance Energy Transfer Studies

This chapter focusses on understanding the differences in the local structural organization of imidazolium-based monocationic ILs (MILs) and dicationic ILs (DILs) through resonance energy transfer studies. The study has been performed with DILs, namely,  $[C_6(mim)_2][NTf_2]_2$  and  $[C_8(mim)_2][NTf_2]_2$  with their monocationic counterparts being  $[C_3mim][NTf_2]$  and  $[C_4mim][NTf_2]$ . Additionally, we have also taken six-membered imidazolium-based IL  $[C_6mim][NTf_2^-]$  and eight-membered imidazolium-based IL,  $[C_8mim][NTf_2^-]$  so that the effect of alkyl chain length can be monitored exclusively (Figure 6). In this study, neat IL has been chosen as donor and a charged species rhodamine 6G (R6G) has been used as an acceptor because of the fact that they satisfy the spectroscopic criteria that are needed for an RET event to take place.<sup>15, 16</sup> In this study, specifically, two imidazolium-based geminal DILs and their monocationic counterparts are used for the present investigations. As stated before, additionally, the studies have also been carried out in some selected MILs where the lengths of the alkyl side chains are kept unchanged for MILs and DILs. Interestingly, the data reveals that the RET interaction is more favorable for DILs than for MILs, even though the DILs are relatively bulkier than their monocationic counterparts. More interestingly, the RET interaction

(as seen from the donor acceptor distance,  $R_{DA}$ , shown in Table 2) is also found to be more favorable for DILs than that for MILs, where the length of the alkyl group is kept fixed for MILs and DILs. The result of the present study delineates that the alkyl chain length on the cation is not the sole factor contributing to the RET outcomes for DILs and MILs but the local structure of DILs also contributes significantly to the same. The current investigation clearly indicates that DILs have a more compact local structure than that of MILs. Essentially, the current study highlights that a cost-effective, noninvasive technique such as RET is quite effective in capturing the differences in the nanostructural organization of MILs and DILs.

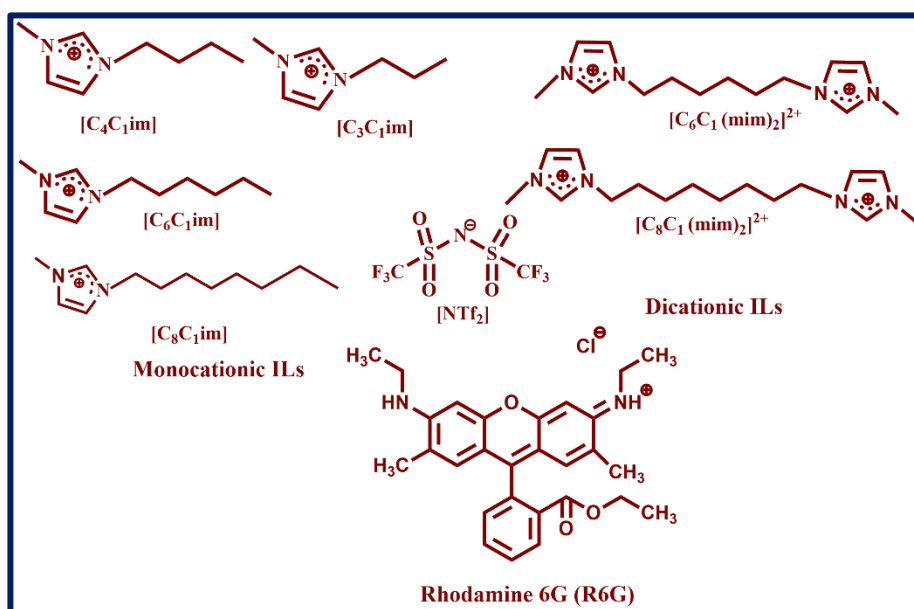


**Figure 6.** Molecular structures of ILs and probes used in this study.

**Table 2.** The FRET parameters obtained from the RET study.

System	$R_{DA}$ (Å)	$E$	$K_{RET}$ ( $10^8$ s $^{-1}$ )
[C <sub>3</sub> mim][NTf <sub>2</sub> <sup>-</sup> ]	37.27	0.65	6.89
[C <sub>4</sub> mim][NTf <sub>2</sub> <sup>-</sup> ]	39.03	0.52	5.49
[C <sub>6</sub> mim][NTf <sub>2</sub> <sup>-</sup> ]	48.26	0.39	3.92
[C <sub>8</sub> mim][NTf <sub>2</sub> <sup>-</sup> ]	55.05	0.31	4.02
[C <sub>6</sub> (mim) <sub>2</sub> ][NTf <sub>2</sub> <sup>-</sup> ] <sub>2</sub>	46.44	0.45	4.72
[C <sub>8</sub> (mim) <sub>2</sub> ][NTf <sub>2</sub> <sup>-</sup> ] <sub>2</sub>	48.61	0.40	4.25

## Chapter 6. The Effect of Lithium Ions on the Structural Organisation of Monocationic and Dicationic Ionic Liquids

In recent times, ionic liquid-based (ILs) electrolytic system has emerged as suitable alternative to the conventional organic solvent-based electrolytic system. However, since, anion of ILs is known to form aggregates in the presence of lithium-ions ( $\text{Li}^+$ ), and this can influence the transport properties of  $\text{Li}^+$  ion in a significant manner, it is, therefore, important to understand how lithium-ions influence the structure and dynamics of ILs.<sup>17, 18</sup>

This chapter describes the intermolecular interaction, structural organization and dynamics of MILs and DIL in the absence and presence of lithium salt. Specifically, for this purpose, two MILs, 1-methyl-3-propylimidazolium bis- (trifluoromethylsulfonyl)imide ( $[\text{C}_3\text{C}_{1\text{im}}][\text{NTf}_2]$ ), 1-hexyl-3-propylimidazolium bis- (trifluoromethylsulfonyl)imide ( $[\text{C}_6\text{C}_{1\text{im}}][\text{NTf}_2]$ ), and a DIL, 1,6-bis(3-methylimidazolium-1-yl)hexane bis(trifluoromethylsulfonyl)amide ( $[\text{C}_6(\text{mim})_2][\text{NTf}_2]_2$ ) (Figure 7) have been chosen in such a way that either the alkyl chain of MILs becomes equal or half of the spacer chain length of DIL. To understand the effect of the addition of lithium-ion on the structural organization of MILs and DIL, steady-state absorption and fluorescence spectroscopies, time-resolved fluorescence anisotropy and nuclear magnetic resonance (NMR) techniques have been used. Structural organization in the apolar and polar domains of ILs has been probed by following the rotational diffusion of suitably chosen solute in the concerned media through time-resolved fluorescence anisotropy (TRFA) measurements. TRFA studies have revealed that with the addition of  $\text{Li}^+$  ion, due to the coordination between the  $\text{Li}^+$  ions and  $\text{NTf}_2$  anions in ILs, the packing of the alkyl chain present in the apolar region of MILs get reduced which is not observed in DILs. This has been depicted by the change in the average friction coefficient

upon addition of lithium ions in both MILs and DIL (Figure 8). Further, measurements of the self-diffusion coefficient through NMR have also supported the observation that  $\text{Li}^+$  ion also perturbs the nanostructural organization of the MIL in a significant manner than that it does for the DIL. The behavior of DIL in the presence of  $\text{Li}^+$  ion, as revealed by the present study, has been rationalized by considering the folded arrangement of DIL in the fluid-structure. Essentially, all of these investigations have suggested that the addition of lithium-ion significantly alters the microscopic behavior of MILs in comparison to that of DIL. The outcome of this study is expected to be helpful in realizing the potentials of these media as electrolytes in battery applications.

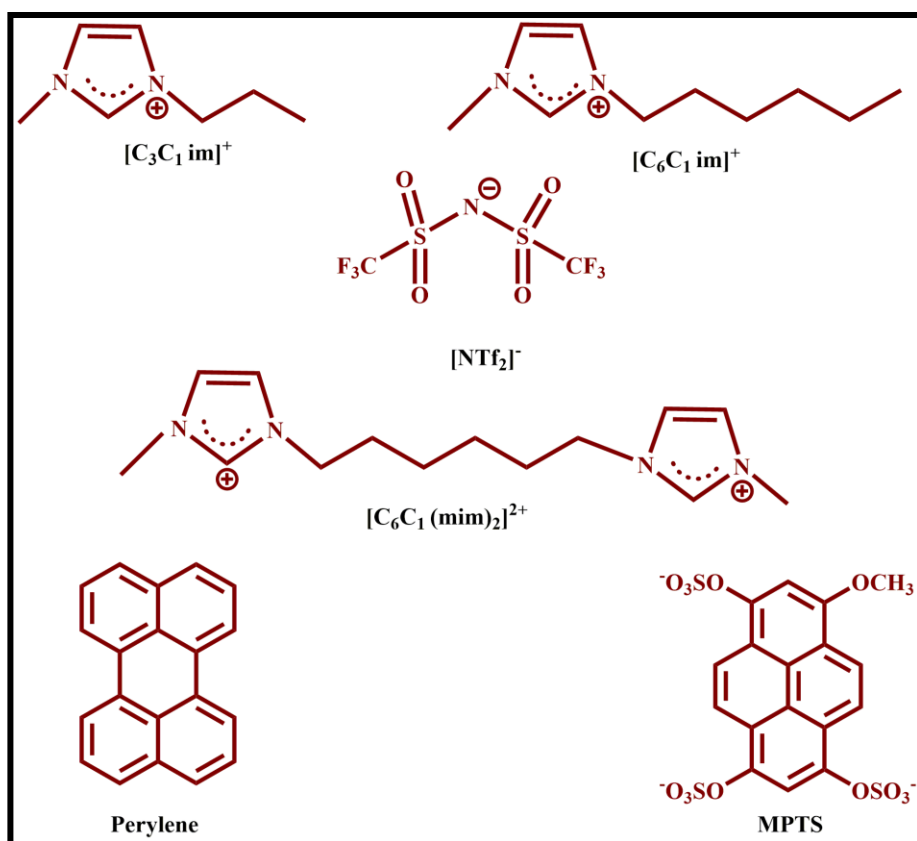


**Figure 7.** Molecular structures of ILs and probes used in this study.

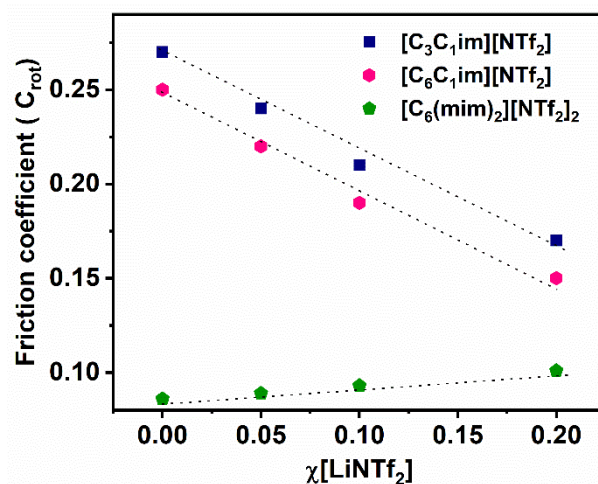


**Figure 8.** Average friction coefficient for perylene in all the systems as a function of Li<sup>+</sup> ion concentration.

In conclusion, the present study has demonstrated the structural organization, intermolecular interactions and solute dynamics in MILs, DILs and the binary mixtures of MILs are very different. The present work provides valuable information with regards to understanding the structure-property correlation in various IL-based solvent systems.

The future prospects are also outlined at the end of the thesis.

## References

1. Rogers Robin, D.; Seddon Kenneth, R., *Science* **2003**, *302* (5646), 792-793.
2. Hallett, J. P.; Welton, T., *Chem. Rev.* **2011**, *111*, 3508-3576.
3. Anderson, J. L.; Ding, R.; Ellern, A.; Armstrong, D. W., *J. Am. Chem. Soc.* **2005**, *127*, 593-604.
4. Villar-Garcia, I. J.; Lovelock, K. R. J.; Men, S.; Licence, P., *Chem. Sci.* **2014**, *5*, 2573-2579.
5. Mandai, T.; Yoshida, K.; Ueno, K.; Dokko, K.; Watanabe, M., *Phys. Chem. Chem. Phys.* **2014**, *16*, 8761-8772.

6. Shirota, H.; Mandai, T.; Fukazawa, H.; Kato, T., *J. Chem. Eng. Data* **2011**, *56*, 2453-2459.
7. Han, X.; Armstrong, D. W., *Org. Lett.* **2005**, *7*, 4205-4208.
8. Niedermeyer, H.; Hallett, J. P.; Villar-Garcia, I. J.; Hunt, P. A.; Welton, T., *Chem. Soc. Rev.* **2012**, *41*, 7780-7802.
9. Chatel, G.; Pereira, J. F. B.; Debbeti, V.; Wang, H.; Rogers, R. D., *Green Chem.* **2014**, *16*, 2051-2083.
10. Clough, M. T.; Crick, C. R.; Gräsvik, J.; Hunt, P. A.; Niedermeyer, H.; Welton, T.; Whitaker, O. P., *Chem. Sci.* **2015**, *6*, 1101-1114.
11. Fleming, G. R., *Chemical applications of ultrafast spectroscopy*. **1986**.
12. Edward, J. T., *J. Chem. Educ.* **1970**, *47*, 261.
13. Dote, J. L.; Kivelson, D.; Schwartz, R. N., *J. Phys. Chem* **1981**, *85*, 2169-2180.
14. Anderton, R. M.; Kauffman, J. F., *J. Phys. Chem* **1994**, *98*, 12117-12124.
15. Lakowicz, J. R., *Principles of fluorescence spectroscopy*. Springer: 2006.
16. Förster, T., *Molecular Fluorescence Principles and Applications*, Wiley-VCH Verlag GmbH, Weinheim, Germany. **1948**, 55-75.
17. Lawler, C.; Fayer, M. D., *J. Phys. Chem B* **2013**, *117*, 9768-9774.
18. Dhale, R. S.; Sahu, P. K.; Sarkar, M., *J. Phys. Chem B* **2017**, *121*, 7934-7945.

## List of Schemes

<b>Sl. No.</b>	<b>Scheme No.</b>	<b>Title</b>	<b>Page No.</b>
1.	Scheme 1.1.	Schematic representation of interconversion of spiropyran and merocyanine with UV light irradiation.	15
2.	Scheme 1.2.	Schematic representation of excitation wavelength dependent fluorescence emission phenomenon.	17
3.	Scheme 2.1.	A schematic diagram for the working principle of TCSPC setup.	32
4.	Scheme 2.2.	Basic configuration of confocal fluorescence microscope	34
5.	Scheme 2.3.	Diffusion of fluorophores through the confocal volume and fluctuations in the relative intensities.	35
6.	Scheme 2.4.	A diagrammatic representation of fluorescence anisotropy measurements.	39

## List of Figures

Sl. No.	Figure No.	Figure title	Page No.
1.	Figure 1.1	Molecular structure of some cations and anions of RTILs	4
2.	Figure 3.1.	Molecular structures of ILs and probes used in the present study (Chapter 3).	50
3.	Figure 3.2.	Variation of the bulk viscosity of [C <sub>4</sub> C <sub>1</sub> ][BF <sub>4</sub> ], [C <sub>4</sub> C <sub>1</sub> ][PF <sub>6</sub> ], Mix I (A), Mix I (B) and Mix I (C) with temperature and its fitting with VFT equation.	54
4.	Figure 3.3.	Schematic representation of interconversion of spiropyran and merocyanine with UV light irradiation.	56
5.	Figure 3.4.	Overlay spectra illustrating the thermal decay of a solution of SP in Mix III after exposure to UV irradiation.	56
6.	Figure 3.5.	First-order kinetic plot of the thermal relaxation of the SP isomer in Mix III after 5 min UV irradiation.	57
7.	Figure 3.6	Representative time resolved fluorescence anisotropy decay profile of (a) perylene and (b) MPTS in Mix I (B) at two different temperatures. The black line denotes the fit to data points.	59
8.	Figure 3.7.	Log( $\tau_r$ ) vs. log( $\eta/T$ ) plot of perylene in (a) Mix I (b) Mix II and (c) Mix III with stick and slip boundary condition limits. The solid black lines indicate the fit to the data points. The red and blue lines represent the stick and slip boundary conditions. The composition of IL-IL mixtures are Mix I (B): [C <sub>4</sub> C <sub>1</sub> ][BF <sub>4</sub> ] <sub>0.6</sub> [PF <sub>6</sub> ] <sub>0.4</sub> ; Mix II (C) : [C <sub>4</sub> C <sub>1</sub> ][PF <sub>6</sub> ] <sub>0.8</sub> [NTF <sub>2</sub> ] <sub>0.2</sub> and Mix III (B) : [C <sub>4</sub> C <sub>1</sub> ][BF <sub>4</sub> ] <sub>0.6</sub> [NTF <sub>2</sub> ] <sub>0.4</sub> .	62
9.	Figure 3.8.	Log( $\tau_r$ ) vs. log( $\eta/T$ ) plot of MPTS in (a) Mix I (b) Mix II and (c) Mix III with stick and slip boundary condition limits. The solid black lines indicate the fit to the data points. The red and blue lines indicate the stick and slip boundary conditions. The composition of IL-IL mixtures are Mix I (B): [C <sub>4</sub> C <sub>1</sub> ][BF <sub>4</sub> ] <sub>0.6</sub> [PF <sub>6</sub> ] <sub>0.4</sub> ; Mix II (C): [C <sub>4</sub> C <sub>1</sub> ][PF <sub>6</sub> ] <sub>0.8</sub> [NTf <sub>2</sub> ] <sub>0.2</sub> and Mix III (B): [C <sub>4</sub> C <sub>1</sub> ][BF <sub>4</sub> ] <sub>0.6</sub> [NTf <sub>2</sub> ] <sub>0.4</sub> .	64
10.	Figure 3.9.	The representative FCS plot for Mix I.	67
11.	Figure 4.1.	Molecular structures of ILs and probes used in the present study (chapter 4).	73
12.	Figure 4.2.	Plot of excess molar volumes ( $V^E$ /cm <sup>3</sup> mol <sup>-1</sup> ) of binary mixtures of ILs for T = 293 K, 298 K, 303 K, 308 K	76

- and 318 K. The solid boxes are for pure imidazolium IL-IL mixture. The open boxes are for pure pyrrolidinium IL-IL mixtures. The solid stars are for mixture of pyrrolidinium IL and imidazolium IL.
13. Figure 4.3. Thermal expansion coefficients of binary mixture of ILs: (i) mole frac. of [C<sub>2</sub>C<sub>1</sub>im] in the [C<sub>2</sub>C<sub>1</sub>im][C<sub>4</sub>C<sub>1</sub>im] mix., (ii) mole frac. of [C<sub>3</sub>C<sub>1</sub>pyr] in the [C<sub>3</sub>C<sub>1</sub>pyr][C<sub>3</sub>C<sub>1</sub>im]mix and (iii) mole frac. of [C<sub>3</sub>C<sub>1</sub>pyr] in the [C<sub>3</sub>C<sub>1</sub>pyr][C<sub>4</sub>C<sub>1</sub>pyr] mix. The black solid rectangle represents the thermal expansion coefficient calculated with Benson Kriyohara criterion. 77
  14. Figure 4.4. Viscosity of binary mixture of ILs: (i) mole frac. of [C<sub>2</sub>C<sub>1</sub>im] in the [C<sub>2</sub>C<sub>1</sub>im][C<sub>4</sub>C<sub>1</sub>im] mix., (ii) mole frac. of [C<sub>3</sub>C<sub>1</sub>pyr] in the [C<sub>3</sub>C<sub>1</sub>pyr][C<sub>3</sub>C<sub>1</sub>im] mix., and (iii) mole frac. of [C<sub>3</sub>C<sub>1</sub>pyr] in the [C<sub>3</sub>C<sub>1</sub>pyr][C<sub>4</sub>C<sub>1</sub>pyr] mix. 79
  15. Figure 4.5. Representative decay of (i) Perylene in [C<sub>2</sub>C<sub>1</sub>im]<sub>0.2</sub>[C<sub>4</sub>C<sub>1</sub>im]<sub>0.8</sub>[NTf<sub>2</sub>] (ii) MPTS in [C<sub>2</sub>C<sub>1</sub>im]<sub>0.2</sub>[C<sub>4</sub>C<sub>1</sub>im]<sub>0.8</sub>[NTf<sub>2</sub>]. 80
  16. Figure 4.6. log-log plots of the average rotational relaxation time of perylene in (i) [C<sub>2</sub>C<sub>1</sub>im] and [C<sub>4</sub>C<sub>1</sub>im] mix. (ii) [C<sub>3</sub>C<sub>1</sub>pyr] and [C<sub>3</sub>C<sub>1</sub>im] mix. (iii) [C<sub>3</sub>C<sub>1</sub>pyr] and [C<sub>4</sub>C<sub>1</sub>pyr] mix. with blue colour stick and red colour slip boundary condition limits. The solid black lines indicate the fit to the data points. 84
  17. Figure 4.7. log-log plots of the average rotational relaxation time of MPTS in (i) [C<sub>2</sub>C<sub>1</sub>im] and [C<sub>4</sub>C<sub>1</sub>im] mix. (ii) [C<sub>3</sub>C<sub>1</sub>pyr] and [C<sub>3</sub>C<sub>1</sub>im] mix. (iii) [C<sub>3</sub>C<sub>1</sub>pyr] and [C<sub>4</sub>C<sub>1</sub>pyr] mix. with blue colour stick and red colour slip boundary condition limits. The solid black lines indicate the fit to the data points. 84
  18. Figure 4.8. The excess diffusion coefficient of neat ILs and their corresponding binary mixtures (i) [C<sub>2</sub>C<sub>1</sub>im] and [C<sub>4</sub>C<sub>1</sub>im] ILs (ii) [C<sub>3</sub>C<sub>1</sub>pyr] and [C<sub>3</sub>C<sub>1</sub>im] ILs (iii) [C<sub>3</sub>C<sub>1</sub>pyr] and [C<sub>4</sub>C<sub>1</sub>pyr] ILs. 87
  19. Figure 5.1. Molecular structures of ILs and probes used in the present study (chapter 5). 94
  20. Figure 5.2. (a) Absorption spectrum of neat [C<sub>3</sub>mim][NTf<sub>2</sub><sup>-</sup>] and (b) Normalized absorption and emission spectra of R6G and [C<sub>3</sub>mim][NTf<sub>2</sub><sup>-</sup>] respectively. The IL ([C<sub>3</sub>mim][NTf<sub>2</sub><sup>-</sup>]) has been excited at 375nm. The overlap region in Figure 5.2(b) is highlighted. 97
  21. Figure 5.3. Decrease in the fluorescence intensity upon gradual addition of DMSO (a) [C<sub>6</sub>(mim)<sub>2</sub>][NTf<sub>2</sub>]<sub>2</sub> (b) [C<sub>3</sub>mim][NTf<sub>2</sub>]. 98
  22. Figure 5.4. Fluorescence correlation plots of neat [C<sub>3</sub>mim][NTf<sub>2</sub>] and [C<sub>6</sub>(mim)<sub>2</sub>][NTf<sub>2</sub>]<sub>2</sub> upon gradual addition of different concentrations of DMSO. 99
  23. Figure 5.5. Variation in the emission intensity of [C<sub>3</sub>mim][NTf<sub>2</sub><sup>-</sup>](λ<sub>exc</sub> = 375 nm) with gradual addition of R6G. The inset indicates that the emission intensity of 101

		[C <sub>3</sub> mim][NTf <sub>2</sub> <sup>-</sup> ] decreases as the acceptor concentration is increased (from 0 μM to 231 μM).	
24.	Figure 5.6.	Fluorescence decay curves of [C <sub>3</sub> mim][NTf <sub>2</sub> <sup>-</sup> ] in absence and presence of the acceptor ( $\lambda_{\text{ex}} = 375$ nm and $\lambda_{\text{em}} = 450$ nm). The solid black line represents fit to the data points.	102
25.	Figure 5.7.	Fluorescence decay profile of the acceptor (R6G) ( $\lambda_{\text{ex}} = 375$ nm and $\lambda_{\text{em}} = 580$ nm; concentration of the acceptor = 231 μM) in presence of the donor [C <sub>3</sub> mim][NTf <sub>2</sub> <sup>-</sup> ]. A clear rise time can be seen in the inset. The solid green line symbolizes fit to the data points.	104
26.	Figure 6.1.	Molecular structures of ILs and probes used in the present study (chapter 6).	117
27.	Figure 6.2.	The excitation wavelength dependent behaviour of ANF in (a) [C <sub>3</sub> C <sub>1</sub> im][NTf <sub>2</sub> ], [LiNTf <sub>2</sub> ] <sub>0.2</sub> [C <sub>3</sub> C <sub>1</sub> im][NTf <sub>2</sub> ] (b) [C <sub>6</sub> C <sub>1</sub> im][NTf <sub>2</sub> ], [LiNTf <sub>2</sub> ] <sub>0.2</sub> [C <sub>6</sub> C <sub>1</sub> im][NTf <sub>2</sub> ], and (c) [C <sub>6</sub> (mim) <sub>2</sub> ][NTf <sub>2</sub> ] <sub>2</sub> and [LiNTf <sub>2</sub> ] <sub>0.2</sub> [C <sub>6</sub> (mim) <sub>2</sub> ][NTf <sub>2</sub> ] <sub>2</sub> .	119
28.	Figure 6.3.	Temperature-dependent viscosities of a) [C <sub>3</sub> C <sub>1</sub> im][NTf <sub>2</sub> ] (MIL) b) [C <sub>6</sub> C <sub>1</sub> im][NTf <sub>2</sub> ] (MIL) c) [C <sub>6</sub> (mim) <sub>2</sub> ][NTf <sub>2</sub> ] <sub>2</sub> (DIL) solutions with different mole fractions of Li <sup>+</sup> ions. The data points are fitted by single exponential fit. The black lines are the fitted lines.	120
29.	Figure 6.4.	(a) Representation of average experimental rotational relaxation time for perylene plotted against dynamic viscosity $\eta$ over $kT$ in case of both MIL (solid symbols) and DIL (open symbols) for $\chi[\text{LiNTf}_2] = 0$ (code: navy blue), 0.05 (code: yellow), 0.1 (code: green) and 0.2 (code: orange). The plots in (b), (c), and (d) are rescaled and shifted for better visualization. Plot (b) is for the MIL, [C <sub>3</sub> C <sub>1</sub> im][NTf <sub>2</sub> ], plot (c) is for MIL, [C <sub>6</sub> C <sub>1</sub> im][NTf <sub>2</sub> ] and plot (d) is for DIL, [C <sub>6</sub> (mim) <sub>2</sub> ][NTf <sub>2</sub> ] <sub>2</sub> . The data points are the least square fitted and show the hydrodynamic diffusion.	122
30.	Figure 6.5.	Log-log plots of average rotational time of perylene in (a) [C <sub>3</sub> C <sub>1</sub> im][NTf <sub>2</sub> ] (b) [C <sub>6</sub> C <sub>1</sub> im][NTf <sub>2</sub> ] and (c) [C <sub>6</sub> (mim) <sub>2</sub> ][NTf <sub>2</sub> ] <sub>2</sub> with red and blue boundary condition indicating the stick and slip boundary conditions respectively. The solid black line indicates the fit to data points.	123
31.	Figure 6.6.	The average friction coefficient for perylene in all the systems as a function of Li <sup>+</sup> ion concentration.	125
32.	Figure 6.7.	Log-log plots of average rotational time of MPTS in (a) [C <sub>3</sub> C <sub>1</sub> im][NTf <sub>2</sub> ] (b) [C <sub>6</sub> C <sub>1</sub> im][NTf <sub>2</sub> ] and (c) [C <sub>6</sub> (mim) <sub>2</sub> ][NTf <sub>2</sub> ] <sub>2</sub> with red and blue boundary condition indicating the stick and slip boundary conditions. The solid black line indicates the fit to data points.	126

33. Figure 6.8. The friction coefficient for MPTS in all the systems as a function of  $\text{Li}^+$  ion concentration at 298 K. 128
34. Figure 6.9 Temperature dependent variation of self-diffusion coefficient neat ILs as well as with the addition of  $\text{Li}^+$  ion. The square solid shapes (brown) and square open shapes (brown) represent the value of  $D$  for  $[\text{C}_3\text{C}_1\text{im}][\text{NTf}_2]$  and  $[\text{LiNTf}_2]_{0.1}[\text{C}_3\text{C}_1\text{im}][\text{NTf}_2]$  respectively. The circle solid shapes (pink) and circle open shapes (pink) represent the value of  $D$  for  $[\text{C}_6\text{C}_1\text{im}][\text{NTf}_2]$  and  $[\text{LiNTf}_2]_{0.1}[\text{C}_6\text{C}_1\text{im}][\text{NTf}_2]$  respectively. The pentagon solid shapes (green) and pentagon open shapes (green) represent the value of  $D$  for  $[\text{C}_6(\text{mim})_2][\text{NTf}_2]_2$  and  $[\text{LiNTf}_2]_{0.1}[\text{C}_6(\text{mim})_2][\text{NTf}_2]_2$  respectively. 130
35. Figure 6.10. Self-diffusion coefficient plotted against  $T/\eta$  in neat ILs as well as with the addition of  $\text{Li}^+$  ion. The dotted lines are the fit to the data points. The square solid shapes (blue) and square open shapes (blue) represent the value of  $D$  for  $[\text{C}_3\text{C}_1\text{im}][\text{NTf}_2]$  and  $[\text{LiNTf}_2]_{0.1}[\text{C}_3\text{C}_1\text{im}][\text{NTf}_2]$  respectively. The circle solid shapes (red) and circle open shapes (red) represent the value of  $D$  for  $[\text{C}_6\text{C}_1\text{im}][\text{NTf}_2]$  and  $[\text{LiNTf}_2]_{0.1}[\text{C}_6\text{C}_1\text{im}][\text{NTf}_2]$  respectively. The pentagon solid shapes (green) and pentagon open shapes (green) represent the value of  $D$  for  $[\text{C}_6(\text{mim})_2][\text{NTf}_2]_2$  and  $[\text{LiNTf}_2]_{0.1}[\text{C}_6(\text{mim})_2][\text{NTf}_2]_2$  respectively. 131

## List of Tables

Sl. No.	Figure No.	Table title	Page No.
1.	Table 1.1.	Physical properties of some monocationic and dicationic ILs.	5
2.	Table 2.1.	Solute dimensions, van der Waals volumes, shape factors and boundary condition parameters ( $C_{slip}$ ) for the solutes.	42
3.	Table 3.1.	Experimental viscosity ( $\eta$ , cP) and density ( $\rho$ , g/cm <sup>3</sup> ) of individual ILs and mixtures.	51
4.	Table 3.2.	The excess molar volumes calculated for IL-IL mixtures.	53
5.	Table 3.3.	Thermal expansion coefficient values of ILs and IL mixtures as a function of temperature.	55
6.	Table 3.4.	Thermal relaxation rate constants of spiropyran derivatives in IL-IL mixtures.	58
7.	Table 3.5.	The reorientation time ( $\tau_r$ ) of perylene and MPTS in [C <sub>4</sub> C <sub>1</sub> ][BF <sub>4</sub> ], [C <sub>4</sub> C <sub>1</sub> ][PF <sub>6</sub> ], [C <sub>4</sub> C <sub>1</sub> ][NTF <sub>2</sub> ], Mix I, Mix II and Mix III.	59
8.	Table 3.6.	Diffusion coefficients of the concerned ILs and IL mixtures at 298 K.	66
9.	Table 3.7.	Parameters obtained through FCS for IL mixtures and constituent ILs at 298 K.	67
10.	Table 4.1.	The experimental density ( $\rho$ ) of neat ILs and their binary mixtures.	74
11.	Table 4.2.	The reorientation time ( $\tau_r$ ) of perylene and MPTS in [C <sub>2</sub> C <sub>1</sub> im] [NTF <sub>2</sub> ], [C <sub>4</sub> C <sub>1</sub> im] [NTF <sub>2</sub> ], [C <sub>3</sub> C <sub>1</sub> im] [NTF <sub>2</sub> ], [C <sub>3</sub> C <sub>1</sub> pyr] [NTF <sub>2</sub> ], [C <sub>4</sub> C <sub>1</sub> pyr] [NTF <sub>2</sub> ] and their corresponding binary mixtures.	80
12.	Table 4.3.	Boundary conditions obtained from DKS model.	85
13.	Table 5.1.	The densities of both MILs and DILs.	95
14.	Table 5.2.	Formula Weight (FW), Molar Volumes (V) (cm <sup>3</sup> . mol <sup>-1</sup> ), Van der Waals volume (V <sub>VWD</sub> ) and the ratio (V <sub>VWD</sub> /V) for all the ILs.	96
15.	Table 5.3.	The relevant parameters obtained from FCS for [C <sub>6</sub> (mim) <sub>2</sub> ][NTf <sub>2</sub> ] <sub>2</sub> and [C <sub>3</sub> mim][NTf <sub>2</sub> ] at 298 K.	100
16.	Table 5.4.	Time constants of the fluorescence decay of the donor (ILs) in the presence of the acceptor (R6G) at different concentrations (where $\lambda_{exc} = 375$ nm and $\lambda_{em} = 450$ nm).	102
17.	Table 5.5.	Time constants of the fluorescence decay of the acceptor (R6G) at different concentrations.	104
18.	Table 5.6.	The magnitude of RET parameters.	107
19.	Table 6.1.	Estimated translational diffusion coefficient of MILs with varying mole fractions of Li <sup>+</sup> ions.	129

## Glossary of Acronyms

ILs	Ionic liquids
RTILs	Room temperature ionic liquids
MILs	Monocationic ionic liquids
DILs	Dicationic ionic liquids
GDIL	Geminal dicationic ionic liquids
NTf <sub>2</sub>	bis(trifluoromethanesulfonyl)imide
BF <sub>4</sub>	tetrafluoroborate
PF <sub>6</sub>	hexafluorophosphate
NO <sub>3</sub>	nitrate
CO <sub>2</sub>	carbon dioxide
SO <sub>2</sub>	sulfur dioxide
CF <sub>3</sub> CO <sub>2</sub>	trifluoroacetate
CH <sub>3</sub> CO <sub>2</sub>	acetate
CH <sub>3</sub> SO <sub>3</sub>	methanesulfonate
CF <sub>3</sub> SO <sub>3</sub>	triflate
Na <sub>2</sub> SO <sub>4</sub>	sodium sulfate
DMSO	dimethyl sulfoxide
DMSO-d <sub>6</sub>	deuterated dimethyl sulfoxide
FAP	tris(pentafluoroethyl) trifluorophosphate
EtAN	ethanolammonium nitrate
$T_d$	Thermal decomposition
$T_g$	Glass transition temperature
$T_m$	Melting temperature

$n_D$	Refractive index
$\rho$	Density
$\eta$	Viscosity
$\sigma$	Specific conductivity
V	Volts
$V^E$	Excess molar volume
$V_M$	Molar volume
FW	Formula weight
$V_{VD}$	Van der Waals volume
$\chi$	Mole fraction
$C_{rot}$	Rotational coupling constant
C <sub>2</sub> mim[X]	1-ethyl-3-methylimidazolium halide
SAXS	Small angle X-ray scattering
FT-IR	Fourier transform infrared spectroscopy
DFT	Density functional theory
PALS	Positron annihilation lifetime spectroscopy
NMR	Nuclear magnetic resonance
OHD-RIKES	Optical heterodyne-detected Raman induced Kerr effect spectroscopy
MD	Molecular dynamics
TSILs	Task specific ionic liquids
REE	Red edge effect
ANF	2-amino-7-nitro fluorene
FRET	Förster resonance energy transfer
PFM-NMR	Pulsed field gradient nuclear magnetic resonance

NOE	Nuclear Overhauser Effect
FCS	Fluorescence correlation spectroscopy
[C <sub>4</sub> C <sub>1</sub> ][BF <sub>4</sub> ]	1-butyl-3-methylimidazolium tetrafluoroborate
[C <sub>4</sub> C <sub>1</sub> ][PF <sub>6</sub> ]	1-butyl-3-methylimidazolium hexafluorophosphate
[C <sub>8</sub> C <sub>1</sub> ][NTf <sub>2</sub> ]	1-octyl-3-methylimidazolium bis(trifluoromethylsulfonyl)imide
[C <sub>6</sub> C <sub>1</sub> ][NTf <sub>2</sub> ]	1-hexyl-3-methylimidazolium bis(trifluoromethylsulfonyl)imide
[C <sub>4</sub> C <sub>1</sub> ][NTf <sub>2</sub> ]	1-butyl-3-methylimidazolium bis(trifluoromethylsulfonyl)imide
[C <sub>2</sub> C <sub>1</sub> im][NTf <sub>2</sub> ]	1-ethyl-3-methylimidazolium bis(trifluoromethylsulfonyl)imide
[C <sub>3</sub> C <sub>1</sub> im][NTf <sub>2</sub> ]	1-propyl-3-methylimidazolium bis(trifluoromethylsulfonyl)imide
[C <sub>3</sub> C <sub>1</sub> pyr][NTf <sub>2</sub> ]	1-methyl-1-propylpyrrolidinium bis(trifluoromethylsulfonyl)imide
[C <sub>4</sub> C <sub>1</sub> pyr][NTf <sub>2</sub> ]	1-methyl-1-butylpyrrolidinium bis(trifluoromethylsulfonyl)imide
[C <sub>6</sub> (Mim) <sub>2</sub> ][Br] <sub>2</sub>	1,6-bis(3-methylimidazolium-1-yl)hexane bromide
[C <sub>6</sub> (mim) <sub>2</sub> ][NTf <sub>2</sub> ] <sub>2</sub>	1,6-bis-(3-methylimidazolium-1-yl)hexane bis-(trifluoromethylsulfonyl)amide
[C <sub>8</sub> (Mim) <sub>2</sub> ][Br] <sub>2</sub>	1,8-bis(3-methylimidazolium-1-yl)octane bromide
[C <sub>8</sub> (mim) <sub>2</sub> ][NTf <sub>2</sub> ] <sub>2</sub>	1,8-bis-(3-methylimidazolium-1-yl)octane bis (trifluoromethylsulfonyl)-amide
6-NO <sub>2</sub> - BIPS	1',3'-dihydro-1',3',3'-trimethyl-6-nitrospiro(2H-1-benzopyran-2,2'- 2H-indole
SP	Spiropyran
MC	Merocyanine
R6G	Rhodamine 6G
MPTS	sodium 8-methoxypyrene-1,3,6- sulfonate
TRFA	Time-resolved fluorescence anisotropy
PMT	Photomultiplier tube

TCSPC	Time-correlated single photon counting
CFD	Constant fraction discriminator
TAC	Time to amplitude converter
MCA	Multichannel analyzer
ADC	Analog-to-digital converter
IRF	Instrument response function
CFM	Confocal fluorescence microscope
CCD	Charged coupled device
SPAD	Single or multiple photon avalanche photodiodes
SNR	Signal to noise ratio
NLLS	Nonlinear least squares
VFT	Vogel-Fulcher-Tammann relationship
R-K	Redlich-Kister equation
SED	Stokes-Einstein-Debye theory
GW	Gierer-Wirtz theory
DKS	Dote-Kivelson-Schwartz theory
D	Diffusion coefficient
$C_{slip}$	Slip boundary limit
$C_{stick}$	Stick boundary limit
$V_h$	Hydrodynamic volume

# **CHAPTER 1**

---

## **Introduction**

---

# ***Chapter 1***

---

## **Introduction**

---

This chapter discusses on the room temperature ionic liquids, their thermophysical properties and their potential applications in the fields of biology and material sciences. This chapter also highlights the importance of binary mixture of ionic liquids, their thermophysical properties and their microscopic behaviour in terms of ideality. Further, discussion on the photophysical processes in ILs such as excitation wavelength dependent emission behaviour, the rotational dynamics of binary mixture of ILs along with concerned neat ILs using different probe molecules, resonance energy transfer process, translational diffusion of ions measured through NMR and fluorescence correlation spectroscopy are provided by illustrating several literature reports. The objective of the thesis along with the recent challenges involved in research areas of ionic liquids are presented in the end of this chapter.

---

### **1.1. Ionic Liquids**

Ionic Liquids (ILs) are special category of molten salts which typically constitutes of bulky and asymmetrical organic cations and organic or inorganic anions with their melting points below 100 °C.<sup>1</sup> In ILs, organic cations are imidazolium, ammonium, pyridinium, pyrrolidinium etc. and the inorganic anions are usually bromide, chloride, sulfate, hexafluorophosphate, tetrafluoroborate etc. In ILs, the charge density of the ions become low due to their diffused charges which results in inefficient lattice packing eventually leading to disruption in their crystalline packing structure. The inefficiency in the packing along with the low charge densities over the constituent ions results in the formation of liquid materials at the ambient temperature (20-30 °C) and pressure (1 bar).<sup>2-4</sup> ILs were originally believed to be within the

conventional scheme of molecular liquids. However, more recently it has been determined that the diverse ordering structures present in the ILs in comparison to the conventional molecular liquids and their structure-ordering are driven by the short-range interactions in combination with long range interactions associated amongst the constituent ions.<sup>5-9</sup> Interestingly, ILs possess several interesting properties such as extremely low vapor pressures, high viscosity, low toxicity, high ionic conductivity, extremely high thermal stability and capability to dissolve a wide range of inorganic, organic compounds making these unique materials suitable for several applications such as in the fields of material and biological sciences.<sup>4, 10-24</sup>

Although the history of ILs mostly credits the German chemist Paul Walden as he was the first to synthesize ionic salt, ethyl-ammonium nitrate (EAN) with a low melting point 12<sup>0</sup>C and a low viscosity in 1914<sup>25</sup> but in 1911, our own Indian Chemist Archarya Prafulla Chandra Ray<sup>26</sup>, synthesized a similar kind of ionic liquid to ethyl ammonium nitrate but was not paid due attention for some unknown reasons. In fact, 40 years later, Hurley and Wier<sup>27</sup> documented the potential benefits of ILs more explicitly by synthesizing organic chloroaluminates from aluminum compounds and alkylpyridinium chloride salts. The product obtained from the synthesis was organic chloroaluminates, considered as first generation ILs.<sup>1, 15</sup> In 1980s, scientific interest on ILs began to spread with the broadening of range of investigations starting from solvents in organic synthesis to materials. In this period, ILs were synthesized with different organic cations namely imidazolium, pyridinium, pyrrolidinium, ammonium, phosphonium etc. and anions mostly consisting of halides.<sup>28</sup> It was observed that the pyridinium as well as imidazolium based chloroaluminates possess a disadvantage of being reactive with water. Interestingly, in 1990, Mike Zaworotko<sup>29</sup> developed methods for synthesizing water-stable anions. Thus, the second generation of ILs were prepared with anions such as nitrate (NO<sub>3</sub>), tetrafluoroborate (BF<sub>4</sub>), hexafluorophosphate (PF<sub>6</sub>) etc. illustrated in Figure 1.1. Next, the third generation ILs<sup>28, 30, 31</sup> were synthesized consisting of perfluorinated

anions such as bis(trifluoromethylsulfonyl)imide (NTf<sub>2</sub>), tris(pentafluoroethyl) trifluorophosphate (FAP) etc (Chart 1). These ILs were hydrophobic in nature possessing low viscosity, low melting points and low conductivity.<sup>32, 33</sup> Some of the disadvantages of these ILs were production cost, high affinity of binding with metal ions resulting in toxicity.<sup>28, 30, 31</sup> In recent times, cost effective task specific ILs were developed for the use in energy materials.<sup>34</sup> Apart from material applications, amino acid based ILs were designed for the use in ionic liquid pharmaceuticals.<sup>35, 36</sup> Other families of ILs like geminal dicationic ILs were also designed as these are thought to have applications in the field of battery related applications.<sup>37-50</sup>

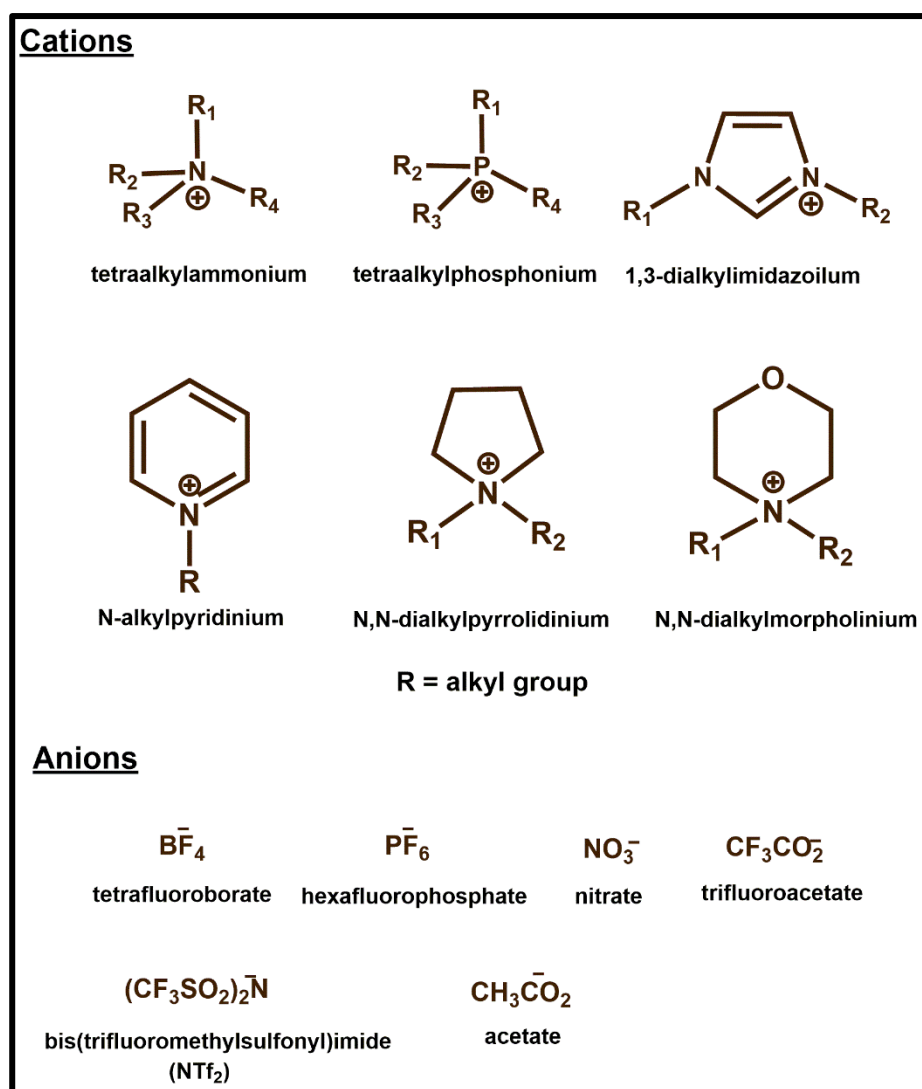


**Figure 1.1.** Molecular structure of some cations and anions of RTILs

### 1.1.1. Characteristic features of ILs

Some of the general properties of ILs as described earlier makes ILs a special solvent system from the usual conventional organic solvents. ILs are known to possess negligible vapour pressure, high chemical thermal stability, non-flammability, wide liquidous range, wide electrical conductivity and the ability to dissolve a wide variety of organic and inorganic substances.<sup>3, 12-15, 18-21, 24, 51-54</sup> As these properties can be tuned by the combination of different cations and anions chosen for a particular application, the ILs are also termed as “designer solvents”.<sup>55</sup> Molecular diagrams of the common imidazolium based ILs are provided in Figure 1.1. Physical properties of the ILs are collected in Table 1.1.

**Table 1.1.** Physical properties of some monocationic<sup>48</sup> and dicationic ILs<sup>48</sup>

Cations	T <sub>m</sub> (K)		T <sub>g</sub> (K)		T <sub>d</sub> (K)		ρ (gcm <sup>-1</sup> )	
	[NTf <sub>2</sub> ] <sup>-</sup>	[BF <sub>4</sub> ] <sup>-</sup>	[NTf <sub>2</sub> ] <sup>-</sup>	[BF <sub>4</sub> ] <sup>-</sup>	[NTf <sub>2</sub> ] <sup>-</sup>	[BF <sub>4</sub> ] <sup>-</sup>	[NTf <sub>2</sub> ] <sup>-</sup>	[BF <sub>4</sub> ] <sup>-</sup>
[C <sub>2</sub> MIm] <sup>+</sup>	269.9	287.8	183.7	182.4	664.3	555.9	1.520	1.279
[C <sub>4</sub> MIm] <sup>+</sup>	269.2	-	188.1	186.3	676.2	565.9	1.438	1.201
[C <sub>6</sub> MIm] <sup>+</sup>	265.9	-	190.4	190.0	635.4	577.2	1.373	1.155
[C <sub>4</sub> (MIm) <sub>2</sub> ] <sup>2+</sup>	332.5	372.3	-	-	706.4	589.2	-	-
[C <sub>6</sub> (MIm) <sub>2</sub> ] <sup>2+</sup>	-	403.9	209.9	-	700.1	639.6	1.546	-

T<sub>m</sub> : Melting Point ; T<sub>g</sub> : glass transition temp. ; T<sub>d</sub> : decomposition temp. ; ρ : density

- **Melting points:** The phenomenon of melting occurs when the crystal lattice gets disrupted and the ions consisting the lattice gets disordered. In case of ILs, sharp melting points are not observed due to the supercooling nature.<sup>19, 56, 57</sup>

- **Glass transition temperature:** The strength of cohesive forces present within a salt is denoted by the glass transition temperature ( $T_g$ ). With the variation in anion-cation combination in ILs, the cohesive interactions are found to vary as the cohesive interactions are found to increase with the attractive Coulomb and van der Waals interactions.<sup>33</sup>
- **Density:** Density of ILs depend on the packing efficiency of ionic constituents in the ILs. ILs are found to be denser than water and the range of density lies within 1.0 to 1.7 g cm<sup>-1</sup>. The density of alkylammonium, alkylimidazolium and alkylpyrrolidinium ILs decreases with increasing alkyl chain length of cation.<sup>58, 59</sup> Further, the nature of cation and anion affect the densities of ILs. The densities and ionic structures of ILs are intricately related with each other. The molar volume has been observed to increase proportionally with an increase in the density of alkyl chain length of cations in ILs.<sup>60</sup> With the introduction of fluoroalkyl chain, the density of ILs increases. For eg., in case of 1-ethyl-3-methylimidazolium cation, density follows the order:  $\text{CH}_3\text{SO}_3^- < \text{BF}_4^-$  and  $\text{CF}_3\text{COO}^- < \text{CF}_3\text{SO}_3^- < (\text{CF}_3\text{SO}_2)_2\text{N}^- < (\text{C}_2\text{F}_5\text{SO}_2)_2\text{N}^-$ .
- **Viscosity:** ILs have considerable high viscosity (typically 10 to 100 times) in comparison to molecular solvents.<sup>61</sup> Viscosity of a medium arises due to the various interactions such as Coulombic interactions within the ions, van der Waals interaction, hydrogen bonding etc. within the fluid system.<sup>61</sup> As the other physical properties are dependent on the nature of anions and cations, viscosity is also affected by the choice of cations and anions. Experimentally, it has been observed that as the chain length of cation increases, the viscosity also increases due to a strong van der Waals interactions.<sup>61</sup> The ability of the anion to participate in the hydrogen bonding affects the viscosity of ILs.<sup>62, 63</sup> ILs having ions such as  $\text{PF}_6^-$  and  $\text{BF}_4^-$ , are found to be more viscous in comparison to  $\text{Tf}_2\text{N}^-$  ion due to the electronic effect arising due to the presence of fluoride atom as well as due to the dispersion of the negative charge on the two sulfoxide groups of  $\text{Tf}_2\text{N}$  anion.<sup>64</sup> It has been observed

that viscosity of ILs are quite affected by the percentage of water present in them.<sup>64</sup> It is to be noted here that the viscosities of ILs are found to obey Vogel-Tammann-Fulcher<sup>65-67</sup> (VFT) equation (1.1) given below:

$$\ln(\eta) = \ln(\eta_0) + \frac{DT_c}{T-T_c} \quad (1.1)$$

In the eq. (1.1),  $\eta_0$  represents viscosity at infinite temperature, D denotes the fragility parameter and  $T_c$  is the viscosity diverging temperature.

- **Conductivity ( $\sigma$ )** : ILs have reasonably good ionic conductivities,<sup>68, 69</sup>  $\sim 10 \text{ mS cm}^{-1}$ , in comparison to organic solvents. However, due to high viscosity, ILs tend to have less conductivity at room temperature as the conductivity of electrolytic solution depends both on mobility and the number of charge carriers.<sup>70</sup> The reduction in the ion mobility can also be caused by the larger size of the constituent ions as well as the tendency of aggregation of these ions. One of the ways to overcome the issue of low conductivity is by mixing co-solvents with the ILs.<sup>69, 71</sup>
- **Electrochemical potential window**: Electrochemical potential is one of the significant criteria for battery applications. The electrochemical potential window (without significant background current) is one of the key factors for any medium to be used in electrochemical applications. Generally, ILs exhibit a large electrochemical window in the range of 4.5-5 V.<sup>25, 72</sup> This potential window range is found to be more than the conventional electrolytic solutions. We would also like to note here that dication-based ILs exhibit even longer electrochemical window.<sup>73</sup>
- **Other properties**: Many other physical properties of ILs such as surface tension, refractive index, molar volumes etc. have been observed to vary with the variation of cation and anions in ILs.<sup>68</sup> As the packing efficiency increases, the surface tension decreases whereas as the ionic or hydrogen bonding interaction increases, an increase in the surface tension is

observed for ILs. By estimating the refractive index ( $n_D$ ) values of ILs, these can be considered as moderately polar media like acetonitrile. However, with an increase in the alkyl chain length of the cationic moiety of the IL, the refractive index is found to decrease.<sup>74</sup> On the other hand, with an addition of hydroxyl group in IL, an increase in the refractive index has been observed.<sup>75</sup> Another important parameter of ILs, is its solubility. The solubility of an IL is mainly governed by the anionic species.<sup>56, 57, 62</sup> In case of PF<sub>6</sub>, NTf<sub>2</sub> anions, the nature of ILs are hydrophobic while for BF<sub>4</sub>, halide anions the nature of ILs are hydrophilic.

### 1.1.2. Binary mixtures of ILs

Binary mixture of ILs are not the simple mixtures of two or more ions of ILs which would have been analogous to the mixtures of organic solvents rather as ILs when mixed together, the ionic associations in the individual ILs are lost and it is difficult to predict which cation/anion is from which ionic liquids.<sup>76</sup> To address this issue, majority of literatures are primarily focused in understanding the ideality and non-ideality of IL mixtures.<sup>77-90</sup> This is usually observed mainly by focusing on the deviation in some well-known physical properties of the IL mixtures.<sup>81</sup> In some of the IL-IL mixtures, the physical properties like density and viscosity were found to follow the mixing laws linearly while properties those were dependent on the specific chemical associations like phase transition were difficult to estimate and often led to non-ideal behaviour portraying the IL-IL mixture model as simple mixtures.<sup>77, 81, 90</sup> It is to be noted here that when two ILs with a different monovalent ions are mixed (for e.g., [A][B] and [C][D]), a scenario with a combination of four different salts [A][B], [B][C], [A][C] and [A][D] are formed. Since it often becomes difficult to predict the properties of the resulting complex solutions, it is found that the concept of double salt might be helpful in elucidating the properties of IL mixtures.<sup>76</sup>

In this context, it is believed that intermolecular interactions such as hydrogen bonding is an important factor for governing the physical properties in IL-IL mixtures. However, hydrogen bonds prevailing in the ions for the IL mixtures have been observed to have negligible effect on the viscosity.<sup>91</sup> Different mixing laws proposed in the literatures such as Katti and Chaudhri law (based on molar volumes),<sup>92</sup> the Grunberg and Nissan law (logarithmic law involving only the viscosity),<sup>93</sup> or the Bingham law (developed by analogy to electric resistors in parallel circuits),<sup>94</sup> are found to be in good agreement between the experimental viscosity data of the IL-IL mixtures. In order to understand the aspect of ideality and non-ideality for the mixtures of ILs, deviation of viscosity in case of IL mixtures from the linear mixing behaviour is calculated.<sup>81, 90, 95</sup>

It may be noted here that the experimental densities of ILs are also found to be in good agreement with the mixing laws available in the literatures.<sup>81, 90</sup> When IL mixtures are composed of three or four ions, a very small deviation in density ( $\sim 0.01 \text{ g cm}^{-3}$ ) is observed which indicates an ideal mixing behaviour. To discuss on the volumetric effect of ions constituting the mixture, calculation of the excess molar volume ( $V^E$ ) is necessary. By definition,  $V^E$  is the difference in the measured molar volume of a mixture from the expected molar volume.<sup>95</sup> It is usually expressed by the equation (1.2):

$$V^E = \frac{\chi \times M_{(A)} + (1-\chi) \times M_{(B)}}{\rho} - (\chi \times V_{M(A)} + (1 - \chi) \times V_{M(B)}) \quad (1.2)$$

where  $\chi$  denotes the mole fraction, M denotes the molecular weight,  $\rho$  corresponds to the density of the mixture,  $V_M$  denotes the molar volume (i.e., volume occupied by one mole of a substance), and A and B denote the two different compounds constituting the binary mixture of ILs. A positive deviation of  $V^E$  has been found to be observed as the volume of binary mixture of IL becomes larger than that expected from mixture of ILs comprising of two -ion ILs. On the contrary, a negative deviation of  $V^E$  has can be found when the volume of the

mixture become smaller than that can be expected when the ILs are mixed. In order to highlight the differences among the ILs and their binary mixtures, an arbitrary line boundary (deviation of  $0.20 \text{ cm}^3 \text{ mol}^{-1}$ ) is usually fixed.<sup>81</sup> Many of the physical properties of these binary mixtures of ILs are still at its infancy. Therefore, under the mechanism of preferential solvation is expected to bring interesting outcomes with respect to properties such as solubility, conductivity, ideal, non-ideal behavior etc. for some specific solutes, solvents, gases and even drugs.

### **1.1.3. Information on structural and dynamic heterogeneity in ILs and their binary mixtures**

Initially, ILs were believed to be homogeneous in nature.<sup>96</sup> But several recent theoretical as well as experimental observations have suggested that ILs are not homogenous in nature rather they form cluster assemblies consisting of ion pairs that shows a mesoscopic pattern (micelle type, H-bonded network structures).<sup>97-101</sup> The inhomogeneity in ILs is referred as micro-heterogenous nature of these media.

Crystal structures of ILs offer clues for the local intermolecular interactions prevailing in the liquid structures.<sup>6-8, 102-106</sup> It has been observed that in ethanolanmonium nitrate (EtAN), two lamellar like layers composed of EtA cations takes vertical configuration while half of the  $[\text{NO}_3]$  anions are situated between adjacent ammonium moieties creating a polar region, while the other  $[\text{NO}_3]$  anions are found to be intercalated between ethyl chains.<sup>107</sup> In contrast to the alkylammonium ILs, crystal structure of imidazolium ILs are found to be different depending on the structure of anion and the chain length of cations.<sup>102, 107</sup> Structural features revealed by the NMR studies on the imidazolium-based ILs,  $\text{C}_2\text{mim}[\text{X}]$  where X denotes the halides, have shown the formation of contact-ion pairs.<sup>108, 109</sup> Indirect evidence of the formation of contact-ion pairs has also been revealed by studying the transport properties of

dialkylimidazolium ILs.<sup>110</sup> Even though the concept of ion pairs is quite helpful to some extent to visualize the liquid structures in electrolytic solutions, it has not been feasible to define the bulk IL structures based on these concepts. It is also believed that in the overall liquid structure, transient ion pairs might also exist in IL matrixes possessing shorter lifetime less than picosecond time scale.<sup>17,111</sup> This hypothesis though help in addressing the overall bulk structure of liquid but are found to be more complicated in comparison to the concept of a continuum of ion pairs or ion couples present in solutions.<sup>9</sup>

The microstructures of EAN were investigated by Atkin,<sup>5</sup> Warr<sup>5</sup> and Umebayashi *et al.*<sup>6</sup> independently using complementary wide-angle X-ray scattering (WAXS) and small-angle neutron scattering (SANS) techniques. All these work have demonstrated the existence of heterogeneity at the length-scale for EAN constituting apolar and polar domains in the bulk liquid matrix. This signifies a disordered, locally smectic bi-continuous liquid structure form of ILs. The nanostructural heterogeneity are thought to be formed due to the solvophobic interactions prevailing among the alkyl units.<sup>9</sup> Several fluorescence studies on ILs have demonstrated the micro-heterogenous nature of ILs.<sup>112-129</sup> Among these, the investigations carried out by Samanta and coworkers<sup>121, 122</sup> are noteworthy in understanding the micro-heterogeneous behavior of several ILs through excitation wavelength dependent fluorescence experiments. Both the experimental<sup>114, 115, 117, 120-124</sup> and theoretical studies<sup>116, 118, 119, 125-129</sup> on ILs have shown that ILs are structurally and dynamically heterogeneous in nature. Excitation wavelength dependent solvation dynamics on ILs carried out by Bhattacharyya<sup>114, 115</sup> and Maroncelli<sup>119, 120</sup> independently have shown that ILs are not just structurally heterogenous but also dynamically heterogeneous in nature. Later on, investigations with IR spectroscopy have revealed the dynamic heterogeneity of ammonium-based ILs.<sup>130</sup> MD simulation studies carried out by Hu and Margulis<sup>118</sup> have also shown the micro heterogenous behaviour of ILs. Moreover, the evidence of heterogeneity in ILs have also been shown with optical heterodyne-detected

Raman induced Kerr effect (OHD-RIKES).<sup>128</sup> As ILs are complex media, further experimental and theoretical studies are necessary to understand the structure-property relationship in these media.

One of the significant observation in a wide variety of IL mixtures is that the structure of these mixtures is highly dominated by coulombic interactions.<sup>77, 78, 84, 85, 89, 117, 131</sup> As the coulombic interactions are present within the cations and anions in IL, the distribution of these ions is random in nature. It is noteworthy to mention here that although coulombic interactions are isotropic in nature but the charge densities will be different of each ion in a polyatomic system and this difference in the charge densities will result in electrostatic interactions purely governed by the shape, size and individual charge density of ions rather than the averaged charge of the whole system.<sup>132</sup> We would also note here that the weaker interactions in IL, like  $\pi - \pi^*$  interactions and hydrogen bonding have been accounted for the formation of ideal and non-ideal IL mixtures.<sup>80, 111, 131</sup> The IL mixtures consisting of anions with different basicities have shown positive excess molar volumes suggesting a greater free volume present in the mixture than that anticipated from the linear interpolation of ILs.<sup>132</sup> Techniques such as small angle X-ray scattering (SAXS), positron annihilation lifetime spectroscopy (PALS) and <sup>129</sup>Xe-NMR techniques have helped in exploring the relationship between the free volume and the thermodynamics of IL mixtures.<sup>132</sup> As this domain of IL mixture has not been explored to its full potential, comprehensive studies focusing the structural organization of IL are very much needed.

#### **1.1.4. Application of ILs and their binary mixtures**

ILs, having several unique properties, have shown great potential in replacing organic solvents in chemical reactions and catalysis.<sup>133-136</sup> As medium polarity of ILs make them a suitable solvent of dissolving wide range of compounds, they are used in several synthesis and catalytic

reactions. They are also used in the crystallization of protein.<sup>137, 138</sup> A major wide-scale applications of ILs in catalysis is that they can be used to immobilize the homogeneous catalysts by forming biphasic systems, where one of the phases in the biphasic system is made up of a catalyst dissolved in IL while the other phase is made with reagents.<sup>138, 139</sup> Interestingly, the electrochemical properties of ILs such as high conductivity, low reactivity, and wide electrochemical window make these material suitable for battery applications.<sup>54, 140-142</sup>

The third generation ILs consisting of task specific ILs (TSIL) have been used in industrial applications such as lubricants,<sup>143, 144</sup> rocket propellants,<sup>144</sup> synthesis of nanomaterials,<sup>145</sup> scavenging of SO<sub>2</sub>, CO<sub>2</sub> etc.<sup>146-148</sup> Another class of ILs, dicationic ILs (DILs) are known to exhibit superior thermophysical properties than the traditional MILs in terms of higher shear viscosity, higher thermal stability, larger liquid density and higher surface tensions.<sup>48</sup> Due to the fact that a large number of cation–anion combinations are possible in DILs, these are expected to show greater structural variability in comparison to MILs making them more tunable and versatile.<sup>39, 48</sup> As DILs have high thermal stability and large electrochemical window than MILs, potential applications of DILs are in the high temperature battery and electrolytic applications.<sup>37, 73, 149-153</sup>

The approach of forming the IL mixtures can effectively reduce the viscosities of the IL mixtures which is expected to show improved transport properties in iodide based binary mixture of ILs to be used in battery applications.<sup>154-159</sup> Lei and coworkers<sup>160</sup> have demonstrated that mixtures of short and long chain imidazolium cations with  $[BF_4]^-$  and  $[NTf_2]^-$  anions show better CO<sub>2</sub> absorption capacity in comparison to their parent ILs. Even though effective extraction of metal ions can be carried out by the neat ILs, the high viscosities and their manufacturing cost can be problematic. To overcome this, the task-specific ILs in combinations with ‘standard’ hydrophobic IL,  $[C_4C_1im][PF_6]$ , decreases the viscosity and thus can effectively be used for the extraction of metals.<sup>161</sup> In the field of biomass processing 100% catalytic

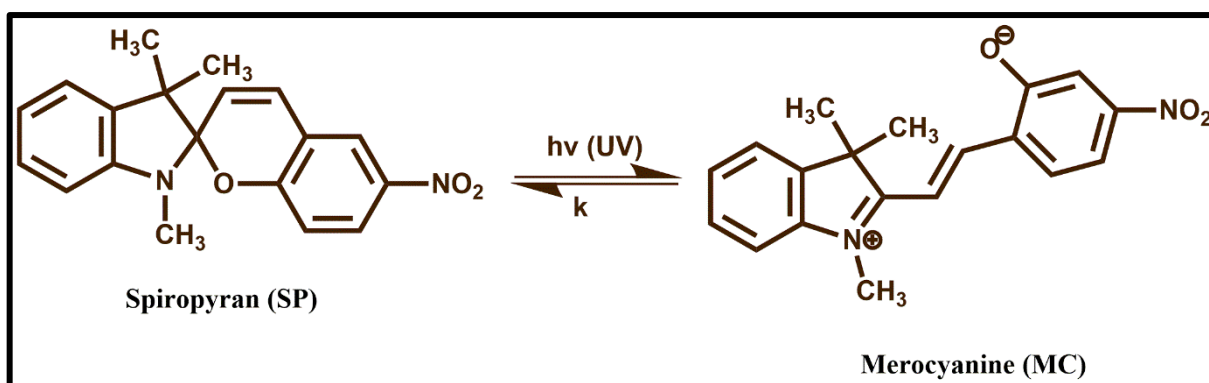
conversion cellulose has been investigated with mixture of ILs. Zhu et al.<sup>162</sup> have shown an effective method of stabilizing Pd (0) nanoparticles using a mixture of IL, [C<sub>4</sub>C<sub>1</sub>im][MeSO<sub>4</sub>]<sub>x</sub>[PF<sub>6</sub>]<sub>(1-x)</sub>.

Focusing on the usage of ILs as electrolytes in lithium-ion batteries, studies have been carried out by emphasizing the coordination effect of Li ions with the ILs.<sup>163-165</sup> In this regard, Varela and co-workers<sup>166</sup> have demonstrated the structural changes of LiNO<sub>3</sub> in alkylammonium nitrate (EAN) IL through SAXS (small-angle X-ray scattering) experiments and atomistic simulations. They have observed that Li<sup>+</sup> ions coordinate with [NO<sub>3</sub>]<sup>-</sup> in a monodentate or bidentate fashion leading to solid-like short-range pseudo lattice ordering in the structure.<sup>166</sup> In this context, it is noteworthy to mention that solvated Li-ions are found to have distinct abilities to coordinate with the IL media which can be successfully connected to the idea of “structure-making” and “structure-breaking”.<sup>167-169</sup> In a separate study carried out by Atkin and co-workers<sup>167</sup> have noted that LiNO<sub>3</sub> has “structure-breaking” effect in EAN due to the incorporation of LiNO<sub>3</sub> into the polar domain of EAN, causing disruption in the neat alignment of ethyl chains in the apolar domain. Conversely, “structure-making” has been found in the case of ethanolanmonium nitrate (EtAN) when LiNO<sub>3</sub> is dissolved in the medium. This phenomenon has been attributed to the long-range rearrangement of EtAN in the presence of Li ions.<sup>167</sup> Fayer and coworkers<sup>170</sup> have also investigated the effect of lithium on ILs through optically heterodyne-detected optical Kerr effect (OHD-OKE) spectroscopy and have observed that medium viscosity increases upon addition of lithium salt to the media which in turn influences the ion mobility and rotational dynamics of ions in IL–Li solvent system. Overall, all the above studies that are carried out on MILs have demonstrated that the Li<sup>+</sup> ion can cause significant changes in the structural organization of the medium.

### 1.1.5. Photophysical processes in ILs

An in-dept understanding of structure and dynamics of ILs at the molecular level is necessary for their effective utilization for various applications. Several theoretical<sup>116, 118, 125-127</sup> and experimental<sup>114, 117, 120, 122, 128</sup> investigations around the globe have been carried out to understand the structure-property relationship in ILs. Several photophysical studies have suggested that unlike conventional organic solvents, ILs are micro-heterogenous in nature.<sup>118, 127, 171-179</sup> This thesis discusses some of the photophysical studies in ILs and their binary mixtures in the subsequent sections given below.

- **Photochromism and kinetics:** Photochromism is the process that involves color changes in a system through electromagnetic irradiation.<sup>180, 181</sup> Although several compounds are known to show photochromic behavior,<sup>181-189</sup> the family of spiropyrans is considered as one of the most frequently used compounds in research field. Spiropyrans such as 1',3',3'-trimethyl-6-nitrospiro(2H-1-benzopyran-2,2'-2H-indole) (referred to as 6-NO<sub>2</sub>- BIPS) are known to exist in two isomeric forms, spiropyran form, SP, and merocyanine form, MC. These forms exist in thermal equilibrium with each other, as shown in Scheme 1. 1.



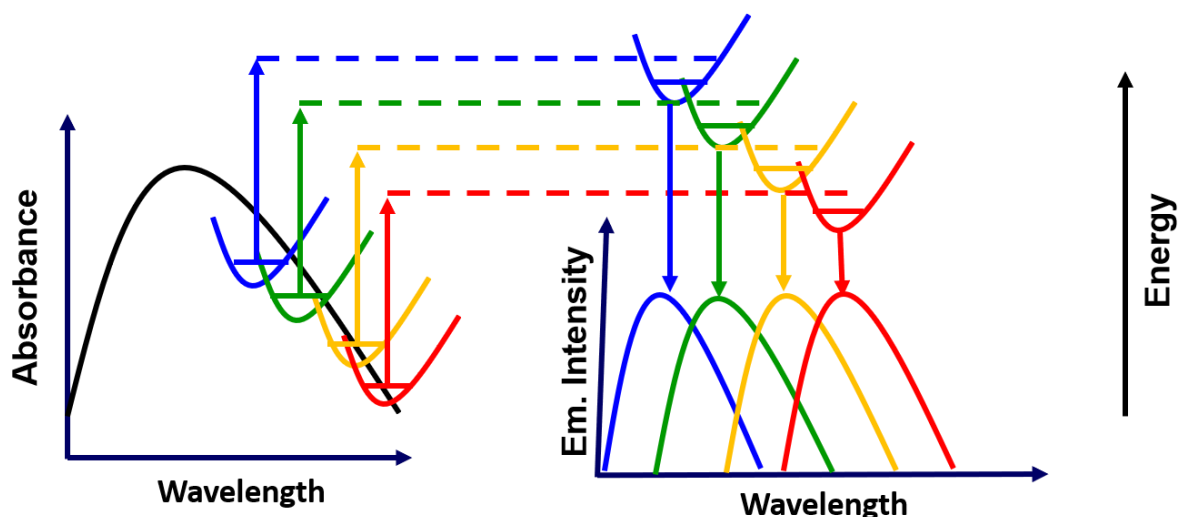
**Scheme 1.1.** Schematic representation of interconversion of spiropyran and merocyanine with UV light irradiation.

6-NO<sub>2</sub>- BIPS, referred to as the normal form, N is considered as thermodynamically more stable isomer with a closed-ring structure.<sup>188</sup> The absorption band lies near UV region,

around 350 nm.<sup>188</sup> The MC form also absorbs in the UV, but unlike N, has a characteristic strong absorption band between 500 and 600 nm.<sup>188</sup> In the absence of UV radiation, the isomer that is most abundant is the N isomer although the presence of MC cannot be neglected as it is in thermal chemical equilibrium with N. Upon UV irradiation, the absorption band of N gets displaced due to the thermal equilibrium between N and MC which results in the increase in the concentration of MC, thereby increasing the intensity of the color. Due to this reason MC is generally considered as the photo isomer. After irradiation formation of N takes place from MC via thermal process which can be measured easily by monitoring the absorbance of MC with time. By this method, kinetics of decolorization can be determined. These kinetic parameters include relaxation time, activation energy, etc. can be correlated with the medium polarity and thus can help in understanding the thermophysical relationships of a given medium.

- ***Excitation wavelength dependence fluorescence study:*** The origin of fluorescence emission is from the lowest vibrational energy level of the lowest excited state having the same multiplicity.<sup>190</sup> According to Kasha's rule, the emission spectrum of a fluorescent molecule is expected to be independent of excitation wavelength.<sup>191-197</sup> However, at times, under certain conditions the emission spectrum of a fluorophore molecule has been observed to be shifted towards longer wavelength as the molecule is excited towards the red end of the absorption spectrum. This phenomenon of excitation dependent emission is called "red edge effect" (REE).<sup>194, 195</sup> To observe REE effect, an ensemble of different energetically associated species must be distributed in the ground state which leads to the inhomogeneous broadening of the absorption spectrum and the excited state relaxation of fluorescent probe showing the REE effect must be slower or comparable to the excited state lifetime of the molecule. Since a molecule in the heterogeneous medium experiences different microenvironment (the cybotactic environment near the vicinity of probe molecule) one can expect a variation of interaction

energies between the solute and the solvent leading to a broadening of the absorption spectrum. REEs have been observed for some organic fluorescent dipolar molecules in ILs.<sup>171</sup> The presence of REE effect in a solvent system gives qualitative idea about the micro heterogeneous nature of the medium. A pictorial representation of REE effect has been shown in Scheme 1.2



**Scheme 1.2.** Schematic representation of excitation wavelength dependent fluorescence emission phenomenon.

- ***Rotational relaxation dynamics through time-resolved fluorescence anisotropy measurements:*** Investigation on the rotational dynamics of a fluorescent probe in a given medium has been experimentally carried out using the time-resolved fluorescence anisotropy measurements. Anisotropy is the extent of emission depolarization of a fluorescent probe that has been generated by the absorption of polarized light.<sup>198</sup> These fluorophores are preferentially excited by the polarized light which creates an anisotropy in the excited electronic state. The average angular displacement of a fluorophore that occurs with an absorption and subsequent emission is measured by the anisotropy. The observed angular displacement depends on the extent and the rate of the rotational diffusion of the excited state fluorophore. Further, the rotational diffusion is found to be dependent on the shape, viscosity or rigidity of the local environment (microenvironment), etc. Moreover, the rotational diffusion of a molecule is very

much related to the solute-solvent interactions (H-bonding, electrostatic interactions etc.). Therefore, studies which focusses on the rotational motion of a solute in a given media is expected to provide valuable information on the local environment of that media which otherwise becomes difficult to obtain.<sup>169, 171, 178, 179, 199</sup> This in turn is expected to be helpful in picturizing the structural organization of the IL media. Detailed discussions on rotational dynamics and its analysis have been made in chapter 2.

- ***Förster resonance energy transfer studies (FRET):*** The phenomenon where the excitation energy of the donor is non-radiatively transferred to the acceptor mole present in the ground state is called FRET.<sup>198</sup> FRET is a distance dependent phenomenon where the distance between the donor and the acceptor typically falls within 10 to 100 Å.<sup>198, 200, 201</sup> As FRET is a distance dependent phenomena, it has been used as a “spectroscopic ruler” in molecular biology.<sup>198, 200, 201</sup> One of important condition for FRET to happen is the overlap between the absorption spectrum of the acceptor and the emission spectrum of the donor. One of the greatest advantages of FRET is to monitor events non-invasively in a heterogenous environment such as cells, protein assemblies, polymer matrices etc.<sup>198, 200</sup> As FRET is a distance dependent phenomenon, a small change in the donor acceptor distance can cause significant effect in the efficiency of FRET process. FRET studies on ILs have provided useful information on the micro-structural organization of ILs.<sup>198</sup> Bhattacharya and co-workers have demonstrated that excitation wavelength dependent FRET study can provide information about the different regions of an ionic liquid-based micellar system.<sup>173, 202</sup> Further, the aggregation behavior of ILs have been explored by Stricolli and co-workers through the FRET studies.<sup>175</sup> However, more studies concerning the FRET process in ILs are essential as these can provide an idea on the structural organization of MILs and DILs.

### 1.1.6. NMR investigations on ILs

$^1\text{H}$  and  $^{13}\text{C}$  NMR is primarily used to characterize organic molecules. However, NMR can also be used to understand the behavior of ILs. For eg., the solute-solvent hydrogen bonding interactions in ILs can be probed through this technique.<sup>203-205</sup> Further, multinuclear NMR techniques are also used for measuring the translational diffusion coefficient, spin-lattice and spin-spin relaxation time in ILs.<sup>205</sup> In this context, it is noteworthy to mention that the pulsed field gradient NMR (PFG-NMR) method can effectively determine the diffusion coefficient of ions in ILs.<sup>204, 206</sup> As measuring the diffusion coefficient can directly be related to the transport properties of the medium, by estimating the diffusion coefficient one can also easily get an idea about the transport properties of ions in ILs.<sup>206</sup> By measuring the diffusion data of  $^1\text{H}$ , the self-diffusion of the cationic moieties can be monitored in ILs.<sup>206</sup> On the other hand,  $^{19}\text{F}$  relaxation data can provide the diffusion of the anionic moieties in ILs.<sup>207</sup> Moreover, the nuclear overhauser effect (NOE) can be employed to understand the anion-cation interactions in ILs.<sup>207-213</sup> These interactions can help in obtaining idea on the structure and interactions between ions in ILs. Also, the inter or intra molecular interactions in ILs have been studied by employing NMR.<sup>207-213</sup>

### 1.1.7. Fluorescence Correlation Spectroscopy (FCS) studies in ILs

Investigations of molecular diffusion, binding studies, protein dynamics etc. at single molecule level can be carried out with the help of FCS. FCS is a technique based on the fluctuations of the fluorescence intensity of a fluorescent sample (in nanomolar range of concentration) in a small confocal volume.<sup>198</sup> The confocal volume ranges from 1.0 to 1.2 femtolitre in the conventional FCS setup.<sup>198, 214</sup> Diffusion of fluorophores through FCS eventually helps in understanding the structural organization of ILs. Kim and coworkers<sup>215, 216</sup> investigated the neat ILs through FCS. They have shown that the fluorescence of neat RTILs is originating from different anion-cation associated species.<sup>215</sup> Baker and coworkers<sup>217</sup> used FCS to investigate

the translational diffusion of charged and neutral fluorophores in ILs. Also, self-aggregation of the alkyl chains of the cationic ring have also been monitored through FCS.<sup>217</sup> Bhattacharya and coworkers<sup>218</sup> have studied the diffusion of neutral and anionic dyes in two imidazolium-based ILs and it has been observed that diffusion coefficients of neutral dye is similar in water and ILs whereas the diffusion coefficient for the anionic dye is found to be ~1.7 times lesser than the same for neutral dye in ILs. This is observed due to the presence of electrostatic interactions between ILs and charged solutes.<sup>218</sup> The results obtained from FCS are often coupled with the fluorescence lifetime data in order to explain the existence of polar and non-polar regions of the ILs and thus micro-heterogeneous behavior.<sup>174, 219, 220</sup> Therefore, FCS study in ILs is essential to obtain useful information on the structural organization of ILs at single molecular level.

## **1.2. Objective of the thesis**

Although extensive theoretical and experimental studies have been undertaken on ILs during the last decade. Many challenges with regard to ionic liquid research has still not been resolved completely. Some of the important issues regarding this are:

- Proper understanding of the solute-solvent interactions in micro-heterogeneous media.
- Understanding the inter-relationship among the intermolecular interaction, structural organization and solute dynamics in various imidazolium and pyrrolidinium based monocation, dicationic ionic liquids and binary mixtures of monocationic ionic liquids.
- Whether important photophysical process like resonance energy transfer can be exploited in understanding the structural organization of ILs. These processes are important to understand the potential of ILs in energy related applications.

- Understanding what lithium ion does to the nano-structural organization of different ILs when the former is added to the later.

The current thesis addresses all the issues raised above in different chapters systematically.

Brief introduction about ionic liquids (ILs) and their physicochemical properties have been made in Chapter 1. In particular, discussions are made on various imidazolium and pyrrolidinium-based ILs. Various applications of ILs and their binary mixtures in the fields of chemical, biological and material sciences have also been highlighted. Next, the study of kinetics using photochromic probes has been illustrated in this chapter. After this, a detailed discussions on the excitation wavelength dependent emission behavior, solute rotation, translational diffusion phenomena in various ILs have been made by illustrating several literature reports. Lastly, the current challenges in ionic liquids research and objective of the present thesis work have been outlined at the end of this chapter.

Basic principles of different experimental techniques used in the present study, such as absorption spectroscopy, steady-state and time-resolved emission spectroscopy have been demonstrated briefly in this chapter. The working principle of time-correlated single photon counting (TCSPC) technique and single molecule fluorescence spectroscopic technique have also been discussed. Further, principles of time-resolved fluorescence anisotropy and pulsed-field-gradient NMR (PFG-NMR) measurements are also described. Methodologies used to obtain the rotational relaxation time and analysis of time resolved fluorescence anisotropy data by using several hydrodynamic models have also been demonstrated. The error limits corresponding to different experimental parameters are provided in the end of this chapter.

This chapter discusses the outcomes of combined thermophysical and photophysical investigations of several binary mixtures of ILs along with the constituent pure neat ILs that they are composed of. Specifically in this study, the mixtures of ILs are chosen with a common

cation, 1-Butyl-3-methylimidazolium [BMIM] with variation in anion namely bistrifluoromethylsulfonylimide [NTf<sub>2</sub>], hexafluorophosphate [PF<sub>6</sub>] and tetrafluoroborate [BF<sub>4</sub>] as shown in Figure 1.1. This has been done to monitor the role of anion, if any, in governing the overall behavior of ILs exclusively. The investigations are also carried out by taking individual pure ILs so that the difference in the behavior of pure IL and (IL + IL) mixtures is understood. Microscopic behavior in terms of solute-solvent interactions have been studied using the steady-state and time-resolved fluorescence spectroscopy, nuclear magnetic resonance (NMR), and fluorescence correlation spectroscopy (FCS). (Chapter 3)

In this chapter the thermophysical properties as well as the structural organization of different binary mixtures of ILs have been investigated by understanding the thermodynamics of mixing ILs. In this work, a systematic study of the IL mixtures has been conducted by taking imidazolium and pyrrolidinium ILs with bis(trifluoromethylsulfonyl)imide [NTf<sub>2</sub>] as the common anion and various cations such as 1-alkyl-3-methylimidazolium with n = 2, 3, 4, [C<sub>2</sub>C<sub>1</sub>im], [C<sub>3</sub>C<sub>1</sub>im], [C<sub>4</sub>C<sub>1</sub>im], and 1-alkyl-3-methylpyrrolidinium with n = 3, 4, [C<sub>3</sub>C<sub>1</sub>pyr] and [C<sub>4</sub>C<sub>1</sub>pyr] (Chart 2). Moreover, imidazolium and pyrrolidinium based ILs are chosen so that the role of cations, in governing the behavior of the said mixture, if any, is properly understood. Investigations have been carried out at the macroscopic level by observing the thermophysical properties, such as molar volume and thermal expansion coefficient, and at the microscopic level with time-resolved fluorescence measurements and the pulse field gradient nuclear magnetic resonance (NMR) technique. (Chapter 4)

The resonance energy transfer (RET) studies have been investigated from neat ionic liquids (donor) to rhodamine 6G (R6G) (acceptor) to understand the local structural organization of different imidazolium based ILs. For this study, we have taken imidazolium based monocationic ILs (MILs) and dicationic ILs (DILs). R6G, being a charged species, is

expected to facilitate the electrostatic interactions with the ILs which are also charged. The RET studies are carried out in such a way that the length of the alkyl side chains is kept unchanged for MILs and DILs. In this work, RET a cost-effective and non-invasive technique is quite effective in capturing the differences in the nanostructural organization of MILs and DILs. (Chapter 5)

In recent times, ionic liquid-based (ILs) electrolytic system has emerged as suitable alternative to the conventional organic solvent-based electrolytic system. Since anion of ILs is known to form aggregates in the presence of lithium-ions ( $\text{Li}^+$ ), the aggregation can significantly influence the transport properties of  $\text{Li}^+$  ion, therefore, it is extremely important to understand how lithium-ions influence the structure and dynamics of ILs. With this objective, in the present study, intermolecular interaction, structural organization, and dynamics of monocationic ILs (MILs) and dicationic IL (DIL) have been studied in the absence and presence of lithium salt. Specifically, for this purpose, two MILs, 1-methyl-3-propylimidazolium bis- (trifluoromethylsulfonyl)imide ( $[\text{C}_3\text{C}_1\text{im}][\text{NTf}_2]$ ), 1-hexyl-3-propylimidazolium bis- (trifluoromethylsulfonyl)imide ( $[\text{C}_6\text{C}_1\text{im}][\text{NTf}_2]$ ), and a DIL, 1,6-bis(3-methylimidazolium-1-yl)hexane bis(trifluoromethylsulfonyl)amide ( $[\text{C}_6(\text{mim})_2][\text{NTf}_2]_2$ ) have been chosen in such a way that either the alkyl chain of MILs becomes equal or half of the spacer chain length of DIL. To understand the effect of the addition of lithium-ion on the structural organization of MILs and DIL, steady-state absorption and fluorescence spectroscopies, time-resolved fluorescence anisotropy and nuclear magnetic resonance (NMR) techniques have been used. The outcome of this study is expected to be helpful in realizing the potentials of these media as electrolytes in battery applications. (Chapter 6)

## **CHAPTER 2**

---

### **Materials, Instrumentations and Methods**

---

## Chapter 2

---

### Materials, Instrumentations and Methods

---

This chapter mainly presents various methodologies and different experimental techniques used in the present thesis work. Briefly, sources of chemicals used, methods of sample preparation and experimental techniques involving spectral measurements are described. The instrumentation details, especially, time-correlated single photon counting setup and time-resolved confocal fluorescence microscope setup have been discussed in detail. This chapter also describes the methodologies adopted to analyze the experimental data.

---

#### 2.1. Materials

The monocationic ILs used in the present thesis work were obtained from Sigma Aldrich, TCI Chemicals (Japan) and Io-Li-Tech (Germany). The purification of ILs were carried out by using the active charcoal and its purity were verified through conventional analytical techniques such as NMR and Mass Spectrometry. For the synthesis of dicationic ILs, 1,6-Bis(3-methylimidazolium-1-yl)hexane bis(trifluoromethylsulfonyl)amide,  $[C_6(\text{Mim})_2][\text{NTf}_2]_2$  and 1,8-Bis(3-methylimidazolium-1-yl)octane bis(trifluoromethylsulfonyl)amide,  $[C_8(\text{Mim})_2][\text{NTf}_2]_2$ , the materials used of synthesis are 1, 6-Dibromohexane (TCI Chemicals), 1, 8-Dibromooctane (Sigma Aldrich), Acetonitrile (Spectrochem), 1-Methylimidazole (TCI Chemicals), Lithium bis(trifluoromethylsulfonyl)amide (TCI Chemicals), Diethyl ether (Spectrochem),  $\text{Na}_2\text{SO}_4$  (99.0% anhydrous, Sigma Aldrich) and activated charcoal (Spectrochem). Synthesis of the dicationic ILs were carried out by following a literature procedure.<sup>48</sup> Thermophysical properties such as viscosity and density were measured and compared with the literature values. All the ILs were dried under high vacuum overnight prior to the spectroscopic studies.

## 2.2 Synthesis procedure of dicationic ionic liquids (DILs)

### 2.2.1. 1,6-Bis(3-methylimidazolium-1-yl)hexane bromide, $[C_6(Mim)_2][Br]_2$ (precursor for target six membered DIL)

1, 6-Dibromohexane (25 gm, 102.5 mmol) was gradually added to an acetonitrile solution (50 mL) of 1-methylimidazole (22 gm, 267.9 mmol) in a round-bottom flask equipped with a reflux condenser and a magnetic stirrer under nitrogen atmosphere, and the solution was stirred at 343 K for 3 days. The solution was then condensed by evaporation, and was washed by diethyl ether. The salt was precipitated as a brown powder. Then the salt was recrystallized from diethyl ether for several times and the purified product was finally obtained as a white solid after it was dried under vacuum at 308 K. The yield was 89%.  $^1H$ -NMR (DMSO- $d_6$ , 400 MHz):  $\delta$  (ppm) = 9.27 (s, 2H), 7.82 (s, 2H), 7.76 (s, 2H), 4.21 (t, 4H), 3.85 (s, 6H), 1.81 (m, 4H) 1.26 (m, 4H).

### 2.2.2. 1,6-Bis(3-methylimidazolium-1-yl)hexane bis(trifluoromethylsulfonyl)amide, $[C_6(Mim)_2][NTf_2]_2$

1, 6-Dibromohexane (15.5 gm, 63 mmol) was gradually added to an acetonitrile solution (30 mL) of 1-methylimidazole (11.7 gm, 143 mmol) in a double neck round-bottom flask equipped with a reflux condenser and a magnetic stirrer under nitrogen atmosphere. The solution was stirred at 343 K for 3 days under nitrogen atmosphere. Condensation by evaporation method was used to obtain the resulting product which was then washed with diethyl ether till a clear residue was obtained. The salt was then recrystallized from diethyl ether and the purified product was obtained as a white solid after it was dried under vacuum at 308 K. The yield obtained was 88%.  $^1H$ -NMR (DMSO- $d_6$ , 400 MHz):  $\delta$  (ppm) = 9.06 (s, 2H), 7.72 (s, 2H), 7.67 (s, 2H), 4.17 (t, 4H), 3.85 (s, 6H), 1.77 (m, 4H) 1.25 (m, 4H). ESI-MS (+ve): 528.13 m/z  $[C_6(mim)_2]^+$

### 2.2.3. 1,8-Bis(3-methylimidazolium-1-yl)octane bromide, $[\text{C}_8(\text{Mim})_2][\text{Br}]_2$ (precursor for target eight membered DIL)

1, 8-Dibromooctane (25 gm, 102.5 mmol) was gradually added to an acetonitrile solution (50 mL) of 1-methylimidazole (22 gm, 267.9 mmol) in a round-bottom flask equipped with a reflux condenser and a magnetic stirrer under nitrogen atmosphere, and the solution was stirred at 343 K for 3 days. The solution was then condensed by evaporation, and was washed by diethyl ether. The salt was precipitated as a brown powder. Then the salt was recrystallized from diethyl ether for several times and the purified product was finally obtained as a white solid after it was dried under vacuum at 308 K. The yield was 86%.  $^1\text{H-NMR}$  (DMSO- $d_6$ , 400 MHz):  $\delta$  (ppm) = 9.23 (s, 2H), 7.80 (s, 2H), 7.72 (s, 2H), 4.16 (t, 4H), 3.83 (s, 6H), 1.81 (m, 4H) 1.23 (m, 8H, b).

### 2.2.4. 1,8-Bis(3-methylimidazolium-1-yl)octane bis(trifluoromethylsulfonyl)amide, $[\text{C}_8(\text{Mim})_2][\text{NTf}_2]_2$

$[\text{C}_8(\text{Mim})_2][\text{Br}]_2$  (7.1 gm, 28.5 mmol) was dissolved in water (30 mL), and aqueous lithium bis(trifluoromethylsulfonyl)amide solution (10.6 gm, 37.1 mmol in 20 mL water) was gradually added to the solution. The resultant mixture was stirred at room temperature for 1 day and the aqueous solution was decanted. The organic layer consisting of ionic liquid was dissolved in ethyl acetate (30 mL) and was washed with water (30 mL  $\times$  5). Anhydrous  $\text{Na}_2\text{SO}_4$  was used for drying the organic layer and was filtered to remove the drying agent. Next the solvent was evaporated and the residue was mixed with activated charcoal in acetonitrile. Removal of the activated charcoal was done by filtration and the solvent was evaporated. The above decolorization with charcoal step was repeated twice. Then, the ionic liquid was dried under vacuum at 308 K for 3 days. The product obtained was a colourless liquid. The yield was 85%.  $^1\text{H-NMR}$  (DMSO- $d_6$ , 400 MHz):  $\delta$  (ppm) = 9.08 (s, 2H), 7.72 (s, 2H), 7.67 (s, 2H), 4.11 (t, 4H), 3.81 (s, 6H), 1.75 (m, 4H) 1.23 (m, 8H, b). ESI-MS (+ve): 556.15 m/z  $[\text{C}_8(\text{mim})_2]^+$

### **2.3. Sample preparation for spectroscopic measurements**

For the steady state and time-resolved fluorescence measurements, ILs were taken in quartz cuvette bearing a long-necked having with path length of 1cm. The long neck allowed proper dissolution of probe molecules. Amount of fluorescence probe dissolved in the ILs was adjusted by measuring the optical density of the probe. The optical density was maintained below 0.4. To avoid moisture adsorption in the samples, proper precautions were maintained during the sample preparation by sealing the cuvettes using the parafilm and rubber septum.

### **2.4. Instrumentations**

#### **2.4.1. Instrumentations used for characterization of samples**

Bruker Avance 400 MHz NMR spectrometer was used to record the NMR spectra. The ESI-MS (Electrospray ionization mass spectrometry) spectra were collected by using Bruker micrOTOF-QII mass spectrometer. Viscosity of ILs was recorded by using a Cone and Plate Viscometer (Brookfield LVDV-III Ultra). Additionally, temperature dependent viscosity measurements were also performed by using a Julabo water circulator bath attached to the viscometer. Additionally, the densities ( $\rho$ ) of the samples were measured by an automated temperature-controlled density analyzer (Anton Paar, model DSA 5000) at variable temperatures.

#### **2.4.2. Instrumental techniques for absorption and steady state emission measurements**

##### **2.4.2.1. Absorption measurements**

The UV-Visible spectroscopy measurements of all the samples were investigated by using a Cary 100 Bio UV-VIS spectrophotometer with a wavelength resolution of 0.15 nm. A xenon lamp has been used as the lamp source. Absorption spectroscopy mainly offers an idea on the ground electronic states of systems. Absorption measurements can help in obtaining information on the nature of electronic transitions possible in the ground state of the chromophore in the concerned samples by visualizing the wavelength of different absorption

bands and molar extinction coefficient. Thus, UV-VIS absorption spectroscopy helps to characterize the various types of chromophoric systems and their neighboring micro-environments.<sup>190, 221, 222</sup> Moreover, UV-VIS absorption spectrum of a chromophoric species is also influenced by polarizability, solvent polarity or hydrogen bonding interaction in the ground state. Hence, UV-Visible absorption spectroscopy is capable of providing useful insights into the interactions existing between the chromophoric species and its surrounding micro-environment present in the ground electronic state.

The UV-Visible absorption spectroscopy follows the Lambert Beer's law, according to which the absorbance ( $A_\lambda$ ) of an absorbing species in a solution at a wavelength  $\lambda$ , is directly proportional to the concentration ( $C$ ) of the species in the solution and its molar extinction coefficient ( $\epsilon_\lambda$ ) at that particular wavelength. It can be expressed by the following relationship<sup>190, 198, 221, 222</sup>

$$A_\lambda = \log\left(\frac{I_0}{I}\right) = \epsilon_\lambda Cl \quad (2.1)$$

where  $I_0$  = Incident light intensity and  $I$  = Transmitted light intensity.  $l$  = path length of the sample in cuvette.

#### **2.4.2.2. Steady state fluorescence measurements**

All the steady-state fluorescence measurements in the present work were performed with a Cary Eclipse fluorescence spectrophotometer of Agilent Technologies (G9800A) where a xenon lamp is used as the lamp source. Additionally, Edinburgh spectrofluorometer FS5 was used to collect temperature dependent fluorescence spectra. A North West (TC 125) temperature controller was used to maintain the temperature by circulating water through the cell holder.

Fluorescence spectroscopy is a widely used and sensitive tool to investigate various types of photochemical and photophysical processes in the excited state of a fluorophore molecule. Slight changes in the environment or interactions of the fluorophore molecules in

the excited state can cause change in the emission maxima, intensity and shape of the emission spectra of the respective species.<sup>190, 198, 221, 222</sup> Therefore, with the help of this technique a better understanding on the micro-environment of the emitting species can be observed.

### 2.4.3. Instrumental techniques for time-resolved studies

#### 2.4.3.1. Fluorescence lifetime measurements

Time-resolved fluorescence measurements are very beneficial in providing valuable information on the kinetics and dynamics of various photochemical and photophysical process. Very short pulsed light is used to excite the fluorescent molecule that results an initial population ( $n_o$ ) of fluorescent molecule in the excited state. The excited state population decays with a rate ( $k_r + k_{nr}$ ) according to the following relation<sup>190, 198, 221-227</sup> (2.2):

$$-\frac{dn(t)}{dt} = (k_r + k_{nr})n(t) \quad (2.2)$$

where  $n(t)$  = number of excited molecules at time  $t$  following the excitation of fluorophore molecule with the very short pulse light. The  $k_r$  and  $k_{nr}$  denotes the radiative and nonradiative rate constant respectively. As emission is considered as a random event, the probability of emission of excited state is fluorophores are same over a given period of time. And the excited state population decays with an exponential manner with the following equation (2.3) is provided below:

$$n(t) = n_o \exp\left(-\frac{t}{\tau}\right) \quad (2.3)$$

From the equation 2.3, as it can be seen that the fluorescence intensity is directly proportional to the number of excited molecules present in the solution. Subsequently, the equation 2.3 can be rewritten in terms of the time dependent intensity  $I(t)$  and the integration of the final equation (2.4) has been provided in the equation below:

$$I(t) = I_o \exp\left(-\frac{t}{\tau_f}\right) \quad (2.4)$$

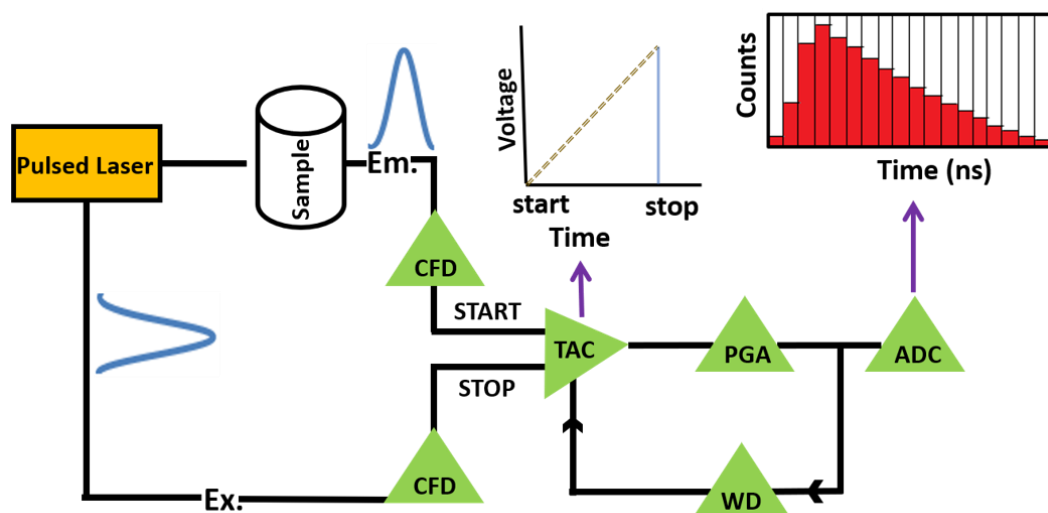
where  $I_0$  = intensity at time (zero),  $\tau_f$  = fluorescence lifetime of the sample that is related to the radiative and non-radiative decay rate constants as per the following equation (2.5):

$$\tau_f = \frac{1}{k_r + k_{nr}} \quad (2.5)$$

The excited state fluorescence lifetime of a fluorophore is estimated through time-correlated single photon counting (TCSPC) technique. In this context, it should be noted here that the time spent by the different molecules in the excited state are different. Therefore, in the excited state, some molecules may emit at a longer time whereas others may emit in a very short time span. Therefore, the time distribution of these emitted photons appears as the measured fluorescence decay of the sample under examination. Henceforth, the estimated lifetime obtained from the TCSPC setup denotes the statistical average of the times that the fluorophore molecules spend in the excited state. All the time-resolved measurements in the present thesis have been carried out by using Edinburgh Life Spec II TCSPC instrument. The fundamental working principles and the important components pertaining to the TCSPC setup are described below.

#### **2.4.3.2. Basic principle of TCSPC setup**

The working principle of TCSPC technique is based on the single photon detection from a sample following a pulsed excitation.<sup>223-227</sup> The TCSPC technique is based on the time dependent probability distribution of the single photon emission from an excited fluorophore. The time dependent probability distribution obtained from the TCSPC technique is equivalent to the time dependent changes in the fluorescence intensity of the sample after its excitation through a short light pulse.<sup>223-227</sup> The working principle of TCSPC setup (in reverse mode) is provided by a schematic diagramed in Scheme 2.1.



**Scheme 2.1.** A schematic diagram for the working principle of TCSPC setup.

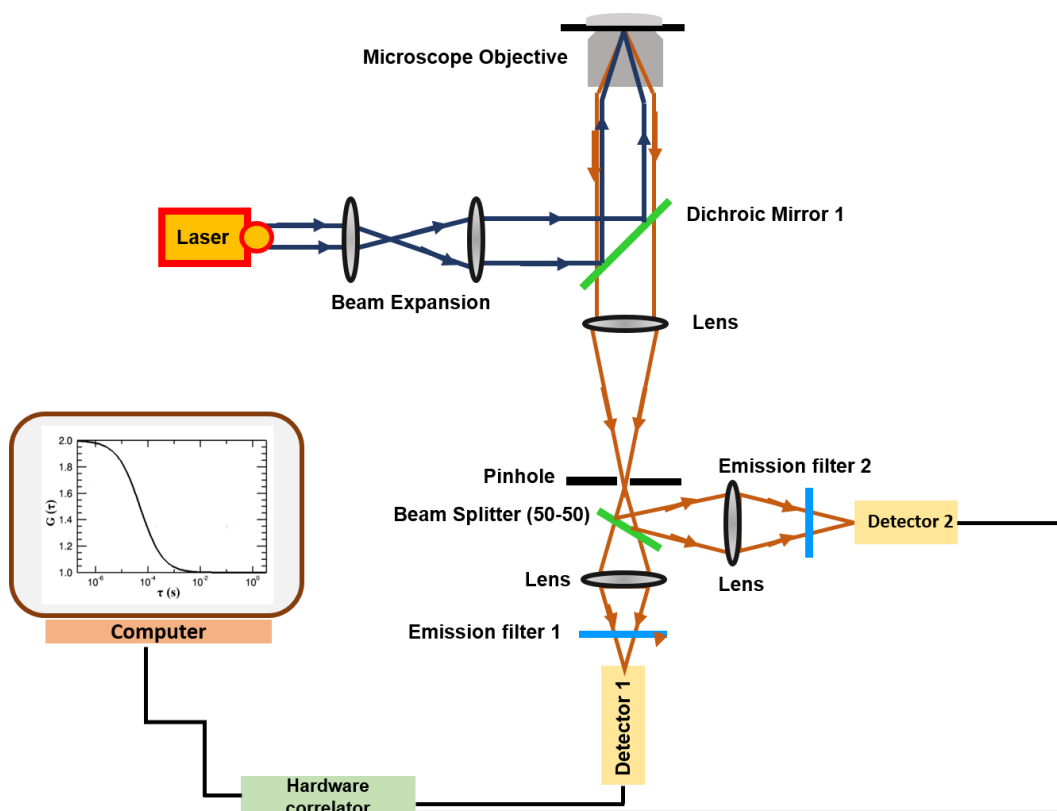
As describe in Scheme 2.1, an excitation pulse is divided into two parts, the first part is used to excite the sample and the second part of the pulse excitation is directed towards the electronics. The optical signal from the emitted photon at the start PMT generates an electrical signal that corresponds to START pulse. The START pulse that passes through the Constant Fraction Discriminator (CFD) helps in measuring the exact arrival time of the pulse. Then the signal arrives through START input to the Time to Amplitude Converter (TAC), which generates a voltage ramp which increases linearly with time. In second channel, consisting of the excited photons passes through the CFD unit and reaches the TAC unit. These signals are basically the STOP pulses which are also passed through the CFD and variable delay line to the STOP the input of the same TAC unit. The TAC unit stops to generate the voltage ramp once it detects the first STOP pulse. Essentially, the TAC unit now contains a voltage that is proportional to the time delay ( $\Delta t$ ) between the excitation and emission pulse. The TAC output pulse signals are then passed through PGA (Pulsed Gain Amplifier) to an ADC (Analog-to-Digital Converter). The ADC generates a numerical value, which is proportional to the height of the TAC output pulse signal. Finally, the data is stored in the multichannel analyser (MCA).

The above cyclic process is repeated again and again for a large number of times resulting in a collection of histogram of counts in the MCA channels. Scheme 2.1 is provided for a TCSPC technique in a “reverse mode”. In present times, almost all TCSPC measurements are done in the "reverse mode".<sup>198</sup> Reverse mode is used because of the high repetition rate of modern pulsed-light-based sources. The TAC has to be reset and set to zero before each start pulse, which takes a finite amount of time. To avoid the loss of information, the TAC can be constantly in reset mode if the start signals arrive too rapidly. It has been observed that the emission signals occur about 1 per 100 excitation pulses, and hence much less frequently than the excitation pulses. These emission pulses are used to start the TAC, and the next subsequent laser pulse is used to stop the TAC. Present electronics for TCSPC setup only allow the detection of the first arrival photon. Analysis procedure for estimation of fluorescence lifetime and anisotropy from the measured fluorescence decay curves is also discussed in the later part of this chapter.

#### **2.4.4. Experimental technique for single-molecule studies**

##### **2.4.4.1. Time-resolved confocal fluorescence microscope**

Optical microscopes are used as a tool to magnify the images of the micro-objects. The overall resolution of microscopes is determined by the excitation wavelength and the numerical aperture of the objective lens. Depending on the excitation source and the configuration of a microscope, it is possible to modulate the resolution of microscope. The generation of confocal fluorescence microscopy (CFM) is important when higher temporal resolution (upto few ns) is required. This has been made possible by employing multiple pinholes in the detection path that allows only the tightly focused light resulting in abbreviation free images. A schematic diagram of the confocal microscope is shown in Scheme 2.2.

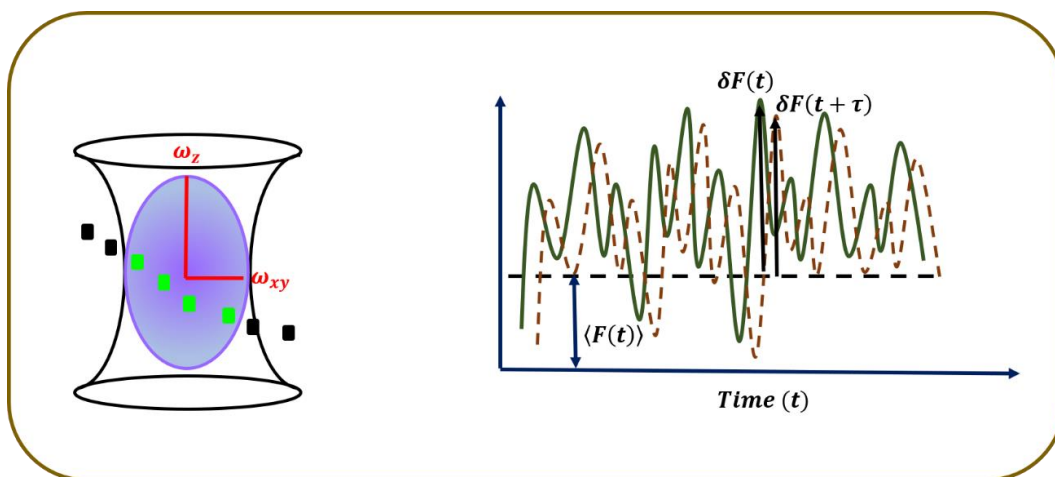


**Scheme 2.2.** Basic configuration of confocal fluorescence microscope.

All the measurements in the present thesis were carried out using MicroTime 200 (PicoQuant) model of time-resolved confocal microscope. As the excitation source, different pulsed picosecond diode lasers (excitation wavelength of 403 nm, 444 nm, 483 nm and 519 nm) was used in the setup. The output of the laser beam was guided to the sample which was placed on a movable stage of an inverted microscope. To control the sample position, a piezo scanning stage is mounted in the microscope body. For manual positioning, micro-meter screws were used along with the software controlled piezo-scanner for precise and repeatable XY scanning and Z –positioning of the sample. Optical fibers, dichroic mirrors, beam splitters and water immersion objective were the main optical components. A charged coupled device (CCD) detector was used to monitor the position of the focal point on the sample. Depending on the measurement techniques different single or multiple photon avalanche photodiodes (SPAD) were used.

### 2.4.4.2. Fluorescence correlation spectroscopy

FCS is a noninvasive fluorescence intensity fluctuations-based technique used to obtain information on the dynamic processes responsible for the fluctuation.<sup>228-230</sup> It is a solution-based technique, where fluorophores diffuse freely through the confocal volume and generate signal fluctuations due to diffusion and other processes. To generate sharp fluctuations, the number of species has to be small. To do this effectively few nanomolar solutions are used as concentrated sample produces nearly constant average signal throughout the measurement time. This gives rise to single molecule sensitivity depending on the size of the observation volume. Signals obtained are then correlated to obtain the correlation curves. Since, FCS is a diffusion-based technique which is a random event, the occupancy of the fluorescent species in the observation volume is described by Poisson statistics. Experimental setup for this technique is same as shown in Scheme 2.2. To increase Signal to Noise ratio (SNR) and achieve better temporal resolution signals are generally cross-correlated.



**Scheme 2.3.** Diffusion of fluorophores through the confocal volume and fluctuations in the relative intensities.

Scheme 2.3 denotes the diffusion of the fluorophore through the ellipsoidal observation volume. The autocorrelation function is defined as the product of the fluctuation of fluorescence intensities at time  $t$ ,  $\delta F(t)$  and  $t+\tau$ ,  $\delta F(t+\tau)$  and averaged over a large number of

measurements. The autocorrelation function,  $G(\tau)$  normalized by the square of average fluorescence intensity ( $\langle F(t) \rangle$ ) is given by the following equation (2.6):

$$G(\tau) = \frac{\langle \delta F(t) \delta F(t+\tau) \rangle}{\langle F(t) \rangle^2} \quad (2.6)$$

Here,  $\delta F(t)$  and  $\delta F(t+\tau)$  are defined as equation (2.7):

$$\delta F(t) = F(t) - \langle F(t) \rangle \text{ and } \delta F(t + \tau) = F(t + \tau) - \langle F(t) \rangle \quad (2.7)$$

Autocorrelation function for pure diffusion in three dimensions can be written as in equation (2.8):

$$G(\tau) = \frac{1}{N} \left(1 + \frac{\tau}{\tau_D}\right)^{-1} \left(1 + \frac{\tau}{\kappa^2 \tau_D}\right)^{-\frac{1}{2}} \quad (2.8)$$

where  $\langle N \rangle$  is the average number of the fluorophore in the observed volume,  $\tau_D$  is the diffusion time,  $\kappa$  is the structure parameter of the observed volume. From the equation 2.8, diffusion coefficient of the fluorescent species can be derived as in equation (2.9):

$$D = \frac{\omega_{xy}^2}{4\tau_D} \quad (2.9)$$

## 2.5. Methods

### 2.5.1. Analysis of the fluorescence decay curves

#### 2.5.1.1. Data analysis

Fluorescence lifetime values obtained from the decay curves were determined using the reconvolution least squares method.<sup>231</sup> The excitation pulse can be expressed as a  $\delta$ -function when the estimated decay time is higher than the pulse-width of the excitation source. Even though, as the excited state lifetime is small, several factors (such as the finite decay time of the source pulse, response time of the photomultiplier tube (PMT) and related electronics) can distort the experimental data. Therefore, the instrument response function (IRF) depends not only on the decay time of the laser pulse but also depends on the response time of the detector (PMT) and associated electronics. As the measured decay function is convolution of the accurate fluorescence decay and IRF. Therefore, it is essential to deconvolute the IRF from the

experimental decay to obtain the fluorescence lifetime. The method can be mathematically expressed as<sup>221, 222, 232, 233</sup> in equation (2.10):

$$I_m(t) = \int_0^t I_R(t-t')R(t')dt' \quad (2.10)$$

where  $I_m(t)$  is the fluorescence intensity at time  $t$ ,  $I_R(t-t')$  is the response function of the experimental system and  $R(t')$  is the intensity of the exciting pulse at time  $t'$ . IRF was estimated using a dilute Ludox solution and deconvolution algorithm was made through iterative reconvolution method.

Then, a nonlinear least squares (NLLS) data processing method is used to fit the ideal decay with some assumed functional form. The least square analysis is only useful if the data points fulfill certain assumptions. The main assumptions involved are there should be sufficient independent data points. The uncertainties in the experimental data points are Gaussian distributed and there should not be any systematic error in the experimental data points. Both  $I_m(t)$  and  $R(t')$  can be obtained experimentally from the TCSPC setup. During the analysis, a decay function  $G(t)$  is first assumed for the sample and this function is deconvoluted with the observed  $R(t')$  according to equation 2.10 to get a calculated curve  $Y(t)$ . The  $Y(t)$  is then compared with the experimentally observed decay curve  $I_m(t)$ .<sup>198, 221, 222, 232</sup> The variables in the function  $G(t)$  are changed iteratively until a good comparison (known as the best fit) between the  $Y(t)$  and  $I_m(t)$  is obtained. The function  $G(t)$  is typically assumed to be a sum of exponentials in such a way represented in equation (2.11):

$$G(t) = \sum_i B_i \exp\left(\frac{-t}{\tau_i}\right) \quad (2.11)$$

where  $B_i$  is the pre-exponential factor for the  $i^{\text{th}}$  component and  $\tau_i$  is the corresponding fluorescence lifetime. The success of an analysis of a fit to the observed decay curve are determined from the judicial judgments of the following statistical parameters.

### 2.5.1.2. Reduced chi-square ( $\chi^2$ ) values

To judge the goodness of a fit, reduced  $\chi^2$  values are monitored and its value approaches unity if the model does fit the data. The reduced  $\chi^2$  is denoted as shown in equation (2.12):

$$\chi^2 = \frac{\sum_i W_i \{Y_i - I_i\}^2}{n-p} \quad (2.12)$$

where  $Y_i$  is the count of  $i^{\text{th}}$  channel of the calculated curve,  $I_i$  is the count at the  $i^{\text{th}}$  channel of the curve measured experimentally.  $W_i$  [ $W_i=I/I_i$ ], is the weighting factor of the counts in the  $i^{\text{th}}$  channel,  $n$  is the number of channels used for the decay to be analyzed and  $p$  is the number of degrees of freedom in the decay function considered for the analysis which is equal to the number of variables in the function  $G(t)$ . For a good fit, the  $\chi^2$  values must be close to unity. Generally, values of  $\chi^2$  ranging between 1.0 to 1.2 is considered to be a good fit to the data points.

### 2.5.1.3. Distribution of weighted residuals

The differences between the measured decay function and the fitted function are denoted by the weighted residuals. The weighted residuals are considered as one of the important parameters for the judgments of the achievement of an analysis of TCSPC data set and are defined by the following equation (2.13):

$$r_i = \sqrt{W_i} (Y_i - I_i) \quad (2.13)$$

where  $W_i$ ,  $Y_i$  and  $I_i$  are defined as previously. For a good fit, random distribution of the weighted residuals about the zero line for the complete data range of the data channels used in the analysis are expected to be obtained.

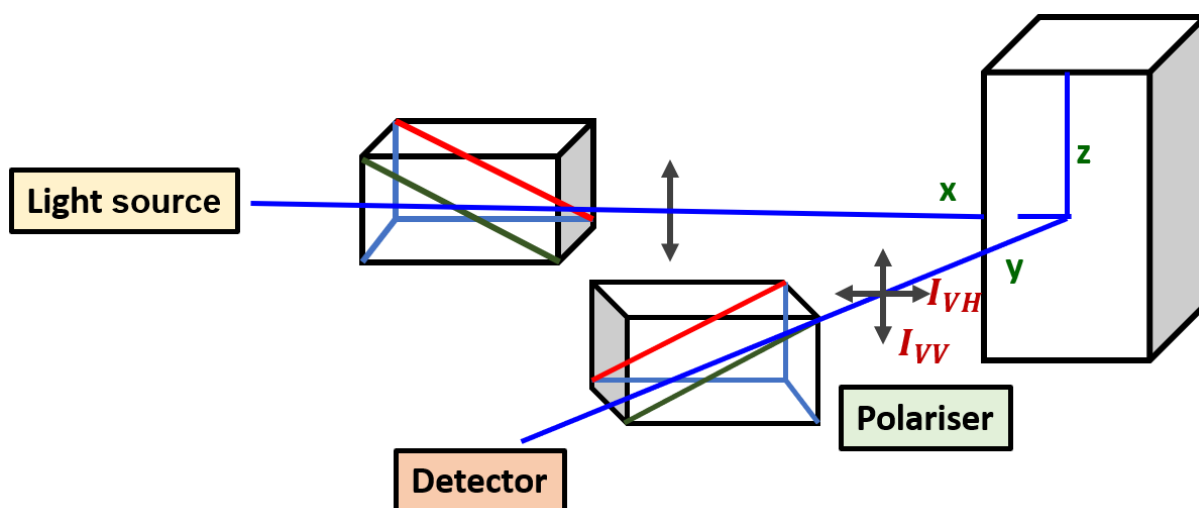
## 2.5.2. Time-resolved fluorescence anisotropy measurements

The fluorescence anisotropy is defined as the extent of the average angular displacement of a fluorophore that occurs between absorption and subsequent emission of a photon.<sup>198</sup> A diagrammatic representation of fluorescence anisotropy measurement is provided in Scheme 2.4.<sup>198</sup> The orientation of the emission polarization is defined by the electric vector of the

excitation pulse.  $I_{VV}$  designates the emission intensity observed with parallel polarization (excitation and emission polarizer are in vertical position) and  $I_{VH}$  denotes the intensity of perpendicularly polarized emission (excitation and emission polarizer are in vertical and horizontal position respectively). The ideal anisotropy  $r(t)$  is defined as in equation (2.14):

$$r(t) = \frac{I_{VV}(t) - I_{VH}(t)}{I_{VV}(t) + 2I_{VH}(t)} \quad (2.14)$$

The anisotropy is considered as a dimensionless quantity as the difference between parallel and perpendicular emission is normalized by the total emission intensity. Moreover, anisotropy is also independent of the fluorophore concentration as well as the total emission intensity.



**Scheme 2.4.** A diagrammatic representation of fluorescence anisotropy measurements.

Since, in TCSPC instrument, sensitivity of experimental setup and electronics (such as monochromator) may influence, the actual anisotropy measurements, therefore, it is necessary to incorporate correction factor ( $G$ ) while estimating the anisotropy,  $r(t)$ . This value of  $G$  represents the relative sensitivity of the detection system to the different polarization.  $G$  varies with the emission wavelength and the band pass filter of the monochromator. It is expressed as in equation (2.15):

$$G = \frac{I_{HH}}{I_{HV}} \quad (2.15)$$

where  $I_{HV}$  and  $I_{HH}$  are the emission intensities when the excitation and emission polarizers are in horizontal-vertical and horizontal-horizontal position respectively. The  $G$  factor is calculated based on the intensity ratio between  $I_{HV}$  and  $I_{HH}$ . The measured anisotropy is then estimated by using the following relation in (2.16):

$$r(t) = \frac{GI_{VV}(t) - I_{VH}(t)}{GI_{VV}(t) + 2I_{VH}(t)} \quad (2.16)$$

In the present work, Edinburgh, Life Spec II TCSPC set-up was used to measure time-resolved fluorescence anisotropy. For time-resolved fluorescence anisotropy measurements, fluorescence intensities at different positions parallel ( $\parallel$ ) and perpendicular ( $\perp$ ) polarization were collected alternatively until a peak difference between parallel ( $\parallel$ ) and perpendicular ( $\perp$ ) decay is  $\sim 5000$  (at  $t = 0$ ) was observed. The same procedure was applied for  $G$ -factor calculation but with horizontal polarization of the exciting laser beam and five cycles of repetitions. The temperature of the cell was monitored by circulating water through the cell holder by a Quantum along with a North West (TC 125) temperature controller. To calculate the rotational relaxation time, fitting of the anisotropy data was performed using the following equation (2.17):

$$r(t) = r_0 e^{-(t/\tau_r)} \quad (2.17)$$

where,  $r_0$  is the initial anisotropy and  $\tau_r$  is the rotational relaxation time or reorientation time. It can be mentioned here that the  $r_0$  values ranges from 0.20 to 0.40 for any single-photon excitation.<sup>198</sup> The data corresponding to time-resolved anisotropy decay measurements were analyzed through hydrodynamic and quasi-hydrodynamic theories.

### 2.5.3. Hydrodynamic and Quasihydrodynamic theories

The rotational reorientation times of different probe molecules in IL-based solvent system have been interpreted using SED hydrodynamic theory.<sup>234, 235</sup> Additional to the SED hydrodynamic theory, different quasihydrodynamic theories<sup>236, 237</sup> are also presented in the subsequent section.

### 2.5.3.1. The Stokes-Einstein-Debye (SED) theory

According to SED theory, as the solute molecule rotates in the solvent continuum its reorientation time  $\tau_r$  is governed by the viscosity  $\eta$  of a given fluid at a temperature  $T$ .<sup>238</sup> The solute properties that dictate the rotation of solute in the solvent are the size and shape of the solute molecule. These factors are incorporated in the SED theory in form of van der Waals volume,  $V$  and shape factor,  $f$  accounting the non-spherical nature of the solute.<sup>238</sup> The solute molecules in this model are treated as either symmetric or asymmetric ellipsoids.<sup>239</sup> Additionally, the coupling between the solute and the solvent plays an important role in controlling the rotational diffusion of a solute molecule. To account this solute-solvent coupling parameter in SED model, usually denoted by  $C$ , the axial ratio of the solute molecule and the two limiting cases are the hydrodynamic boundaries stick and slip are considered.<sup>240</sup> The stick boundary conditions assumes a perfect coherence between the motion of the solute and the neighboring solvent.<sup>240</sup> On the other hand, the slip boundary condition assumes that the solvent can exert no tangential stress on the rotating solute.<sup>240</sup> Stick boundary condition is found to be appropriate for rotating bodies that are considerably larger than the surrounding fluid molecules. On the other hand, the validity of slip boundary condition begins as the rotating body is smaller of comparable size than the fluid molecules. The two limiting values for  $C$  are the hydrodynamic slip ( $C_{\text{slip}}$ ), which satisfies the inequality  $0 < C_{\text{slip}} \leq 1$  and hydrodynamic stick with  $C = 1$ . Thus, the expression for the rotational reorientation time  $\tau_r$  is given by equation (2.18):

$$\tau_r = \frac{\eta V f C}{kT} \quad (2.18)$$

where  $k$  is the Boltzmann constant. The product  $VfC$  is known as the hydrodynamic volume,  $V_h$ , which is the volume experienced by the solute molecule in the solvent medium. In case of SED, while calculating the boundary parameter condition, the size of the solute molecule only is taken into consideration. Despite this limitation, the SED theory is reasonably successful in

describing the rotational diffusion of medium-sized solute molecules in different kinds of solvents.<sup>241</sup> To apply SED theory for the systems described in this thesis, van der Waals volume of the solute molecules perylene and sodium 8-methoxypyrene-1,3,6- sulfonate (MPTS) were obtained using Edward's increment method.<sup>235</sup> Solute dimensions, van der Waals volumes, shape factors and boundary condition parameters ( $C_{slip}$ ) for the solutes perylene and MPTS have been calculated and listed in Table 2.1.

**Table 2.1.** Solute dimensions, van der Waals volumes, shape factors and boundary condition parameters ( $C_{slip}$ ) for the solutes.

Solute	$V/\text{\AA}^3$	$f$	$C_{slip}$
Perylene	225	1.76	0.085
MPTS	343	1.33	0.11

### 2.5.3.2. Quasi-hydrodynamic theories

As mentioned in the previous section, the SED theory takes into the hydrodynamic volume of the solute is independent of the solvent continuum. However, this assumption is valid only when the size of the solute is considerably larger compared to the size of the solvent. However, when SED theory fails in analyzing the hydrodynamic behaviour, different theories such as “quasi-hydrodynamic theories”<sup>236, 237</sup> are formulated after considering both the sizes of solvent and solute molecules. Other models such as the “Solventberg”<sup>242</sup> or “Nee Zwanzig”<sup>243</sup> are also sometime used to explain the rotational dynamics of a solute molecule.

The quasi-hydrodynamic theories that are successful in explaining the solvent size dependent rotational behavior of solute molecules are the Gierer-Wirtz (GW)<sup>236</sup> and Dote-Kivelson-Schwartz (DKS)<sup>237</sup> theories. GW theory states that the solvent molecule is made up of concentric shells of spherical particles surrounding the spherical solute molecules and the boundary parameter ( $C_{GW}$ ) in this condition is estimated by the angular viscosity that decreases as successive concentric shells around the solute molecule increases. On the other hand, DKS

theory takes into consideration of the free space between the solute and the solvent molecule along with the size of the solute and solvent molecule.<sup>237</sup> According the DKS theory, when the size of the solute is compared to the free space of the solvent, a weak coupling between the solute and solvent is observed. In this scenario, the solute experiences less friction leading to a faster rotation of the rotating solute in the solvent continuum.

The boundary condition parameter,  $C_{GW}$  in accordance to the GW quasihydrodynamic theory is given by the following equation (2.19):

$$C_{GW} = \sigma C_0 \quad (2.19)$$

The parameter  $\sigma$  and  $C_0$  are given by the following equations (2.20) and (2.21):

$$\sigma = [1 + 6(V_s/V)^{1/3} C_0]^{-1} \quad (2.20)$$

$$C_0 = \left[ \frac{6(V_s/V)^{1/3}}{[1+2(V_s/V)^{1/3}]^4} + \frac{1}{[1+4(V_s/V)^{1/3}]^3} \right]^{-1} \quad (2.21)$$

In these equations,  $V_s$  and  $V$  are the volume of the solvent and solute respectively.

The boundary conditions in case of DKS theory are given by the following equation (2.22):

$$C_{DKS} = (1 + \gamma/\phi)^{-1} \quad (2.22)$$

$\gamma/\phi$  is a measure of the ratio of the free volume of the solvent to the effective size of the solute molecule. It is represented as in equations (2.23), (2.24) and (2.25):

$$\gamma = \frac{\Delta V}{V_p} \left( 4 \left( \frac{V_p}{V_s} \right)^{2/3} + 1 \right) \quad (2.23)$$

$\Delta V$  is the smallest volume of free space per solvent molecule, which is empirically related to the viscosity.

$$\Delta V = V_m - V_s \quad (2.24)$$

$$\phi = f C_{slip} \quad (2.25)$$

$V_m$  is the solvent molar volume divided by the Avogadro number.

The solute-solvent interactions in ILs in presence of different solutes can provide information which are crucial for their potential applications. It has been established that rotational motion gets affected significantly due to solute-solvent interaction and the studies on rotational motion of the fluorescent probes in ILs through time-resolved anisotropic techniques can provide information on the solute-solvent interactions and hence the solvent properties of the medium. With this objective in mind, various research groups have done this type of investigation.<sup>169, 179, 244-246</sup> These investigations have revealed that the solute rotation not only depends on the medium viscosity but also depends on the specific solute-solvent interactions. The specific solute-solvent interactions in terms of hydrogen bonding can significantly affect the rotational motion of solute in ILs.<sup>199, 246</sup> Moreover as ILs are made up of ions, the electrostatic interactions among the charged solutes and ions of ILs also influence the rotational dynamics of charged probe molecules. However, the extent of electrostatic as well as hydrogen bonding interactions is still a debatable topic. We note here that studies have shown that rotational dynamics of charged probe in ILs depends solely on the viscosity of the medium. Even though some studies on rotational dynamic are available for neat ILs,<sup>169, 179, 244, 246</sup> such studies on binary mixtures of ILs are very limited.

## 2.6. NMR measurements

NMR studies have been carried out by using a 9.4 Tesla Bruker Avance NMR spectrometer at Larmor frequencies of 400.1MHz for <sup>1</sup>H measurement. For measuring translational diffusion coefficients ( $D$ ), stimulated echo bipolar pulse-gradient pulse (stebpgp) sequence has been used at different temperatures (298 K to 328 K). By varying the gradient strength from 2 to 95% of the maximum gradient pulse strength (50 G/cm) measurements of echo heights were made with 16 identical intervals. The echo heights were then fit to the relation (2.26):

$$S(g) = S(0) \exp \left[ -D\gamma^2 \delta^2 g^2 \left( \frac{\Delta - \delta}{3} \right) \right] \quad (2.26)$$

where  $S(g)$  and  $S(0)$  denote the echo height at the gradient strength  $g$  and  $0$  respectively.  $\gamma$  = gyromagnetic ratio of the proton,  $\delta$  denotes the gradient pulse length.  $\Delta$  = duration between the two gradient pulses.

## 2.7. Quantum yield calculations

The (anthracence in ethanol 0.27),<sup>247</sup> is have been used as a standard to assess the quantum yields ( $\Phi_s$ ) of neat ILs by using the following equation (2.27):

$$\Phi_S = \frac{I_s}{I_r} \times \frac{n_s^2}{n_r^2} \times \Phi_r \quad (2.27)$$

where  $I_s$  and  $I_r$  are the integrated fluorescence emission of the sample and the reference, respectively.  $\Phi_r$  is the quantum yields of the reference (anthracence,  $\Phi_r = 0.27$ ). The  $n_s$  and  $n_r$  are the refractive indices of the sample and the reference respectively. The values of  $I_s$  and  $I_r$  are determined by integrating the emission intensity over the spectral range. The sample and reference are excited at optically method condition.

## 2.8. Standard error limits

Standard error limits involved in the experimental results were

Viscosity ( $\eta$ )	$\pm 2\%$
Density	$\pm 2\%$
$\lambda_{\max}$ (abs./flu.)	$\pm 1-2$ nm
$\tau_f$ ( $> 1$ ns)	$\pm 5\%$
Rotational relaxation time	$\pm 5-10\%$
The energy transfer rate	$\pm 5\%$
Diffusion coefficient (through NMR)	$\pm 5\%$
Diffusion coefficient (through FCS)	$\pm 5-10\%$

## CHAPTER 3

---

# Thermophysical and Spectroscopic Investigations on Imidazolium-based Monocationic ILs and their Binary Mixtures with Common Cation

---

---

Chakraborty, M.; Ahmed, T.; Dhale, R. S.; Majhi, D.; Sarkar, M. *J. Phys. Chem. B* **2018**, *122*, 12114–12130

## Chapter 3

---

### Thermophysical and Spectroscopic Investigations on Imidazolium-based Monocationic ILs and their Binary Mixtures with Common Cation

---

Recently, mixing of ionic liquids with suitable chemical composition have been proposed in order to develop a useful new solvent system. However, current knowledge about the microscopic behavior of these systems is rather limited. The present study is undertaken with an objective to understand the microscopic behavior in terms of intermolecular interaction, structure and dynamics of these solvent systems. In the present study, few IL-IL mixtures are chosen with a common cation 1-butyl-3-methyl imidazolium, [C<sub>4</sub>C<sub>1</sub>im] and with a variation of anion namely, bis(trifluoromethylsulfonyl)amide [NTf<sub>2</sub>], hexafluorophosphate [PF<sub>6</sub>] and tetrafluoroborate [BF<sub>4</sub>]. Initially, investigations are done by studying the thermophysical properties of the concerned mixtures. Synergistic effect existing between the mixtures and the neat ILs are also studied through photochromism. Further, investigations on these mixtures are performed through steady state and time resolved fluorescence spectroscopy, nuclear magnetic resonance (NMR) and fluorescence correlation spectroscopy (FCS). The analysis of data essentially reveals that the mixtures of ILs that are used in the current study do not behave like a non-ideal solution. The behavior of the IL mixtures is observed to be more like quasi-ideal type.

---

#### 3. 1. Introduction

Ionic Liquids (ILs) are now considered as one of the most important classes of material due to their unique physiochemical properties such as large electrochemical window, negligible vapor pressure, high viscosity, high thermal stability etc.<sup>4, 17, 51, 248-250</sup> Another interesting aspect of

ILs is that the physiochemical properties of ILs can be tuned by an appropriate selection of cation and anion. Because of this reason, they are also known as “designer solvents.”<sup>55</sup> One of the ways through which the properties of ILs can be tuned is to combine two or more ILs through simple mixing.<sup>82</sup> Tuning of ILs by simple mixing is economical and less cumbersome than altering the molecular structure of the concerned ILs by chemical synthesis. It is interesting to note that an increase conductivity is observed for the mixture of ILs in comparison to individual ILs.<sup>17, 19, 251</sup> The IL-IL mixtures are interesting solvent systems but the usefulness of these system as a fluid material for several applications can only be realized when the solute-solvent interactions as well as the solvent-solvent interactions within the constitute of this material is completely understood. However, very limited numbers of studies have been carried out on these systems.

Welton’s group have discussed the ideal and non-ideal behavior of ionic liquid mixtures mainly focusing on their properties and applications.<sup>86</sup> A major finding consistent with the range of IL mixtures predicts the structure of IL mixtures dominated by the random distribution of ions driven by Columbic interaction.<sup>77, 78, 84, 85, 89, 91</sup> In the context of ideal and non-ideal behavior of IL mixture, the work by Marrucho and co-workers<sup>91</sup> is noteworthy. With the help of estimated the densities, viscosities and the molar volume of many IL mixtures, they have concluded that mixtures of ILs that are used in that study do not deviate in a significant extent from the ideal behavior.<sup>91</sup> A few studies on IL mixtures have also looked at the effect of H-bonding interactions with the IL mixtures.<sup>80, 252, 253</sup> Recently, Ludwig and coworkers<sup>88</sup> through molecular dynamics (MD) simulation studies have demonstrated that the behaviors of the protic ionic mixtures yield to a simple statistical analysis based upon the number of hydrogen bonding sites of the constituent ions. From the above discussions it is evident that though some studies on IL- IL mixtures are carried out but studies which aim to understand kinship among the interactions, structure and dynamics of the IL-IL mixtures are rather limited.

In this context, we would like to note that time-resolved fluorescence anisotropy, NMR, and fluorescence correlation spectroscopy (FCS) techniques have proven to be quite effective in providing molecular-level understanding on the microscopic behavior of the ILs<sup>254, 255</sup> and therefore these techniques are also expected to be quite helpful in understanding the intermolecular interactions, dynamics, and nanostructural organization of the IL-IL mixtures.

Keeping the above facts in mind, this chapter deals with different spectroscopic investigations on IL-IL mixtures (Figure 3.1). The IL-IL mixtures are constituted by mixing the concerned ILs in a definite mole fraction varying from 0.2 to 0.8. Prior to spectroscopic studies, thermophysical properties of IL mixtures have also been investigated. Synergistic behavior between the combining ILs have also been investigated through the photochromism studies. Solute-solvent and solvent-solvent interactions in the IL mixtures are carried out using the time-resolved fluorescence anisotropy studies. The data on mixtures of ILs have also been compared with the constituent pure IL so that the synergism that exists between the individual ILs are also understood. Additionally, all the relevant systems have been investigated through NMR and FCS so that a comprehensive understanding on the microscopic behavior in terms of intermolecular interaction, structure and dynamics of IL mixtures are obtained.

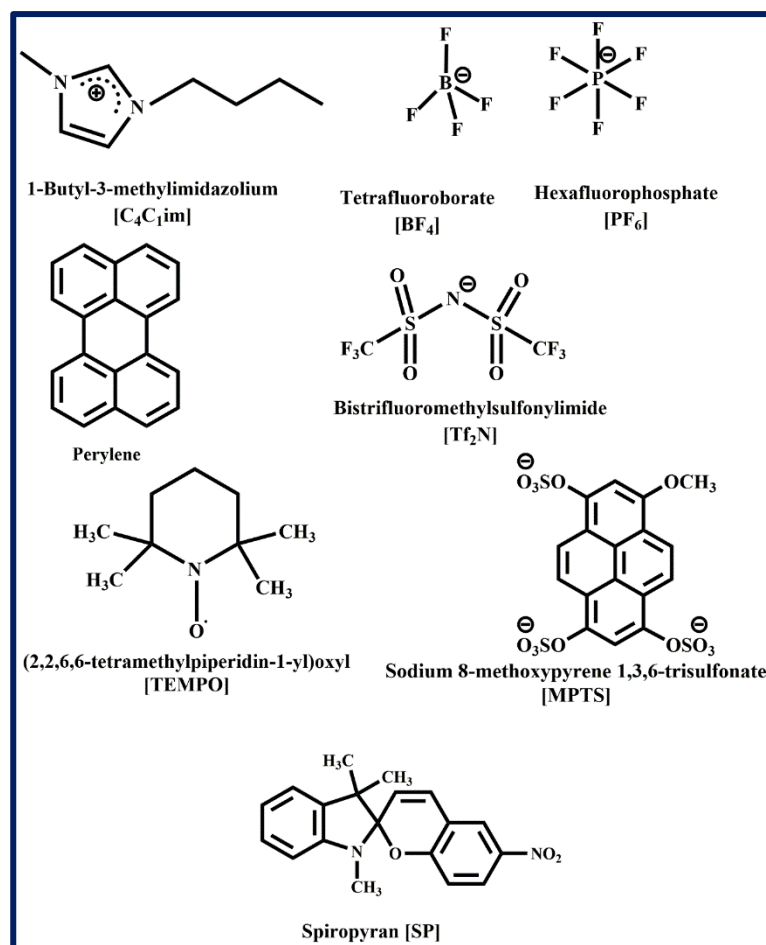


**Figure 3.1.** Molecular structures of ILs and probes used in the present study (Chapter 3).

### 3.2. Experimental techniques and methods

The ionic liquids [C<sub>4</sub>C<sub>1</sub>][BF<sub>4</sub>] and [C<sub>4</sub>C<sub>1</sub>][NTf<sub>2</sub>] were purchased from TCI Chemicals (>98% purity), and [C<sub>4</sub>C<sub>1</sub>][PF<sub>6</sub>] was obtained from Sigma-Aldrich (>99% purity). The halide ions and water content in these ILs are < 100 ppm. Spiropyran (SP), Perylene and MPTS were purchased from Sigma-Aldrich and used as received. The sample preparation procedures and experimental methods for thermophysical study, photochromism study, steady-state and time-resolved fluorescence studies, translational diffusion studies through NMR and fluorescence correlation study through FCS are described in detail in Chapter 2.

### 3.3. Results and discussion

#### 3.3.1. Thermophysical properties of ILs and IL-IL mixtures

Since many applications of a given solvent system depend on its physio-chemical properties,<sup>81, 256-259</sup> we have tried to understand the thermophysical properties<sup>257</sup> of IL mixtures

along with their constituent ILs. In this study, variation in viscosities and densities of the IL mixtures and that of individual ILs at different temperatures are illustrated in Table 3.1.

**Table 3.1.** Experimental viscosity ( $\eta$ ,cP) and density ( $\rho$ ,g/cm<sup>3</sup>) of individual ILs and mixtures

Neat ILs						
[C <sub>4</sub> C <sub>1</sub> ][BF <sub>4</sub> ]		[C <sub>4</sub> C <sub>1</sub> ][PF <sub>6</sub> ]		[C <sub>4</sub> C <sub>1</sub> ][NTf <sub>2</sub> ]		
T (K)	$\eta^a$	$\rho^b$	$\eta^a$	$\rho^b$	$\eta^a$	$\rho^b$
293	113.3	1.129	223.7	1.370	63.6	1.436
298	84.2	1.126	164.8	1.368	49.6	1.431
303	64.3	1.121	126.9	1.365	40.4	1.428
308	50.9	1.116	100.7	1.362	33.4	1.424
313	40.8	1.112	81.1	1.358	27.5	1.420
318	33.1	1.108	65.4	1.352	23.3	1.417
323	27.4	1.102	53.6	1.349	19.8	1.413
328	23.2	0.998	45.8	1.345	16.9	1.408
Mix I						
Mix I (A) <sup>x</sup>		Mix I (B) <sup>y</sup>		Mix I (C) <sup>z</sup>		
T (K)	$\eta^a$	$\rho^b$	$\eta^a$	$\rho^b$	$\eta^a$	$\rho^b$
293	142.6	1.236	184.4	1.274	202.5	1.315
298	122.6	1.228	136.1	1.271	143.6	1.308
303	110.7	1.221	113.4	1.265	105.7	1.298
308	91.5	1.214	86.3	1.261	79.5	1.291
313	80.5	1.206	71.9	1.256	59.5	1.282
318	71.6	1.201	53.6	1.250	44.2	1.274
323	62.4	1.192	44.5	1.244	32.4	1.268
328	48.3	1.180	36.7	1.239	24.6	1.256
Mix II						
Mix II (A) <sup>m</sup>		Mix II (B) <sup>n</sup>		Mix II (C) <sup>o</sup>		
T (K)	$\eta^a$	$\rho^b$	$\eta^a$	$\rho^b$	$\eta^a$	$\rho^b$

293	95.5	1.362	100.6	1.387	153.4	1.408
298	81.3	1.358	88.6	1.379	114.6	1.401
303	73.3	1.353	76.5	1.371	89.6	1.397
308	60.4	1.342	65.4	1.365	71.3	1.391
313	49.4	1.334	51.3	1.353	57.4	1.388
318	36.2	1.327	44.2	1.349	47.1	1.382
323	22.4	1.321	36.4	1.341	38.9	1.377
328	18.2	1.313	29.5	1.335	32.5	1.373
Mix III						
Mix III (A) <sup>p</sup>		Mix III (B) <sup>q</sup>			Mix III (C) <sup>r</sup>	
T (K)	$\eta^a$	$\rho^b$	$\eta^a$	$\rho^b$	$\eta^a$	$\rho^b$
293	70.5	1.318	83.4	1.339	88.4	1.367
298	52.4	1.313	64.5	1.333	69.5	1.361
303	45.5	1.305	51.9	1.328	58.8	1.354
308	39.6	1.294	42.4	1.324	46.3	1.346
313	30.3	1.282	34.8	1.317	38.4	1.338
318	24.3	1.271	29.1	1.310	31.5	1.329
323	19.5	1.267	24.6	1.303	26.4	1.321
328	14.6	1.261	21.0	1.300	21.2	1.316
<sup>x</sup> Mix I (A): [C <sub>4</sub> C <sub>1</sub> ][BF <sub>4</sub> ] <sub>0.4</sub> [PF <sub>6</sub> ] <sub>0.6</sub> ; <sup>y</sup> Mix I (B): [C <sub>4</sub> C <sub>1</sub> ][BF <sub>4</sub> ] <sub>0.6</sub> [PF <sub>6</sub> ] <sub>0.4</sub> ; <sup>z</sup> Mix I (C): [C <sub>4</sub> C <sub>1</sub> ][BF <sub>4</sub> ] <sub>0.8</sub> [PF <sub>6</sub> ] <sub>0.2</sub>						
<sup>m</sup> Mix II (A): [C <sub>4</sub> C <sub>1</sub> ][PF <sub>6</sub> ] <sub>0.4</sub> [NTf <sub>2</sub> ] <sub>0.6</sub> ; <sup>n</sup> Mix II (B) : [C <sub>4</sub> C <sub>1</sub> ][PF <sub>6</sub> ] <sub>0.6</sub> [NTf <sub>2</sub> ] <sub>0.4</sub> ; <sup>o</sup> Mix II (C): [C <sub>4</sub> C <sub>1</sub> ][PF <sub>6</sub> ] <sub>0.8</sub> [NTf <sub>2</sub> ] <sub>0.2</sub>						
<sup>p</sup> Mix III (A) : [C <sub>4</sub> C <sub>1</sub> ][BF <sub>4</sub> ] <sub>0.4</sub> [NTf <sub>2</sub> ] <sub>0.6</sub> ; <sup>q</sup> Mix III (B) : [C <sub>4</sub> C <sub>1</sub> ][BF <sub>4</sub> ] <sub>0.6</sub> [NTf <sub>2</sub> ] <sub>0.4</sub> ; <sup>r</sup> Mix III (C) : [C <sub>4</sub> C <sub>1</sub> ][BF <sub>4</sub> ] <sub>0.8</sub> [NTf <sub>2</sub> ] <sub>0.2</sub>						
<sup>a</sup> Error limit: $\pm 7\%$ ; <sup>b</sup> Error limit: $\pm 0.6\%$						

Interestingly, the data in Table 3.1 depicts the viscosities and densities of IL mixtures fall in between the individual ILs that they are composed of. This observation indicates that the viscosity and density of mixture of ILs is not a simple average of the viscosity and density of

individual ILs which constitute the mixture. To throw more light on the nature of these IL mixtures calculation of excess molar volume is necessary. The corresponding data of excess molar volume are collected in Table 3.2.

**Table 3.2:** The excess molar volumes calculated for IL-IL mixtures.

Systems	Excess molar volume ( $V_E^m$ )
Mix I (A)	$0.09 \pm 0.012$
Mix I (B)	$0.11 \pm 0.014$
Mix I (C)	$0.07 \pm 0.015$
Mix II (A)	$0.13 \pm 0.011$
Mix II (B)	$0.15 \pm 0.013$
Mix II(C)	$0.17 \pm 0.014$
Mix III(A)	$0.08 \pm 0.015$
Mix III(B)	$0.12 \pm 0.012$
Mix III (C)	$0.06 \pm 0.013$

Further, it has also been observed that the estimated values for excess molar volumes of IL-IL mixtures in the present study (Table 3.2) and the study carried out by Seddon and co-workers<sup>81</sup> are very similar. It has been found that the excess molar volume for these IL mixtures are lower than 0.5% of the molar volume of the concerned mixtures. These data essentially indicate that the mixture is not behaving like a non-ideal mixture rather the behaviour of the mixture is quasi-ideal type. Again, the temperature dependent viscosities of Mix I along with the concerned ILs are further analyzed by fitting the data using Vogel-Fulcher-Tammann (VFT) relationship<sup>65-67</sup> (Figure 3.2). From the Figure 3.2, it can be understood that the viscosity of IL-IL mixtures lies within the broad limits of viscosity values of the individual ILs.

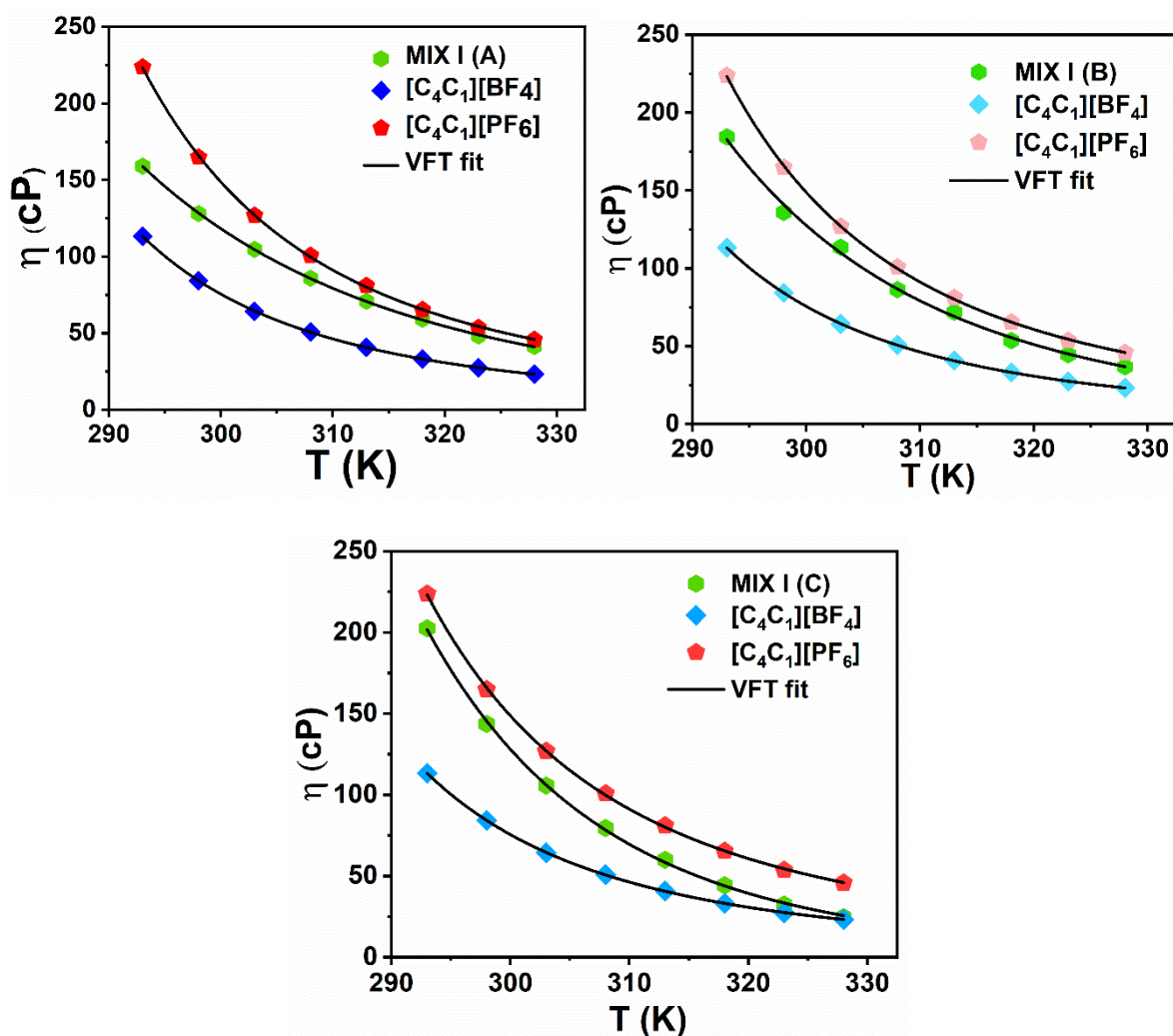


**Figure 3.2.** Variation of the bulk viscosity of  $[C_4C_1][BF_4]$ ,  $[C_4C_1][PF_6]$ , Mix I (A), Mix I (B) and Mix I (C) with temperature and its fitting with VFT equation.

We have also estimated the thermal expansion coefficients ( $\alpha$ ) of the individual ILs and their mixtures in Table 3.3. Please note that the thermal expansion coefficient describes the tendency of a material to change in shape, size, area and volume in a response to a change in temperature.<sup>260</sup> Therefore, the thermal expansion coefficient ( $\alpha_p$ ) is also known as volume expansivity.<sup>261</sup> As seen from the Table 3.3 that with increase in temperature the change in  $\alpha$  corresponding to IL mixtures is different to that of corresponding individual ILs. It can be also noted that the thermal expansion coefficient of Mix I and Mix II falls within the limits of the  $\alpha_p$  of the individual ILs. However, in case of Mix III,  $\alpha_p$  goes beyond the limits of neat ILs.

Perhaps this data points out that the structural organization and intermolecular interactions within the IL mixtures are quite different to that of the individual ILs.

**Table 3.3.** Thermal expansion coefficient values of ILs and IL mixtures as a function of temperature.

	Temperature (K)						
	Systems	293	298	303	308	313	318
$\alpha^{\#} \times 10^4 \text{ (K}^{-1}\text{)}$	[C <sub>4</sub> C <sub>1</sub> ][BF <sub>4</sub> ]	8.04	8.07	8.10	8.14	8.17	8.20
	[C <sub>4</sub> C <sub>1</sub> ][PF <sub>6</sub> ]	6.61	6.64	6.68	6.70	6.73	6.75
	[C <sub>4</sub> C <sub>1</sub> ][NTf <sub>2</sub> ]	5.27	5.28	5.30	5.32	5.34	5.37
	Mix I (A)	7.80	7.83	7.86	7.89	7.92	7.95
	Mix I (B)	7.55	7.58	7.61	7.64	7.67	7.70
	Mix I (C)	7.36	7.39	7.42	7.45	7.47	7.50
	Mix II (A)	6.99	7.01	7.04	7.06	7.09	7.11
	Mix II (B)	6.73	6.76	6.78	6.80	6.83	6.85
	Mix II (C)	6.50	6.52	6.54	6.56	6.58	6.61
	Mix III (A)	7.10	7.13	7.15	7.18	7.20	7.23
	Mix III (B)	6.97	6.99	7.02	7.05	7.07	7.10
	Mix III (C)	6.79	6.82	6.85	6.87	6.89	6.92

# Error limit:  $\pm 0.5\%$

### 3.3.2. Photochromic behavior of spiropyran in ILs and IL-IL mixtures

In this study, we have chosen different combinations of ILs along with parent ILs and have investigated the synergism existing between them through photochromic study. In this study, spiropyrans are known to exist in two isomeric forms, spiropyran form, SP and merocyanine form, MC exist in thermal equilibrium with each other and are represented in Figure 3.3. We would also like to note here that an idea about synergism between the two solvents can be obtained by following the dependence of relaxation rate of one isomer with the mole fraction of the solvent.<sup>180</sup>

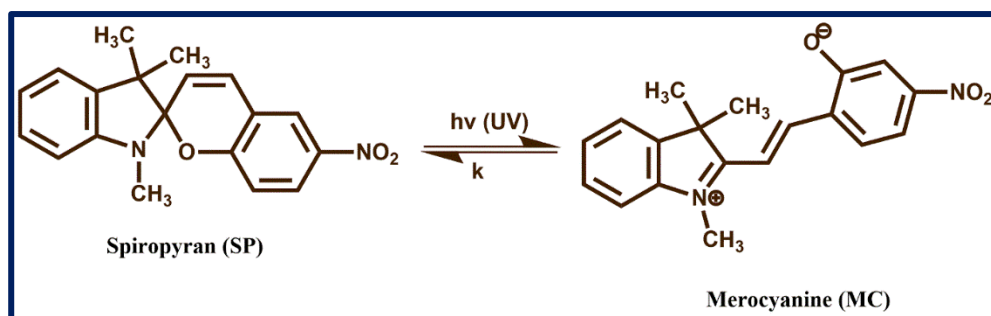


**Figure 3.3.** Schematic representation of interconversion of spiropyran and merocyanine with UV light irradiation.

The spiropyrans give rise to pale violet to violet colors when being dissolved in the IL mixtures. Please note that under UV light irradiation, the thermal equilibrium between SP and MC is disturbed and a change in color is seen due to the formation of MC.<sup>188</sup> It is also important to mention that after UV light irradiation, MC can thermally relaxes back to SP which can be easily monitored by following the decrease in absorption of MC.<sup>188</sup> Additionally it has been observed that the solution when stored in the dark lead to a gradual decay of the absorption band comprising of colored MC form, suggesting a conversion of the merocyanine form to the spiropyran form (MC  $\rightarrow$  SP). We have estimated the thermal relaxation rate constants of spiropyran derivative, 6-NO<sub>2</sub>-BIPS, in the IL mixtures where mole fractions of the concerned ILs are varied.

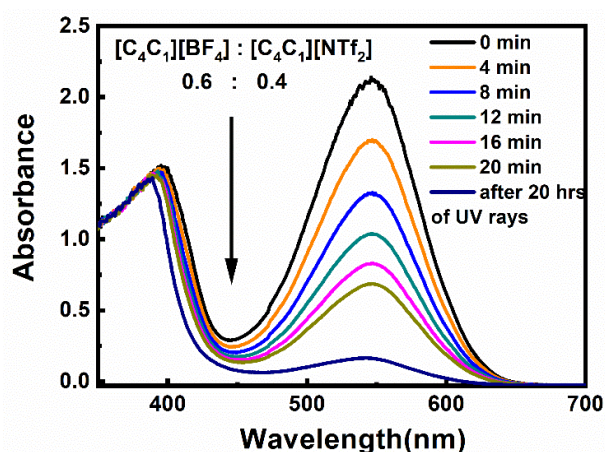


**Figure 3.4.** Overlay spectra illustrating the thermal decay of a solution of SP in Mix III after exposure to UV irradiation.

The representative time evolution of the absorbance band ( $\lambda_{\text{max}}^{\text{abs}}$ ) of MC in Mix I(B) for 0.6 mole fraction of  $[\text{C}_4\text{C}_1][\text{BF}_4]$  at 25 °C is given in Figure 3.4. After this, the decay rates of thermal relaxation from MC to SP have been estimated. The decay rate constants for the thermal relaxation of MC in ILs are obtained by monitoring absorption changes in regular interval for a MC-rich solution kept in the dark at constant temperatures (T) using the following equations 3.1 and 3.2:

$$A(t) = (A_0 - A_i)e^{-t/\tau} + A_i \quad (3.1)$$

$$\log\{A(t) - A_i/A_0 - A_i\} = -kt \quad (3.2)$$

$A(t)$  = absorbance at time  $t$

$A_0$  = absorbance just when irradiation is stopped

$A_i$  = absorbance before irradiation/ at after long time after UV irradiation/ absorbance of MC at equilibrium time

$k$  = thermal decay rate constant

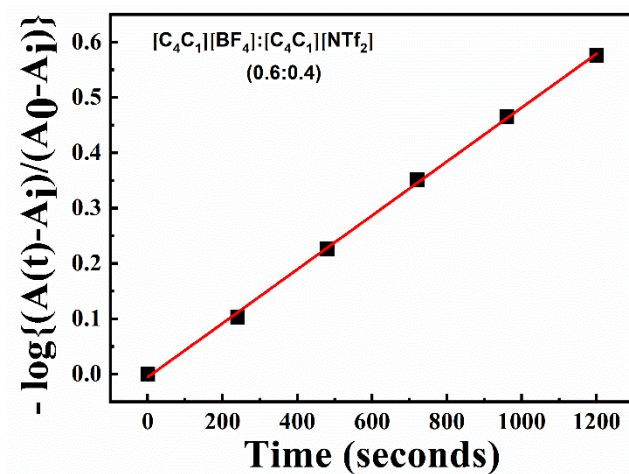


**Figure 3.5.** First-order kinetic plot of the thermal relaxation of the SP isomer in Mix III after 5 min UV irradiation.

The process of relaxation of the MC isomer to the Spiro form (SP) follows first order kinetics.<sup>188</sup> Here, we would like to mention that the average solvation time in ILs fall in ps-ns time scale.<sup>120, 262</sup> Figure 3.5 depicts the linear time evolution of the kinetics for thermal back isomerization process, MC  $\rightarrow$  SP for Mix III.

**Table 3.4.** Thermal relaxation rate constants of spiropyran derivatives in IL-IL mixtures.

Mix I		Mix II		Mix III	
$\chi_{[BMIM][BF_4]}$ in Mix I	k $\times 10^5$	$\chi_{[BMIM][PF_6]}$ in Mix II	k $\times 10^5$	$\chi_{[BMIM][BF_4]}$ in Mix III	k $\times 10^5$
0	5.88	0	4.78	0	4.89
0.2	15.48	0.2	21.38	0.2	15.13
0.4	28.84	0.4	30.90	0.4	24.54
0.6	53.70	0.6	33.11	0.6	48.97
0.8	19.05	0.8	22.38	0.8	15.84
1	10.01	1	5.75	1	12.58

The thermal relaxation rate constant values of spiropyran derivative in different IL mixtures are collected in Table 3.4. From Table 3.4 it can be observed that relaxation rate for all the different IL-IL mixtures having different constituent ILs are different indicating that the microscopic behavior of these solvent systems is quite different from each other. One can also see from Table 3.4 that for a particular IL mixtures relaxation rate constant, k, changes with a change in mole fraction of the constituent ILs. Additionally, one can note there exist synergistic effect in this photochromism study with respect to the mole fraction. This synergism is found in IL-IL mixtures with comparison to the neat ILs as the relaxation rate of IL-IL mixtures is very much composition dependent.

### 3.3.3. Time-resolved fluorescence study

In the present work through time resolved fluorescence anisotropy study, rotational motion of two structurally similar but chemically different organic solutes perylene and MPTS are investigated in IL-IL mixtures along with their constituent ILs at different temperatures. Structurally similar but chemically distinguishable solutes are chosen so that the solute solvent interactions prevailing in the particular medium are exclusively monitored. Analysis of the time

resolved fluorescence anisotropy data through hydrodynamic theory (explained in chapter 2) has proven to be quite useful in unraveling microscopic behavior of a given solvent system.

### 3.3.3.1. Perylene

A representative time resolved anisotropy decay of perylene and MPTS in IL mixtures (Mix I B) along with the constituent ILs are shown in Figure 3.6(a) and Figure 3.6(b) respectively. The rotational relaxation time for perylene in different ILs and (IL+IL) mixtures are listed in Table 3.5. From the Table 3.5, it can be mentioned that  $\tau_r$  decreases with the increase in temperature for all the systems due to the decrease in the bulk viscosity of the concerned medium upon increasing the temperature.

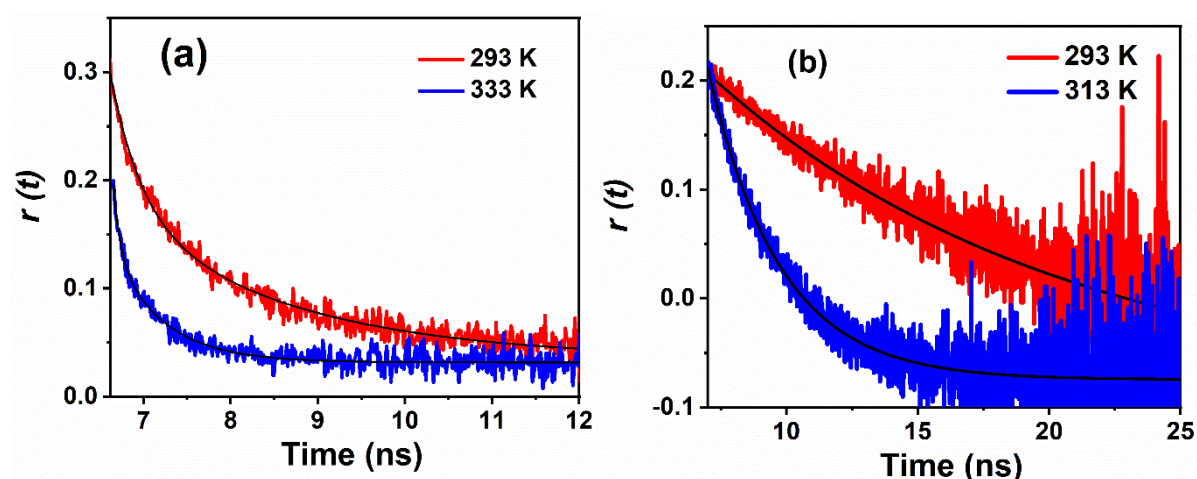


**Figure 3.6.** Representative time resolved fluorescence anisotropy decay profile of (a) perylene and (b) MPTS in Mix I (B) at two different temperatures. The black line denotes the fit to data points.

**Table 3.5.** The reorientation time ( $\tau_r$ ) of perylene and MPTS in  $[C_4C_1][BF_4]$ ,  $[C_4C_1][PF_6]$ ,  $[C_4C_1][NTF_2]$ , Mix I, Mix II and Mix III.

	Perylene			MPTS	
	Temp. (K)	$\tau_r^b$ (ns)	$C_{rot} <avg>$	$\tau_r^b$ (ns)	$C_{rot} <avg>$
$[C_4C_1][BF_4]$	293	1.23	$0.13 \pm 0.02$	12.51	$1.08 \pm 0.011$
	298	1.03		10.14	
	303	0.83		7.80	

	308	0.65		6.21	
	313	0.55		5.31	
[C <sub>4</sub> C <sub>1</sub> ][PF <sub>6</sub> ]	293	2.16	0.11 ± 0.013	20.00	1.04 ± 0.017
	298	1.71		16.83	
	303	1.34		14.66	
	308	1.08		12.56	
	313	0.84		11.10	
[C <sub>4</sub> C <sub>1</sub> ][NTf <sub>2</sub> ]	293	1.27	0.21 ± 0.015	10.47	1.39 ± 0.016
	298	1.02		8.63	
	303	0.84		7.85	
	308	0.68		6.89	
	313	0.58		6.04	
Mix I (A)	293	1.57	0.12 ± 0.016	16.71	1.01 ± 0.017
	298	1.41		14.44	
	303	1.23		12.13	
	308	1.02		9.79	
	313	0.95		8.87	
Mix I (B)	293	1.61	0.11 ± 0.018	15.54	0.80 ± 0.018
	298	1.32		12.11	
	303	1.11		9.91	
	308	0.89		7.56	
	313	0.72		6.40	
Mix I (C)	293	1.76	0.11 ± 0.011	21.67	0.98 ± 0.016
	298	1.58		18.81	
	303	1.46		16.13	
	308	1.34		14.92	
	313	1.18		12.82	
Mix II (A)	293	1.23	0.13 ± 0.019	13.41	1.28 ± 0.012
	298	1.11		11.86	

	303	0.95		10.43	
	308	0.82		9.28	
	313	0.68		7.98	
Mix II (B)	293	0.97	$0.13 \pm 0.016$	10.74	$1.22 \pm 0.018$
	298	0.81		9.62	
	303	0.74		8.67	
	308	0.67		7.83	
	313	0.58		6.92	
Mix II (C)	293	1.51	$0.12 \pm 0.015$	14.84	$1.24 \pm 0.011$
	298	1.27		11.67	
	303	1.00		9.98	
	308	0.85		7.21	
	313	0.66		6.56	
Mix III (A)	293	0.94	$0.15 \pm 0.012$	7.46	$1.09 \pm 0.014$
	298	0.75		6.37	
	303	0.65		5.32	
	308	0.57		4.86	
	313	0.44		4.12	
Mix III (B)	293	1.15	$0.16 \pm 0.019$	8.86	$1.10 \pm 0.018$
	298	0.91		7.17	
	303	0.76		6.34	
	308	0.62		5.14	
	313	0.46		4.71	
Mix III (C)	293	1.25	$0.16 \pm 0.02$	9.21	$1.07 \pm 0.017$
	298	0.98		7.83	
	303	0.85		6.92	
	308	0.69		5.54	
	313	0.62		5.02	

---

<sup>b</sup> Experimental error =  $\pm 5\%$

---

The data has been analysed further through Stokes-Einstein-Debye (SED) hydrodynamic model<sup>234, 235</sup> so as to get a comprehensive understanding of the solute dynamics in a given medium.

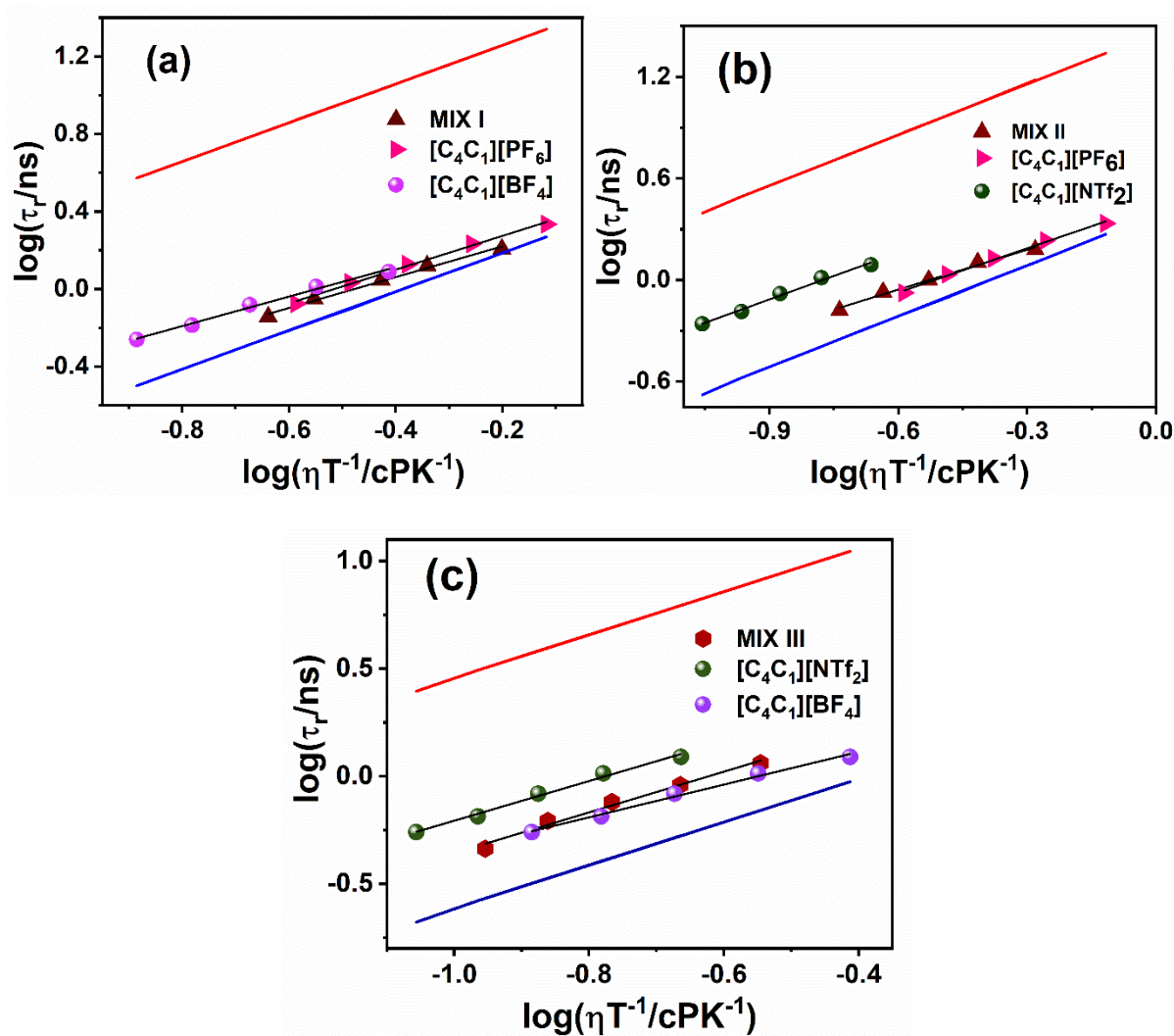


**Figure 3.7.** Log( $\tau_r$ ) vs. log( $\eta/T$ ) plot of perylene in (a) Mix I (b) Mix II and (c) Mix III with stick and slip boundary condition limits. The solid black lines indicate the fit to the data points. The red and blue lines represent the stick and slip boundary conditions. The composition of IL-IL mixtures are Mix I (B): $[C_4C_1][BF_4]_{0.6}[PF_6]_{0.4}$ ; Mix II (C) :  $[C_4C_1]PF_6]_{0.8}[NTf_2]_{0.2}$  and Mix III (B) :  $[C_4C_1][BF_4]_{0.6}[NTf_2]_{0.4}$ .

The SED plots pertaining to perylene motion in a particular composition of IL mixtures along with neat ILs are illustrated in Figure 3.7. However, upon a careful look at the plot one

can also see that in all the cases the behavior of perylene in IL mixtures are quite different than that of constituent ILs. We have further analyzed  $\tau_r$  by fitting  $\tau_r$  to an empirical relationship  $\tau_r = A(\eta/T)^n$  where  $A$  and  $n$  are constants.<sup>121, 178</sup> The exponent  $n$  represent the non-linearity in  $\tau_r$  vs  $\eta/T$  plot. Usually, rotational relaxation time is expected to linearly depend on the bulk viscosity of the solvent. The departure of the  $n$  value from unity can therefore be attributed to the decoupling of the rotational diffusion motion of the solute from the bulk viscosity of the medium.<sup>121, 178, 263, 264</sup> It has been shown earlier by our group and others that the viscosity-diffusion decoupling behavior in ILs can be caused due to the micro-heterogeneous nature of the medium.<sup>121, 178, 263, 264</sup>

Following relations are obtained for perylene:

Perylene in [C <sub>4</sub> C <sub>1</sub> ][BF <sub>4</sub> ]:	$\tau_r = (2.61 \pm 0.02)(\eta/T)^{0.67 \pm 0.03}$	(N = 5, R = 0.99)
Perylene in [C <sub>4</sub> C <sub>1</sub> ][PF <sub>6</sub> ]:	$\tau_r = (2.75 \pm 0.03)(\eta/T)^{0.61 \pm 0.03}$	(N = 5, R = 0.98)
Perylene in [C <sub>4</sub> C <sub>1</sub> ][NTf <sub>2</sub> ]:	$\tau_r = (4.89 \pm 0.06)(\eta/T)^{0.72 \pm 0.02}$	(N = 5, R = 0.98)
Perylene in Mix I (A):	$\tau_r = (1.63 \pm 0.04)(\eta/T)^{0.68 \pm 0.03}$	(N = 5, R = 0.99)
Perylene in Mix I (B):	$\tau_r = (2.34 \pm 0.07)(\eta/T)^{0.65 \pm 0.04}$	(N = 5, R = 0.98)
Perylene in Mix I (C):	$\tau_r = (1.46 \pm 0.05)(\eta/T)^{0.62 \pm 0.04}$	(N = 5, R = 0.98)
Perylene in Mix II (A):	$\tau_r = (1.93 \pm 0.04)(\eta/T)^{0.71 \pm 0.03}$	(N = 5, R = 0.99)
Perylene in Mix II (B):	$\tau_r = (1.53 \pm 0.03)(\eta/T)^{0.74 \pm 0.04}$	(N = 5, R = 0.98)
Perylene in Mix II (C):	$\tau_r = (2.57 \pm 0.02)(\eta/T)^{0.68 \pm 0.04}$	(N = 5, R = 0.99)
Perylene in Mix III (A):	$\tau_r = (2.13 \pm 0.05)(\eta/T)^{0.78 \pm 0.04}$	(N = 5, R = 0.99)
Perylene in Mix III (B):	$\tau_r = (1.77 \pm 0.02)(\eta/T)^{0.71 \pm 0.06}$	(N = 5, R = 0.98)
Perylene in Mix III (C):	$\tau_r = (2.28 \pm 0.03)(\eta/T)^{0.81 \pm 0.05}$	(N = 5, R = 0.99)

The deviation of  $n$  from unity indicates the micro-heterogeneity of the medium. This data in general illustrates that the microenvironment experienced by perylene in IL mixtures which again is found to be different in comparison to the neat ILs. More importantly, this data

categorically demonstrates that IL mixtures are not only spatially heterogeneous but they are also dynamically heterogeneous.

### 3.3.3.2 MPTS

Investigation has also been carried out by taking MPTS (negatively charged anion) solute and the rotational relaxation parameters are collected in Table 3.5. Interestingly, it can be seen that unlike perylene, the rotation of MPTS is much hindered in all the ILs and their mixtures. The data also suggests a stronger solute-solvent interaction in case of MPTS than that of perylene in the concerned media. Figure 3.8 represent the log-log plot of  $\tau_r$  vs  $\eta/T$  of MPTS for few compositions of IL mixtures along with the slip and stick boundary lines.

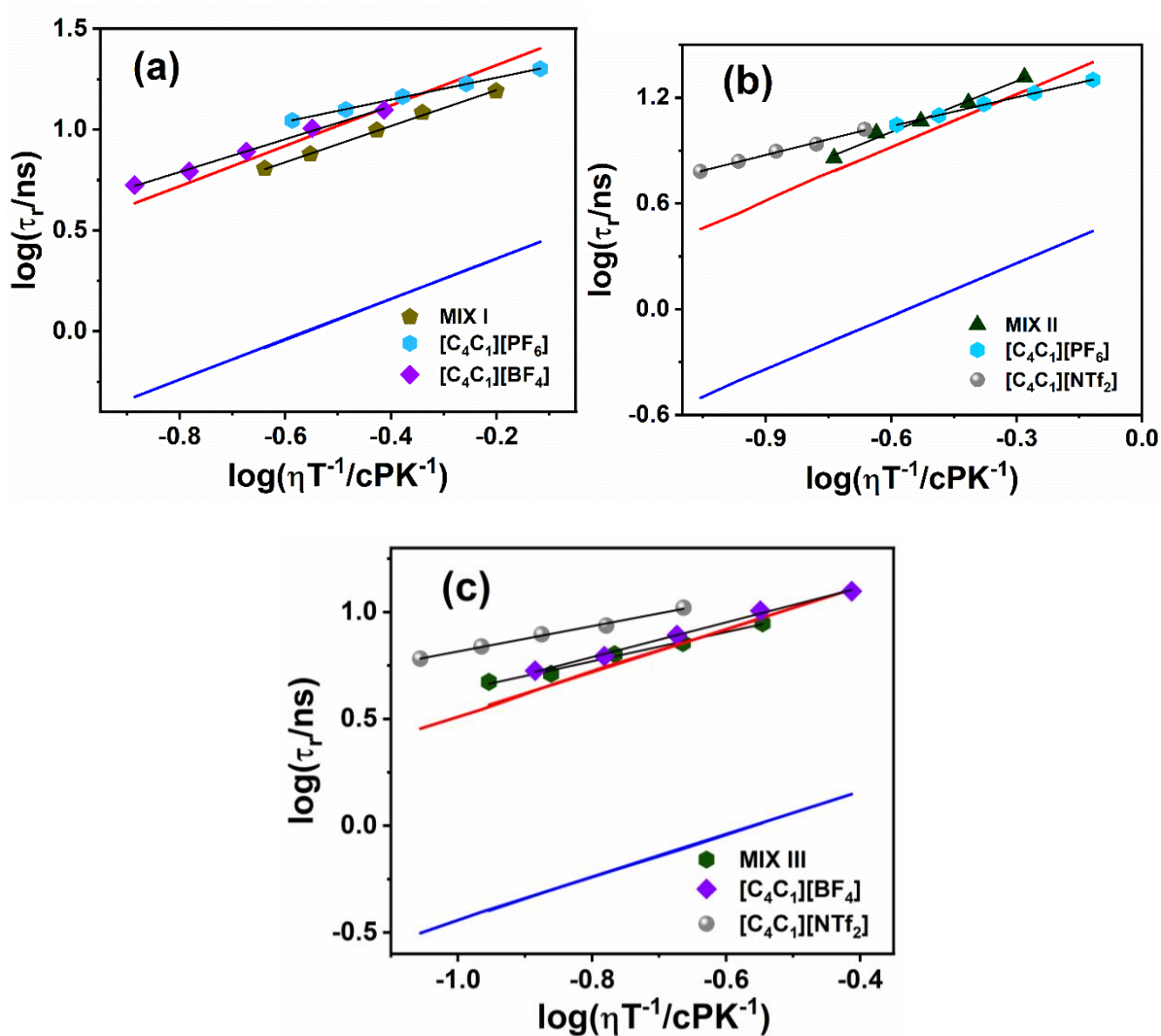


**Figure 3.8.** Log( $\tau_r$ ) vs. log( $\eta/T$ ) plot of MPTS in (a) Mix I (b) Mix II and (c) Mix III with stick and slip boundary condition limits. The solid black lines indicate the fit to the data points. The

red and blue lines indicate the stick and slip boundary conditions. The composition of IL-IL mixtures are Mix I (B): [C<sub>4</sub>C<sub>1</sub>][BF<sub>4</sub>]<sub>0.6</sub>[PF<sub>6</sub>]<sub>0.4</sub>; Mix II (C): [C<sub>4</sub>C<sub>1</sub>][PF<sub>6</sub>]<sub>0.8</sub>[NTf<sub>2</sub>]<sub>0.2</sub> and Mix III (B): [C<sub>4</sub>C<sub>1</sub>][BF<sub>4</sub>]<sub>0.6</sub>[NTf<sub>2</sub>]<sub>0.4</sub>.

From Figure 3.8, it can be observed that for all the systems the experimental rotational time lie above the stick line. In the hydrodynamic terminology this situation of rotation of MPTS is known as super-stick situation. This hindered rotation of MPTS essentially indicates strong solute-solvent interaction. The stronger solute-solvent interaction for MPTS has also been realized by estimating the rotational coupling constant ( $C_{rot}$ ), where  $C_{rot} = \tau_{r_{exp}}/\tau_{r_{stk}}$ .  $C_{rot}$  essentially indicates the extent of specific solute-solvent interaction. We note here that this super stick behavior arises due to the specific solute-solvent interaction prevailing in the medium.<sup>178, 199, 215, 265-267</sup> In this context, we would like to mention that the super stick behavior of monocationic ILs is also observed independently by many groups like Fayer<sup>266</sup>, Dutt<sup>267</sup> and by us.<sup>178</sup> The super stick behavior of MPTS in ILs can be attributed to the formation of strong hydrogen bonding interaction between the acidic C(2) hydrogen of imidazole and the sulphate groups of MPTS.<sup>268</sup> It has been shown that the highly acidic nature ( $pK_a \sim 28.3$ )<sup>268</sup> of C(2) hydrogen of imidazole is capable of forming hydrogen bonds with the negatively charged MPTS moiety. In the present study, SED plots (Figure 3.8) and  $C_{rot}$  values (Table 3.5) demonstrate the structural organization of IL-IL mixtures along with the neat ILs.

### 3.3.4. NMR and FCS studies

#### 3.3.4.1. NMR studies

Recently the PFG-NMR technique has proven to be quite useful in providing information about the translational diffusion of cations and anions of ILs.<sup>269-272</sup> The outcome of PFG-NMR study can provide an idea about the size and the diffusivity of the diffusing species which in turn helps us in viewing the microscopic structural organization of ILs. The translational diffusion coefficient for the mixtures of ILs along with the constituent neat ILs at room temperature are enlisted in Table 3.6. The diffusion data illustrates the diffusion of the

“cationic moiety” in case of all the systems. In case of IL-IL mixtures, the diffusion coefficient data is an averaged-out effect of the cations arising from the neat ILs.

**Table 3.6.** Diffusion coefficients of the concerned ILs and IL mixtures at 298 K.

Systems	Diffusion coefficient (m <sup>2</sup> /s)
[C <sub>4</sub> C <sub>1</sub> ][BF <sub>4</sub> ]	1.203 × 10 <sup>-11</sup>
[C <sub>4</sub> C <sub>1</sub> ][PF <sub>6</sub> ]	0.952 × 10 <sup>-11</sup>
[C <sub>4</sub> C <sub>1</sub> ][NTf <sub>2</sub> ]	2.751 × 10 <sup>-11</sup>
Mix I	0.825 × 10 <sup>-11</sup>
Mix II	1.086 × 10 <sup>-11</sup>
Mix III	1.768 × 10 <sup>-11</sup>

From the Table 3.6, it is observed that the diffusion coefficient for Mix I is lower than the diffusion coefficients of concerned ILs, whereas in case of Mix II the diffusion coefficient is found to be slightly higher than the diffusion coefficients of the individual ILs involved. It is quite interesting to note that in case of Mix III, diffusion coefficient of the averaged cationic radii is estimated to be in between the values estimated for concerned pure ILs. This data indicates that the structural organization of these IL-IL mixtures are different in comparison to individual ILs.

### 3.3.4.2. FCS studies

To understand the various intermolecular interactions involving fluorescent molecules, measuring the diffusion coefficient of fluorescent species through FCS is quite helpful as the diffusion coefficient depends on the molecular mass, size and the shape of the diffusing fluorescent species.<sup>174, 177, 215, 220, 273-276</sup> The representative diffusion curve of Mix I has been illustrated in Figure 3.9 and the data corresponding to the translation diffusion coefficient of the IL-IL mixtures and constituent ILs estimated from the FCS study are collected in Table 3.7.

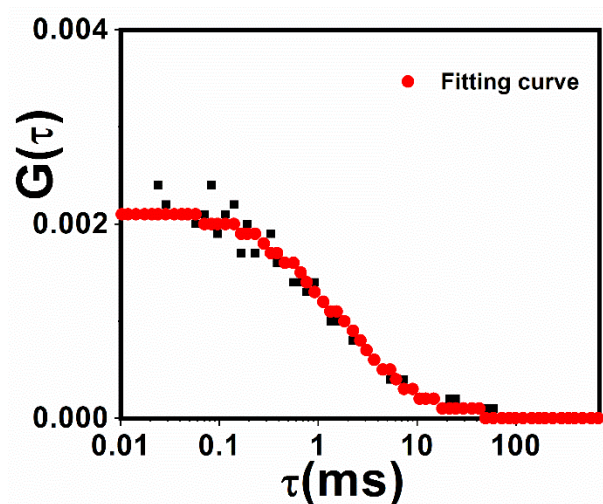


**Figure 3.9.** The representative FCS plot for Mix I.

**Table 3.7.** Parameters obtained through FCS for IL mixtures and constituent ILs at 298 K.

Systems	Conc.(nM)	$D(\mu\text{m}^2\text{s}^{-1})$	Viscosity(cP)	$R(\text{\AA})$
$[\text{C}_4\text{C}_1][\text{BF}_4]$	$1141 \pm 11$	$6.55 \pm 0.72$	$84.2 \pm 0.65$	3.9
$[\text{C}_4\text{C}_1][\text{PF}_6]$	$706 \pm 16$	$2.16 \pm 0.26$	$164.8 \pm 0.61$	6.1
$[\text{C}_4\text{C}_1][\text{NTf}_2]$	$1842 \pm 14$	$10.02 \pm 0.78$	$49.6 \pm 0.69$	4.4
Mix I	$1267 \pm 36$	$3.98 \pm 0.42$	$136.1 \pm 0.68$	4.0
Mix II	$1075 \pm 44$	$4.09 \pm 0.28$	$114.6 \pm 0.61$	4.6
Mix III	$1770 \pm 14$	$8.03 \pm 0.68$	$64.5 \pm 0.66$	4.2

The hydrodynamic radii of Mix I,  $[\text{C}_4\text{C}_1][\text{BF}_4]$  and  $[\text{C}_4\text{C}_1][\text{PF}_6]$  are estimated to be 4.0 Å, 3.9 Å and 6.1 Å respectively. Further, hydrodynamic radii of Mix I, Mix II and Mix III are estimated to be 4.0 Å, 4.6 Å and 4.2 Å respectively. This observation shows that the hydrodynamic radii of IL-IL mixtures are different from each other. In general, both diffusion coefficients that are estimated from NMR and FCS studies demonstrate that the nano structural organizations of these IL mixtures are quasi-ideal in nature with respect to the concerned pure constituent ILs. All these data essentially signify that the microscopic behavior of these IL mixtures depicts a new picture of these mixtures in comparison to its bulk nature.

### 3.4. Conclusion

This chapter delineates the outcome of a combined steady state, time-resolved fluorescence, NMR and FCS investigations of several binary mixtures of ILs along with the constituent pure ILs that they are composed of. The microscopic behavior in terms of intermolecular interaction, structure and dynamics of the binary mixtures of ILs and pure ILs have been carried so that the differences in behavior between pure ILs and IL mixtures are understood. Viscosity, density and thermal expansion coefficient values of ILs and IL-IL mixtures that are obtained from thermophysical studies have revealed that the thermophysical parameters for IL-IL mixtures are within the broad limits of the concerned parameter of neat ILs constituting the mixture. Studies on excess molar volume calculations do not reveal any non-ideal behavior of the mixtures. Again, the time resolved fluorescence anisotropy studies have also revealed that IL-IL mixtures are not only spatially heterogeneous but they are dynamically heterogeneous too. Measurements of both rotational diffusion through TRFA studies and measurements of translational diffusion coefficients of the diffusing species through NMR and FCS studies have provided idea about the nano-structural organization within these binary mixtures of ILs. The analysis of the data essentially reveals that the mixtures of ILs that are used in the current study do not behave like a non-ideal solution. The behavior of the IL mixtures is observed to be more like quasi-ideal type. The outcome of the present study is expected to be useful in understanding the microscopic behavior of IL-IL mixtures and their use towards various applications.

## CHAPTER 4

---

# Thermophysical and Spectroscopic Investigations on Imidazolium and Pyrrolidinium-based Monocationic ILs and their Binary Mixtures with Common Anion

---

---

Chakraborty, M.; Barik, S.; Mahapatra, A.; Sarkar, M. *J. Chem. Phys.* **2021**, *154*, 224507.

## Chapter 4

---

### Thermophysical and Spectroscopic Investigations on Imidazolium and Pyrrolidinium-based Monocationic ILs and their Binary Mixtures with Common Anion

---

The mixing of ILs provide an opportunity to fine tune the physicochemical properties of ILs such that these resultant mixtures can be used in various targeted applications. However, a suitable mixture having desired properties can only be designed when the physicochemical properties of the mixtures of ILs along with their spectroscopic properties are well understood. With an aim to achieve this objective three different mixtures with a common anion namely  $[C_2C_1im][C_4C_1im][NTf_2]$ ,  $[C_3C_1pyr][C_4C_1pyr][NTf_2]$  and  $[C_3C_1im][C_3C_1pyr][NTf_2]$  are investigated in the current study. Investigations are carried out at the macroscopic level by observing the thermophysical properties like molar volume, thermal expansion coefficient etc. and at microscopic level with the time-resolved fluorescence measurements and pulse field gradient NMR technique. The present investigation reveals that the mixtures show appreciable deviation from ideal behaviour and the departure from the ideal behaviour is caused due to the generation of free volume in the resultant mixture.

---

#### 4. 1. Introduction

Mixing of two or more ILs with known properties may allow one to finely tune these properties to obtain an interesting solvent system with desired properties.<sup>87</sup> As ILs are mixed together, unique interactions within the IL mixtures may arise.<sup>76</sup> Recently, Knorr et al.<sup>277</sup> have also found the existence of hydrogen bonding not only between anions and cations but also among cations themselves. They have also observed spectroscopic evidence of jumping and pecking (intermolecular attractions) of the cholinium cation on anions in ILs as well as the H-

bond enhanced cation–cation interaction in the same ILs.<sup>277</sup> These observations essentially indicate that the properties of IL mixtures are quite complex in nature. However, knowledge on the mixture of ILs is rather limited in terms of understanding the kinship among structure–property relationships. Therefore, an understanding of the structure and physicochemical properties of ILs is very much needed so that the mixing approach can be successfully employed to develop suitable solvent systems for targeted applications. In recent times, keeping in mind the potential applications of the binary mixture of ILs, some investigations have been carried out by employing both experimental and theoretical methods.<sup>79, 278-280</sup> Moreover, recent works on IL mixtures have demonstrated that intermolecular hydrogen bonding within the IL mixture may lead to the formation of ideal and non-ideal mixtures.<sup>90, 117, 281-283</sup> For example, a set of binary mixtures of imidazolium ILs shows a significant positive excess molar volume, depicting a non-ideal mixture, whereas in another set of binary mixture of IL, it has been found that the mixture does not deviate significantly from the ideal behavior. These variations in the behavior of IL mixtures are expected to arise from their structural organization.<sup>9, 82, 132, 284</sup> Some studies on ILs have pointed out that intermolecular interactions such as hydrogen bonding interaction within a particular mixture can play an important role in the formation of ideal and non-ideal mixtures. The recent work by Brooks et al.<sup>132</sup> on this aspect is found to be extremely significant. They have shown a linkage between the spatial arrangement and the free volume of IL mixtures containing a common  $[C_4C_{1im}]^+$  cation and different anions through different experimental techniques. The obtained results pertaining to the free volume are found to strongly correlate with each other despite the vast difference in their experimental timescale.<sup>132</sup> Moreover, it has been shown that fluxional processes such as hydrogen bonding do not significantly contribute to the free volumes of the IL–IL mixtures as compared to the spatial arrangement of ions arising from the size, shape, and electrostatic interaction.<sup>132</sup> The above-mentioned discussion clearly shows that the arena of the binary

mixture of ILs still remains hazy. Consequently, assigning a particular IL mixture an ideal, non-ideal, or some other behavior different from that mentioned in these concepts is still a matter of challenge. To overcome this issue, comprehensive studies focusing on the structure–property relationship in the IL mixture are needed. Although some studies have been carried out on the IL–IL mixture with variation in anions, studies aimed at understanding the interactions and the role of ions in the structure–property relationship in a binary mixture of ILs with variation in cations are rather limited.

Keeping the above-mentioned facts in mind, the work in this chapter have been carried out to understand the behavior of the binary mixture of ILs (Figure 4.1), which are formed by taking imidazolium and pyrrolidinium ILs with bis(trifluoromethylsulfonyl)imide [NTf<sub>2</sub>] as the common anion and various cations such as 1-alkyl-3- methylimidazolium with n = 2, 3, 4, [C<sub>2</sub>C<sub>1</sub>im], [C<sub>3</sub>C<sub>1</sub>im], [C<sub>4</sub>C<sub>1</sub>im], and 1-alkyl-3-methylpyrrolidinium with n = 3, 4, [C<sub>3</sub>C<sub>1</sub>pyr] and [C<sub>4</sub>C<sub>1</sub>pyr]. Moreover, imidazolium and pyrrolidinium based ILs are purposefully chosen so that the role of cations (imidazolium and pyrrolidinium ILs) in governing the thermodynamic properties of the said mixtures, if any, is understood. The binary mixtures of ILs are constituted by mixing the concerned ILs in a definite mole fraction. Variation in the mole fraction has been set from 0.2 to 0.8. Our first set of the binary IL–IL mixture constitutes of pure imidazolium moieties, [C<sub>2</sub>C<sub>1</sub>im][C<sub>4</sub>C<sub>1</sub>im][NTf<sub>2</sub>], the second set of the IL–IL mixture constitutes of pure pyrrolidinium moieties, [C<sub>3</sub>C<sub>1</sub>pyr][C<sub>4</sub>C<sub>1</sub>pyr][NTf<sub>2</sub>], and the third set of the binary IL mixture is formed with the combination of imidazolium and pyrrolidinium ILs, [C<sub>3</sub>C<sub>1</sub>im][C<sub>3</sub>C<sub>1</sub>pyr][NTf<sub>2</sub>]. Investigations are carried out using TRFA and PFG-NMR techniques. Analysis of the present study depicts that the structural organization in the case of the binary mixture of imidazolium ILs is very different from that of pyrrolidinium ILs. The present work demonstrates some interesting correlation between free volume and structural

organization of ILs and their mixture. The study shows that the behavior of the binary mixture of ILs is found to be neither ideal nor non-ideal; rather, it is quasi-ideal in nature.

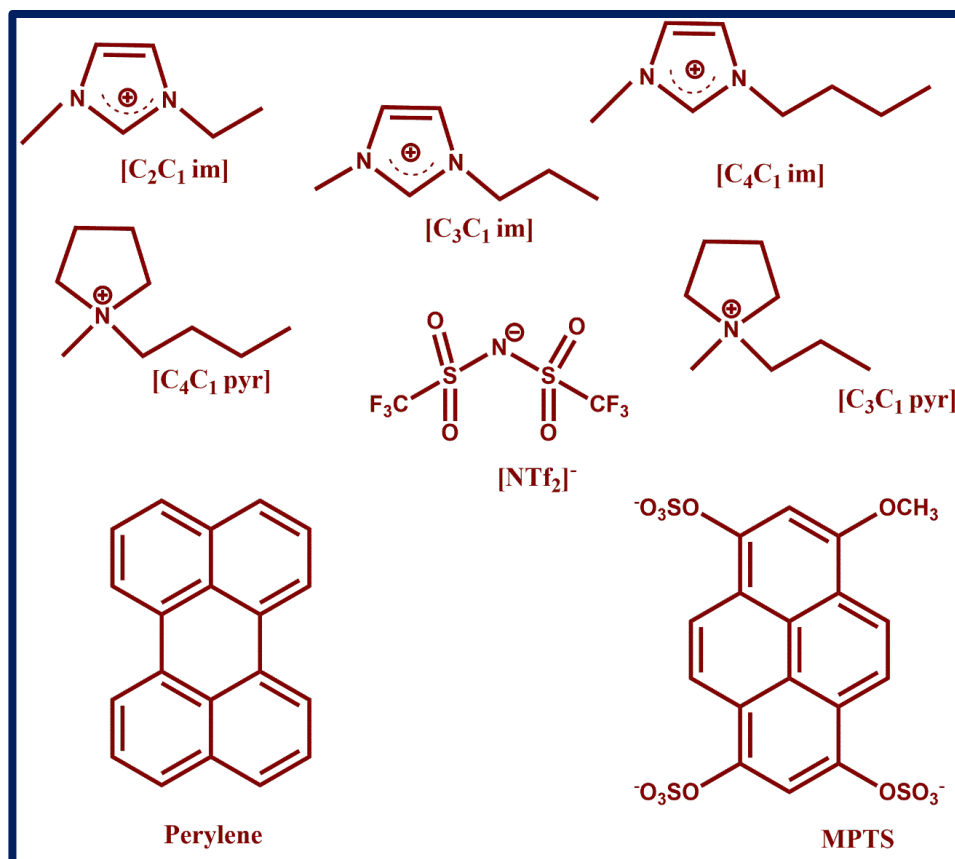


**Figure 4.1.** Molecular structures of ILs and probes used in the present study (chapter 4).

#### 4.2. Experimental techniques and methods

The ionic liquids [C<sub>2</sub>C<sub>1</sub>im][NTf<sub>2</sub>], [C<sub>4</sub>C<sub>1</sub>im][NTf<sub>2</sub>], [C<sub>3</sub>C<sub>1</sub>im][NTf<sub>2</sub>], [C<sub>3</sub>C<sub>1</sub>pyr][NTf<sub>2</sub>], and [C<sub>4</sub>C<sub>1</sub>pyr][NTf<sub>2</sub>] were purchased from TCI Chemicals (>98% purity). Perylene and MPTS were purchased from Sigma-Aldrich and used as received. Prior to the usage, the ILs were kept in high vacuum to avoid moisture. Instrumental techniques for time-resolved fluorescence as well as NMR experiments have been described in Chapter 2. Details of procedures for data analysis have also been discussed in Chapter 2.

### 4.3. Results and discussions

#### 4.3.1. Thermophysical properties of ILs and their binary mixtures

Densities of the neat ILs and their binary mixtures have been estimated at various temperatures, which are listed in Table 4.1. To minimize the error in the estimated parameters, all the measurements have been carried out multiple times. During the investigations, it has been observed that with an increase in temperature, densities of the neat ILs as well as their binary mixtures decreases. Moreover, the analysis of the data also reveals that the density in the case of IL–IL binary mixtures is not a simple averaged-out effect arising out of individual ILs that constitute the mixture.

**Table 4.1.** The experimental density ( $\rho$ ) of neat ILs and their binary mixtures.

Systems	293 K	298 K	303 K	308 K	313 K
	$\rho^b$ (g/cm <sup>3</sup> )				
[C <sub>2</sub> C <sub>1</sub> im] [NTF <sub>2</sub> ]	1.521	1.516	1.512	1.506	1.502
[C <sub>4</sub> C <sub>1</sub> im] [NTF <sub>2</sub> ]	1.436	1.431	1.428	1.424	1.42
[C <sub>3</sub> C <sub>1</sub> pyr] [NTF <sub>2</sub> ]	1.454	1.449	1.444	1.439	1.433
[C <sub>3</sub> C <sub>1</sub> im] [NTF <sub>2</sub> ]	1.479	1.474	1.469	1.464	1.459
[C <sub>4</sub> C <sub>1</sub> pyr] [NTF <sub>2</sub> ]	1.399	1.394	1.389	1.384	1.379
[C <sub>2</sub> C <sub>1</sub> im] <sub>0.2</sub> [C <sub>4</sub> C <sub>1</sub> im] <sub>0.8</sub>	1.183	1.176	1.171	1.165	1.161
[C <sub>2</sub> C <sub>1</sub> im] <sub>0.4</sub> [C <sub>4</sub> C <sub>1</sub> im] <sub>0.6</sub>	1.263	1.259	1.251	1.244	1.239
[C <sub>2</sub> C <sub>1</sub> im] <sub>0.6</sub> [C <sub>4</sub> C <sub>1</sub> im] <sub>0.4</sub>	1.305	1.297	1.291	1.284	1.278
[C <sub>2</sub> C <sub>1</sub> im] <sub>0.8</sub> [C <sub>4</sub> C <sub>1</sub> im] <sub>0.2</sub>	1.373	1.368	1.361	1.353	1.349
[C <sub>3</sub> C <sub>1</sub> pyr] <sub>0.2</sub> [C <sub>3</sub> C <sub>1</sub> im] <sub>0.8</sub>	1.471	1.466	1.461	1.456	1.45
[C <sub>3</sub> C <sub>1</sub> pyr] <sub>0.4</sub> [C <sub>3</sub> C <sub>1</sub> im] <sub>0.6</sub>	1.472	1.461	1.454	1.45	1.445
[C <sub>3</sub> C <sub>1</sub> pyr] <sub>0.6</sub> [C <sub>3</sub> C <sub>1</sub> im] <sub>0.4</sub>	1.461	1.456	1.451	1.446	1.44

[C <sub>3</sub> C <sub>1</sub> pyr] <sub>0.8</sub> [C <sub>3</sub> C <sub>1</sub> im] <sub>0.2</sub>	1.456	1.451	1.446	1.441	1.435
[C <sub>3</sub> C <sub>1</sub> pyr] <sub>0.2</sub> [C <sub>4</sub> C <sub>1</sub> pyr] <sub>0.8</sub>	1.407	1.402	1.397	1.392	1.387
[C <sub>3</sub> C <sub>1</sub> pyr] <sub>0.4</sub> [C <sub>4</sub> C <sub>1</sub> pyr] <sub>0.6</sub>	1.418	1.413	1.408	1.403	1.397
[C <sub>3</sub> C <sub>1</sub> pyr] <sub>0.6</sub> [C <sub>4</sub> C <sub>1</sub> pyr] <sub>0.4</sub>	1.429	1.424	1.419	1.414	1.408
[C <sub>3</sub> C <sub>1</sub> pyr] <sub>0.8</sub> [C <sub>4</sub> C <sub>1</sub> pyr] <sub>0.2</sub>	1.44	1.435	1.43	1.425	1.419

---

<sup>b</sup>Experimental error:  $\pm 0.001$

---

To have a proper understanding of the nature of the IL–IL binary mixture, calculation of excess molar volume is necessary. The excess molar volume ( $V_M^E$ ) of all the mixtures have been calculated by the following eq. (4.1):

$$V_M^E/cm^3 mol^{-1} = \frac{(x_1 M_1 + x_2 M_2)}{\rho_{12}} - \left( \frac{x_1 M_1}{\rho_1} \right) - \left( \frac{x_2 M_2}{\rho_2} \right) \quad (4.1)$$

where  $\rho_{12}$  denotes densities of the mixture and  $x_1$ ,  $M_1$ ,  $\rho_1$  and  $x_2$ ,  $M_2$ ,  $\rho_2$  are mole fractions, molecular weights and densities of pure components 1 and 2 respectively. The excess molar volume is found to be less than 0.5% of the mixture volume, showing a near ideal condition in the mixture. Additionally, to gain more insight on the ideal behaviour of mixture, the excess molar volume for the mixture of ILs have been fitted by reduced Redlich-Kister (R-K)<sup>285</sup> equation shown in Figure 4.2. The reduced R-K function is more sensitive as it accounts for the various hidden interactions within the ionic liquids.<sup>285</sup> The reduced R-K equation at fixed temperature T is given as below eq. (4.2):

$$Y^E = x_1(1 - x_1) \sum_{p=0}^{p=n} A_{n,p,T} (2x_1 - 1)^p \quad (4.2)$$

where  $Y^E$  denotes  $V_M^E$  and  $n$  is the optimal number of parameters ( $n = 3$  or  $4$ ). The coefficients  $A_{n,p,T}$  in equation 2 are regressed by applying the least-square fit method. The values of  $V_M^E$  obtained for different mixtures of ILs are not smaller than the experimental uncertainty

(uncertainty of the density measurement is found to be more than  $0.1 \text{ cm}^3 \text{ mol}^{-1}$ ) indicating that these values are significant.

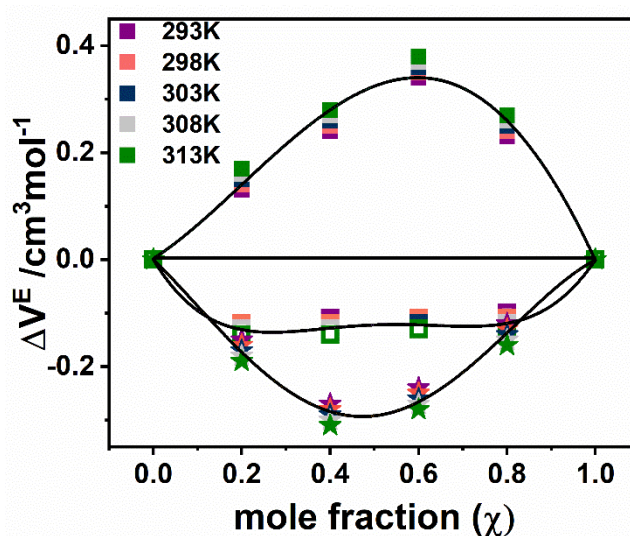


**Figure 4.2.** Plot of excess molar volumes ( $V^E / \text{cm}^3 \text{ mol}^{-1}$ ) of binary mixtures of ILs for  $T = 293 \text{ K}$ ,  $298 \text{ K}$ ,  $303 \text{ K}$ ,  $308 \text{ K}$  and  $318 \text{ K}$ . The solid boxes are for pure imidazolium IL-IL mixture. The open boxes are for pure pyrrolidinium IL-IL mixtures. The solid stars are for mixture of pyrrolidinium IL and imidazolium IL.

In the present study, as can be seen from the Figure 4.2, a positive deviation in the excess molar volume have been observed for  $[\text{C}_2\text{C}_1\text{im}][\text{C}_4\text{C}_1\text{im}]$ . This increase in the excess molar volume can be due to the free volume (vide infra) generated by the alkyl chain.<sup>286</sup> In this context, we would like to mention that a very small positive deviation in the excess molar volumes in imidazolium-based IL-IL mixtures composed of similar cations but different anions had also been observed by us earlier.<sup>219</sup> Further, from the Figure 4.2, it can be seen that the pyrrolidinium based IL-IL mixture show a small negative deviation that perhaps has arisen due to the fact that the density of pyrrolidinium based ILs is lower than that of imidazolium IL causing an increase in the free volume. Such negative deviations have also been observed by other researchers in mixtures containing  $\text{BF}_4$  (tetrafluoroborate) and  $\text{NTf}_2$  based ILs.<sup>287</sup> Furthermore, as can be seen from Figure 4.2, in case of a mixture of imidazolium and pyrrolidinium IL, the excess deviation in the molar volume is found to be somewhat negative

and suggests the presence of free volume in the said mixture. In addition, to get more insight into the behavior of the IL–IL mixture, the isobaric thermal expansivity has been determined from the density of neat ILs as well as their mixture. Thermal expansion coefficient ( $\alpha$ ) has been obtained by using the following eq. (4.3):

$$\alpha_{\rho} = -\frac{1}{\rho} \left( \frac{\delta\rho}{\delta T} \right)_{\rho} = -\frac{A_3}{A_2 + A_3 T} \quad (4.3)$$

where  $A_2$ ,  $A_3$  are the fitting parameters,  $\alpha$  and  $T$  are the thermal expansion coefficient and absolute temperature respectively. To evaluate the deviation of IL-IL mixture from the ideal condition, Benson and Kiyohara criterion<sup>288</sup> have been used to define the ideal thermal expansivity. The experimental values of thermal expansivity in the binary mixture of ILs have been depicted in Figure 4.3.

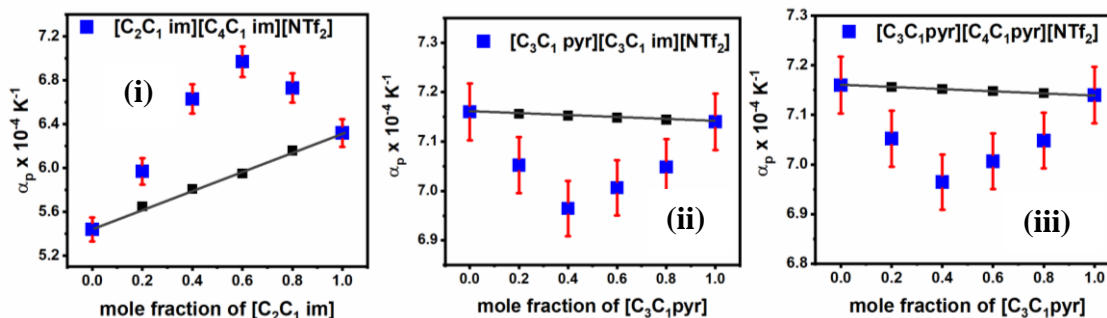


**Figure 4.3.** Thermal expansion coefficients of binary mixture of ILs: (i) mole frac. of  $[\text{C}_2\text{C}_1\text{im}]$  in the  $[\text{C}_2\text{C}_1\text{im}][\text{C}_4\text{C}_1\text{im}]$  mix., (ii) mole frac. of  $[\text{C}_3\text{C}_1\text{pyr}]$  in the  $[\text{C}_3\text{C}_1\text{pyr}][\text{C}_3\text{C}_1\text{im}]$  mix. and (iii) mole frac. of  $[\text{C}_3\text{C}_1\text{pyr}]$  in the  $[\text{C}_3\text{C}_1\text{pyr}][\text{C}_4\text{C}_1\text{pyr}]$  mix. The black solid rectangle represents the thermal expansion coefficient calculated with Benson Kiyohara criterion.

From the Figure 4.3, one can vividly see that the IL-IL mixtures used in the present study do not fit into the ideal model. It is important to mention here that with regards to composition dependence, the experimental values are distributed with a positive deviation from the ideal condition in case of imidazolium-based IL mixtures, while a negative deviation for both pyrrolidinium based IL mixtures as well as a combination of imidazolium and pyrrolidinium based IL mixture. These deviations are not within the limit of experimental uncertainty

indicating a quasi-ideal behaviour of IL-IL mixtures. To have further understanding on the behavior of the IL mixtures, viscosities of all the ILs and their binary mixtures have been measured and plotted in Figure 4.4. A decrease in viscosity of ILs as well as their mixture has been observed with an increase in temperature. Unlike densities, viscosities do not show linear dependence with the mole fraction of the components of mixture.<sup>82</sup> To understand the behaviour of IL mixtures in terms of ideal and non-ideal conditions, several mixing rules available in the literature.<sup>289</sup> In this work, we have used the mixing rule proposed by Grunberg and Nissan to note the extent of non-ideality in mixtures.<sup>93</sup> In order to measure the extent of non-ideality in a mixture, Grunberg and Nissan mixing laws are proposed. The eq. (4.4) below denotes the mixing law. The mixing laws accounts for additional term ‘ $G$ ’ indicating the extent of non-ideality.

$$\log \eta = \chi \log \eta_1 + (1 - \chi) \log \eta_2 + \chi(1 - \chi) G_{12} \quad (4.4)$$

where  $\eta_1$  and  $\eta_2$  represent the viscosities of neat IL 1 and neat IL 2 respectively,  $\eta$  represents the viscosity of IL mixture,  $\chi$  represents the mole fractions of neat ILs present in the mixture and  $G_{12}$  is the additional term indicating the extent of non-ideality which depends on the strength of interaction between the two components of the mixture. The expression of  $G_{12}$  is shown below in eq. (4.5):

$$G_{12} = \ln \left( \frac{\eta}{\eta_{calc}^{id}} \right) / \chi_1 \chi_2 ; \eta_{calc}^{id} = \eta_1^{\chi_1} \eta_2^{\chi_2} \quad (4.5)$$

Figure 4.3. show that  $\log \eta(x)$  of the IL-IL mixture is not a strict linear function of the composition of the IL, one can find a very small deviation indicating the IL mixtures are not completely ideal rather the behaviour of IL mixture is more of quasi-ideal in nature.

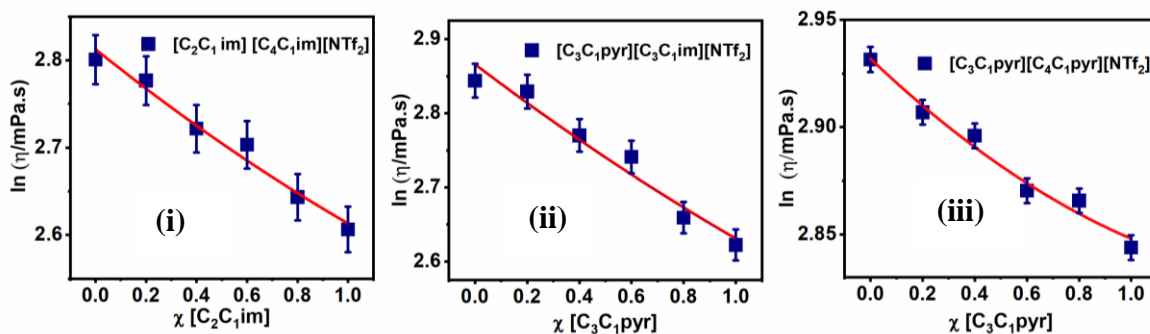


**Figure 4.4.** Viscosity of binary mixture of ILs: (i) mole frac. of  $[C_2C_1im]$  in the  $[C_2C_1im][C_4C_1im][NTf_2]$  mix., (ii) mole frac. of  $[C_3C_1pyr]$  in the  $[C_3C_1pyr][C_3C_1im][NTf_2]$  mix. and (iii) mole frac. of  $[C_3C_1pyr]$  in the  $[C_3C_1pyr][C_4C_1pyr][NTf_2]$  mix.

#### 4.3.2. Time-resolved fluorescence anisotropy

The microscopic behavior of a medium is intricately related to the solute solvent interaction and free volume of the concerned medium which in turn is closely related to macroscopic properties of the medium.<sup>132</sup> It is, therefore, also important to know the microscopic behavior of the systems that are used in the present study. TRFA is a powerful tool for exploring the solute–solvent and solvent–solvent interactions, which play an important role in determining physicochemical properties of liquid and solution.<sup>199, 265</sup> The time-resolved fluorescence anisotropy data and the analysis of the data through hydrodynamic theories (details of the different hydrodynamic theories have been explained in chapter 2) are found to be helpful in providing ideas about the free volume of the given solvent system. Investigations have been carried out on two structurally similar but chemically distinguishable probes, such as perylene and MPTS, in the binary mixtures of ILs along with the constituent ILs comprising the mixture at different temperatures through time-resolved fluorescence anisotropy. These probes are purposefully chosen to exclusively monitor the solute–solvent interactions in the medium. The representative decay plot of perylene and MPTS in the mixture  $[C_2C_1im][C_4C_1im]$  have been shown in Figure 4.5.

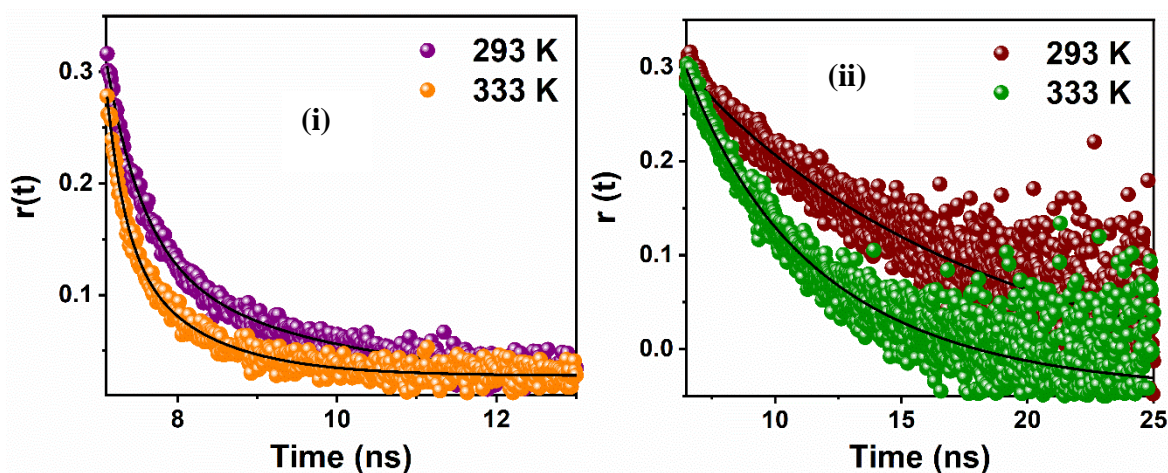


**Figure 4.5.** Representative decay of (i) Perylene in  $[C_2C_{1im}]_{0.2}[C_4C_{1im}]_{0.8}[NTF_2]$  (ii) MPTS in  $[C_2C_{1im}]_{0.2}[C_4C_{1im}]_{0.8}[NTF_2]$ .

**Table 4.2.** The reorientation time ( $\tau_r$ ) of perylene and MPTS in  $[C_2C_{1im}] [NTF_2]$ ,  $[C_4C_{1im}] [NTF_2]$ ,  $[C_3C_{1im}] [NTF_2]$ ,  $[C_3C_{1pyr}] [NTF_2]$ ,  $[C_4C_{1pyr}] [NTF_2]$  and their corresponding binary mixtures.

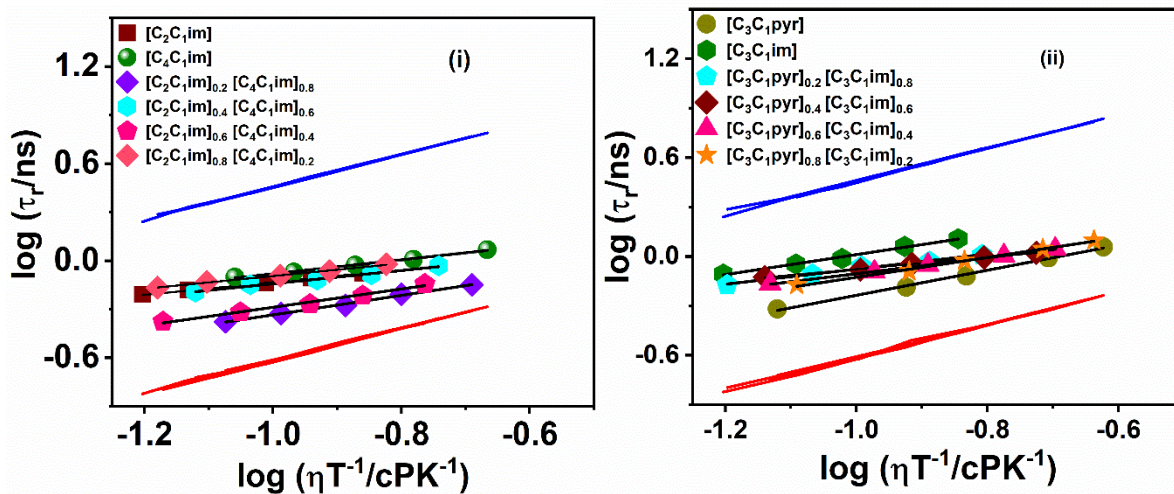
Systems	Perylene			MPTS	
	Temp. (K)	$\tau_r^b$ (ns)	$C_{rot} <avg>$	$\tau_r^b$ (ns)	$C_{rot} <avg>$
$[C_2C_{1im}] [NTF_2]$	293	0.87	$0.27 \pm 0.011$	4.85	$1.13 \pm 0.013$
	298	0.75		4.15	
	303	0.71		3.58	
	308	0.66		2.87	
	313	0.62		2.37	
$[C_4C_{1im}] [NTF_2]$	293	1.17	$0.25 \pm 0.012$	10.5	$1.78 \pm 0.017$
	298	1.02		8.63	
	303	0.94		7.85	
	308	0.85		6.89	
	313	0.79		6.04	
$[C_3C_{1pyr}] [NTF_2]$	293	1.14	$0.18 \pm 0.013$	8.58	$1.13 \pm 0.014$
	298	0.98		7.3	
	303	0.76		5.63	
	308	0.65		4.61	
	313	0.48		3.73	

[C <sub>3</sub> C <sub>1</sub> im] [NTF <sub>2</sub> ]	293	1.28	0.36 ± 0.02	12.06	2.71 ± 0.015
	298	1.15		10.12	
	303	0.97		8.3	
	308	0.87		7.52	
	313	0.8		5.84	
[C <sub>4</sub> C <sub>1</sub> pyr] [NTF <sub>2</sub> ]	293	1.56	0.23 ± 0.011	14.6	1.92 ± 0.012
	298	1.33		12.5	
	303	1.02		10.43	
	308	0.85		8.31	
	313	0.75		7.46	
[C <sub>2</sub> C <sub>1</sub> im] <sub>0.2</sub> [C <sub>4</sub> C <sub>1</sub> im] <sub>0.8</sub>	293	0.71	0.14 ± 0.015	6.70	1.18 ± 0.017
	298	0.62		5.71	
	303	0.53		4.93	
	308	0.47		4.41	
	313	0.42		3.82	
[C <sub>2</sub> C <sub>1</sub> im] <sub>0.4</sub> [C <sub>4</sub> C <sub>1</sub> im] <sub>0.6</sub>	293	0.93	0.23 ± 0.013	6.03	1.33 ± 0.015
	298	0.82		5.62	
	303	0.76		5.03	
	308	0.71		4.68	
	313	0.64		3.96	
[C <sub>2</sub> C <sub>1</sub> im] <sub>0.6</sub> [C <sub>4</sub> C <sub>1</sub> im] <sub>0.4</sub>	293	0.72	0.17 ± 0.012	5.83	1.22 ± 0.013
	298	0.61		5.07	
	303	0.54		4.36	
	308	0.48		3.87	
	313	0.42		3.32	
[C <sub>2</sub> C <sub>1</sub> im] <sub>0.8</sub> [C <sub>4</sub> C <sub>1</sub> im] <sub>0.2</sub>	293	0.95	0.21 ± 0.013	6.92	1.46 ± 0.012
	298	0.86		5.70	
	303	0.81		4.93	
	308	0.74		3.84	

	313	0.68		3.38	
[C <sub>3</sub> C <sub>1</sub> pyr] <sub>0.2</sub> [C <sub>3</sub> C <sub>1</sub> im] <sub>0.8</sub>	293	1.02	0.28 ± 0.016	11.12	2.32 ± 0.012
	298	0.93		9.35	
	303	0.87		7.81	
	308	0.78		6.85	
	313	0.66		5.58	
[C <sub>3</sub> C <sub>1</sub> pyr] <sub>0.4</sub> [C <sub>3</sub> C <sub>1</sub> im] <sub>0.6</sub>	293	1.08	0.26 ± 0.019	9.92	1.74 ± 0.016
	298	0.96		8.54	
	303	0.9		6.87	
	308	0.83		6.03	
	313	0.75		4.74	
[C <sub>3</sub> C <sub>1</sub> pyr] <sub>0.6</sub> [C <sub>3</sub> C <sub>1</sub> im] <sub>0.4</sub>	293	1.16	0.24 ± 0.016	9.28	1.54 ± 0.018
	298	1.01		8.01	
	303	0.84		6.41	
	308	0.78		5.67	
	313	0.71		4.34	
[C <sub>3</sub> C <sub>1</sub> pyr] <sub>0.8</sub> [C <sub>3</sub> C <sub>1</sub> im] <sub>0.2</sub>	293	1.25	0.23 ± 0.014	8.45	1.35 ± 0.013
	298	1.11		7.31	
	303	0.94		5.85	
	308	0.81		5.17	
	313	0.67		4.12	
[C <sub>3</sub> C <sub>1</sub> pyr] <sub>0.2</sub> [C <sub>4</sub> C <sub>1</sub> pyr] <sub>0.8</sub>	293	1.18	0.20 ± 0.017	9.45	1.35 ± 0.013
	298	1.03		8.3	
	303	0.83		6.05	
	308	0.71		5.16	
	313	0.56		4.37	
[C <sub>3</sub> C <sub>1</sub> pyr] <sub>0.4</sub> [C <sub>4</sub> C <sub>1</sub> pyr] <sub>0.6</sub>	293	1.3	0.21 ± 0.012	10.77	1.45 ± 0.011
	298	1.15		9.21	
	303	0.87		7.4	

	308	0.75		6.01	
	313	0.61		5.12	
[C <sub>3</sub> C <sub>1</sub> pyr] <sub>0.6</sub> [C <sub>4</sub> C <sub>1</sub> pyr] <sub>0.4</sub>	293	1.38	0.22 ± 0.015	11.62	1.67 ± 0.017
	298	1.23		9.93	
	303	0.95		8.08	
	308	0.75		6.46	
	313	0.62		5.67	
[C <sub>3</sub> C <sub>1</sub> pyr] <sub>0.8</sub> [C <sub>4</sub> C <sub>1</sub> pyr] <sub>0.2</sub>	293	1.45	0.22 ± 0.015	13.35	1.86 ± 0.011
	298	1.26		12.37	
	303	0.98		9.43	
	308	0.8		7.47	
	313	0.68		6.51	

<sup>b</sup> Experimental error = ± 5%



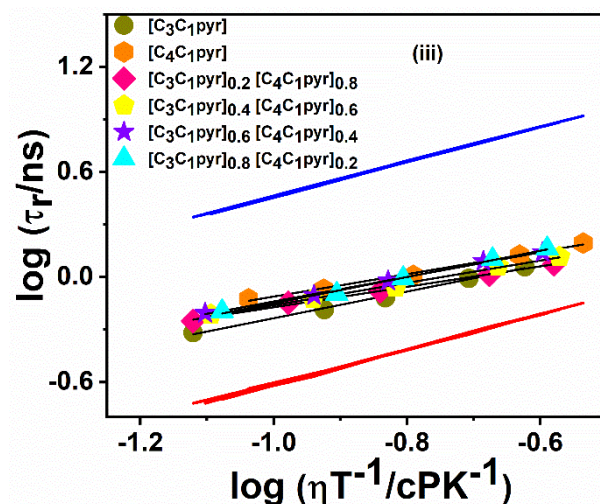


**Figure 4.6** log-log plots of the average rotational relaxation time of perylene in (i)  $[\text{C}_2\text{C}_1\text{im}]$  and  $[\text{C}_4\text{C}_1\text{im}]$  mix. (ii)  $[\text{C}_3\text{C}_1\text{pyr}]$  and  $[\text{C}_3\text{C}_1\text{im}]$  mix. (iii)  $[\text{C}_3\text{C}_1\text{pyr}]$  and  $[\text{C}_4\text{C}_1\text{pyr}]$  mix. with blue colour stick and red colour slip boundary condition limits. The solid black lines indicate the fit to the data points.

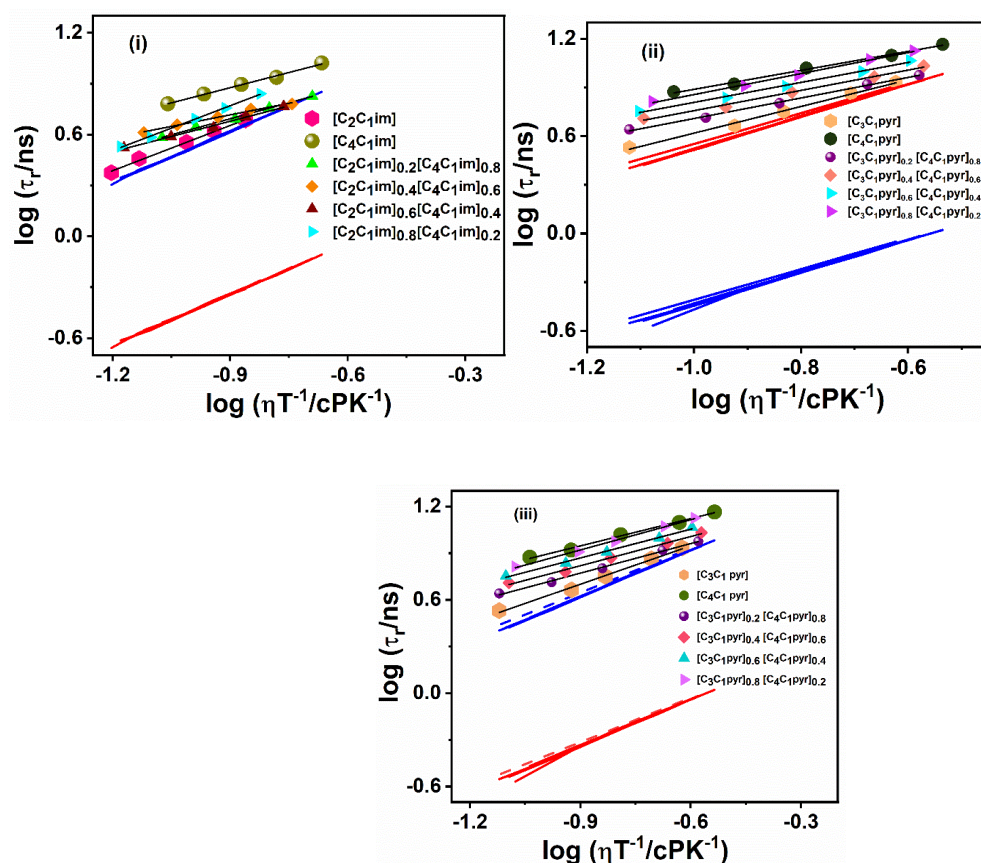


**Figure 4.7.** log-log plots of the average rotational relaxation time of MPTS in (i)  $[\text{C}_2\text{C}_1\text{im}]$  and  $[\text{C}_4\text{C}_1\text{im}]$  mix. (ii)  $[\text{C}_3\text{C}_1\text{pyr}]$  and  $[\text{C}_3\text{C}_1\text{im}]$  mix. (iii)  $[\text{C}_3\text{C}_1\text{pyr}]$  and  $[\text{C}_4\text{C}_1\text{pyr}]$  mix. with blue colour stick and red colour slip boundary condition limits. The solid black lines indicate the fit to the data points.

The Stokes–Einstein–Debye (SED) hydrodynamic model<sup>234, 235</sup> has been used for obtaining a comprehensive understanding of the solute dynamics in a given medium. Details of the SED theory has been explained in chapter 2. The rotational relaxation time for perylene and MPTS in different ILs and their corresponding binary mixtures is listed in Table 4.2. Figures 4.6 and 4.7 illustrate the SED plots pertaining to the rotational motion of perylene and MPTS, respectively, in the neat ILs and their corresponding binary mixtures of ILs. From Fig. 4.6, one can say that perylene rotates within the limits predicted by SED theory. Interestingly, it can be observed that unlike perylene, MPTS shows a hindered rotation in all ILs and their corresponding binary mixtures [Figure 4.7]. The hindered rotation of MPTS clearly indicates a stronger solute–solvent interaction in the concerned media.<sup>219, 266</sup> In the present study, the electrostatic interaction along with hydrogen bonding ability, highly acidic C(2) hydrogen (pKa  $\sim$  28.3),<sup>268</sup> is the main reason behind the retardation motion of MPTS in the IL medium. On the contrary, in the case of pyrrolidinium based ILs, the rotational dynamics of MPTS are also hindered due to strong electrostatic interaction.<sup>290</sup>

**Table 4.3.** Boundary conditions obtained from DKS model.

System	$C_{DKS}$
[C <sub>2</sub> C <sub>1</sub> im] [NTF <sub>2</sub> ]	0.068 $\pm$ 0.002
[C <sub>4</sub> C <sub>1</sub> im] [NTF <sub>2</sub> ]	0.052 $\pm$ 0.003
[C <sub>3</sub> C <sub>1</sub> pyr] [NTF <sub>2</sub> ]	0.087 $\pm$ 0.001
[C <sub>3</sub> C <sub>1</sub> im] [NTF <sub>2</sub> ]	0.053 $\pm$ 0.002
[C <sub>4</sub> C <sub>1</sub> pyr] [NTF <sub>2</sub> ]	0.088 $\pm$ 0.001
[C <sub>2</sub> C <sub>1</sub> im] <sub>0.2</sub> [C <sub>4</sub> C <sub>1</sub> im] <sub>0.8</sub>	0.047 $\pm$ 0.002
[C <sub>2</sub> C <sub>1</sub> im] <sub>0.4</sub> [C <sub>4</sub> C <sub>1</sub> im] <sub>0.6</sub>	0.053 $\pm$ 0.001
[C <sub>2</sub> C <sub>1</sub> im] <sub>0.6</sub> [C <sub>4</sub> C <sub>1</sub> im] <sub>0.4</sub>	0.057 $\pm$ 0.003
[C <sub>2</sub> C <sub>1</sub> im] <sub>0.8</sub> [C <sub>4</sub> C <sub>1</sub> im] <sub>0.2</sub>	0.064 $\pm$ 0.002
[C <sub>3</sub> C <sub>1</sub> pyr] <sub>0.2</sub> [C <sub>3</sub> C <sub>1</sub> im] <sub>0.8</sub>	0.060 $\pm$ 0.001

$[C_3C_1pyr]_{0.4}[C_3C_1im]_{0.6}$	$0.068 \pm 0.002$
$[C_3C_1pyr]_{0.6}[C_3C_1im]_{0.4}$	$0.078 \pm 0.002$
$[C_3C_1pyr]_{0.8}[C_3C_1im]_{0.2}$	$0.090 \pm 0.001$
$[C_3C_1pyr]_{0.2}[C_4C_1pyr]_{0.8}$	$0.091 \pm 0.001$
$[C_3C_1pyr]_{0.4}[C_4C_1pyr]_{0.6}$	$0.078 \pm 0.003$
$[C_3C_1pyr]_{0.6}[C_4C_1pyr]_{0.4}$	$0.073 \pm 0.002$
$[C_3C_1pyr]_{0.8}[C_4C_1pyr]_{0.2}$	$0.075 \pm 0.002$

---

To account for the extent of free volume present in ILs and their binary mixture, the Dote–Kivelson–Schwartz<sup>237, 291</sup> model has been considered, which not only considers the solvent size but also incorporates the cavities or free spaces created by the solvent around the probe molecule while calculating the boundary condition. This theory has been discussed in detail in chapter 2. Table 4.3 lists the average rotational relaxation time of perylene in different solvent systems with boundary condition parameters obtained from the DKS model. The boundary condition obtained from the DKS model is supposed to be different from the same for the SED model as it takes the free volume into consideration. From Table 4.3, one can say that in the case of a mixture composed of  $[C_2C_1im]$  and  $[C_4C_1im]$ , there is a decrease of 3% in the  $C_{DKS}$  ( $C$  refers to the solute–solvent coupling constant) value compared with the  $C_{slip}$  boundary condition of SED. The decrease in  $C_{DKS}$  illustrates a decrease in the solute–solvent coupling constant, which is indicative of an increase in the free volume of the system considered. In the present study, the free volume in the mixture  $[C_2C_1im][C_4C_1im]$  is more than that in either  $[C_3C_1pyr][C_4C_1pyr]$  or  $[C_3C_1pyr][C_3C_1im]$ . The increase in the free volume for the mixture of  $[C_2C_1im]$  and  $[C_4C_1im]$  has resulted in faster rotation of perylene. The slight hindrance in the rotation of perylene in both  $[C_3C_1pyr][C_4C_1pyr]$  and  $[C_3C_1pyr][C_3C_1im]$  in comparison to that in  $[C_2C_1im][C_4C_1im]$  indicates a decrease in the free volume for  $[C_3C_1pyr][C_4C_1pyr]$  and  $[C_3C_1pyr][C_3C_1im]$ . The results obtained from rotational diffusion of

perylene are in sync with the excess free volume observed in the thermophysical study. The observation demonstrates that the extent of free volume in the binary mixture of ILs play an important role in the structural organization of the mixture of ILs. The variation in the extent of free volume indicates that the structural organization of the binary mixture of ILs is different.

### 4.3.3. NMR studies

The PFG–NMR<sup>269, 271-273, 275</sup> technique provides information on translational diffusion of cations and anions in the ILs by estimating the size and the diffusivity of the diffusing species.<sup>269</sup> The translational diffusion coefficient ( $D$ ) of the diffusing species in a given medium is influenced not only by factors such as mass, shape, and size of ions in the ILs but also by the effect of free volume in ILs along with cation–anion interaction.<sup>132</sup> Since free volume of a given media is intricately related to the structural organization of the medium,  $D$  is expected to vary with variation in the free volume of that concerned medium.<sup>132</sup> The implications of these effects change the structural organization of ILs.<sup>273, 275</sup> In the present work,  $D$  tabulated in Table 4.4 and estimated through PFG-NMR shows the diffusive nature of the “cationic moiety” in all cases.  $D$  measured for the binary mixture of ILs is an averaged-out effect of the cations arising from the constituent neat ILs.

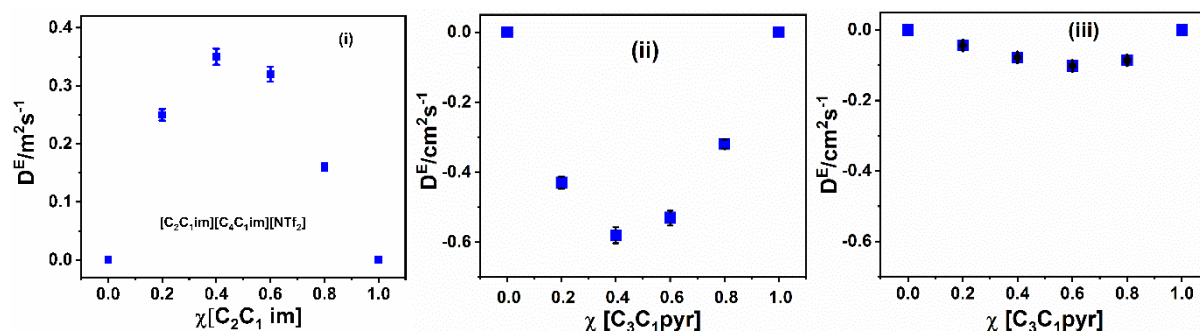


**Figure 4.8.** The excess diffusion coefficient ( $D^E$ ) of neat ILs and their corresponding binary mixtures (i)  $[C_2C_1im]$  and  $[C_4C_1im]$  ILs (ii)  $[C_3C_1pyr]$  and  $[C_3C_1im]$  ILs (iii)  $[C_3C_1pyr]$  and  $[C_4C_1pyr]$  ILs.

From Figure 4.8, one can observe that in the case of the binary mixture of  $[\text{C}_2\text{C}_1\text{im}][\text{C}_4\text{C}_1\text{im}]$ , a small positive deviation is observed for D from respective neat ILs while in the case of the binary mixture of  $[\text{C}_3\text{C}_1\text{pyr}][\text{C}_4\text{C}_1\text{pyr}]$  and  $[\text{C}_3\text{C}_1\text{pyr}][\text{C}_3\text{C}_1\text{im}]$ , there is a small negative deviation. As discussed earlier, the deviation in D in the case of binary mixtures of ILs might have arisen due to an excess molar volume linked with the generation of free volume by the alkyl chain of imidazolium and pyrrolidinium moiety, causing a faster diffusion in  $[\text{C}_2\text{C}_1\text{im}][\text{C}_4\text{C}_1\text{im}]$  than in  $[\text{C}_4\text{C}_1\text{pyr}][\text{C}_3\text{C}_1\text{pyr}]$  and  $[\text{C}_3\text{C}_1\text{pyr}][\text{C}_3\text{C}_1\text{im}]$ . Keeping the above-mentioned facts in mind, the present study shows that the binary mixture of ILs is not obviously non-ideal or ideal; rather, these IL–IL mixtures have a slight deviation from a completely ideal behavior. Henceforth, the behavior of these IL–IL mixtures is more quasi-ideal in nature.

#### 4.4. Conclusion

Even though the mixing of ILs in designing and developing a new solvent system having desired properties is an interesting approach, the success of this approach is entirely dependent on our understanding of the concerned media at both macroscopic and microscopic level. With an aim to fulfill this objective, in this chapter, we have studied the thermophysical properties as well as the structural organization of different binary mixtures comprising of imidazolium and pyrrolidinium based ILs such as  $[\text{C}_2\text{C}_1\text{im}][\text{C}_4\text{C}_1\text{im}][\text{NTf}_2]$ ,  $[\text{C}_3\text{C}_1\text{pyr}][\text{C}_4\text{C}_1\text{pyr}][\text{NTf}_2]$ , and  $[\text{C}_3\text{C}_1\text{im}][\text{C}_3\text{C}_1\text{pyr}][\text{NTf}_2]$ . Moreover, imidazolium and pyrrolidinium based ILs are chosen so that the role of cations, in governing the behavior of the said mixture, if any, is understood. Thermophysical studies on these mixtures have shown a small but non-negligible increase in the excess molar volume of the binary mixture of ILs. These studies and some recent literature findings have also indicated that in the case of the binary mixture of imidazolium ILs, the generation of excess molar volume may be linked to the free volume created by the alkyl chain whereas in the case of the binary mixture of pyrrolidinium ILs, lowering of density can give rise to free volume. In order to understand the microscopic behavior of the medium in terms of

free volume and solute-solvent interactions through TRFA as well as the PFG-NMR techniques have been employed for investigation purposes. Analysis of TRFA data has provided clear evidence in favor of the presence of free volume in the binary mixture of ILs. Thus, the results have pointed out that the deviation from the ideal behavior in the binary mixture of ILs is intricately related to its free volume. The outcome of the present study has essentially shown that the mixtures show appreciable but not large deviation from the ideal behavior and the change in the free volume of the mixture from its constituent ILs is caused due to change in the structural organization of the resultant mixture during the mixing process. The outcome of the current investigations has led us to conclude that the binary mixtures of ILs used in this study can be best described as quasi-ideal rather than ideal or non-ideal.

## CHAPTER 5

---

# Understanding the Structural Organisation of Monocationic and Dicationic Room Temperature Ionic Liquids through Resonance Energy Transfer (RET) Studies

---

---

Chakraborty, M.; Ahmed, T.; Sarkar, M. *Langmuir* **2019**, *35*, 16172–16184.

## Chapter 5

---

### Understanding the Structural Organization of Monocationic and Dicationic Room Temperature Ionic Liquids through Resonance Energy Transfer (RET) Studies

---

This chapter aims to understand the differences in the local structural organization of the imidazolium-based monocationic ionic liquids (MILs) and dicationic ionic liquids (DILs) through resonance energy transfer (RET) studies. In this study, neat IL is used as donor and a charged species rhodamine 6G (R6G) is used as the acceptor unit due to the fact that they satisfy the spectroscopic criteria that are needed for RET event to take place. Interestingly, the present data reveal that the RET interaction is more favorable for DILs than for MILs even though the DILs are relatively bulkier than their monocationic counterparts. More interestingly, RET interaction is also found to be more favorable for DILs than that for those MILs where the length of alkyl group is kept fixed for MILs and DILs. The result of the present study delineates that the length of the alkyl chain length on the cation is not the sole factor contributing to the RET outcomes for DILs and MILs but the local structure of DILs also contribute significantly to the same. The current investigation clearly indicates DILs have a more compact local structure than that of MILs.

---

#### 5. 1. Introduction

In recent times, the room-temperature ionic liquids (ILs) have emerged as special solvent systems because of their applications in the field of catalysis, batteries, fuel cell photovoltaics, super capacitors, and so forth.<sup>3, 14, 22, 51, 292-296</sup> The innumerable applications of ILs have been possible because of their fascinating physicochemical properties such as low melting point, low vapor pressure, high thermal stability etc.<sup>14, 17, 249</sup> Because ILs are composed of cations and anions, different combinations of these cations and anions are feasible, which in turn can offer

high tunability in their chemical properties.<sup>19, 29</sup> However, several studies have revealed that the structural organizations of ILs are quite complex and the current understanding on this issue still remains hazy. In the past decade, extensive research efforts have been put forward by focusing on the structure–property relationship of monocationic ionic liquids (MILs).<sup>48, 119, 123, 124, 129, 219, 254, 256, 262, 297-302</sup> Essentially, the outcome of the studies aimed to understand the structure–property relationship have indicated ILs to be microheterogeneous in nature and the length of micro-heterogeneity spans over a few nanometers.<sup>48, 118, 129, 219, 256, 300-305</sup> The segregation of the alkyl chain leads to the formation of polar and nonpolar domains, which is thought to be the main cause of the microheterogeneous behavior of ILs.<sup>111, 116, 126, 306</sup> Very recently, dicationic ionic liquids (DILs) have been designed and developed.<sup>37-50</sup> These include imidazolium<sup>43, 47</sup> and ammonium<sup>38, 39, 46</sup>-based DILs. DILs are expected to be more attractive solvent systems than MILs because of the fact that a large number of cation–anion combinations are possible in the former than in the latter.<sup>48</sup> This would eventually make the physicochemical properties of DILs more favorable than those of MILs. Some initial works on DILs have also revealed that DILs are more advantageous than MILs in terms of viscosity, surface tension, thermal stability, and so forth.<sup>48</sup> In this regard, Anderson et al.<sup>37</sup> have investigated the physicochemical properties of imidazolium- and pyrrolidinium-based DILs and illustrated that DILs possess a higher thermal stability than MILs. Sahu and Sarkar<sup>179, 307</sup> have also observed that a six-membered alkyl spacer (linker) chain bearing imidazolium-based DIL has a different dynamical behavior than a hexyl chain-bearing imidazolium-based MIL. Cummings and co-workers<sup>42, 43, 308</sup> using a molecular dynamics (MD) simulation study have shown the difference in the structural organization of DILs and MILs, which depends on the alkyl linker and tail chain length of the former and latter systems, respectively. Again in a study done by Moosavi and co-workers,<sup>309</sup> the spatial structures of germinal dicationic liquids have been explained using the heterogeneity order parameter (HOP) values HOP. They have also

shown that the DILs can exist in a folded form.<sup>309</sup> In the case of imidazolium-based DILs, Bhargava<sup>310, 311</sup> and Palchowdhury<sup>311</sup> through MD simulations have shown the aggregation behavior. The above discussions pertaining to DILs have explained that even though some work has been carried out on them, experimental studies that focus on the understanding of microscopic structural organization of DILs are rather limited. Apart from the studies discussed above, few studies based on steady-state and time-resolved fluorescence<sup>220</sup> and nuclear magnetic resonance (NMR)<sup>220, 269</sup> have also been carried out to shed light on the structure–property relationship in DIL systems. Recently, studies conducted by Mandal and co-workers<sup>176, 312</sup> are noteworthy in which the impact of cationic and anionic moieties on the nanostructural organization of MILs has been successfully demonstrated by exploiting resonance energy-transfer (RET) studies. The efficiency of RET process is highly dependent on the distance between the donor, and as a consequence, it has been found to be one of the most sensitive tools in monitoring events in various types of heterogeneous assemblies.<sup>173, 313</sup> In a separate work, Sarkar and co-workers<sup>244</sup> have also demonstrated that RET studies can differentiate the microscopic structural organization of planar and nonplanar cation-based ILs. It is very exciting to note the use of a simple cost-effective method such as RET in comparison to neutron diffraction studies in understanding the fluid structure of ILs. However, we would like to note here that all the above-mentioned studies are done only on MILs, and no attempts have so far been made to understand the nanostructure organization of DILs by exploiting RET.

Keeping the above facts in mind, the RET process between several neat ILs (donor) and rhodamine (acceptor) has been studied in an organized manner. In this study, we have chosen six-membered and eight-membered alkyl imidazolium DILs, namely,  $[C_6(\text{MIm})_2][\text{NTf}_2]_2$  and  $[C_8(\text{MIm})_2][\text{NTf}_2]_2$ , respectively, along with their monocationic counterparts, the three-membered and four-membered alkyl imidazolium IL systems, namely,  $[C_3\text{mim}][\text{NTf}_2^-]$  and  $[C_4\text{mim}][\text{NTf}_2^-]$ , respectively. Additionally, we have also taken six-

membered and eight-membered alkyl imidazolium MILs, namely,  $[\text{C}_6\text{mim}][\text{NTf}_2^-]$  and  $[\text{C}_8\text{mim}][\text{NTf}_2^-]$  so that the effect of alkyl chain length can be monitored exclusively. A systematic variation of cation is maintained while the anions are kept constants. The choice of rhodamine 6G (R6G) dye as the acceptor molecule lies in the fact that a significant overlap between the absorption spectrum of R6G with the emission spectrum of the concerned IL could be observed. Additionally, R6G being the charged species is also expected to facilitate the electrostatic interaction with ILs which are also charged. An electrostatic interaction is expected to facilitate the closer approach of acceptor molecules to the donor ILs and thus helps to facilitate sufficient RET communication between them. In the RET studies, the steady-state measurements and time-resolved fluorescence measurements of ILs (donor) and R6G (acceptor) have been carried out. Molecular diagrams of the systems used in the present study are depicted in Figure 5.1.

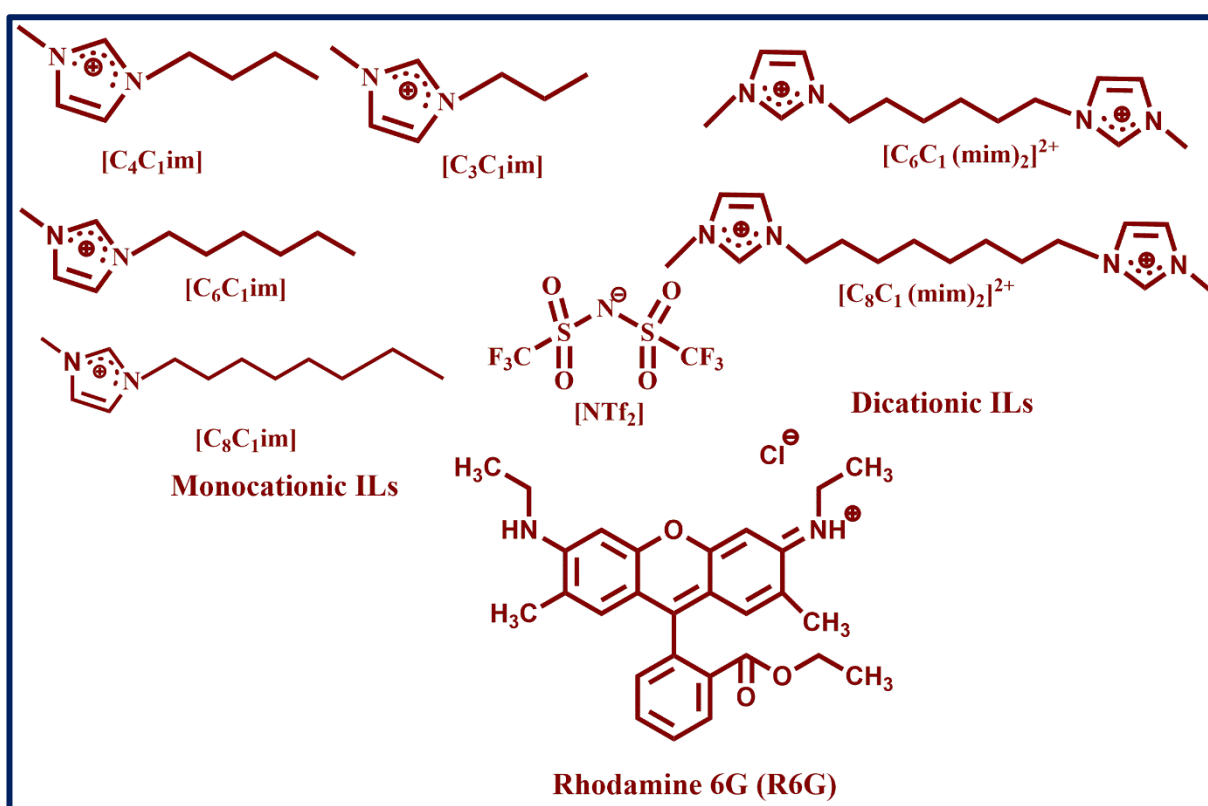


**Figure 5.1.** Molecular structures of ILs and probes used in the present study (chapter 5).

## 5.2. Experimental techniques and methods

The monocationic ionic liquids [C<sub>3</sub>C<sub>1</sub>][NTf<sub>2</sub>], [C<sub>4</sub>C<sub>1</sub>][NTf<sub>2</sub>] and [C<sub>6</sub>C<sub>1</sub>][NTf<sub>2</sub>] were purchased from Sigma and TCI Chemicals (>98% purity). The halide ions and water content in these ILs are < 100 ppm. The dicationic ILs, [C<sub>6</sub>(mim)<sub>2</sub>][NTf<sub>2</sub><sup>-</sup>]<sub>2</sub> and [C<sub>8</sub>(mim)<sub>2</sub>][NTf<sub>2</sub><sup>-</sup>]<sub>2</sub> were synthesized. The synthesis procedure of dicationic ILs were explained in detailed in chapter 2. Anhydrous DMSO and Rhodamine 6G (R6G) was purchased from Sigma-Aldrich and used as received. The sample preparation procedures and experimental methods for steady-state and time-resolved fluorescence studies and fluorescence correlation study through FCS are described in detail in Chapter 2.

## 5.3. Results and discussions

### 5.3.1. Thermophysical properties of neat ILs

The thermophysical properties of ILs depend on its constituent cation and anions. Table 5.1, illustrates the densities of both the monocationic ionic liquids along with the dicationic ionic liquids.

**Table 5.1.** The densities of both MILs and DILs.

$\rho / \text{gm.cm}^{-3}$						
Temp. (K)	[C <sub>3</sub> mim][NTf <sub>2</sub> ]	[C <sub>4</sub> mim][NTf <sub>2</sub> ]	[C <sub>6</sub> mim][NTf <sub>2</sub> ]	[C <sub>8</sub> mim][NTf <sub>2</sub> ]	[C <sub>6</sub> (mim) <sub>2</sub> ][NTf <sub>2</sub> <sup>-</sup> ] <sub>2</sub>	[C <sub>8</sub> (mim) <sub>2</sub> ][NTf <sub>2</sub> <sup>-</sup> ] <sub>2</sub>
293	1.472	1.436	1.354	1.286	1.557	1.517
298	1.465	1.431	1.348	1.279	1.546	1.508
303	1.460	1.428	1.341	1.273	1.539	1.496
308	1.453	1.424	1.336	1.268	1.531	1.490
313	1.446	1.420	1.329	1.261	1.526	1.483
318	1.439	1.417	1.322	1.255	1.520	1.476

323      1.431      1.413      1.317      1.248      1.514      1.469

---

Instrumental error: 0.5%

---

From the Table 5.1, the densities of DILs are always found to be higher than the corresponding MILs. For e.g. the densities of C<sub>6</sub> for a dicationic IL is ~ 5 % higher than that of C<sub>3</sub> monocationic IL. Additionally, to have a deeper insight on this issue, the free volume difference existing between the MILs and DILs have been calculated. Initially we calculated the van der Waals volumes (V<sub>VWD</sub>) of the ILs using van der Waals increment method<sup>235</sup> and the ratios between the van der Waals volume and the molar volume (V), V<sub>VWD</sub>/V have been calculated. The molar volume of an IL has been estimated from the density and its formula weight ( $V = FW/d$ ). The ratio, V<sub>VWD</sub>/V estimates the extent of space (unit space) occupied by a molecule or a pair of ions.<sup>48</sup> The values of V<sub>VWD</sub>/V for the ILs are listed in the in Table 5.2.

**Table 5.2.** Formula Weight (FW), Molar Volumes (V) (cm<sup>3</sup>. mol<sup>-1</sup>), Van der Waals volume (V<sub>VWD</sub>) and the ratio (V<sub>VWD</sub>/V) for all the ILs.

Cation	Formula Weight (FW)	Molar Volumes (V) (cm <sup>3</sup> . mol <sup>-1</sup> )	Van der Waals volume (V <sub>VWD</sub> )	V <sub>VWD</sub> / V
[C <sub>3</sub> mim][NTf <sub>2</sub> <sup>-</sup> ]	405	276.5	171.2	0.623
[C <sub>4</sub> mim][NTf <sub>2</sub> <sup>-</sup> ]	419	292.8	181.4	0.622
[C <sub>6</sub> mim][NTf <sub>2</sub> <sup>-</sup> ]	447	331.6	201.9	0.619
[C <sub>8</sub> mim][NTf <sub>2</sub> <sup>-</sup> ]	489	382.3	243.1	0.617
[C <sub>6</sub> (mim) <sub>2</sub> ][NTf <sub>2</sub> <sup>-</sup> ] <sub>2</sub>	808.7	523.1	335.5	0.642
[C <sub>8</sub> (mim) <sub>2</sub> ][NTf <sub>2</sub> <sup>-</sup> ] <sub>2</sub>	836.7	554.8	356	0.637

From the Table 5.2, it can be said that the value for V<sub>VWD</sub>/Vis more in DILs are larger than that in monocationic ILs having same anions and cations with equivalent alkyl groups. These data essentially indicates that the compactness in case of DILs is more than that of MILs.

### 5.3.2. Fluorescent property in neat ILs

Before the spectroscopic investigation, all the ILs are carefully purified. A thorough examination of the absorption and fluorescence behavior for all the neat ILs has been done before RET studies. Figure 5.2 depicts the representative absorption and emission spectra of neat IL,  $[\text{C}_3\text{mim}][\text{NTf}_2^-]$ . The absorption profile of neat ILs shows a significant absorption observed for all the ILs in the UV region. Moreover, in the case of all the other ILs, a long tail (beyond 400 nm) has been observed. This long tail of absorption indicates the different energetically associated species present in the ground state.<sup>121, 122, 175</sup> Essentially, the nature of absorption spectra in these ILs is quite similar to other imidazolium-based ILs.<sup>121, 122, 124, 175, 254, 262</sup> The emission spectra of all the neat ILs show a broad band with a maximum at  $\sim 450$  nm (Figure 5.2b).

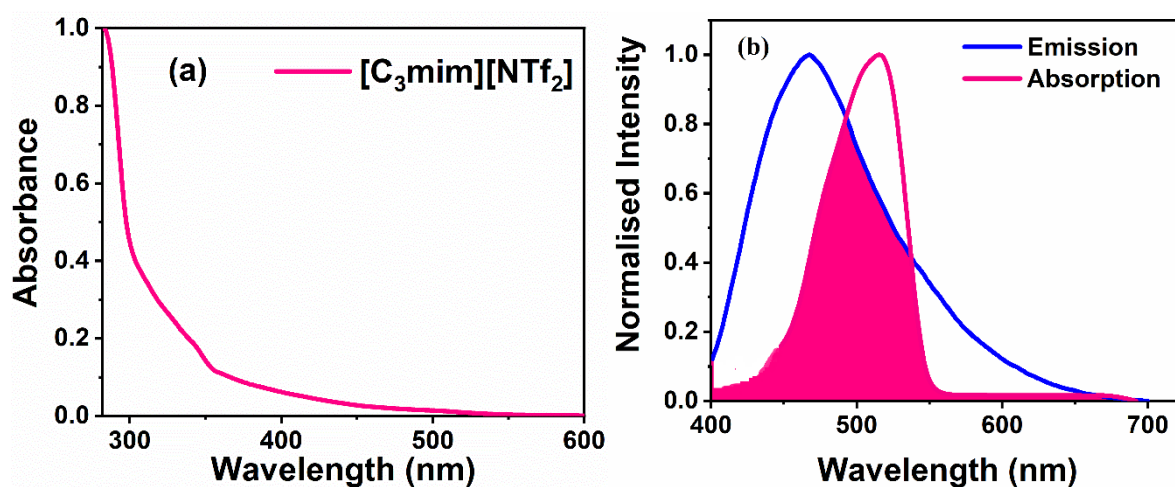


**Figure 5.2.** (a) Absorption spectrum of neat  $[\text{C}_3\text{mim}][\text{NTf}_2^-]$  and (b) Normalized absorption and emission spectra of R6G and  $[\text{C}_3\text{mim}][\text{NTf}_2^-]$  respectively. The IL ( $[\text{C}_3\text{mim}][\text{NTf}_2^-]$ ) has been excited at 375nm. The overlap region in Figure 5.1(b) is highlighted.

Prior to the RET studies, the fluorescence behavior of neat MILs and DILs has been investigated by steady-state fluorescence and FCS. It has been suggested for some MILs previously that the associated species of ILs, not the monomeric forms of ILs, are responsible for their fluorescence behavior.<sup>121, 254</sup> In this context, it is relevant to mention that

Weingärtner<sup>17</sup> has shown that imidazolium-based MILs can exist as ion pair and ion clusters. In the present work, steady-state fluorescence measurements have been performed in neat ILs along with gradual addition of DMSO to MILs and DILs separately. In order to verify whether the fluorescence of the IL is due to the associated structures rather than the monomeric form of ILs, in the present study, we have used DMSO as a solvent system because of the fact that DMSO is nicely soluble in the IL with no biphasic separation. The effect of other solvents on the neat IL emission has already been shown by Kim and co-workers.<sup>215</sup> They have also observed the breaking down of associated structures with aqueous and organic solvents. A representative figure which shows the effect of DMSO in neat ILs is shown in Figure 5.3.

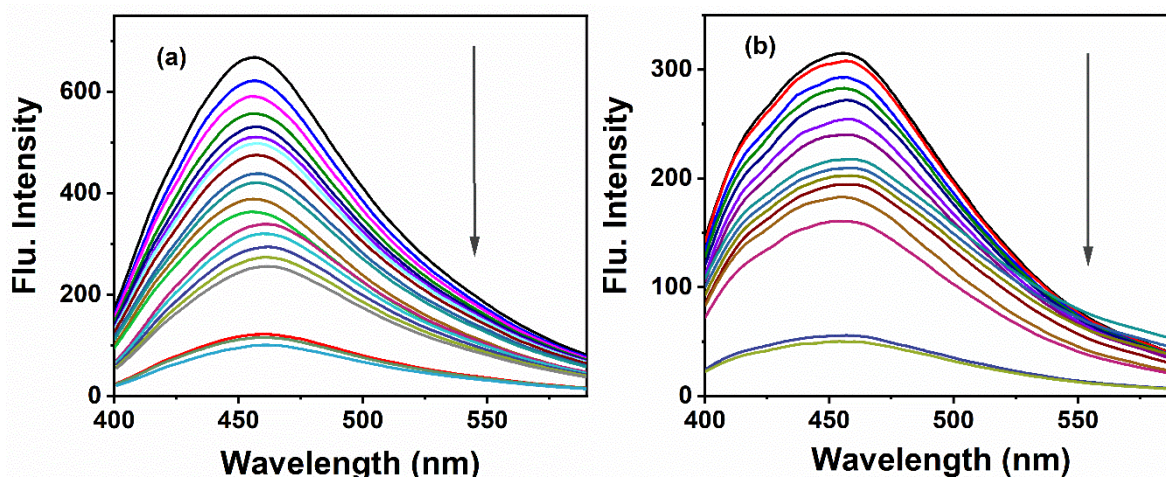


**Figure 5.3.** Decrease in the fluorescence intensity upon gradual addition of DMSO (a) [C<sub>6</sub>(mim)<sub>2</sub>][NTf<sub>2</sub>]<sub>2</sub>(b) [C<sub>3</sub>mim][NTf<sub>2</sub>].

As can be seen from Figure 5.3, the fluorescence intensity decreases gradually for both MILs and DILs upon addition of DMSO to the respective neat ILs. The fluorescence intensity of the concerned ILs is almost diminished after 10 folds of dilution. The present study suggests that the molecular association within the ILs breaks down, which ultimately causes a drop in the fluorescence intensity. The reduction in the fluorescence intensity of neat ILs upon addition of DMSO is not due to the effect of concentration but rather due to the breaking of IL aggregates. This indicates the dissociation of the associated structure of ILs.<sup>215</sup> For an in-depth

understanding on this aspect, we have further performed FCS study on neat ILs in the absence and presence of DMSO. Kim and co-workers<sup>215</sup> have shown the breaking of aggregates with other organic solvents. FCS allows a precise measurement of the number of fluorescent species in the confocal volume.<sup>174, 177, 198, 216</sup> The relevant data obtained from the FCS measurements for the concerned ILs are collected in Table 3. The data obtained from FCS measurements has been fitted to a single diffusion model. Please note that the single diffusion model is found to be appropriate in determining the diffusion constant of a fluorescing species in IL media.<sup>174, 215, 216, 254</sup> It can be observed from Figure 5.4 that upon dilution of ILs with DMSO, there is a decrease in the number of fluorescent species. Please note that  $G(0)$  is inversely proportional to the quantity of fluorophore in a given sample. The diffusion time  $\tau_d$  of the concerned fluorescing species is also found to decrease as the DMSO content is increased. These observations indicate that the fluorescence of neat ILs originates from its molecular aggregates. Therefore, the present steady-state fluorescence measurements and FCS study on MILs and DILs clearly demonstrate that the associated structures of ILs are primary responsible for their emission behavior.

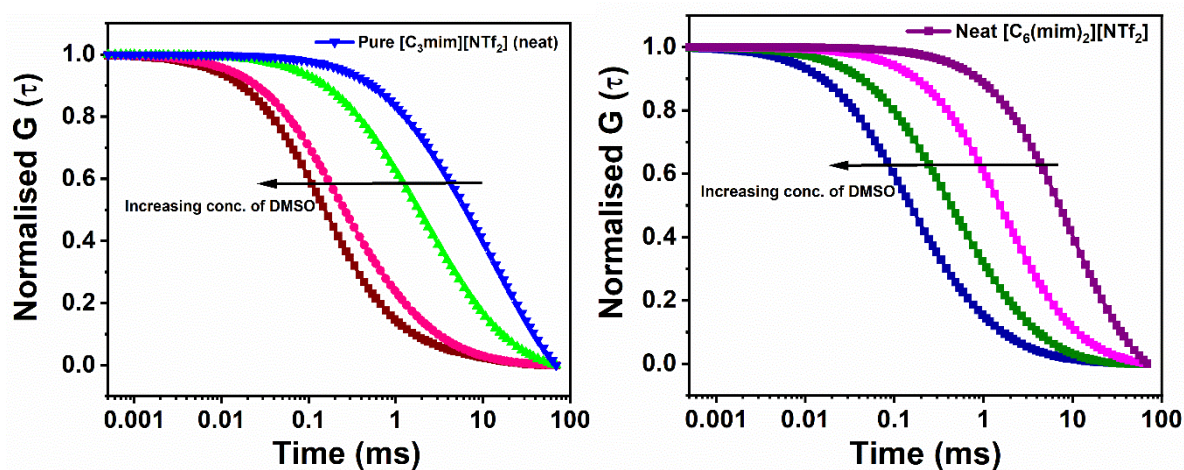


**Figure 5.4.** Fluorescence correlation plots of neat  $[C_3\text{mim}][\text{NTf}_2]$  and  $[C_6(\text{mim})_2][\text{NTf}_2]$  upon gradual addition of different concentrations of DMSO.

**Table 5.3.** The relevant parameters obtained from FCS for [C<sub>6</sub>(mim)<sub>2</sub>][NTf<sub>2</sub>]<sub>2</sub> and [C<sub>3</sub>mim][NTf<sub>2</sub>] at 298 K.

Systems	Concentration (nM)	D ( $\mu\text{m}^2\text{s}^{-1}$ )	$\tau_d$ (ms)
[C <sub>6</sub> (mim) <sub>2</sub> ][NTf <sub>2</sub> ] <sub>2</sub> (neat)	548 ± 15	1.25 ± 0.41	10.4 ± 0.36
[C <sub>6</sub> (mim) <sub>2</sub> ][NTf <sub>2</sub> ] <sub>2</sub> : DMSO (1: 0.05)	537 ± 21	2.11 ± 0.36	6.1 ± 0.23
[C <sub>6</sub> (mim) <sub>2</sub> ][NTf <sub>2</sub> ] <sub>2</sub> : DMSO (1: 0.4)	330 ± 26	10.5 ± 0.45	1.25 ± 0.71
[C <sub>6</sub> (mim) <sub>2</sub> ][NTf <sub>2</sub> ] <sub>2</sub> : DMSO (1:1)	34 ± 10	39.8 ± 0.31	0.33 ± 0.24
[C <sub>3</sub> mim][NTf <sub>2</sub> ] (neat)	9587 ± 115	10 ± 0.68	1.3 ± 0.26
[C <sub>3</sub> mim][NTf <sub>2</sub> ] : DMSO (1:0.5)	6589 ± 109	25.5 ± 0.51	0.51 ± 0.18
[C <sub>3</sub> mim][NTf <sub>2</sub> ] : DMSO (1:1)	3098 ± 143	53 ± 0.74	0.25 ± 0.12
[C <sub>3</sub> mim][NTf <sub>2</sub> ] : DMSO (1:1.5)	2162 ± 120	59.3 ± 0.48	0.22 ± 0.15

### 5.3.3. Resonance energy transfer (RET) study

As stated earlier, the ionic dye R6G is purposefully chosen for the current investigation, anticipating that the negative charge of the dye will facilitate the dye (acceptor) to have an electrostatic interaction with positive charge of the imidazolium moiety (donor) and thereby allow the close approach between donor and acceptor to undergo an efficient electrostatic interaction, which is required for RET process.

### 5.3.3.1. Probing the RET process using steady state measurements

Initially, the steady-state fluorescence measurements have been carried out to investigate the interactions between the donor (IL) and the acceptor (R6G) unit. For performing the fluorescence measurements, the concerned systems are excited at 375 nm, where a maximum absorption of the donor is found with a minimum absorption of the acceptor. The emission spectra of the donor (neat  $[\text{C}_3\text{mim}][\text{NTf}_2^-]$ ) with and without successive addition of the acceptor (R6G) are also provided in Figure 5.5. Similar plot has also been obtained for other ILs.

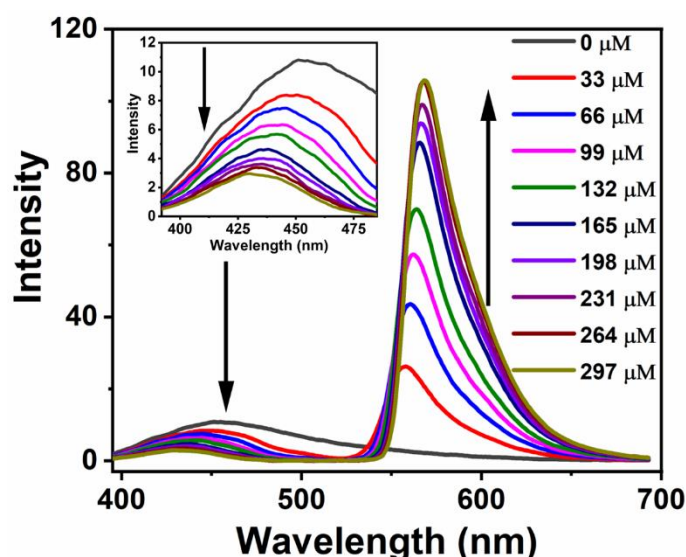


**Figure 5.5.** Variation in the emission intensity of  $[\text{C}_3\text{mim}][\text{NTf}_2^-]$  ( $\lambda_{\text{exc}} = 375 \text{ nm}$ ) with gradual addition of R6G. The inset indicates that the emission intensity of  $[\text{C}_3\text{mim}][\text{NTf}_2^-]$  decreases as the acceptor concentration is increased (from  $0 \mu\text{M}$  to  $231 \mu\text{M}$ ).

From Figure 5.5, we can clearly observe that with an increase in the concentration of the acceptor, there is a gradual decrease in the emission of the donor with a simultaneous increase in the emission of the acceptor (Figure 5.5). The decrease in the intensity of donor emission with respect to the acceptor indicates that the donor (IL) and the acceptor (R6G) are in RET communication. Also, a change in the emission maxima of the donor toward high energy (blue end) is observed (Figure 5.5). Interestingly, in the presence of the acceptor molecule, a red shift

in the emission of the acceptor has also been observed. The shift in the emission spectra for both donor and acceptor perhaps arise because of the change in the electronic environment of the donor and acceptor molecule upon association of acceptor to donor.<sup>244</sup>

### 5.3.3.2. RET process through time-resolved measurements

To confirm whether the quenching of donor emission by acceptor is mediated via a static or dynamic quenching process, time-resolved fluorescence measurements have been performed. Figure 5.6 represents the decay profile of [C<sub>3</sub>mim][NTf<sub>2</sub><sup>-</sup>] in the absence and presence of R6G and the corresponding decay parameters are listed in Table 5.4. Figure 5.7 represents the decay profile of the acceptor (R6G) in presence of the donor [C<sub>3</sub>mim][NTf<sub>2</sub><sup>-</sup>] and the corresponding time constants of the fluorescence decay of the acceptor (R6G) are listed in Table 5.5.

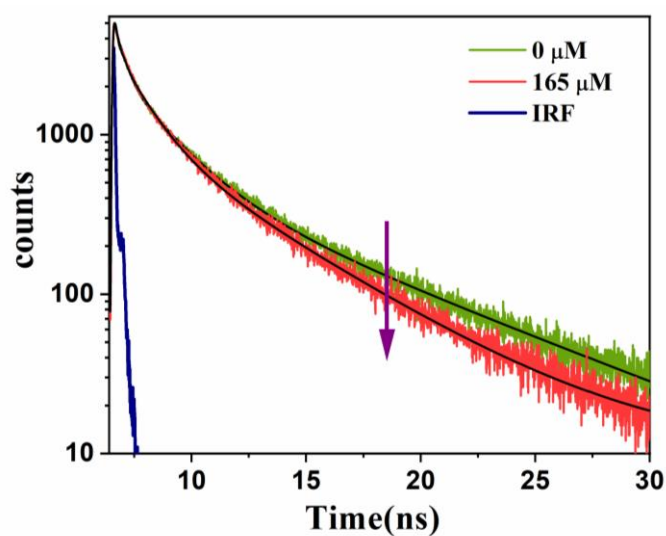


**Figure 5.6.** Fluorescence decay curves of [C<sub>3</sub>mim][NTf<sub>2</sub><sup>-</sup>] in absence and presence of the acceptor ( $\lambda_{\text{ex}} = 375$  nm and  $\lambda_{\text{em}} = 450$  nm). The solid black line represents fit to the data points.

**Table 5.4.** Time constants of the fluorescence decay of the donor (ILs) in the presence of the acceptor (R6G) at different concentrations (where  $\lambda_{\text{exc}} = 375$  nm and  $\lambda_{\text{em}} = 450$  nm).

System	Concentration ( $\mu\text{M}$ )	B <sub>1</sub>	$\tau_1$ (ns)	B <sub>2</sub>	$\tau_2$ (ns)	B <sub>3</sub>	$\tau_3$	$\langle\tau\rangle^a$
[C <sub>3</sub> mim][NTf <sub>2</sub> <sup>-</sup> ]	0	0.10	0.39	0.07	2.93	0.35	8.57	2.65

	33	0.05	0.34	0.04	2.81	0.30	8.34	2.51
	66	0.05	0.33	0.05	2.78	0.25	8.24	2.47
	99	0.6	0.31	0.04	2.72	0.2	8.11	2.40
	132	0.06	0.30	0.04	2.59	0.2	7.91	2.34
	165	0.07	0.29	0.05	2.55	0.19	7.85	2.18
[C <sub>4</sub> mim][NTf <sub>2</sub> <sup>-</sup> ]	0	0.55	0.97	0.23	3.41	0.03	1132	2.00
	33	0.62	0.93	0.21	3.47	0.02	11.53	1.85
	66	0.41	0.55	0.25	2.74	0.03	9.76	1.78
	99	0.43	0.50	0.25	2.65	0.03	9.62	1.67
	132	0.43	0.42	0.25	2.62	0.04	8.54	1.58
	165	0.48	0.41	0.26	2.61	0.03	8.42	1.50
[C <sub>6</sub> mim][NTf <sub>2</sub> <sup>-</sup> ]	0	0.22	0.33	0.11	2.43	0.03	8.27	1.68
	33	0.23	0.34	0.12	2.39	0.03	8.04	1.59
	66	0.24	0.30	0.12	2.26	0.03	7.93	1.54
	99	0.25	0.29	0.12	2.21	0.04	7.53	1.46
	132	0.27	0.25	0.13	2.07	0.04	7.43	1.34
	165	0.25	0.2	0.13	1.77	0.04	6.92	1.27
[C <sub>8</sub> mim][NTf <sub>2</sub> <sup>-</sup> ]	0	0.17	0.46	0.12	2.27	0.03	7.58	1.72
	33	0.2	0.42	0.13	2.21	0.02	7.46	1.65
	66	0.21	0.38	0.13	2.17	0.03	7.33	1.52
	99	0.22	0.34	0.14	2.08	0.03	7.09	1.43
	132	0.23	0.26	0.15	1.88	0.03	6.65	1.34
	165	0.29	0.20	0.13	1.71	0.04	6.26	1.23
[C <sub>6</sub> (mim) <sub>2</sub> ][NTf <sub>2</sub> <sup>-</sup> ] <sub>2</sub>	0	0.48	1.09	0.16	2.73	0.02	8.58	1.73
	33	0.51	1.03	0.18	2.70	0.02	8.70	1.64
	66	0.42	0.89	0.21	2.35	0.02	7.64	1.55
	99	0.54	0.83	0.26	2.16	0.03	7.33	1.50
	132	0.50	0.75	0.26	2.03	0.04	6.99	1.46
	165	0.51	0.70	0.26	2.01	0.04	6.32	1.42

[C <sub>8</sub> (mim) <sub>2</sub> ][NTf <sub>2</sub> <sup>-</sup> ] <sub>2</sub>	0	0.23	0.76	0.12	2.41	0.02	8.87	1.57
	33	0.22	0.59	0.15	1.96	0.02	7.34	1.48
	66	0.24	0.60	0.14	2.08	0.01	8.18	1.42
	99	0.23	0.45	0.16	1.90	0.02	7.63	1.36
	132	0.60	0.21	0.29	1.59	0.11	5.96	1.24
	165	0.60	0.20	0.29	1.50	0.12	5.51	1.21

<sup>a</sup> Experimental error: ± 5%

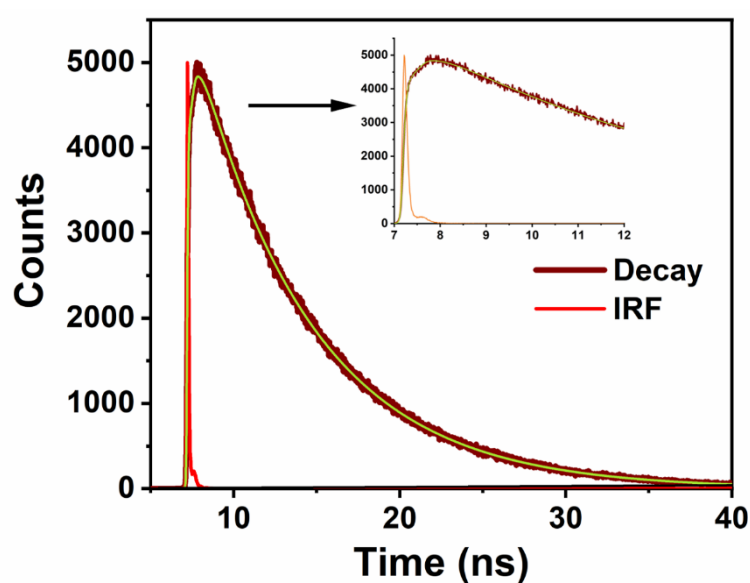


**Figure 5.7.** Fluorescence decay profile of the acceptor (R6G) ( $\lambda_{\text{ex}} = 375$  nm and  $\lambda_{\text{em}} = 580$  nm; concentration of the acceptor =  $231 \mu\text{M}$ ) in presence of the donor [C<sub>3</sub>mim][NTf<sub>2</sub><sup>-</sup>]. A clear rise time can be seen in the inset. The solid green line symbolizes fit to the data points.

**Table 5.5.** Time constants of the fluorescence decay of the acceptor (R6G) at different concentrations.

System	Concentration ( $\mu\text{M}$ )	Rise time (ns) <sup>a</sup>	Lifetime (ns)
[C <sub>3</sub> mim][NTf <sub>2</sub> <sup>-</sup> ]	165	1.45	7.15
	198	1.45	7.26
[C <sub>4</sub> mim][NTf <sub>2</sub> <sup>-</sup> ]	165	1.83	5.88
	198	1.84	5.92
[C <sub>6</sub> mim][NTf <sub>2</sub> <sup>-</sup> ]	165	2.51	8.12

	198	2.55	8.24
[C <sub>8</sub> mim][NTf <sub>2</sub> <sup>-</sup> ]	165	2.48	8.26
	198	2.50	8.33
[C <sub>6</sub> (mim) <sub>2</sub> ][NTf <sub>2</sub> <sup>-</sup> ] <sub>2</sub>	165	2.11	7.25
	198	2.12	7.30
[C <sub>8</sub> (mim) <sub>2</sub> ][NTf <sub>2</sub> <sup>-</sup> ] <sub>2</sub>	165	2.35	7.31
	198	2.37	7.35
<sup>a</sup> Experimental error: ± 5%			

From both Figure 5.7 and Table 5.5, one can clearly see that with an increase in the concentration of the acceptor, the lifetime of the donor (ILs) decreases. For example, by varying the concentration of the acceptor from 0 to 264  $\mu\text{m}$ , the average lifetime of the donor decreases by 25%. The decrease in the fluorescence lifetime of the donor with an increase in the concentration of the acceptor alone cannot completely prove the RET process between the donor (IL) and the acceptor (R6G) moiety.<sup>194, 198</sup> In this context, it is important to note that there are numerous reasons other than RET which can cause quenching.<sup>194, 198</sup> Hence, it is essential to evaluate the process diligently. By monitoring the fluorescence lifetime of the acceptor, one can verify the occurrence of RET process.<sup>194, 198, 201</sup> For example, if the RET process actually takes place for the current donor– acceptor system, a clear rise time at the time of monitoring the decay of acceptor is expected to be seen. Please note that the rise time also indicates the time constant for the RET process.<sup>176, 312</sup> The rise time ( $\tau = 1/K_{\text{RET}}$ ) is the growth observed in the fluorescence decay profile of the acceptor resulting from the energetically coupled donor and acceptor. In the present scenario, because of the energy transfer from donor to acceptor, the acceptor goes to the excited state after receiving the transferred energy from the donor. Therefore, when fluorescent decay is measured by monitoring the acceptor fluorescence, a growth/rise time (formation) is also observed along with the usual decay of the acceptor moiety. In the current study, Figure 5.7 depicts the acceptor's (R6G) decay profile in

the presence of donor, and the relevant parameters pertaining to the decay behavior of the concerned systems are listed in Table 5.4. From Table 5.5, a clear rise time can be observed for all the IL-R6G pairs. The rise time (inset of Figure 5.7) along with the decay of the acceptor conclusively proves the RET communication between the donor (IL) and the acceptor (R6G). To realize whether there are any differences in the outcomes of the RET process involving MILs and DILs, RET studies have been carried out by taking two DILs  $[C_6(\text{mim})_2][\text{NTf}_2^-]_2$  and  $[C_8(\text{mim})_2][\text{NTf}_2^-]_2$  and their monocationic counterparts  $[C_3\text{mim}][\text{NTf}_2^-]$  and  $[C_4\text{mim}][\text{NTf}_2^-]$ , respectively, as the chemical structure of MILs is considered half of the DILs.<sup>179, 220, 307</sup> In view of this, one can anticipate that the estimated time constant for the RET process for MILs and DILs would also follow the same order. However, from Table 5.5, it has been observed that the rise times for  $[C_6(\text{mim})_2][\text{NTf}_2^-]_2$  and  $[C_8(\text{mim})_2][\text{NTf}_2^-]_2$  are 2.12 and 2.37 ns, respectively, while those for  $[C_3\text{mim}][\text{NTf}_2^-]$  and  $[C_4\text{mim}][\text{NTf}_2^-]$  are 1.45 and 1.84 ns, respectively. From this observation, it is quite clear that although MILs by the virtue of its chemical formula may represent half of DILs, structural organization of the MILs is different in comparison to DILs. To shed more light on this aspect, studies are further extended by employing new MILs where the length of the alkyl side chain is kept the same as that of the spacer length of the DILs. These sets of ILs are judiciously chosen so that comparison of the experimental data corresponding to ILs having the same alkyl chain length in MILs and the same alkyl spacer in DILs can categorically reveal whether the length of alkyl groups or the local structure of DILs has any influence on the RET process. If one assumes that the hydrophobic alkyl chain of the MILs and DILs used in this study is solely responsible for the FRET event, then one can anticipate a similar value of rise time for the acceptor moiety for the ILs. However, the rise times of  $[C_6(\text{mim})_2][\text{NTf}_2^-]_2$  and  $[C_6(\text{mim})][\text{NTf}_2^-]$  are estimated to be 2.12 and 2.55 ns, respectively. Similar responses in the rise time have also been observed (Table 5.5) in the case of  $[C_8(\text{mim})_2][\text{NTf}_2^-]_2$  and  $[C_8(\text{mim})][\text{NTf}_2^-]$ . This observation reveals

that the length of the hydrophobic alkyl chain is not the only factor which is controlling the RET process from IL to R6G, but the local structural organization of ILs can also play a significant role for the same. Keeping the above facts and the present observation together in mind, one can say that the structural organization of DILs and MILs used in the current study is different.

To have a deep understanding of the microscopic environment of the ILs, data that are collected during the RET study are analyzed further with the help of Förster theory.<sup>194, 198, 201</sup> Förster theory has been explained in detailed manner in Chapter 2. Already it has been shown that the fluorescence of the neat ILs originates from the associated structures of the monomeric form of ILs. This fluorescing unit acts as the donor. In the present study, the distance between this fluorescing unit and the acceptor moiety (R6G) is described as the donor–acceptor distance. The parameters relating to the RET process are estimated with the help of Förster theory and are collected in Table 5.6.

**Table 5.6.** The magnitude of RET parameters.

System	$\phi_D$	$J(\lambda)(10^{16})$ ( $M^{-1}cm^{-1}nm^{-4}$ )	$\tau_D^0$ (ns)	$\tau_{rise}$ (ns)	$R_0$ ( $\text{\AA}$ )	$R_{DA}$ ( $\text{\AA}$ )	$E$	$K_{RET}$ ( $10^8 s^{-1}$ )
[C <sub>3</sub> mim][NTf <sub>2</sub> <sup>-</sup> ]	0.03	1.72	2.65	1.45	41.22	37.27	0.65	6.89
[C <sub>4</sub> mim][NTf <sub>2</sub> <sup>-</sup> ]	0.02	1.82	2.00	1.92	39.92	39.03	0.52	5.49
[C <sub>6</sub> mim][NTf <sub>2</sub> <sup>-</sup> ]	0.04	1.96	1.68	2.55	44.64	48.26	0.39	3.92
[C <sub>8</sub> mim][NTf <sub>2</sub> <sup>-</sup> ]	0.06	1.88	1.72	2.50	46.21	55.05	0.31	4.02
[C <sub>6</sub> (mim) <sub>2</sub> ][NTf <sub>2</sub> <sup>-</sup> ] <sub>2</sub>	0.05	1.67	1.73	2.12	44.90	46.44	0.45	4.72
[C <sub>8</sub> (mim) <sub>2</sub> ][NTf <sub>2</sub> <sup>-</sup> ] <sub>2</sub>	0.07	1.56	1.57	2.35	45.45	48.61	0.40	4.25

From Table 5.6, it is interesting to note that the donor–acceptor distance for [C<sub>6</sub>(mim)<sub>2</sub>][NTf<sub>2</sub><sup>-</sup>]<sub>2</sub> is found to be 46.44  $\text{\AA}$  and its monocationic counterpart [C<sub>3</sub>mim][NTf<sub>2</sub><sup>-</sup>]

is found to be 37.27 Å. Also, in the case of  $[\text{C}_8(\text{mim})_2][\text{NTf}_2^-]_2$ , the donor–acceptor distance is estimated to be 48.61 Å, while the donor–acceptor distance for  $[\text{C}_4\text{mim}][\text{NTf}_2^-]$  is 39.03 Å. Because, from the view of chemical formula, the above MILs can be considered as half of their DIL counterparts, the donor–acceptor distance for the DILs is expected to be half of the corresponding MILs. However, the estimated donor–acceptor distance obtained from the RET parameters has indicated clearly that the local structure of DILs is different from that of MILs. The data have essentially indicated that DILs have a more compact structural organization than MILs. To shed more light on this effect, in particular, to investigate the influence of the length of apolar alkyl group (side-chain MILs and spacer chain length in DILs) in the ensuing RET event, we have also estimated the donor–acceptor distance by introducing MILs whose alkyl chain length is the same as that of the spacer chain length in DILs and the relevant data are mentioned in Table 5.6. Interestingly, the data in Table 5.6 reveals that even though the length of nonpolar alkyl chain is found to be the same for both the sets of ILs, the donor–acceptor distances for  $[\text{C}_6\text{mim}][\text{NTf}_2^-]$  and  $[\text{C}_8\text{mim}][\text{NTf}_2^-]$  donors are found to be 48.26 and 55.05 Å, respectively, while the donor–acceptor distances for  $[\text{C}_6(\text{mim})_2][\text{NTf}_2^-]_2$  and  $[\text{C}_8(\text{mim})_2][\text{NTf}_2^-]_2$  are found to be 46.44 and 48.61 Å, respectively. This result clearly depicts that the RET does not only depend on the alkyl chain length but also depend on the local structure of the cationic moiety of the concerned ILs. The data are further analyzed by looking at other relevant parameters such as energy-transfer efficiency (E) and rate of energy transfer ( $K_{\text{RET}}$ ). From Table 5.6, it can be observed that the rate of energy transfer ( $K_{\text{RET}}$ ) as well as the energy-transfer efficiency (E) in  $[\text{C}_3\text{mim}][\text{NTf}_2^-]$  and  $[\text{C}_4\text{mim}][\text{NTf}_2^-]$  are found to be higher than that of  $[\text{C}_6(\text{mim})_2][\text{NTf}_2^-]_2$  and  $[\text{C}_8(\text{mim})_2][\text{NTf}_2^-]_2$  but is not as high as expected from their chemical formula. However, E and  $K_{\text{RET}}$  are found to be greater in DILs  $[\text{C}_6(\text{mim})_2][\text{NTf}_2^-]_2$  and  $[\text{C}_8(\text{mim})_2][\text{NTf}_2^-]_2$  than in  $[\text{C}_6\text{mim}][\text{NTf}_2^-]$  and  $[\text{C}_8\text{mim}][\text{NTf}_2^-]$ . All

these parameters illustrate that the microscopic structures of DILs and MILs are different from each other.

Now, if we consider all the important RET parameters ( $\tau_{\text{rise}}$ ,  $E$ ,  $K_{\text{RET}}$  and  $R_{\text{DA}}$ ) that have been obtained from the current investigation (Table 5.6) together for all the ILs, the following observations could be made. Among the MILs, it has been observed that the time constant of RET process for short-chain MILs  $[\text{C}_3\text{mim}][\text{NTf}_2^-]$  and  $[\text{C}_4\text{mim}][\text{NTf}_2^-]$  is significantly less than that for long-chain MILs  $[\text{C}_6\text{mim}][\text{NTf}_2^-]$  and  $[\text{C}_8\text{mim}][\text{NTf}_2^-]$ . While  $E$  and  $K_{\text{RET}}$  are found to be higher in short-chain MILs in comparison to long-chain MILs,  $R_{\text{DA}}$  is also found to be less for the former in comparison to the latter. These observations clearly demonstrates that the RET between ILs and R6G is more favorable in shorter alkyl chain containing ILs as compared to relatively longer ILs. These observations indicate that the alkyl chain length in ILs plays an important role in controlling the donor–acceptor interaction during the FRET event. In this regard, it is noteworthy to mention that Leal and co-workers,<sup>314</sup> through both theory and experiments, have illustrated that the fluid structure of small alkyl chain containing ILs are dominated by the polar domains whereas for the long alkyl chain containing ILs, the apolar domains formed by the alkyl chain dominate the fluid structure.<sup>314</sup> Also, the nanostructural organization of DILs is found to have a mixture of unfolded and highly folded DILs. As a result of this, in the current study, the RET process involving the donor and the acceptor has been observed favorable for shorter alkyl chain containing ILs in comparison to the longer alkyl chain containing ILs. Again, if we compare all the RET data (Tables 5.6) obtained during the present study for MILs and DILs, one can observe that the RET process in DILs is very different from their monocationic imidazolium counterparts. More interestingly, the present data also reveal that the RET interaction is more favorable in DILs than in MILs, even though in a scenario where the length of the alkyl group is kept the same for both the ILs. The observation of a relatively more favorable RET process in DILs than in MILs despite the

facts that (a) DILs have the same alkyl group in their cationic part and (b) DILs are relatively bulkier because of the presence of an extra unit of imidazolium moiety in their dication indicates that the local structures of DILs are very different from that of MILs in a sense that DILs have a more compact structure than MILs. The observation also indicates that the length of the alkyl group (chain) is not the sole factor which can contribute to the RET outcomes for DILs and MILs, but the local structure of DILs and MILs can also play a key role for the same event. In the present study, the RET process involved a small alkyl chain containing MIL (e.g., C<sub>3</sub>C<sub>1</sub> and C<sub>4</sub>C<sub>1</sub>) different from a long alkyl chain MIL (e.g., C<sub>6</sub>C<sub>1</sub> and C<sub>8</sub>C<sub>1</sub>). This illustrates that the alkyl chain length plays a crucial role in governing RET events pertaining to ILs. Essentially, the RET data for our own system indicates the compactness in the structure of DILs. To get more evidence in favor of the compact structure of DILs as compared to MILs, we have also estimated the densities of DILs and MILs. The data on the density measurements for both MILs and DILs have shown that the DILs have a larger density in comparison to MILs. These data clearly suggest that DILs are more compact than the corresponding MILs. Therefore, this observation is suggestive of the fact that the local structures of DILs and MILs are different. Also, it is quite evident from the recent studies based on simulations<sup>244, 311</sup> and NMR diffusion experiments<sup>269</sup> that DILs having a medium/longer alkyl chain containing flexible spacer can have a folded structure. In view of these, we can say that the difference in the outcomes of an RET event for DILs and MILs can be attributed to the difference in the microscopic structural arrangements of the concerned media.

#### **5.4. Conclusion**

The objective of the present work is to understand the differences in the microscopic structural organization of imidazolium-based MILs and DILs by exploiting RET studies. The use of RET study in achieving the objective of this work stems from the fact that RET is a distance-sensitive technique, and therefore, the outcome of the FRET events will be directly related to the change

in the donor–acceptor distance, which in turn may arise because of the change in the local structural arrangements of the concerned ILs. In the current work, prior to the RET studies, the fluorescence behavior of neat ILs is investigated. Both steady-state fluorescence study and FCS have shown that the associated structure of imidazolium moiety is primarily responsible for the emission in neat ILs. The occurrence of RET process from the donor to the acceptor units has been clearly established by the observation of a rise time during the estimation of the fluorescence intensity decay of the acceptor. The analysis of the data based on Förster theory has demonstrated that the RET interaction is more favorable for DILs than for MILs. The present data also illustrate that the donor–acceptor distance in DILs is found to be less than in MILs even though DILs are relatively bulkier because of the presence of an extra imidazolium unit in their dication. More interestingly, the data also reveal that the RET interaction is found to be more favorable for DILs than for MILs even in a scenario where the alkyl chain length is kept constant in both DILs and MILs. This suggests that the alkyl chain length on the imidazolium cation is not the only contributing factor in the ensuing RET process between DILs and MILs, but the local structure of imidazole dication also plays a significant role in the RET process. The current results clearly indicate more compactness in the local structural organization of DILs as compared to the MILs. When the outcome of the current study is visualized along with the outcomes of recent simulation and NMR diffusion studies which suggested the folded structure of DILs with a medium/ longer alkyl chain containing flexible spacer, one can perhaps also reasonably assume that the compact structural organization in DILs is caused due to their folded structure. The current study is also interesting because it highlights the usefulness of a simple and noninvasive technique, RET, in capturing the different nanostructural organizations of structurally similar MILs and DILs.

## CHAPTER 6

---

# The Effect of Lithium Ions on the Structural Organisation of Monocationic and Dicationic Ionic Liquids

---

---

Chakraborty, M.; Barik, S.; Mahapatra, A and Sarkar, M. *J. Phys. Chem. B* **2021**, *125*, 13015-13026.

## Chapter 6

---

### The Effect of Lithium Ions on the Structural Organisation of Monocationic and Dicationic Ionic Liquids

---

In recent times, ionic liquid-based (ILs) electrolytic system has emerged as suitable alternative to the conventional organic solvent-based electrolytic system. However, since, anion of ILs is known to form aggregates in the presence of lithium ions ( $\text{Li}^+$ ), and this can influence the transport properties of  $\text{Li}^+$  ion in a significant manner, it is, therefore, important to understand how lithium-ions influence the structure and dynamics of ILs. With this objective, the studies that are done in the present chapter focuses on intermolecular interaction, structural organization, and dynamics of monocationic ILs (MILs) and dicationic IL (DIL) in the absence and presence of lithium salt. Specifically, for this purpose, two MILs,  $[\text{C}_3\text{C}_{1\text{im}}][\text{NTf}_2]$ ,  $[\text{C}_6\text{C}_{1\text{im}}][\text{NTf}_2]$ , and a DIL,  $[\text{C}_6(\text{mim})_2][\text{NTf}_2]_2$  are chosen in such a way that either the alkyl chain of MILs becomes equal or half of the spacer chain length of DIL. To understand the effect of the addition of lithium-ion on the structural organization of MILs and DIL, steady-state fluorescence spectroscopy, time-resolved fluorescence anisotropy and nuclear magnetic resonance (NMR) techniques are used. Essentially, all of these investigations suggest that the addition of lithium-ion significantly alters the microscopic behavior of MILs in comparison to that of DIL.

---

#### 6. 1. Introduction

Room temperature ionic liquids (RTILs) have attracted considerable interest for their unique physicochemical properties such as a broad electrochemical window, negligible vapor pressure, and non-flammability.<sup>4, 17, 51, 248-250</sup> Due to these properties, ILs are also perceived to be promising materials to be used as electrolytes in lithium-ion and lithium metal batteries.<sup>315</sup>

In other words, the use of RTILs-based electrolytic systems in comparison to organic solvent-based electrolytic systems will be advantageous in avoiding hazards (fire and explosion) that are usually associated with conventional organic solvents. Apart from the safety issues, IL-based electrolytic systems are found to exhibit good electrochemical performance<sup>316-318</sup> and are also cost-effective. While the majority of the research work in this regard is carried out by employing monocationic-based ILs, such studies on another type of ILs, for example, geminal dicationic ILs (GDILs), are very limited.<sup>157, 246, 319-325</sup> Moreover, since recent studies have demonstrated that anions of ILs aggregates in the presence of lithium-ion leading to an increase in viscosity of the medium, proper understanding on the structure and dynamics of ILs in the absence and the presence of lithium-ion becomes a worthwhile objective.

Focusing on the usage of ILs as electrolytes in lithium-ion batteries, studies have been carried out by emphasizing the coordination effect of Li ions with the ILs.<sup>322, 326</sup> In this context, it is noteworthy to mention that solvated Li-ions are found to have distinct abilities to coordinate with the IL media.<sup>167, 327</sup> This coordination can be successfully connected to the idea of “structure-making” and “structure-breaking”.<sup>167-169</sup> This idea can be extended to the solvation of inorganic ions, which induce a different local structure of water molecules in the first and even the second or third solvation shells to accommodate the dissolved species.<sup>327</sup> In a separate study carried out by Atkin and co-workers<sup>168</sup> have noted LiNO<sub>3</sub> has “structure-breaking” effect in EAN due to the incorporation of LiNO<sub>3</sub> into the polar domain of EAN, causing disruption in the neat alignment of ethyl chains in the apolar domain. Conversely, “structure-making” has been found in the case of ethanolanmonium nitrate (EtAN) when LiNO<sub>3</sub> is dissolved in the medium. While investigating the effect of lithium bis(trifluoromethylsulfonyl)imide ([LiNTf<sub>2</sub>]) on the IL 1-butyl-3-methylimidazolium bis(trifluoromethylsulfonyl)imide ([C<sub>4</sub>C1im][NTf<sub>2</sub>]) by Fayer and co-workers<sup>328</sup> through optically heterodyne-detected optical Kerr effect (OHD-OKE) spectroscopy have observed that

medium viscosity increases upon addition of lithium salt to the media which in turn influences the ion mobility and rotational dynamics of ions in IL–Li solvent system. Overall, all the above studies that are carried out on MILs have demonstrated that the  $\text{Li}^+$  ion can cause significant changes in the structural organization of the medium.

As discussed above, several studies in search of an efficient electrolytic medium with various MIL-based systems have been studied. However, recent investigation has also highlighted that despite the decent stability of MILs, many of these systems are susceptible to chemical and thermal degradation which can cause serious problems in the functioning of lithium-ion batteries.<sup>329</sup> To overcome this challenge, new types of ILs having higher chemical and thermal stabilities are desirable. In this context, geminal dicationic ionic liquids (GDILs) are thought to be a good candidate due to their higher thermal and chemical stability than many MILs.<sup>37, 73, 149-153</sup> In fact, it has also been shown that the properties of GDILs are superior than the MILs in terms of the higher glass transition temperature, higher surface tension, and larger electrochemical window.<sup>73</sup> We note that, due to the large electrochemical window of the GDILs, an electrolytic system comprising of GDILs and lithium-ion is expected to be beneficial in improving the electrochemical stability of the electrolytic medium at higher voltages.<sup>150-152</sup> All these properties make GDILs as an attractive electrolytic medium for high temperature batteries and dye sensitized solar cells despite the fact that they have high density.<sup>153</sup> Since the above discussions depict many of the previous works that have been carried in understanding the behavior of MILs in the absence and presence of lithium-ion, studies on this aspect by employing GDILs are expected to be interesting. Moreover, as reported earlier introduction of lithium-ion to the IL medium can cause significant changes in the structure and dynamics of the concerned media and all these matters are all intricately related to the performance of a suitable electrolytic medium in the lithium-ion battery. Proper

knowledge of the intermolecular interactions, structure, and dynamics of the concerned medium (MILs and GDILs) is necessary.

Keeping the above facts in mind, the work done in this chapter has been carried out with an aim to understand the influence of lithium-ion in both monocationic and dicationic ionic liquids. For the study we have chosen two monocationic ionic liquid (MIL), namely  $[\text{C}_3\text{C}_{1\text{im}}][\text{NTf}_2]$  and  $[\text{C}_6\text{C}_{1\text{im}}][\text{NTf}_2]$ , along with a dicationic ionic liquid (DIL),  $[\text{C}_6(\text{mim})_2][\text{NTf}_2]_2$  (Figure 6.1). Investigations have been carried out using steady-state fluorescence, time-resolved fluorescence anisotropy, and NMR diffusion techniques. To understand the difference in the structural organization between MILs and DIL in the absence and presence of lithium-ion, the MILs are chosen in a way that either the alkyl chain of MILs becomes equal or half of the spacer chain length of DIL. The microheterogeneity in these systems has been estimated with the help of excitation wavelength-dependent studies. Structural organization in the apolar and polar domains of ILs have been probed by following the rotational diffusion of suitably chosen solute in the concerned media through time-resolved fluorescence anisotropy (TRFA) measurements. Furthermore, NMR diffusion also throws light on the translational diffusion of cations of ILs in the absence and presence of lithium-ion. Outcomes of these investigations will have serious implications in formulating electrolytic systems for lithium-ion battery applications.

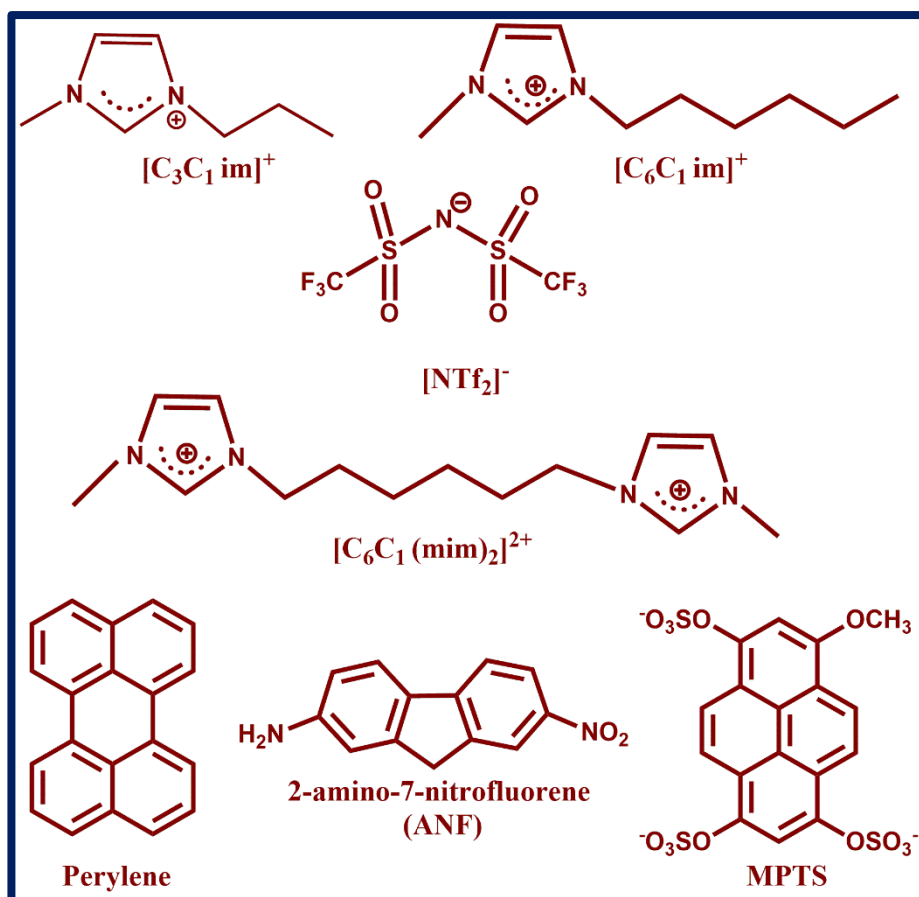


**Figure 6.1.** Molecular structures of ILs and probes used in the present study (chapter 6).

## 6.2. Experimental techniques and methods

The ionic liquids  $[C_3C_1][NTf_2]$  and  $[C_6C_1][NTf_2]$  were purchased from Sigma Aldrich (>99% purity) and TCI Chemicals (>98% purity). The dicationic IL,  $[C_6(\text{mim})_2][NTf_2]_2$  was synthesized by following a literature procedure explained in chapter 2. Perylene and MPTS were purchased from Sigma-Aldrich and used as received. ANF was received from Biosynth Carbosynth. The sample preparation procedures and experimental methods for steady-state and time-resolved fluorescence studies, and translational diffusion studies through NMR are described in detail in Chapter 2.

## 6.3. Results and discussions

### 6.3.1. Steady-state fluorescence studies

Unlike the conventional solvents, ILs are made of ions which gives rise to the complex microheterogeneity character to these media. As the microheterogeneity of a given media is known to be intricately related to the physiochemical properties of the media,<sup>124, 171, 173, 262, 330-333</sup> it is therefore essential to understand the microheterogeneous behavior of different solvent systems chosen for the study. Specifically, one needs to estimate the extent of microheterogeneity caused by the addition of LiNTf<sub>2</sub> for both the MILs and DIL. Experimentally, to determine the extent of microheterogeneity in a given media, excitation wavelength-dependent fluorescence measurements are beneficial. It is well documented that excitation wavelength-dependent fluorescence studies can qualitatively demonstrate the extent of spatial heterogeneity in a given liquid system.<sup>332</sup> In the present study, the extent of microheterogeneity in the case of MILs and DIL and the effect of Li<sup>+</sup> ions on the microheterogeneity of the medium can be estimated by the  $\lambda_{exc}$  dependent fluorescence behavior of 2-amino-7-nitrofluorene (ANF) having a relatively shorter excited state lifetime (~100ps).<sup>334</sup> The ANF has been chosen for the study due to the fact that the relatively shorter excited state lifetime, fluorescence signature of ANF in IL media is expected to be more responsive to the short-lived “transient” domains, created upon the nanostructural organization of ILs.<sup>262</sup> Figure 6.2 illustrates the plot of  $\lambda_{em}^{max}$  versus  $\lambda_{exc}$  of ANF at 298 K for MILs and DIL in the absence and presence of LiNTf<sub>2</sub>.

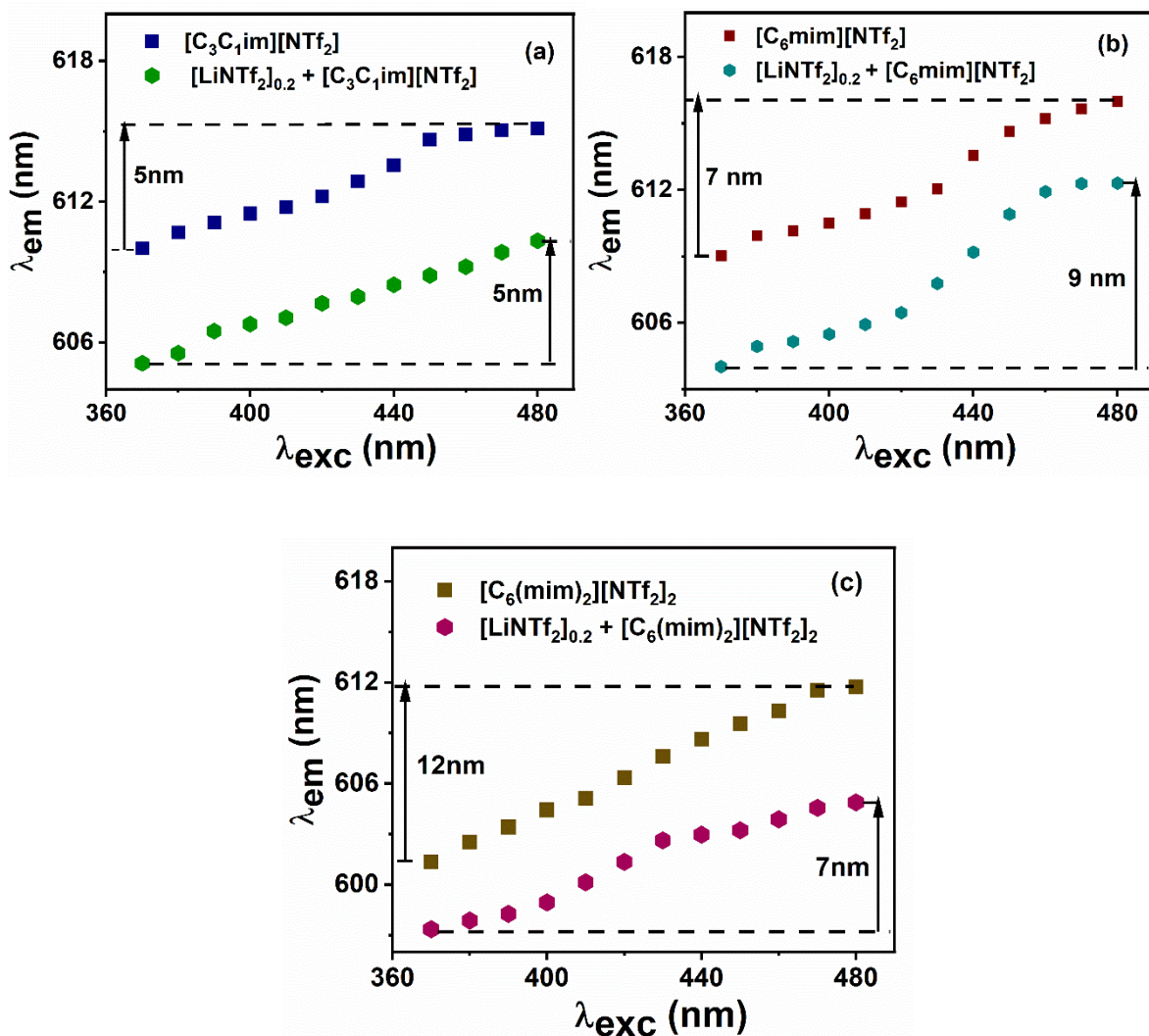


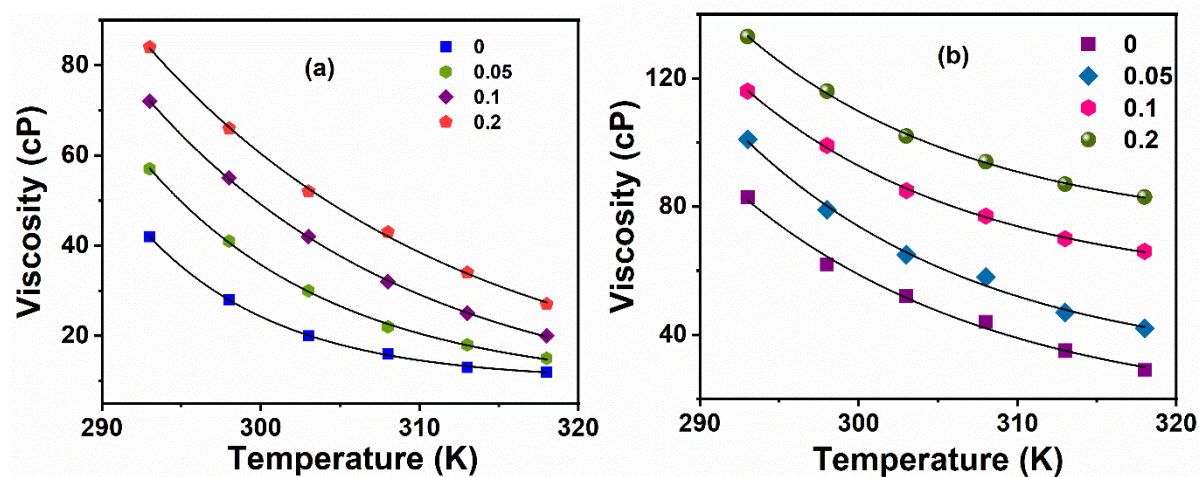
**Figure 6.2.** The excitation wavelength dependent behaviour of ANF in (a)  $[C_3C_1im][NTf_2]$ ,  $[LiNTf_2]_{0.2}[C_3C_1im][NTf_2]$  (b)  $[C_6C_1im][NTf_2]$ ,  $[LiNTf_2]_{0.2}[C_6C_1im][NTf_2]$ , and (c)  $[C_6(mim)_2][NTf_2]_2$  and  $[LiNTf_2]_{0.2}[C_6(mim)_2][NTf_2]_2$ .

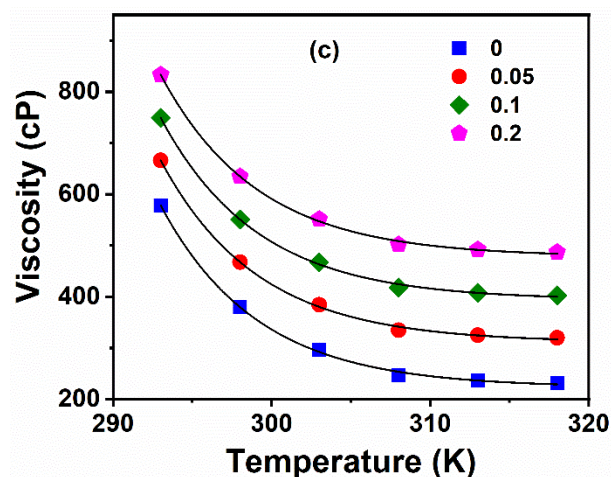
As observed from Figure 6.2, upon increasing the  $\lambda_{exc}$  gradually, an increase in the  $\lambda_{em}^{max}$  is observed for all the solvents systems; however, the total shift in all the cases is found to be different. For example, in the case of MILs in the absence of  $[LiNTf_2]$ ,  $[C_3C_1im][NTf_2]$ , and  $[C_6C_1im][NTf_2]$ , the total shift in the emission maxima has been observed to be 5 nm and 7 nm, respectively. While in the presence of 0.2 mole fraction of  $[LiNTf_2]$ , the total shift in the emission maxima for the same is 5 nm and 9 nm, respectively. On the other hand, in the case of DIL,  $[C_6(mim)_2][NTf_2]_2$  in the absence and presence of 0.2 mole fraction of  $[LiNTf_2]$ , the total shift in emission maxima has been found to be 12 nm and 7 nm respectively. These observations indicate that neat ILs (MILs and DIL) and IL + Li salt mixture,

used in the current study, are spatially heterogeneous. It further demonstrates that while the micro-heterogeneous behavior of neat MILs does not change much in the presence of Li salts, the same is reduced appreciably for neat DILs in the presence of  $\text{Li}^+$  ions. The observation of the total shift of  $\lambda_{em}$  with a change in the  $\lambda_{exc}$  is estimated to be more in DIL as compared to that of MIL (Figure 6.2), indicating that DIL is more heterogeneous than MIL.

### 6.3.2. Time-resolved fluorescence anisotropy studies

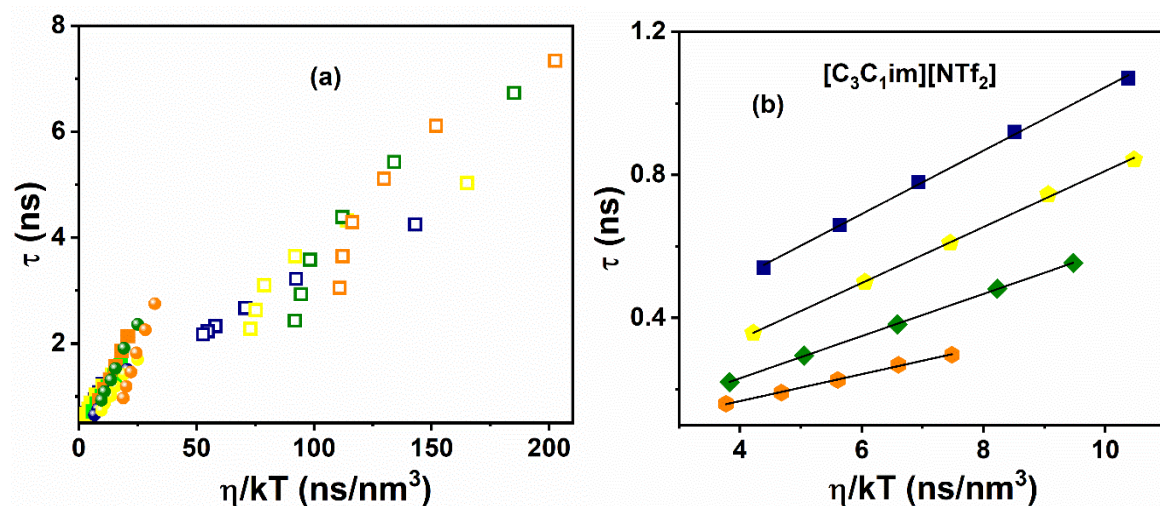
In the present study, investigations have been carried out using two probes found to be structurally similar but chemically distinguishable in nature, perylene, and MPTS. Perylene being apolar and MPTS being polar and negatively charged, expected to help monitor solute-solvent interactions at the apolar and polar domain of the given medium, such as ILs where polar and non-polar domains are the part of their nanostructural organization. Specifically, to understand the temperature dependence of viscosity of the medium more clearly, viscosities of MILs and DIL with increasing concentrations of  $\text{Li}^+$  ion are plotted at various temperatures.





**Figure 6.3.** Temperature-dependent viscosities of a)  $[C_3C_1im][NTf_2]$  (MIL) b)  $[C_6C_1im][NTf_2]$  (MIL) c)  $[C_6(mim)_2][NTf_2]_2$  (DIL) solutions with different mole fractions of  $Li^+$  ions. The data points are fitted by single exponential fit. The black lines are the fitted lines.

From the temperature-dependent viscosities plots that are shown in Figure 6.3, one can also see that the viscosity of IL media increases with the adding of  $Li^+$  ion concentration. From the data plotted in Figure 6.3, one can also see that the increase in viscosity of DIL with the addition of  $Li^+$  ion is about two folds higher than that has been found in both the MILs. This observation suggests that the alkyl spacer chain of DIL may have a considerable influence on the bulk viscosity of ionic liquid-based electrolyte systems.



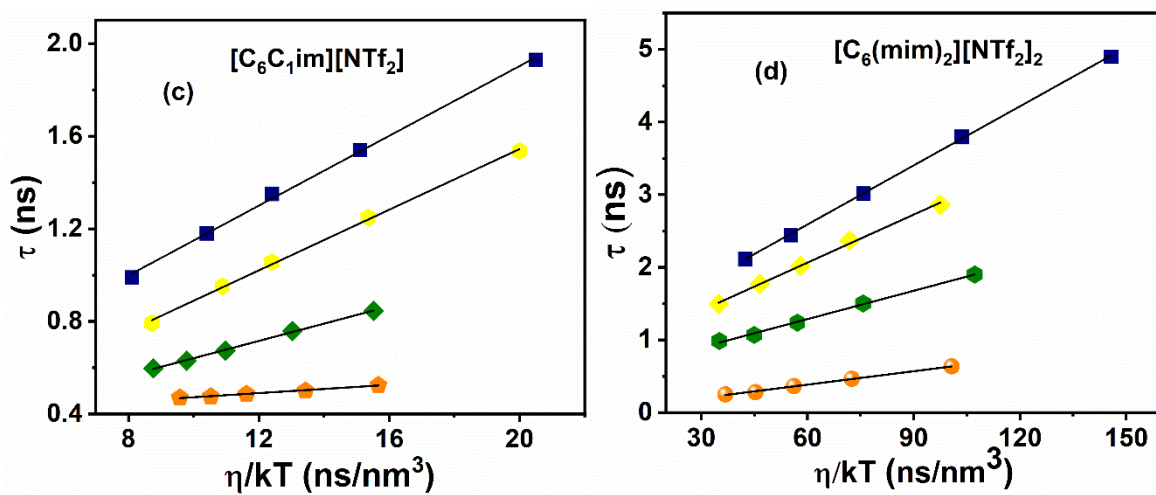


**Figure 6.4.** (a) Representation of average experimental rotational relaxation time for perylene plotted against dynamic viscosity  $\eta$  over  $kT$  in case of both MIL (solid symbols) and DIL (open symbols) for  $\chi[LiNTf_2] = 0$  (colour code: navy blue), 0.05 (colour code: yellow), 0.1 (colour code: green) and 0.2 (colour code: orange). The plots in (b), (c), and (d) are rescaled and shifted for better visualization. Plot (b) is for the MIL,  $[C_3C_{1im}][NTf_2]$ , plot (c) is for MIL,  $[C_6C_{1im}][NTf_2]$  and plot (d) is for DIL,  $[C_6(mim)_2][NTf_2]_2$ . The data points are the least square fitted and show the hydrodynamic diffusion.

In Figure 6.4, the experimental values of rotational time ( $\tau_r$ ) taken over a temperature range in the case of perylene for each lithium added (in mole fraction) in IL solution have been plotted against  $\eta/kT$ . As can be seen from Figure 6.4, in case of MILs and DIL, as the mole fraction of  $Li^+$  ion increases, the  $\tau_r$  value also increases. However, it is also essential to realize whether the increase in the  $\tau_r$  value for perylene upon increasing  $Li^+$  ion concentration is solely dependent on the bulk viscosity of the medium or the micro-viscosity, which is caused due by the change in the structural organization of the IL medium in the presence of lithium salt.

To have a better realization of the solute dynamics, in particular how the solute dynamics are affected by the micro-viscosity of a media that have been used in the present study, the TRFA data has further been analyzed in the light of Stokes-Einstein-Debye (SED) hydrodynamic model.<sup>269</sup> Details of hydrodynamic theories are explained in chapter 2.

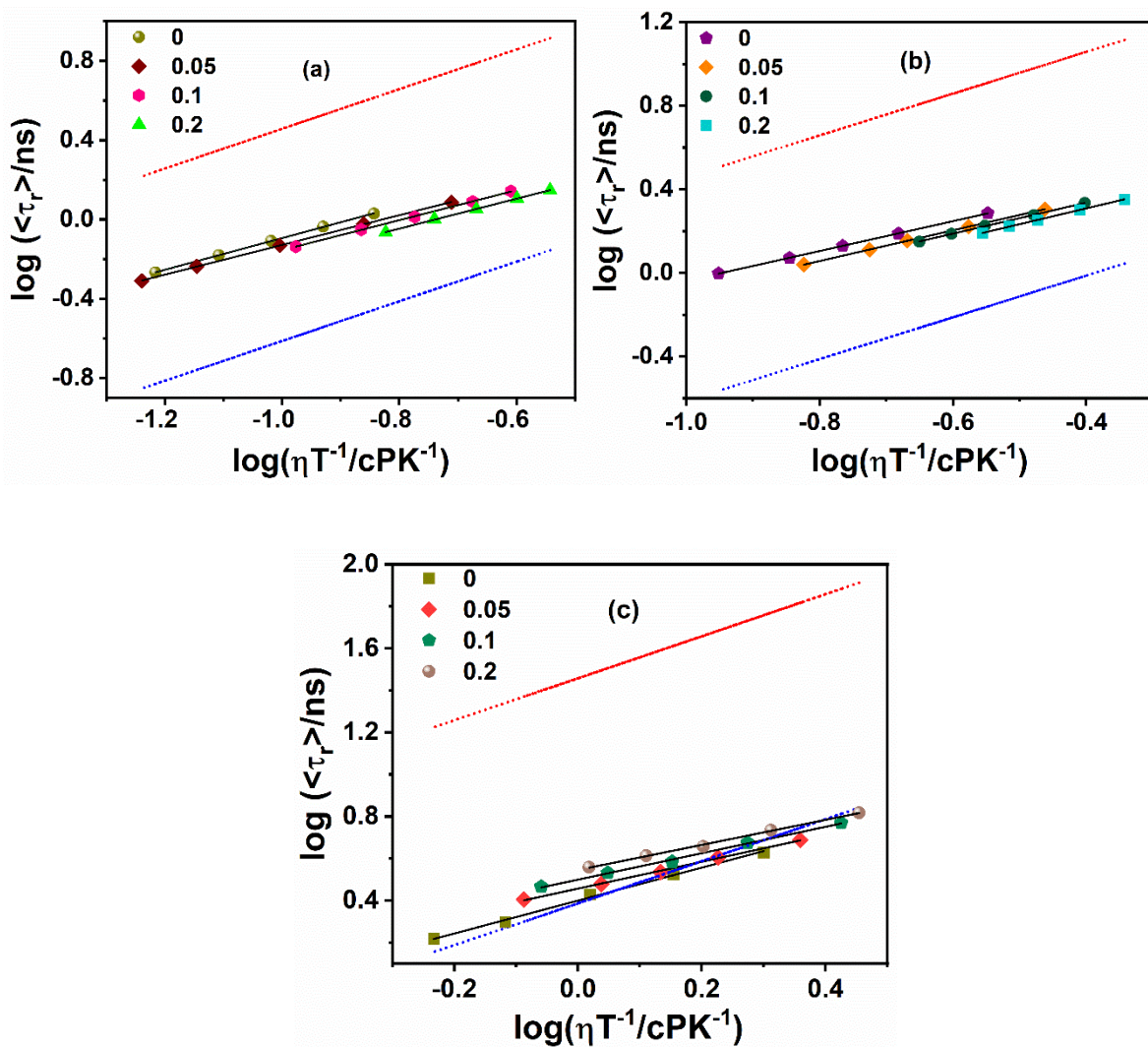


**Figure 6.5.** Log-log plots of average rotational time of perylene in (a)  $[\text{C}_3\text{C}_1\text{im}][\text{NTf}_2]$  (b)  $[\text{C}_6\text{C}_1\text{im}][\text{NTf}_2]$  and (c)  $[\text{C}_6(\text{mim})_2][\text{NTf}_2]_2$  with red and blue boundary condition indicating the stick and slip boundary conditions respectively. The solid black line indicates the fit to data points.

Figure 6.5 represents the log-log plots of average rotational relaxation time  $\langle \tau_r \rangle$  versus  $\eta/T$  for perylene in MILs and DIL with the gradual addition of  $\text{Li}^+$  ions at various temperatures. As can be seen from Figure 6.5, in the case of  $[\text{C}_3\text{C}_1\text{im}][\text{NTf}_2]$  and  $[\text{C}_6\text{C}_1\text{im}][\text{NTf}_2]$ , the rotational relaxation behavior of perylene remains within the boundary conditions imposed by SED theory. However, with an increase in the  $\text{Li}^+$  ion concentration, a departure in the hydrodynamic behavior of the solute in the same medium is noted in a sense that the rotational relaxation behavior of perylene in both the MILs gradually becomes faster

(approaches to the slip boundary) with the gradual increase in the  $\text{Li}^+$  ion concentration. Essentially, this observation indicates a faster rotation relaxation of perylene in the said media. It is an interesting observation in the sense that rotational motion of perylene becomes faster despite the fact bulk viscosity of the concerned medium increases as the concentration of  $\text{Li}^+$  ion increases. This non-obeyance of hydrodynamic behavior of the probe solute or in other words, the departure of the rotational diffusion of the solute with the bulk viscosity of the medium (IL + Li salt) indicates that the role of micro-viscosity of the concerned media is more important than the bulk viscosity in terms of governing the solute rotation. It may also be noted here that such type of viscosity-diffusion decoupling behavior has also been observed by other researchers, and they have rationalized this behaviour by considering the change in the micro heterogeneous behavior of the concerned media.<sup>169, 245, 333, 335</sup> Therefore, the present observation also indicates that the structural organization of neat ILs changes considerably in the presence of  $\text{Li}^+$  ion and thereby causing a change in the micro-heterogenous behavior of the medium. More interestingly, in the case of DIL, one can see that the rotational relaxation behavior of perylene at a lower temperature is significantly faster than that in MIL (Figure 6.5). This observation, as per hydrodynamic terminology, can be interpreted as the sub-slip behavior of the solute. The present sub-slip behavior of perylene in DILs indicates that it is located in the apolar region of the medium. However, upon a careful look at Figure 6.5 (b) and (c), one can also observe that the rotation of DIL is significantly faster even though the length of the alkyl chain corresponding to  $[\text{C}_6\text{mim}][\text{NTf}_2]$  (MIL) and the  $[\text{C}_6(\text{mim})_2][\text{NTf}_2]_2$  (DIL) remains same. This indicates that the length of the alkyl chain (side chain in MIL and spacer chain in DIL) are not solely responsible for the observed behavior in the respective medium; rather, it indicates that the nanostructural organization of MILs and DILs are very different and due to that the micro-viscosity felt by the rotating solute is very different in these two media. Moreover, with the addition of  $\text{Li}^+$  ion in the DIL medium, the rotational motion of perylene

becomes slower (hindered). Also, in this case too, the non-obeyance of hydrodynamic behavior can be easily seen (Figure 6.5). Overall, one can quickly note that the hydrodynamic behavior in the case of MILs and DIL are very different, in a sense that with the gradual addition of  $\text{Li}^+$  ion, the solute rotation becomes faster in MIL. In contrast, not much change in the rotation of solute has been observed in the case of DIL. The observation of the faster rotation of perylene in MILs upon addition of  $\text{Li}^+$  ion indicates that  $\text{Li}^+$  and  $\text{NTf}_2^-$  binding reduces the packing of the alkyl chain present in the apolar region of MILs. These observations show that the behavior of (MIL + Li) mixtures is significantly different from that of (DIL + Li) mixtures.

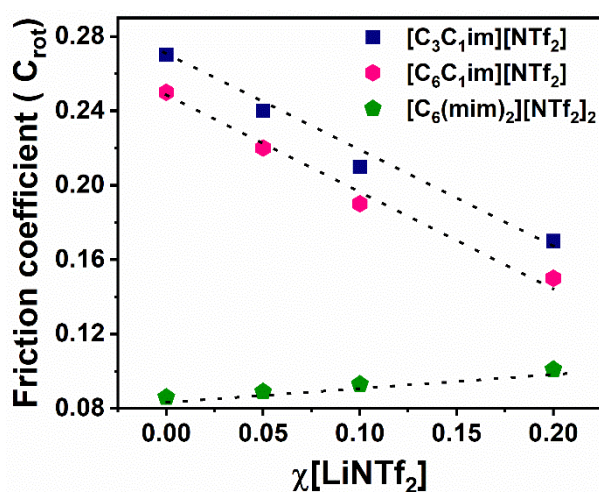


**Figure 6.6.** The average friction coefficient for perylene in all the systems as a function of  $\text{Li}^+$  ion concentration.

Another useful approach to understand the consequence of increasing viscosity upon addition of  $\text{Li}^+$  ion in the respective media on the rotational relaxation behavior of perylene is obtained by calculating the friction coefficient  $C_{rot}$ , where  $C_{rot}$  is expressed as  $C_{rot} = \tau_{theory}/\tau_{exp}$ . This unitless friction coefficient  $C_{rot}$  is considered a helpful parameter as it represents the coupling between the solute and solvent to be independent of the temperature and viscosity of the medium. Figure 6.6 is a plot of friction coefficients of both MILs and DIL as a function of  $\text{Li}^+$  ion concentration. As can be seen from Figure 6.6, there is a gradual change in the friction coefficient upon the addition of  $\text{Li}^+$  ion. However, from Figure

6.6, it can be observed that the effect of  $\text{Li}^+$  ion concentration in both MILs and DIL is not the same. While a significant decrease in the  $C_{rot}$  value has been observed in the case of MILs, the change in DIL is not large. These findings indicate that the addition of  $\text{Li}^+$  ion induces a change in the apolar domain in MILs, whereas the nanostructural organization of DILs remains more or less unperturbed with  $\text{Li}^+$  ion addition.

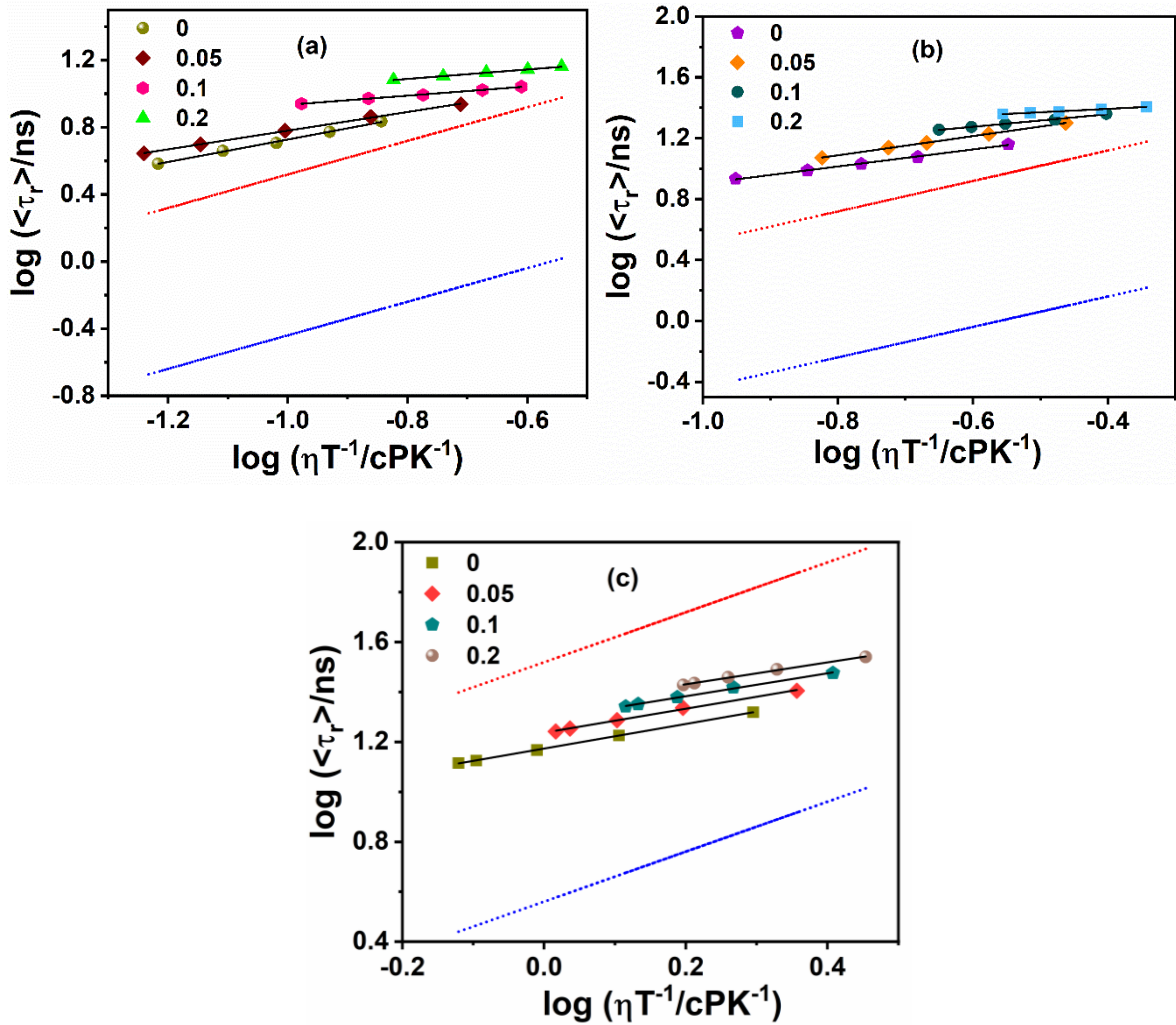


**Figure 6.7.** Log-log plots of average rotational time of MPTS in (a)  $[\text{C}_3\text{C}_{1\text{im}}][\text{NTf}_2]$  (b)  $[\text{C}_6\text{C}_{1\text{im}}][\text{NTf}_2]$  and (c)  $[\text{C}_6(\text{mim})_2][\text{NTf}_2]_2$  with red and blue boundary condition indicating the stick and slip boundary conditions. The solid black line indicates the fit to data points.

To order to probe how the nanostructural organization of the polar domains of ILs is influenced by the presence of  $\text{Li}^+$  ion, a negatively charged solute MPTS has been used for the study. Specifically, the influence of  $\text{Li}^+$  ion on the MILs and DIL have been studied by monitoring the rotational diffusion of MPTS in the respective media in the absence and

presence of  $\text{Li}^+$  ion. Figure 6.7 illustrates the log-log plots of average rotational relaxation time  $\langle\tau_r\rangle$  versus  $\eta/T$  for MPTS in  $[\text{C}_3\text{C}_1\text{im}][\text{NTf}_2]$ ,  $[\text{C}_6\text{C}_1\text{im}][\text{NTf}_2]$  and  $[\text{C}_6(\text{mim})_2][\text{NTf}_2]$  with gradual addition of  $\text{Li}^+$  ions at various temperature. As seen from Figure 6.7, in the case of MILs, the rotational relaxation behavior of MPTS is significantly hindered as compared to that has been observed in the case of perylene. The hindered rotation is due to the strong solute-solvent-specific interaction caused by the specific hydrogen bonding interaction can occur between the highly acidic C (2) hydrogen ( $\text{pK}_a \sim 28.3$ )<sup>268</sup> of imidazolium moiety and the sulfate anions of the solute MPTS. The hindered rotation of MPTS in the MILs also suggests that unlike perylene MPTS is located in the polar region of ILs. Now, when the  $\text{Li}^+$  ions are gradually added to both the MILs independently, the rotational relaxation behavior of MPTS gets more hindered in the concerned media (Figure 6.7). This hindrance of solute rotation with an increase in the  $\text{Li}^+$  ion concentration is suggestive of the fact that the polar domains of MILs gradually become more compact with an increase in the concentration of  $\text{Li}^+$  ions. On the contrary, in the case of DILs, the MPTS rotation is found not to be as hindered as is observed in MILs as seen from the SED theory. This observation indicates relatively weaker solute-solvent interaction in the DIL medium. The relatively weaker solute-solvent interaction in DIL despite the fact that DIL consists of two imidazolium moiety with two acidic C(2) hydrogen, indicates that the structural organization of DILs are different from that of MILs, which eventually facilitate relatively less hindered motion of MPTS in the solvent continuum. In this context, recent literature has depicted that DIL having a six-member alkyl spacer can remain in a folded form where anions are arranged between two imidazolium moieties alternatively.<sup>179, 220, 308-311, 336</sup> Perhaps because of this folded structural arrangement of DILs, it becomes difficult for bulkier MPTS to make stronger interaction with the C(2) hydrogen of imidazolium moiety. Interestingly with  $\text{Li}^+$  ion addition to DILs, the rotation of MPTS is observed to be slightly hindered in (DIL + Li) mixture. We note here that the change in the rotational diffusion of

MPTS is observed to be much higher when  $\text{Li}^+$  ion is added to MILs than that of a situation when  $\text{Li}^+$  ion is added to DILs (Figure 6.7). These observations indicate that polar domains of DIL remain relatively unperturbed than that of MILs with the addition of  $\text{Li}^+$  ions in the respective media. This behavior can also be realized clearly when the friction coefficient values ( $C_{rot}$ ) estimated for both MILs and DIL are plotted against the mole fraction of lithium salt added to the neat ILs (Figure 6.8). As can be seen from Figure 6.8, the change in the friction coefficient for MPTS in the case of MILs is observed to be relatively higher than that of DIL. This indicates that the introduction of  $\text{Li}^+$  ion in MILs and DIL are not the same because, in the presence of  $\text{Li}^+$  ion, the nanostructural organization of MILs gets more perturbed than that of DIL. This observation again demonstrates that due to the difference in the fluid structure of MILs and DIL, the effect of  $\text{Li}^+$  ion on the structurally similar MILs and DIL are quite different from each other.

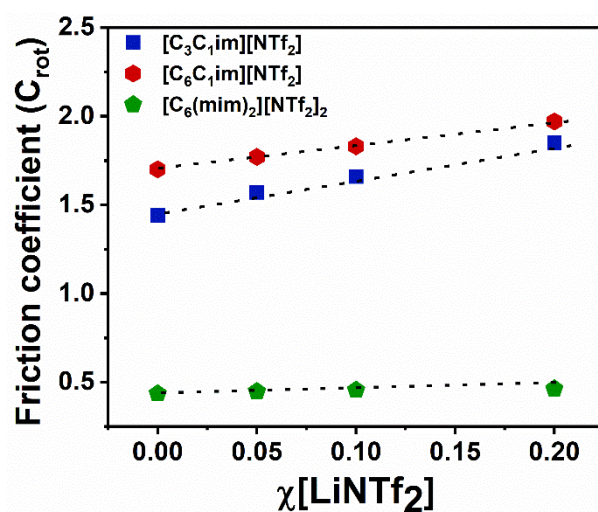


**Figure 6.8.** The friction coefficient for MPTS in all the systems as a function of  $\text{Li}^+$  ion concentration at 298 K.

Overall, the above TRFA studies on MILs and DIL in the absence and presence of  $\text{Li}^+$  ion have demonstrated that interaction between  $\text{Li}^+$  ion and  $\text{NTf}_2^-$  of MILs is relatively stronger than that of  $\text{Li}^+$  ion and  $\text{NTf}_2^-$  of DIL. The difference in the  $\text{Li}^+$  ion-anion interaction for the MILs and DIL happens due to the fact that the structural organization of MILs and DIL are very different

in the sense that while DIL remains in folded form, MILs stay in the straight chain conformation in their respective fluid structure. Because of this relatively stronger lithium-ion anion interaction in the polar domains of MILs, the structural organization at the apolar region of MILs also changes significantly compared to the changes that happen in the apolar region of DIL. Therefore, the outcome of the above investigation demonstrates that the addition of Li<sup>+</sup> ion can cause structure-breaking of ILs where the effect is more pronounced in MILs than DIL.

### 6.3.3. NMR studies

Pulse field gradient NMR (PFG-NMR) technique used for measuring the translational diffusion of ions in a given media is expected to be helpful in understanding the microscopic structural organization of the fluid system.<sup>269, 323, 333, 337</sup> In view of this, we have investigated the translational diffusion of the ILs, specifically the cationic part of the ILs, in the absence and presence of lithium salt by monitoring the <sup>1</sup>H NMR. Table 6.1 and Figure 6.9 illustrates the *D* value of both MILs and DIL in the absence and presence of lithium salt in a temperature range of 298-318 K.

**Table 6.1.** Estimated translational diffusion coefficient of MILs with varying mole fractions of Li<sup>+</sup> ions.

Systems	$\chi[LiNTf_2]$	$D^a \times 10^{-11} \text{ (m}^2\text{s}^{-1}\text{)}$			
		298 K	303 K	308 K	313 K
[C <sub>3</sub> C <sub>1</sub> im] [NTf <sub>2</sub> ]	0	3.11	4.01	5.2	6.91
	0.05	2.82	3.7	5.01	6.32
	0.1	2.49	3.21	3.9	5.1
	0.2	2.3	2.79	3.31	3.9
[C <sub>6</sub> C <sub>1</sub> im] [NTf <sub>2</sub> ]	0	1.34	1.63	1.94	2.42
	0.05	1.20	1.53	1.77	2.24

	0.1	1.16	1.37	1.54	1.73
	0.2	1.04	1.20	1.33	1.46
[C <sub>6</sub> (mim) <sub>2</sub> ] [NTf <sub>2</sub> ] <sub>2</sub>	0	0.21	0.29	0.4	0.51
	0.05	0.18	0.26	0.35	0.46
	0.1	0.15	0.23	0.31	0.41

<sup>a</sup>Experimental error:  $\pm 5\%$

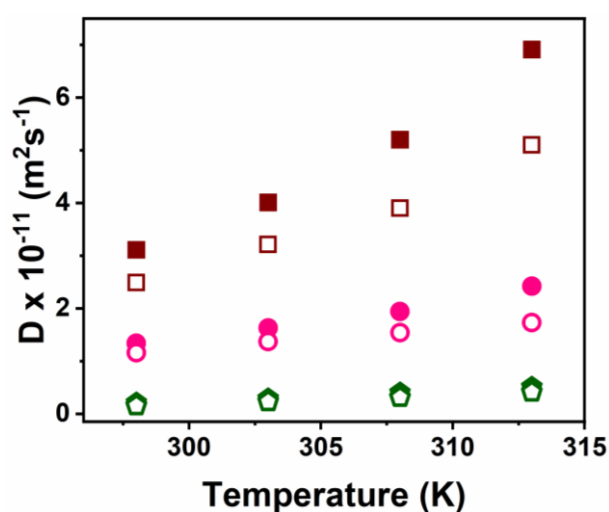


**Figure 6.9.** Temperature dependent variation of self-diffusion coefficient of neat ILs as well as with the addition of  $Li^+$  ion. The square solid shapes (brown) and square open shapes (brown) represent the value of  $D$  for [C<sub>3</sub>C<sub>1</sub>im] [NTf<sub>2</sub>] and [LiNTf<sub>2</sub>]<sub>0.1</sub> [C<sub>3</sub>C<sub>1</sub>im] [NTf<sub>2</sub>] respectively. The circle solid shapes (pink) and circle open shapes (pink) represent the value of  $D$  for [C<sub>6</sub>C<sub>1</sub>im] [NTf<sub>2</sub>] and [LiNTf<sub>2</sub>]<sub>0.1</sub> [C<sub>6</sub>C<sub>1</sub>im] [NTf<sub>2</sub>] respectively. The pentagon solid shapes (green) and pentagon open shapes (green) represent the value of  $D$  for [C<sub>6</sub>(mim)<sub>2</sub>] [NTf<sub>2</sub>]<sub>2</sub> and [LiNTf<sub>2</sub>]<sub>0.1</sub> [C<sub>6</sub>(mim)<sub>2</sub>] [NTf<sub>2</sub>]<sub>2</sub> respectively.

From Table 6.1, we can see that at any particular temperature, the value of  $D$  is found to be smallest for [C<sub>6</sub>(mim)<sub>2</sub>] [NTf<sub>2</sub>]<sub>2</sub>. In contrast, for MIL, [C<sub>3</sub>C<sub>1</sub>im][NTf<sub>2</sub>], it is found to be the largest according to their relative masses. Further, the  $D$  value increases with an increase in the temperature, attributed to the decrease in the medium viscosity. Moreover, upon the addition of Li salt in ILs, the value of  $D$  has been found to decrease in both the MILs and DIL which is also consistent with an increase in medium viscosity. However, upon a careful

inspection it can be noted that the decrease in diffusion coefficient with an increase in viscosity on the addition of lithium salt does not follow a linear relationship. For example, negligible change in the value of  $D$  (0.21 to 0.15 with the addition of 0.1 mole fraction of Li salt) upon addition of lithium salt has been observed in the case of DIL even though the change in viscosity is significant for the same. However, an appreciable change in the value of  $D$  is noted in the case of  $[\text{C}_3\text{C}_{1\text{im}}][\text{NTf}_2]$  with the addition of lithium salt (Figure 6.9). This clearly indicates that the extent of influence of lithium salt on the structural organization of MILs and DILs is different. To support this above observation, we have analyzed the diffusion data through the Stokes-Einstein equation.<sup>86</sup>

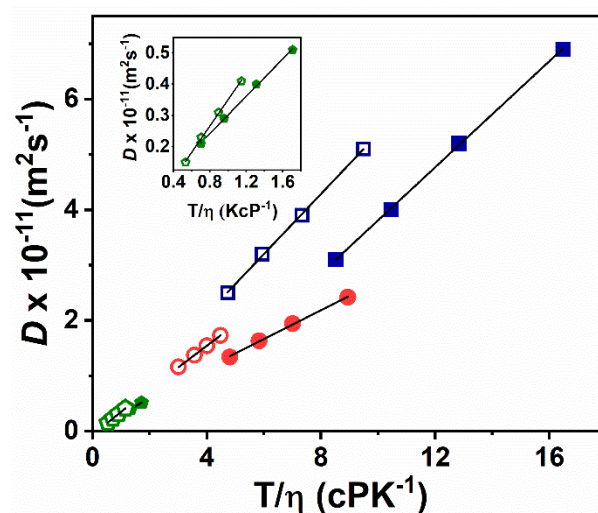


**Figure 6.10.** Self-diffusion coefficient plotted against  $T/\eta$  in neat ILs as well as with the addition of  $\text{Li}^+$  ion. The dotted lines are the fit to the data points. The square solid shapes (blue) and square open shapes (blue) represent the value of  $D$  for  $[\text{C}_3\text{C}_{1\text{im}}][\text{NTf}_2]$  and  $[\text{LiNTf}_2]_{0.1}[\text{C}_3\text{C}_{1\text{im}}][\text{NTf}_2]$  respectively. The circle solid shapes (red) and circle open shapes (red) represent the value of  $D$  for  $[\text{C}_6\text{C}_{1\text{im}}][\text{NTf}_2]$  and  $[\text{LiNTf}_2]_{0.1}[\text{C}_6\text{C}_{1\text{im}}][\text{NTf}_2]$  respectively. The pentagon solid shapes (green) and pentagon open shapes (green) represent the value of  $D$  for  $[\text{C}_6(\text{mim})_2][\text{NTf}_2]_2$  and  $[\text{LiNTf}_2]_{0.1}[\text{C}_6(\text{mim})_2][\text{NTf}_2]_2$  respectively.

Figure 6.10 shows the plot of  $D$  versus  $T/\eta$  and as expected from the Stokes-Einstein equation,<sup>338</sup> a linear relationship is obtained for all the systems. The slope obtained from the plot of  $D$  versus  $T/\eta$  is stated as  $k/(6\pi a)$ , where ‘ $a$ ’ indicates the hydrodynamic radius. It is interesting to note here that the slope of DIL is found to be 0.3 while that of MIL,

[C<sub>6</sub>C<sub>1</sub>im][NTf<sub>2</sub>] and [C<sub>3</sub>C<sub>1</sub>im][NTf<sub>2</sub>] are found to be 0.26 and 0.48 respectively. This observation indicates that the structural arrangement of DIL is neither same as that of [C<sub>6</sub>C<sub>1</sub>im][NTf<sub>2</sub>] nor it's same as [C<sub>3</sub>C<sub>1</sub>im][NTf<sub>2</sub>]; rather, DIL remains in the folded form in the fluid structure. Further, upon the addition of Li<sup>+</sup> ion to both MILs and DIL, the slope increases for both the (MIL+ Li) mixture and the (DIL + Li) mixture. In case of [C<sub>3</sub>C<sub>1</sub>im][NTf<sub>2</sub>] and [C<sub>6</sub>C<sub>1</sub>im][NTf<sub>2</sub>], the slope increases from 0.46 to 0.6 and from 0.26 to 0.4 upon addition of 0.2 mole fraction of Li<sup>+</sup> ion in the respective media while in case of [C<sub>6</sub>(mim)<sub>2</sub>] [NTf<sub>2</sub>]<sub>2</sub> the slope increases from 0.3 to 0.4 upon addition of 0.1 mole fraction of Li<sup>+</sup> ion. These data show that the effect of perturbation by Li<sup>+</sup> ion is greater in the case of MILs than that of DILs. This also indicates that the folded structure of DIL remains intact even upon the addition of Li<sup>+</sup> ions. Moreover, the measurements of the translational diffusion coefficients of these systems corroborate with the findings obtained from the rotational dynamic study.

#### **6.4. Conclusion**

The present study reports the investigation on the intermolecular interaction, structure, and dynamics of MILs and DIL in the absence and presence of lithium salt. The excitation wavelength-dependent fluorescence emission study has demonstrated that the microheterogeneity of the respective MILs and DIL increases upon the addition of lithium salt. How Li<sup>+</sup> ion induces the change in the structural organization of apolar and polar domains of ILs is monitored by following the rotation of apolar solute perylene and a polar ionic solute MPTS through TRFA measurements. TRFA measurements have revealed that upon addition of Li<sup>+</sup> ion, the rotational behavior of the probe solutes changes in both MILs and DIL. However, the difference in the rotational behavior of the solute rotors (in comparison to MILs without Li<sup>+</sup> ion) is found to be significant in MILs than that observed in DIL, indicating the influence of Li<sup>+</sup> ion on MILs is relatively greater than that on DIL. Since LiNTf<sub>2</sub> is known to coordinate with anions of ILs, the outcome of the rotational behavior of solute suggests that interaction

between  $\text{Li}^+$  ions and  $\text{NTf}_2^-$  ions in the case of MILs is relatively stronger than that in DIL. Interestingly, faster rotation of perylene in ILs upon addition of  $\text{Li}^+$  ion also indicates that due to the  $\text{Li}^+$  and  $\text{NTf}_2^-$  binding in the ionic regions of ILs, the packing of alkyl chain present in the apolar region of MILs get reduced. On the other hand, when  $\text{Li}^+$  ion is added to the DIL, not much change in the structural organization of the apolar region of the DIL has been observed. Moreover, measurements from the diffusion coefficient of a cationic moiety of ILs through NMR studies have also supported the observation that  $\text{Li}^+$  ion can perturb the nanostructural organization of MIL in relatively more significant manner than it does for DIL. The differences in the behavior of DIL (as compared to MILs) in the presence of  $\text{Li}^+$  ion has been rationalized by considering the folded arrangement of DIL in its fluid structure. Overall, both fluorescence and NMR studies have clearly demonstrated that the addition of lithium-ion can cause significant structure breaking for MILs compared to that for DIL. The outcome of the present investigation is expected to be helpful in formulating a suitable IL-based electrolytic system for lithium-ion battery applications. Moreover, the results obtained from this study also suggest that the influence of lithium-ion on MILs could be helpful in tuning the organic reactions that are dependent on the change in the behavior of the apolar region of the given medium.

## Summary and Future Prospects

Thermophysical and photophysical studies are carried out on some monocationic ILs, dicationic ILs and binary mixtures of monocationic ILs in order to understand the intermolecular interactions, structure and dynamical behavior of these solvent systems. For this purpose, several neat imidazolium and pyrrolidinium based ILs and their binary mixtures along with some imidazolium-based dicationic ILs have been investigated by using several methods. Specifically, the density, viscosity, thermal expansion coefficient, time-resolved fluorescence anisotropy, NMR, fluorescence correlation spectroscopy (FCS) studies have been carried out to understand the behavior of these solvent systems. Several interesting results in relation to understanding the basics of solute-solvent and solvent-solvent interaction and its relationship with the structural organization of the media have emerged from the present work. The key findings of the present thesis are summarized as follows:

- (1) The intermolecular interactions observed through the rotation of probes in ILs as well as the mixtures of imidazolium ILs are found to be different for different mixtures indicating that the binary mixtures of ILs are micro-heterogeneous in nature.
- (2) The outcome of combined steady state and time-resolved studies have demonstrated that ILs and their mixtures are not only spatially heterogeneous but also, they are dynamically heterogeneous. The study eventually reveals that the binary mixtures of imidazolium and pyrrolidinium-based ILs show appreciable deviation from ideal behavior and the deviation from the ideal behavior is caused due to the generation of free volume in the resultant mixture.
- (3) The outcomes of the RET studies have indicated that the alkyl chain length on the cation is not the sole factor contributing to the RET process in DILs and MILs but the local

structure of DILs play an important role. The results of the RET studies have also indicated that DILs have a more compact local structure than that of MILs.

- (4) The outcome of the investigation on the intermolecular interaction, structure, and dynamics of MILs and DIL in the absence and presence of lithium salt reveals that with an addition of  $\text{Li}^+$  ion cause significant structure breaking for MILs in comparison to DIL. Since  $\text{LiNTf}_2$  is known to coordinate with anions of ILs, the relatively stronger lithium-ion anion interaction in the polar domains of MILs can cause a significant change in the structural organization at the apolar region of MILs than the apolar domain of the DIL.

The present work provides valuable new information in understanding the structure-property correlation in terms of intermolecular interaction, structural organization and solute dynamics in various imidazolium and pyrrolidinium based MILs, DILs and binary mixtures of MILs. Since, neat ILs are fluorescent in nature, they can be used for energy related applications. The outcome of the studies reveals that ILs-based electrolytes can be used in high temperature battery related applications.

## REFERENCES

1. Wilkes, J. S., *Green Chem.* **2002**, *4*, 73-80.
2. Seddon, K. R. S., Annegret; Torres, M.-J., *J. Pure Appl. Chem.* **2000**, *72*, 2275-2287.
3. Wasserscheid, P.; Keim, W., *Angew. Chem. Int. Ed.* **2000**, *39*, 3772-3789.
4. Welton, T., *Chem. Rev.* **1999**, *99*, 2071-2084.
5. Atkin, R.; Warr, G. G., *J. Phys. Chem. B* **2008**, *112*, 4164-4166.
6. Umebayashi, Y.; Chung, W.-L.; Mitsugi, T.; Fukuda, S.; Takeuchi, M.; Fujii, K.; Takamuku, T.; Kanzaki, R.; Ishiguro, S.-i., *J. Comput. Chem., Jpn.* **2008**, *7*, 125-134.
7. Hayes, R.; Imberti, S.; Warr, G. G.; Atkin, R., *J. Phys. Chem C* **2014**, *118*, 13998-14008.
8. Greaves, T. L.; Kennedy, D. F.; Kirby, N.; Drummond, C. J., *Phys. Chem. Chem. Phys.* **2011**, *13*, 13501-13509.
9. Wang, Y.-L.; Li, B.; Sarman, S.; Mocci, F.; Lu, Z.-Y.; Yuan, J.; Laaksonen, A.; Fayer, M. D., *Chem. Rev.* **2020**, *120*, 5798-5877.
10. Xue, H.; Verma, R.; Shreeve, J. n. M., *J. Fluorine Chem.* **2006**, *127*, 159-176.
11. Pandey, S., *Anal. Chim. Acta* **2006**, *556*, 38-45.
12. Seddon Kenneth, R., *J. Am. Chem. Soc.* **2003**, *125*, 7480-7480.
13. Hayashi, S.; Hamaguchi, H.-o., *Chem. Lett.* **2004**, *33*, 1590-1591.
14. Dupont, J.; de Souza, R. F.; Suarez, P. A. Z., *Chem. Rev.* **2002**, *102*, 3667-3692.
15. Sheldon, R., *Chem. Commun.* **2001**, 2399-2407.
16. Imperato, G.; König, B.; Chiappe, C., *Eur. J. Org. Chem.* **2007**, *2007*, 1049-1058.
17. Weingärtner, H., *Angew. Chem. Int. Ed.* **2008**, *47*, 654-670.
18. Rogers, R. D.; Voth, G. A., *Acc. Chem. Res.* **2007**, *40*, 1077-1078.
19. Chiappe, C.; Pieraccini, D., *J. Phys. Org. Chem.* **2005**, *18*, 275-297.
20. Plechkova, N. V.; Seddon, K. R., *Chem. Soc. Rev.* **2008**, *37*, 123-150.

21. Hough, W. L.; Rogers, R. D., *Bull. Chem. Soc. Jpn.* **2007**, *80*, 2262-2269.
22. Hallett, J. P.; Welton, T., *Chem. Rev.* **2011**, *111*, 3508-3576.
23. Mazille, F.; Fei, Z.; Kuang, D.; Zhao, D.; Zakeeruddin, S. M.; Grätzel, M.; Dyson, P. J., *Inorg. Chem.* **2006**, *45*, 1585-1590.
24. Wishart, J. F., *Energy Environ. Sci.* **2009**, *2*, 956-961.
25. Walden, P., *Bull. Acad. Imper. Sci. St. Petersburg* **1914**, 1800.
26. Ray, P. C.; Rakshit, J. N. *J. Chem. Soc., Trans.*, **1911**, *99*, 1470.
27. Hurley, F. H.; Wier, T. P., *J. Electrochem. Soc.* **1951**, *98*, 203.
28. Wasserscheid, P. W., Tom, Ionic Liquids in Synthesis Edited by P. Wasserscheid and T. Welton. Wiley-VCH: Weinheim. 2003. **2003**.
29. Wilkes, J. S.; Zaworotko, M. J., *J. Chem. Soc., Chem. Commun.* **1992**, 965-967.
30. Polyakov, O. G.; Ivanova, S. M.; Gaudinski, C. M.; Miller, S. M.; Anderson, O. P.; Strauss, S. H., *Organometallics* **1999**, *18*, 3769-3771.
31. J. Golding, J.; R. MacFarlane, D.; Spiccia, L.; J. Golding, J.; Forsyth, M.; W. Skelton, B.; H. White, A., *Chem. Commun.* **1998**, 1593-1594.
32. Larsen, A. S.; Holbrey, J. D.; Tham, F. S.; Reed, C. A., *J. Am. Chem. Soc.* **2000**, *122*, 7264-7272.
33. Xu, W.; Wang, L.-M.; Nieman, R. A.; Angell, C. A., *J. Phys. Chem B* **2003**, *107*, 11749-11756.
34. Watanabe, M.; Thomas, M. L.; Zhang, S.; Ueno, K.; Yasuda, T.; Dokko, K., *Chem. Rev.* **2017**, *117*, 7190-7239.
35. Caparica, R.; Júlio, A.; Baby, A. R.; Araújo, M. E.; Fernandes, A. S.; Costa, J. G.; Santos de Almeida, T., *Pharmaceutics* **2018**, *10*.
36. Md Moshikur, R.; Chowdhury, M. R.; Fujisawa, H.; Wakabayashi, R.; Moniruzzaman, M.; Goto, M., *ACS Sustainable Chem. Eng.* **2020**, *8*, 13660-13671.

37. Anderson, J. L.; Ding, R.; Ellern, A.; Armstrong, D. W., *J. Am. Chem. Soc.* **2005**, *127*, 593-604.
38. Bhatt, D. R.; Maheria, K. C.; Parikh, J. K., *RSC Adv.* **2015**, *5*, 12139-12143.
39. Han, X.; Armstrong, D. W., *Org. Lett.* **2005**, *7*, 4205-4208.
40. Jin, C.-M.; Ye, C.; Phillips, B. S.; Zabinski, J. S.; Liu, X.; Liu, W.; Shreeve, J. n. M., *J. Mater. Chem.* **2006**, *16*, 1529-1535.
41. Kim, J. Y.; Kim, T. H.; Kim, D. Y.; Park, N.-G.; Ahn, K.-D., *J. Power Sources* **2008**, *175*, 692-697.
42. Li, S.; Bañuelos, J. L.; Zhang, P.; Feng, G.; Dai, S.; Rother, G.; Cummings, P. T., *Soft Matter* **2014**, *10*, 9193-9200.
43. Li, S.; Zhao, W.; Feng, G.; Cummings, P. T., *Langmuir* **2015**, *31*, 2447-2454.
44. Moosavi, M.; Khashei, F., *Fluid Phase Equilib.* **2018**, *460*, 135-145.
45. Moosavi, M.; Khashei, F.; Sharifi, A.; Mirzaei, M., *J. Chem. Thermodyn.* **2017**, *107*, 1-7.
46. Payagala, T.; Huang, J.; Breitbach, Z. S.; Sharma, P. S.; Armstrong, D. W., *Chem. Mater.* **2007**, *19* (24), 5848-5850.
47. Serva, A.; Migliorati, V.; Lapi, A.; Aquilanti, G.; Arcovito, A.; D'Angelo, P., *Phys. Chem. Chem. Phys.* **2016**, *18*, 16544-16554.
48. Shirota, H.; Mandai, T.; Fukazawa, H.; Kato, T., *J. Chem. Eng. Data* **2011**, *56*, 2453-2459.
49. Yu, G.; Yan, S.; Zhou, F.; Liu, X.; Liu, W.; Liang, Y., *Tribol. Lett.* **2007**, *25*, 197-205.
50. Zeng, Z.; Phillips, B. S.; Xiao, J.-C.; Shreeve, J. n. M., *Chem. Mater.* **2008**, *20*, 2719-2726.
51. Rogers Robin, D.; Seddon Kenneth, R., *Science* **2003**, *302* (5646), 792-793.

52. Enomoto, T.; Nakamori, Y.; Matsumoto, K.; Hagiwara, R., *J. Phys. Chem. C* **2011**, *115*, 4324-4332.
53. Ngo, H. L.; LeCompte, K.; Hargens, L.; McEwen, A. B., *Thermochim. Acta* **2000**, *357-358*, 97-102.
54. Lewandowski, A.; Świdarska-Mocek, A., *J. Power Sources* **2009**, *194*, 601-609.
55. Freemantle, M., *Chem. Eng. News* **2007**, *85*, 23-26.
56. Carda-Broch, S.; Berthod, A.; Armstrong, D. W., *Anal. Bioanal. Chem.* **2003**, *375*, 191-199.
57. Dzyuba, S. V.; Bartsch, R. A., *ChemPhysChem* **2002**, *3*, 161-166.
58. Zhou, Z.-B.; Matsumoto, H.; Tatsumi, K., *Chem. Lett.* **2004**, *33*, 1636-1637.
59. Zhou, Z.-B.; Matsumoto, H.; Tatsumi, K., *Chem. Eur. J.* **2006**, *12*, 2196-2212.
60. Wang, H.; Wang, J.; Zhang, S., *J. Chem. Eng. Data* **2012**, *57*, 1939-1944.
61. Bonhôte, P.; Dias, A.-P.; Papageorgiou, N.; Kalyanasundaram, K.; Grätzel, M., *Inorg. Chem.* **1996**, *35*, 1168-1178.
62. Holbrey, J. D.; Turner, M. B.; Reichert, W. M.; Rogers, R. D., *Green Chem.* **2003**, *5*, 731-736.
63. Branco, L. C.; Rosa, J. N.; Moura Ramos, J. J.; Afonso, C. A. M., *Chem. Eur. J.* **2002**, *8*, 3671-3677.
64. Bagno, A.; Butts, C.; Chiappe, C.; D'Amico, F.; Lord, J. C. D.; Pieraccini, D.; Rastrelli, F., *Org. Biomol. Chem.* **2005**, *3*, 1624-1630.
65. Vogel, H., *Physikalische Zeitschrift (in German)* **1921**, *22*, 645.
66. Fulcher, G. S., *J. Am. Ceram. Soc.* **1925**, *8*, 339-355.
67. Tammann, G.; Hesse, W., *Zeitschrift für anorganische und allgemeine Chemie (in German)* **1926**, *156*, 245-257.

68. Greaves, T. L.; Weerawardena, A.; Fong, C.; Krodkiewska, I.; Drummond, C. J., *J. Phys. Chem B* **2006**, *110*, 22479-22487.
69. Hirao, M.; Sugimoto, H.; Ohno, H., *J. Electrochem. Soc.* **2000**, *147*, 4168.
70. MacFarlane, D. R.; Meakin, P.; Sun, J.; Amini, N.; Forsyth, M., *J. Phys. Chem B* **1999**, *103*, 4164-4170.
71. Tokuda, H.; Baek, S.-J.; Watanabe, M., *Electrochemistry* **2005**, *73*, 620-622.
72. Hapiot, P.; Lagrost, C., *Chem. Rev.* **2008**, *108*, 2238-2264.
73. Zhang, Z.; Zhou, H.; Yang, L.; Tachibana, K.; Kamijima, K.; Xu, J., *Electrochim. Acta* **2008**, *53*, 4833-4838.
74. Almeida, H. F. D.; Carvalho, P. J.; Kurnia, K. A.; Lopes-da-Silva, J. A.; Coutinho, J. A. P.; Freire, M. G., *Fluid Phase Equilib.* **2016**, *409*, 458-465.
75. Zhou, J.; Dong, S.-K.; He, Z.-H.; Zhang, Y.-H., *Chinese Phys. B* **2020**, *29*, 047801.
76. Chatel, G.; Pereira, J. F. B.; Debbeti, V.; Wang, H.; Rogers, R. D., *Green Chem.* **2014**, *16*, 2051-2083.
77. Abbott, A. P.; Frisch, G.; Garrett, H.; Hartley, J., *Chem. Commun.* **2011**, *47*, 11876-11878.
78. Andanson, J.-M.; Beier, M. J.; Baiker, A., *J. Phys. Chem. Lett.* **2011**, *2*, 2959-2964.
79. Bruce, D. W.; Cabry, C. P.; Canongia Lopes, J. N.; Costen, M. L.; D'Andrea, L.; Grillo, I.; Marshall, B. C.; McKendrick, K. G.; Minton, T. K.; Purcell, S. M.; Rogers, S.; Slattery, J. M.; Shimizu, K.; Smoll, E.; Tesa-Serrate, M. A., *J. Phys. Chem B* **2017**, *121*, 6002-6020.
80. Brüssel, M.; Brehm, M.; Pensado, A. S.; Malberg, F.; Ramzan, M.; Stark, A.; Kirchner, B., *Phys. Chem. Chem. Phys.* **2012**, *14*, 13204-13215.
81. Canongia Lopes, J. N.; Cordeiro, T. C.; Esperança, J. M. S. S.; Guedes, H. J. R.; Huq, S.; Rebelo, L. P. N.; Seddon, K. R., *J. Phys. Chem B* **2005**, *109*, 3519-3525.

82. Clough, M. T.; Crick, C. R.; Gräsvik, J.; Hunt, P. A.; Niedermeyer, H.; Welton, T.; Whitaker, O. P., *Chem. Sci.* **2015**, *6*, 1101-1114.
83. Fillion, J. J.; Brennecke, J. F., *J. Chem. Eng. Data* **2017**, *62*, 1884-1901.
84. Hollóczki, O.; Malberg, F.; Welton, T.; Kirchner, B., *Phys. Chem. Chem. Phys.* **2014**, *16*, 16880-16890.
85. Lui, M. Y.; Crowhurst, L.; Hallett, J. P.; Hunt, P. A.; Niedermeyer, H.; Welton, T., *Chem. Sci.* **2011**, *2*, 1491-1496.
86. Matthews, R. P.; Villar-Garcia, I. J.; Weber, C. C.; Griffith, J.; Cameron, F.; Hallett, J. P.; Hunt, P. A.; Welton, T., *Phys. Chem. Chem. Phys.* **2016**, *18*, 8608-8624.
87. Niedermeyer, H.; Hallett, J. P.; Villar-Garcia, I. J.; Hunt, P. A.; Welton, T., *Chem. Soc. Rev.* **2012**, *41*, 7780-7802.
88. Paschek, D.; Golub, B.; Ludwig, R., *Phys. Chem. Chem. Phys.* **2015**, *17*, 8431-8440.
89. Payal, R. S.; Balasubramanian, S., *Phys. Chem. Chem. Phys.* **2013**, *15*, 21077-21083.
90. Stoppa, A.; Buchner, R.; Hefter, G., *J. Mol. Liq.* **2010**, *153*, 46-51.
91. Almeida, H. F. D.; Canongia Lopes, J. N.; Rebelo, L. P. N.; Coutinho, J. A. P.; Freire, M. G.; Marrucho, I. M., *J. Chem. Eng. Data* **2016**, *61*, 2828-2843.
92. Katti, P. K.; Chaudhri, M. M., *J. Chem. Eng. Data* **1964**, *9*, 442-443.
93. Grunberg, L.; Nissan, A. H., *Nature* **1949**, *164*, 799-800.
94. Bingham, E. C., *Fluidity and plasticity*, McGraw-Hill, New York. **1922**.
95. Benson, G. C.; Kiyohara, O., *J. Chem. Thermodyn.* **1979**, *11*, 1061-1064.
96. Bernal, J. D., *Proc. R. Soc. London, Ser. A.* **1964**, *280*, 299.
97. Lo Celso, F.; Yoshida, Y.; Lombardo, R.; Jafta, C.; Gontrani, L.; Triolo, A.; Russina, O., *C R Chim.* **2018**, *21*, 757-770.
98. Liu, X.; Zhou, G.; Huo, F.; Wang, J.; Zhang, S., *J. Phys. Chem C* **2016**, *120*, 659-667.

99. Abe, H.; Imai, Y.; Takekiyo, T.; Yoshimura, Y., *J. Phys. Chem B* **2010**, *114*, 2834-2839.
100. Triolo, A.; Russina, O.; Bleif, H.-J.; Di Cola, E., *J. Phys. Chem B* **2007**, *111*, 4641-4644.
101. Nemoto, F.; Kofu, M.; Yamamuro, O., *J. Phys. Chem B* **2015**, *119*, 5028-5034.
102. Bodo, E.; Postorino, P.; Mangialardo, S.; Piacente, G.; Ramondo, F.; Bosi, F.; Ballirano, P.; Caminiti, R., *J. Phys. Chem B* **2011**, *115*, 13149-13161.
103. Campetella, M.; Macchiagodena, M.; Gontrani, L.; Kirchner, B., *Mol. Phys.* **2017**, *115*, 1582-1589.
104. Jiang, H. J.; FitzGerald, P. A.; Dolan, A.; Atkin, R.; Warr, G. G., *J. Phys Chem B* **2014**, *118*, 9983-9990.
105. Mariani, A.; Caminiti, R.; Campetella, M.; Gontrani, L., *Phys. Chem. Chem. Phys.* **2016**, *18*, 2297-2302.
106. Usui, K.; Hunger, J.; Bonn, M.; Sulpizi, M., *J. Chem. Phys.* **2018**, *148*, 193811.
107. Henderson, W. A.; Fylstra, P.; De Long, H. C.; Trulove, P. C.; Parsons, S., *Phys. Chem. Chem. Phys.* **2012**, *14*, 16041-16046.
108. Avent, A. G.; Chaloner, P. A.; Day, M. P.; Seddon, K. R.; Welton, T., *J. Chem. Soc, Dalton Trans.* **1994**, 3405-3413.
109. Gebbie Matthew, A.; Valtiner, M.; Banquy, X.; Fox Eric, T.; Henderson Wesley, A.; Israelachvili Jacob, N., *J. N. Proc. Natl. Acad. Sci. U.S.A.* **2013**, *110*, 9674-9679.
110. Every, H. A.; Bishop, A. G.; MacFarlane, D. R.; Orädd, G.; Forsyth, M., *Phys. Chem. Chem. Phys.* **2004**, *6*, 1758-1765.
111. Hayes, R.; Warr, G. G.; Atkin, R., *Chem. Rev.* **2015**, *115*, 6357-6426.
112. Schrödle, S.; Annat, G.; MacFarlane, D. R.; Forsyth, M.; Buchner, R.; Hefter, G., *Chem. Commun.* **2006**, 1748-1750.

113. Turton, D. A.; Sonnleitner, T.; Ortner, A.; Walther, M.; Hefter, G.; Seddon, K. R.; Stana, S.; Plechkova, N. V.; Buchner, R.; Wynne, K., *Faraday Discuss.* **2012**, *154*, 145-153.
114. Adhikari, A.; Das, D. K.; Sasmal, D. K.; Bhattacharyya, K., *J. Phys. Chem A* **2009**, *113*, 3737-3743.
115. Bhattacharyya, K.; Bagchi, B., *J. Chem. Sci.* **2007**, *119*, 113-121.
116. Canongia Lopes, J. N. A.; Pádua, A. A. H., *J. Phys. Chem B* **2006**, *110*, 3330-3335.
117. Cha, S.; Kim, D., *Phys. Chem. Chem. Phys.* **2015**, *17*, 29786-29792.
118. Hu, Z.; Margulis Claudio, J., *J. N. Proc. Natl. Acad. Sci. U.S.A.* **2006**, *103*, 831-836.
119. Ingram, J. A.; Moog, R. S.; Ito, N.; Biswas, R.; Maroncelli, M., *J. Phys. Chem B* **2003**, *107*, 5926-5932.
120. Ito, N.; Arzhantsev, S.; Heitz, M.; Maroncelli, M., *J. Phys. Chem B* **2004**, *108*, 5771-5777.
121. Khara, D. C.; Samanta, A., *J. Phys. Chem B* **2012**, *116*, 13430-13438.
122. Paul, A.; Mandal, P. K.; Samanta, A., *J. Phys. Chem B* **2005**, *109*, 9148-9153.
123. Roy, D.; Patel, N.; Conte, S.; Maroncelli, M., *J. Phys. Chem B* **2010**, *114*, 8410-8424.
124. Samanta, A., *J. Phys. Chem B* **2006**, *110*, 13704-13716.
125. Santos, L. M. N. B. F.; Canongia Lopes, J. N.; Coutinho, J. A. P.; Esperança, J. M. S. S.; Gomes, L. R.; Marrucho, I. M.; Rebelo, L. P. N., *J. Am. Chem. Soc.* **2007**, *129*, 284-285.
126. Urahata, S. M.; Ribeiro, M. C. C., *J. Chem. Phys.* **2004**, *122*, 024511.
127. Wang, Y.; Voth, G. A., *J. Phys. Chem B* **2006**, *110*, 18601-18608.
128. Xiao, D.; Rajian, J. R.; Cady, A.; Li, S.; Bartsch, R. A.; Quitevis, E. L., *J. Phys. Chem B* **2007**, *111*, 4669-4677.

129. Zheng, Z.-P.; Fan, W.-H.; Roy, S.; Mazur, K.; Nazet, A.; Buchner, R.; Bonn, M.; Hunger, J., *Angew. Chem. Int. Ed.* **2015**, *54*, 687-690.
130. Dieter, K. M.; Dymek, C. J.; Heimer, N. E.; Rovang, J. W.; Wilkes, J. S., *J. Am. Chem. Soc.* **1988**, *110*, 2722-2726.
131. Matthews, R. P.; Welton, T.; Hunt, P. A., *Phys. Chem. Chem. Phys.* **2014**, *16*, 3238-3253.
132. Brooks, N. J.; Castiglione, F.; Doherty, Cara M.; Dolan, A.; Hill, A. J.; Hunt, P. A.; Matthews, R. P.; Mauri, M.; Mele, A.; Simonutti, R.; Villar-Garcia, I. J.; Weber, C. C.; Welton, T., *Chem. Sci.* **2017**, *8*, 6359-6374.
133. Tanaka, K.; Toda, F., *Chem. Rev.* **2000**, *100*, 1025-1074.
134. Kajimoto, O., *Chem. Rev.* **1999**, *99*, 355-390.
135. Seddon, K. R., *Nature (Materials)* **2003**, *2*, 363-365.
136. Muzart, J., *Adv. Synth. Catal.* **2006**, *348*, 275-295.
137. Judge, R. A.; Takahashi, S.; Longenecker, K. L.; Fry, E. H.; Abad-Zapatero, C.; Chiu, M. L., *Cryst. Growth Des.* **2009**, *9*, 3463-3469.
138. Garlitz, J. A. S., C. A.; Flowers, R. A.; Borgstahl, G. E. O., *Act Crystallogr., Sect D* **1999**, *55*.
139. Ranu, B. C.; Banerjee, S., *Org. Lett.* **2005**, *7*, 3049-3052.
140. Khan, I. A.; Gnezdilov, O. I.; Filippov, A.; Shah, F. U., *ACS Sustain. Chem. Eng.* **2021**, *9*, 7769-7780.
141. Ding, J.; Zhou, D.; Spinks, G.; Wallace, G.; Forsyth, S.; Forsyth, M.; MacFarlane, D., *Chem. Mater.* **2003**, *15*, 2392-2398.
142. Armand, M.; Endres, F.; MacFarlane, D. R.; Ohno, H.; Scrosati, B., *Nat. Mater.* **2009**, *8*, 621-629.
143. Zhou, Y.; Qu, J., *ACS Appl. Mater. Interfaces* **2017**, *9*, 3209-3222.

144. Qu, J.; Truhan, J. J.; Dai, S.; Luo, H.; Blau, P. J., *Tribol. Lett.* **2006**, *22*, 207-214.
145. Surette, J. K. D.; Green, L.; Singer, R. D., *Chem. Commun.* **1996**, 2753-2754.
146. Bates, E. D.; Mayton, R. D.; Ntai, I.; Davis, J. H., *J. Am. Chem. Soc.* **2002**, *124*, 926-927.
147. Huang, K.; Zhang, X.-M.; Li, Y.-X.; Wu, Y.-T.; Hu, X.-B., *J. Membr. Sci.* **2014**, *471*, 227-236.
148. Wang, C.; Cui, G.; Luo, X.; Xu, Y.; Li, H.; Dai, S., *J. Am. Chem. Soc.* **2011**, *133*, 11916-11919.
149. Vélez, J. F.; Vázquez-Santos, M. B.; Amarilla, J. M.; Herradón, B.; Mann, E.; del Río, C.; Morales, E., *J. Power Sources* **2019**, *439*, 227098.
150. Pitawala, J.; Matic, A.; Martinelli, A.; Jacobsson, P.; Koch, V.; Croce, F., *J. Phys Chem B* **2009**, *113*, 10607-10610.
151. Chatterjee, K.; Pathak, A. D.; Lakma, A.; Sharma, C. S.; Sahu, K. K.; Singh, A. K., *Sci. Rep.* **2020**, *10*, 9606.
152. Claros, M.; Galleguillos, H. R.; Brito, I.; Graber, T. A., *J. Chem. Eng. Data* **2012**, *57*, 2147-2152.
153. Duan, J.; Yuan, R.; Huang, H.; Sun, C.; Lei, J.; Yuan, X.; Fan, J.; Chen, Z.; Zheng, M.; Dong, Q., *ACS Appl. Mater. Interfaces* **2021**, *13*, 16238-16245.
154. Leclère, M.; Bernard, L.; Livi, S.; Bardet, M.; Guillermo, A.; Picard, L.; Duchet-Rumeau, J., *J. Nanomater.* **2018**, *8* (6).
155. Miyamoto, H.; Yokota, Y.; Imanishi, A.; Inagaki, K.; Morikawa, Y.; Fukui, K.-i., *Phys. Chem. Chem. Phys.* **2018**, *20*, 19408-19415.
156. Lahiri, A.; Schubert, T. J. S.; Iliev, B.; Endres, F., *Phys. Chem. Chem. Phys.* **2015**, *17*, 11161-11164.

157. Russina, O.; Caminiti, R.; Méndez-Morales, T.; Carrete, J.; Cabeza, O.; Gallego, L. J.; Varela, L. M.; Triolo, A., *J. Mol. Liq.* **2015**, *205*, 16-21.
158. Vardar, G.; Sleightholme, A. E. S.; Naruse, J.; Hiramatsu, H.; Siegel, D. J.; Monroe, C. W., *ACS Appl. Mater. Interfaces* **2014**, *6*, 18033-18039.
159. Prabhu, S. R.; Dutt, G. B., *J Phys. Chem B* **2015**, *119*, 6311-6316.
160. Lei, Z.; Yuan, J.; Zhu, J., *J. Chem. Eng. Data* **2010**, *55*, 4190-4194.
161. Platzer, S.; Kar, M.; Leyma, R.; Chib, S.; Roller, A.; Jirsa, F.; Krachler, R.; MacFarlane, D. R.; Kandioller, W.; Keppler, B. K., *J. Hazard. Mater.* **2017**, *324*, 241-249.
162. Zhu, Y.; Chuanzhao, L.; Sudarmadji, M.; Hui Min, N.; Biying, A. O.; Maguire, J. A.; Hosmane, N. S., *ChemistryOpen* **2012**, *1*, 67-70.
163. Umecky, T.; Saito, Y.; Okumura, Y.; Maeda, S.; Sakai, T., *J. Phys. Chem B* **2008**, *112*, 3357-3364.
164. Lassègues, J.-C.; Grondin, J.; Aupetit, C.; Johansson, P., *J. Phys. Chem A* **2009**, *113*, 305-314.
165. Dubnikova, F.; Zeiri, Y., *J. Phys. Chem A* **2016**, *120*, 3079-3087.
166. Méndez-Morales, T.; Carrete, J.; Cabeza, Ó.; Russina, O.; Triolo, A.; Gallego, L. J.; Varela, L. M., *J. Phys. Chem B* **2014**, *118*, 761-770.
167. Hjalmarsson, N.; Atkin, R.; Rutland, M. W., *J. Phys. Chem C* **2016**, *120*, 26960-26967.
168. Hayes, R.; Bernard, S. A.; Imberti, S.; Warr, G. G.; Atkin, R., *J. Phys. Chem C* **2014**, *118*, 21215-21225.
169. Prabhu, S. R.; Dutt, G. B., *J. Phys. Chem B* **2015**, *119*, 15040-15045.
170. Nicolau, B. G.; Sturlaugson, A.; Fruchey, K.; Ribeiro, M. C. C.; Fayer, M. D., *J. Phys. Chem B* **2010**, *114*, 8350-8356.
171. Mandal, P. K.; Paul, A.; Samanta, A., *J. Photochem. Photobiol.* **2006**, *182*, 113-120.

172. Jin, H.; Baker, G. A.; Arzhantsev, S.; Dong, J.; Maroncelli, M., *J. Phys. Chem B* **2007**, *111*, 7291-7302.
173. Adhikari, A.; Das, D. K.; Sasmal, D. K.; Bhattacharyya, K., *J. Phys. Chem A* **2009**, *113* (16), 3737-3743.
174. Patra, S.; Samanta, A., *J. Phys Chem B* **2012**, *116*, 12275-12283.
175. Binetti, E.; Panniello, A.; Triggiani, L.; Tommasi, R.; Agostiano, A.; Curri, M. L.; Striccoli, M., *J. Phys. Chem B* **2012**, *116*, 3512-3518.
176. Ghosh, A.; De, C. K.; Chatterjee, T.; Mandal, P. K., *Phys. Chem. Chem. Phys.* **2015**, *17*, 16587-16593.
177. Guo, J.; Baker, G. A.; Hillesheim, P. C.; Dai, S.; Shaw, R. W.; Mahurin, S. M., *Phys. Chem. Chem. Phys.* **2011**, *13*, 12395-12398.
178. Das, S. K.; Sahu, P. K.; Sarkar, M., *J. Phys. Chem B* **2013**, *117*, 636-647.
179. Sahu, P. K.; Das, S. K.; Sarkar, M., *Phys. Chem. Chem. Phys.* **2014**, *16*, 12918-12928.
180. Jacques, P., *J. Chem. Educ.* **1991**, *68*, 347.
181. Durr, H.; Bouas-Laurent, H., *Photochromism: molecules and systems*. Elsevier: 2003.
182. Bertelson, R. C., *Techniques in Chemistry: Photochromism*; Brown, C. H., Ed.; Wiley-Interscience: New York, Chapter 1. **1971**, *Vol. 3*.
183. Ault, A.; Kouba, C., *J. Chem. Educ.* **1974**, *51*, 395.
184. Zaczek, N. M.; Levy, W. D.; Jordan, M. L.; Niemyer, J. A., *J. Chem. Educ.* **1982**, *59*, 705.
185. Petersen, R. L.; Harris, G. L., *J. Chem. Educ.* **1985**, *62*, 802.
186. Hutton, A. T., *J. Chem. Educ.* **1986**, *63*, 888.
187. Pickering, M., *J. Chem. Educ.* **1980**, *57*, 833.
188. Negri, R. M.; Prysztajn, H. E., *J. Chem. Educ.* **2001**, *78*, 645.
189. Chibisov, A. K.; Görner, H., *J. Phys. Chem A* **1997**, *101*, 4305-4312.

190. Birks, J. B., *Photophysics of Aromatic Molecules*. Wiley-Interscience, London **1970**, 74, 1294-1295.
191. Demchenko, A. P., In *Topics in Fluorescence Spectroscopy*; Lakowicz, J. R., Ed.; Plenum Press: New York. **1991**, Vol. 3.
192. Demchenko, A. P., The red-edge effects: 30 years of exploration. *Luminescence* **2002**, 17, 19-42.
193. Lakowicz, J. R.; Keating-Nakamoto, S., *Biochemistry* **1984**, 23, 3013-3021.
194. Valeur, B.; Weber, G., *J. Chem. Phys.* **1978**, 69, 2393-2400.
195. Weber, G.; Shinitzky, M., *Proceedings of the National Academy of Sciences* **1970**, 65, 823-830.
196. Itoh, K. i.; Azumi, T., *J. Chem. Phys.* **1975**, 62, 3431-3438.
197. Chattopadhyay, A.; Mukherjee, S., *Biochemistry* **1993**, 32, 3804-3811.
198. Lakowicz, J. R., *Principles of fluorescence spectroscopy*. Springer: 2006.
199. Dutt, G. B., *ChemPhysChem* **2005**, 6, 413-418.
200. Valeur, B.; Berberan-Santos, M. N., *Molecular fluorescence: principles and applications*. John Wiley & Sons: 2012.
201. Förster, T., *Molecular Fluorescence Principles and Applications*, Wiley-VCH Verlag GmbH, Weinheim, Germany. **1948**, 55-75.
202. Das, D. K.; Das, A. K.; Mondal, T.; Mandal, A. K.; Bhattacharyya, K., *J. Phys. Chem B* **2010**, 114, 13159-13166.
203. Koch, M.; Rosspeintner, A.; Angulo, G.; Vauthey, E., *J. Am. Chem. Soc.* **2012**, 134, 3729-3736.
204. Damodaran, K., Chapter Four - Recent NMR Studies of Ionic Liquids. In *Annual Reports on NMR Spectroscopy*, Webb, G. A., Ed. Academic Press: 2016; Vol. 88, pp 215-244.

205. Dias, N.; Shimizu, K.; Morgado, P.; Filipe, E. J. M.; Canongia Lopes, J. N.; Vaca Chávez, F., *J. Phys. Chem B* **2014**, *118* (21), 5772-5780.
206. Kruk, D.; Meier, R.; Rachocki, A.; Korpała, A.; Singh, R. K.; Rössler, E. A., *J. Chem. Phys.* **2014**, *140*, 244509.
207. Noda, A.; Hayamizu, K.; Watanabe, M., *J. Phys. Chem B* **2001**, *105*, 4603-4610.
208. Alam, T. M.; Dreyer, D. R.; Bielwaski, C. W.; Ruoff, R. S., *J. Phys. Chem A* **2011**, *115*, 4307-4316.
209. Antony, J. H.; Mertens, D.; Dölle, A.; Wasserscheid, P.; Carper, W. R., *ChemPhysChem* **2003**, *4*, 588-594.
210. Wahlbeck, P. G.; Carper, W. R., *Chem. Eng. Commun.* **2007**, *194*, 1160-1168.
211. Han, K. S.; Li, S.; Hagaman, E. W.; Baker, G. A.; Cummings, P.; Dai, S., *J. Phys. Chem C* **2012**, *116*, 20779-20786.
212. Garaga, M. N.; Nayeri, M.; Martinelli, A., *J. Mol. Liq.* **2015**, *210*, 169-177.
213. Matveev, V. V.; Markelov, D. A.; Chizhik, V. I.; Ingman, P.; Lähderanta, E., *Russ. Chem. Bull.* **2013**, *62*, 1985-1990.
214. Chen, H.; Farkas, E. R.; Webb, W. W., Chapter 1 In Vivo Applications of Fluorescence Correlation Spectroscopy. In *Methods in Cell Biology*, Academic Press: 2008; Vol. 89, pp 3-35.
215. Cha, S.; Shim, T.; Ouchi, Y.; Kim, D., *J. Phys. Chem B* **2013**, *117*, 10818-10825.
216. Cha, S.; Kim, D., *J. Korean Phys. Soc.* **2012**, *61*, 1555-1559.
217. Werner, J. H.; Baker, S. N.; Baker, G. A., *Analyst* **2003**, *128*, 786-789.
218. Sasmal, D. K.; Mondal, T.; Sen Mojumdar, S.; Choudhury, A.; Banerjee, R.; Bhattacharyya, K., *J. Phys. Chem B* **2011**, *115*, 13075-13083.
219. Chakraborty, M.; Ahmed, T.; Dhale, R. S.; Majhi, D.; Sarkar, M., *J. Phys. Chem B* **2018**, *122*, 12114-12130.

220. Majhi, D.; Seth, S.; Sarkar, M., *Phys. Chem. Chem. Phys.* **2018**, *20*, 7844-7856.
221. Gilbert, A. B., J.; Wagner, P. J., *Essential of Molecular Photochemistry*; Blackwell science Inc.: Cambridge, USA. **1991**.
222. Rohatgi-Mukherjee, K. K., *Fundamentals of photochemistry*. **1978**.
223. Becker, W., *Advanced time-correlated single photon counting techniques*. Springer Science & Business Media: 2005; Vol. 81.
224. Demas, J. N., CHAPTER 2 - Methods of Measuring Lifetimes. In *Excited State Lifetime Measurements*, Demas, J. N., Ed. Academic Press: 1983; pp 12-27.
225. O'Connor, D. V. P. D., *Time-correlated single photon counting*. Academic Press: London; Orlando, 1984.
226. Ware, W. R.; Lamola, A. A., *Creation and Detection of the Excited State*. M. Dekker: 1976; Vol. 4.
227. Van Dyke, D. A.; Pryor, B. A.; Smith, P. G.; Topp, M. R., *J. Chem. Educ.* **1998**, *75*, 615.
228. Magde, D.; Elson, E.; Webb, W. W., *Phys. Rev. Lett.* **1972**, *29*, 705-708.
229. Magde, D.; Elson, E. L.; Webb, W. W., Fluorescence correlation spectroscopy. II. An experimental realization. *Biopolymers* **1974**, *13*, 29-61.
230. Haustein, E.; Schwille, P., Fluorescence correlation spectroscopy: an introduction to its concepts and applications. *Biophysics Textbook Online* **2004**, *94*, 1-33.
231. Bevington, P. R.; Robinson, D. K., *Data reduction and error analysis*. McGraw-Hill, New York **2003**.
232. McKinnon, A. E.; Szabo, A. G.; Miller, D. R., *J. Phys. Chem* **1977**, *81*, 1564-1570.
233. O'Connor, D. V.; Ware, W. R.; Andre, J. C., *J. Phys. Chem* **1979**, *83*, 1333-1343.
234. Fleming, G. R., *Chemical applications of ultrafast spectroscopy*. **1986**.
235. Edward, J. T., *J. Chem. Educ.* **1970**, *47*, 261.

236. Gierer, A.; Wirtz, K., *Zeitschrift für Naturforschung A* **1953**, *8*, 532-538.
237. Dote, J. L.; Kivelson, D.; Schwartz, R. N., *J. Phys. Chem* **1981**, *85*, 2169-2180.
238. Hu, C. M.; Zwanzig, R., *J. Chem. Phys.* **1974**, *60*, 4354-4357.
239. Chuang, T. J.; Eissenthal, K. B., *J. Chem. Phys.* **1972**, *57*, 5094-5097.
240. Kurnikova, M.; Waldeck, D.; Coalson, R., *J. Chem. Phys.* **1996**, *105*, 628-638.
241. Hartman, R. S.; Konitsky, W. M.; Waldeck, D. H., *J. Am. Chem. Soc.* **1993**, *115*, 9692-9700.
242. Spears, K. G.; Cramer, L. E., *J. Chem. Phys.* **1978**, *30*, 1-8.
243. Nee, T. W.; Zwanzig, R., *J. Chem. Phys.* **1970**, *52*, 6353-6363.
244. Majhi, D.; Sarkar, M., *Phys. Chem. Chem. Phys.* **2017**, *19*, 23194-23203.
245. Tarif, E.; Mukherjee, K.; Kumbhakar, K.; Barman, A.; Biswas, R., *J. Chem. Phys.* **2019**, *151*, 154902.
246. Lawler, C.; Fayer, M. D., *J. Phys. Chem B* **2013**, *117*, 9768-9774.
247. Brouwer, A. M., *Pure Appl. Chem.* **2011**, *83*, 2213-2228.
248. Endres, F.; Zein El Abedin, S., *Phys. Chem. Chem. Phys.* **2006**, *8*, 2101-2116.
249. Castner, E. W.; Wishart, J. F., *J. Chem. Phys.* **2010**, *132*, 120901.
250. Dupont, J., *Acc. Chem. Res.* **2011**, *44*, 1223-1231.
251. Simon, P.; Gogotsi, Y., *Nat. Mater.* **2008**, *7*, 845-854.
252. Pereiro, A. B.; Araújo, J. M. M.; Oliveira, F. S.; Bernardes, C. E. S.; Esperança, J. M. S. S.; Canongia Lopes, J. N.; Marrucho, I. M.; Rebelo, L. P. N., *Chem. Commun.* **2012**, *48*, 3656-3658.
253. Oliveira, F. S.; Pereiro, A. B.; Araújo, J. M. M.; Bernardes, C. E. S.; Canongia Lopes, J. N.; Todorovic, S.; Feio, G.; Almeida, P. L.; Rebelo, L. P. N.; Marrucho, I. M., *Phys. Chem. Chem. Phys.* **2013**, *15*, 18138-18147.
254. Majhi, D.; Pabbathi, A.; Sarkar, M., *J. Phys. Chem B* **2016**, *120*, 193-205.

255. Vila, J.; Franjo, C.; Pico, J.; Varela, L.; Cabeza, O., *Port. Electrochim. Acta* **2007**, *25*, 163.
256. Rilo, E.; Varela, L. M.; Cabeza, O., *J. Chem. Eng. Data* **2012**, *57*, 2136-2142.
257. Fredlake, C. P.; Crosthwaite, J. M.; Hert, D. G.; Aki, S. N. V. K.; Brennecke, J. F., *J. Chem. Eng. Data* **2004**, *49*, 954-964.
258. Song, D.; Chen, J., *J. Chem. Eng. Data* **2014**, *59*, 257-262.
259. Costa, A. J. L.; Esperança, J. M. S. S.; Marrucho, I. M.; Rebelo, L. P. N., *J. Chem. Eng. Data* **2011**, *56*, 3433-3441.
260. Tipler, P. A.; Mosca, G., *Physics for scientists and engineers*. Macmillan: 2007.
261. Muhammad, N.; Man, Z. B.; Bustam, M. A.; Mutalib, M. I. A.; Wilfred, C. D.; Rafiq, S., *J. Chem. Eng. Data* **2011**, *56*, 3157-3162.
262. Samanta, A., *J. Phys. Chem. Lett.* **2010**, *1*, 1557-1562.
263. Prabhu, S. R.; Dutt, G. B., *J. Phys. Chem B* **2015**, *119*, 2019-2025.
264. Dutt, G. B., *J. Phys. Chem B* **2010**, *114*, 8971-8977.
265. Das, S.; Mukherjee, B.; Biswas, R., *J. Chem. Phys.* **2018**, *148*, 193839.
266. Fruchey, K.; Fayer, M. D., *J. Phys. Chem B* **2010**, *114*, 2840-2845.
267. Mali, K. S.; Dutt, G. B.; Mukherjee, T., *J. Chem. Phys.* **2008**, *128*, 054504.
268. Amyes, T. L.; Diver, S. T.; Richard, J. P.; Rivas, F. M.; Toth, K., *J. Am. Chem. Soc.* **2004**, *126*, 4366-4374.
269. Kumar Sahu, P.; Ghosh, A.; Sarkar, M., *J. Phys. Chem B* **2015**, *119*, 14221-14235.
270. Inamura, Y.; Yamamuro, O.; Hayashi, S.; Hamaguchi, H.-o., *Phys. B: Condens. Matter* **2006**, *385-386*, 732-734.
271. Mao, Y.; Damodaran, K., *J. Chem. Phys.* **2014**, *440*, 87-93.
272. Ordikhani Seyedlar, A.; Stapf, S.; Mattea, C., *Phys. Chem. Chem. Phys.* **2015**, *17*, 1653-1659.

273. Lovelock, K. R. J.; Ejigu, A.; Loh, S. F.; Men, S.; Licence, P.; Walsh, D. A., *Phys. Chem. Chem. Phys.* **2011**, *13*, 10155-10164.
274. Mukherjee, K.; Das, A.; Choudhury, S.; Barman, A.; Biswas, R., *J. Phys. Chem B* **2015**, *119*, 8063-8071.
275. Habasaki, J.; Ngai, K. L., *J. Chem. Phys.* **2008**, *129* (19), 194501.
276. Tsuzuki, S., *Annu. Rep. Prog. Chem., Sect. C: Phys. Chem.* **2012**, *108*, 69-95.
277. Knorr, A.; Fumino, K.; Bansa, A.-M.; Ludwig, R., *Phys. Chem. Chem. Phys.* **2015**, *17*, 30978-30982.
278. Smith, J. A.; Webber, G. B.; Warr, G. G.; Atkin, R., *J. Phys. Chem B* **2013**, *117*, 13930-13935.
279. Cosby, T.; Kapoor, U.; Shah, J. K.; Sangoro, J., *J. Phys. Chem. Lett.* **2019**, *10*, 6274-6280.
280. Voroshylova, I. V.; Ferreira, E. S. C.; Malček, M.; Costa, R.; Pereira, C. M.; Cordeiro, M. N. D. S., *Phys. Chem. Chem. Phys.* **2018**, *20*, 14899-14918.
281. Gouveia, A. S. L.; Bernardes, C. E. S.; Lozinskaya, E. I.; Shaplov, A. S.; Canongia Lopes, J. N.; Marrucho, I. M., *Phys. Chem. Chem. Phys.* **2019**, *21*, 23305-23309.
282. Cha, S.; Kim, D., *J. Chem. Phys.* **2018**, *148*, 193827.
283. Avula, N. V. S.; Mondal, A.; Balasubramanian, S., *J. Phys. Chem. Lett.* **2018**, *9*, 3511-3516.
284. Umeda, K.; Kobayashi, K.; Minato, T.; Yamada, H., *J. Phys. Chem. Lett.* **2020**, *11*, 1343-1348.
285. Brandani, V.; Prausnitz, J. M., *Proc. Natl. Acad. Sci. U.S.A.* **1982**, *79*, 5729-5733.
286. Gardas, R. L.; Costa, H. F.; Freire, M. G.; Carvalho, P. J.; Marrucho, I. M.; Fonseca, I. M. A.; Ferreira, A. G. M.; Coutinho, J. A. P., *J. Chem. Eng. Data* **2008**, *53*, 805-811.
287. Navia, P.; Troncoso, J.; Romani, L., *J. Chem. Eng. Data* **2007**, *52*, 2542-2542.

288. Benson, G. C.; Kiyohara, O., *J. Chem. Thermodyn.* **1979**, *11*, 1061-1064.
289. Tariq, M.; Altamash, T.; Salavera, D.; Coronas, A.; Rebelo, L. P.; Lopes, J. N. C., *ChemPhysChem* **2013**, *14*, 1956-1968.
290. Guo, J.; Mahurin, S. M.; Baker, G. A.; Hillesheim, P. C.; Dai, S.; Shaw, R. W., *J. Phys. Chem B* **2014**, *118*, 1088-1096.
291. Anderton, R. M.; Kauffman, J. F., *J. Phys. Chem* **1994**, *98*, 12117-12124.
292. Wang, P.; Wenger, B.; Humphry-Baker, R.; Moser, J.-E.; Teuscher, J.; Kantlehner, W.; Mezger, J.; Stoyanov, E. V.; Zakeeruddin, S. M.; Grätzel, M., *J. Am. Chem. Soc.* **2005**, *127*, 6850-6856.
293. Sun, X.; Luo, H.; Dai, S., *Chem. Rev.* **2012**, *112*, 2100-2128.
294. Borra, E. F.; Seddiki, O.; Angel, R.; Eisenstein, D.; Hickson, P.; Seddon, K. R.; Worden, S. P., *Nature* **2007**, *447*, 979-981.
295. MacFarlane, D. R.; Tachikawa, N.; Forsyth, M.; Pringle, J. M.; Howlett, P. C.; Elliott, G. D.; Davis, J. H.; Watanabe, M.; Simon, P.; Angell, C. A., *Energy Environ. Sci.* **2014**, *7*, 232-250.
296. Gélinas, B.; Natali, M.; Bibienne, T.; Li, Q. P.; Dollé, M.; Rochefort, D., *J. Phys. Chem C* **2016**, *120*, 5315-5325.
297. Arzhantsev, S.; Jin, H.; Baker, G. A.; Maroncelli, M., *J. Phys. Chem B* **2007**, *111*, 4978-4989.
298. Ren, Z.; Ivanova, A. S.; Couchot-Vore, D.; Garrett-Roe, S., *J. Phys. Chem. Lett.* **2014**, *5*, 1541-1546.
299. Berquist, E. J.; Daly, C. A.; Brinzer, T.; Bullard, K. K.; Campbell, Z. M.; Corcelli, S. A.; Garrett-Roe, S.; Lambrecht, D. S., *J. Phys. Chem B* **2017**, *121*, 208-220.
300. Bailey, H. E.; Wang, Y.-L.; Fayer, M. D., *J. Chem. Phys.* **2018**, *149*, 044501.
301. Araque, J. C.; Daly, R. P.; Margulis, C. J., *J. Chem. Phys.* **2016**, *144*, 204504.

302. Kim, D.; Park, S.-W.; Shim, Y.; Kim, H. J.; Jung, Y., *J. Chem. Phys.* **2016**, *145*, 044502.
303. Rilo, E.; Domínguez-Pérez, M.; Vila, J.; Varela, L. M.; Cabeza, O., *J. Chem. Thermodyn.* **2012**, *49*, 165-171.
304. Dela Cruz, J. L.; Blanchard, G. J., *J. Phys. Chem A* **2002**, *106*, 10718-10724.
305. Daschakraborty, S.; Ranjit, B., *J. Phys. Chem B* **2011**, *115*, 4011-4024.
306. Annapureddy, H. V. R.; Kashyap, H. K.; De Biase, P. M.; Margulis, C. J., *J. Phys. Chem B* **2010**, *114*, 16838-16846.
307. Sahu, P. K.; Sarkar, M., *Chem. Phys. Lett.* **2016**, *652*, 177-183.
308. Li, S.; Feng, G.; Bañuelos, J. L.; Rother, G.; Fulvio, P. F.; Dai, S.; Cummings, P. T., *J. Phys. Chem C* **2013**, *117*, 18251-18257.
309. Moosavi, M.; Khashei, F.; Sedghamiz, E., *Phys. Chem. Chem. Phys.* **2018**, *20*, 435-448.
310. Bhargava, B. L.; Klein, M. L., *J. Phys. Chem B* **2011**, *115*, 10439-10446.
311. Palchowdhury, S.; Bhargava, B. L., *Phys. Chem. Chem. Phys.* **2015**, *17*, 11627-11637.
312. Ghosh, A.; Chatterjee, T.; Roy, D.; Das, A.; Mandal, P. K., *J. Phys. Chem C* **2014**, *118*, 5051-5057.
313. Banerjee, C.; Mandal, S.; Ghosh, S.; Kuchlyan, J.; Kundu, N.; Sarkar, N., *J. Phys. Chem B* **2013**, *117*, 3927-3934.
314. Dávila, M. J.; Aparicio, S.; Alcalde, R.; García, B.; Leal, J. M., *Green Chem.* **2007**, *9*, 221-232.
315. Opallo, M.; Lesniewski, A., *J. Electroanal. Chem.* **2011**, *656*, 2-16.
316. Popovic, J.; Höfler, D.; Melchior, J. P.; Münchinger, A.; List, B.; Maier, J., *J. Phys. Chem. Lett.* **2018**, *9*, 5116-5120.

317. Elia, G. A.; Ulissi, U.; Jeong, S.; Passerini, S.; Hassoun, J., *Energy Environ. Sci.* **2016**, *9*, 3210-3220.
318. Bayley, P. M.; Best, A. S.; MacFarlane, D. R.; Forsyth, M., *ChemPhysChem* **2011**, *12*, 823-827.
319. Ray, P.; Vogl, T.; Balducci, A.; Kirchner, B., *J. Phys. Chem B* **2017**, *121*, 5279-5292.
320. Prabhu, S. R.; Dutt, G., *J. Phys. Chem B* **2016**, *120*, 13118-13124.
321. Kadyan, A.; Pandey, S., *J. Phys. Chem B* **2018**, *122*, 5106-5113.
322. Duluard, S.; Grondin, J.; Bruneel, J.-L.; Pianet, I.; Grélard, A.; Campet, G.; Delville, M.-H.; Lassègues, J.-C., *J. Raman Spectrosc.* **2008**, *39* (5), 627-632.
323. Dhale, R. S.; Sahu, P. K.; Sarkar, M., *J. Phys. Chem B* **2017**, *121*, 7934-7945.
324. Aguilera, L.; Völkner, J.; Labrador, A.; Matic, A., *Phys. Chem. Chem. Phys.* **2015**, *17*, 27082-27087.
325. Casalegno, M.; Raos, G.; Appetecchi, G. B.; Passerini, S.; Castiglione, F.; Mele, A., *J. Phys. Chem. Lett.* **2017**, *8*, 5196-5202.
326. Huang, Q.; Lourenço, T. C.; Costa, L. T.; Zhang, Y.; Maginn, E. J.; Gurkan, B., *J. Phys. Chem B* **2019**, *123*, 516-527.
327. Méndez-Morales, T.; Carrete, J.; Rodriguez, J. R.; Cabeza, O.; Gallego, L. J.; Russina, O.; Varela, L. M., *Phys. Chem. Chem. Phys.* **2015**, *17*, 5298-5307.
328. Nicolau, B. G.; Sturlaugson, A.; Fruchey, K.; Ribeiro, M. C.; Fayer, M., *J. Phys. Chem B* **2010**, *114*, 8350-8356.
329. Balducci, A., *Top Curr. Chem.* **2017**, *375*, 20.
330. Jin, H.; Li, X.; Maroncelli, M., *J. Phys. Chem B* **2007**, *111*, 13473-13478.
331. Sasmal, D. K.; Mojumdar, S. S.; Adhikari, A.; Bhattacharyya, K., *J. Phys. Chem B* **2010**, *114*, 4565-4571.
332. Das, A.; Das, S.; Biswas, R., *J. Chem. Phys.* **2015**, *142*, 034505.

333. Barik, S.; Chakraborty, M.; Sarkar, M., *J. Phys. Chem B* **2020**, *124*, 2864-2878.
334. Saroja, G.; Soujanya, T.; Ramachandram, B.; Samanta, A., *J. Fluoresc.* **1998**, *8*, 405-410.
335. Sahu, P. K.; Das, S. K.; Sarkar, M., *J. Phys. Chem. B* **2014**, *118*, 1907-1915.
336. Chakraborty, M.; Ahmed, T.; Sarkar, M., *Langmuir* **2019**, *35*, 16172-16184.
337. Pramanik, R.; Sarkar, S.; Ghatak, C.; Rao, V. G.; Sarkar, N., *J. Phys. Chem B* **2011**, *115*, 2322-2330.
338. Einstein, A., *Ann. Phys.* **1905**, *322*, 549-560.